**Doctoral Dissertation**

# Swelling and mechanical characteristics of sand treated with a paper sludge ash-based stabilizer.

ペーパースラッジ灰系改質材で改質した砂の膨潤性と力学的特性

by

**DJANDJIEME MALIKI OTIEBOAME**

**ジャンジェメ　マリキ　オチボアメ**

A dissertation submitted to

Graduate School of Urban Innovation

of Yokohama National University

In partial fulfilment of the requirements for the award of the degree of

**Doctor of Philosophy in Engineering**

Academic Supervisor

**Professor KIMITOSHI HAYANO**

Yokohama National University

Yokohama, Japan

**December 2023**

**YOKOHAMA NATIONAL UNIVERSITY**

**GRADUATE SCHOOL OF URBAN INNOVATION**

This dissertation, written by Djandjieme Maliki Otieboame, has been accepted by his supervisor and dissertation committee members. It is submitted to the Graduate School of Urban innovation-Yokohama National university-Japan in partial fulfilment of the requirement for the award of the degree of Doctor of Philosophy in Engineering.

**Committee members:**

- Prof. Kimitoshi HAYANO, Chair

Faculty of Urban Innovation – Yokohama National University

- Prof. Mamoru KIKUMOTO

Faculty of Urban Innovation – Yokohama National University

- Assoc. Prof. Ying CUI

Faculty of Urban Innovation – Yokohama National University

- Assoc. Prof. Hiroshi TAMURA

Faculty of Urban Innovation – Yokohama National University

- Prof. Chikako FUJIYAMA

Faculty of Urban Innovation – Yokohama National University

## Abstract

The thesis aims to investigate the potential of using a Paper Sludge Ash-Based Stabilizer (PSAS) to improve the engineering properties of sand intended for use as backfill material around underground pipes. The study focuses on enhancing the swelling potential and strength characteristics of the sand through the application of PSAS, and a comprehensive set of laboratory tests was conducted to analyse its performance.

In parallel with PSAS-treated sand, ordinary Portland cement (OPC) was also utilized as a stabilizing agent to allow for a comparative analysis. Swelling potential tests were performed on both PSAS-treated and OPC-treated sands at varying moisture contents. The results indicated that PSAS-treated sand, with a water content of 0%, exhibited significant expansion during soaking, similar to the expansion observed in OPC-treated sand. However, the test findings revealed that controlling the moisture content of PSAS-treated sand can effectively reduce its potential for expansion, depending on the duration of its temporary placement at the construction site. This highlights the importance of proper moisture regulation during construction activities.

Further insights into the strength characteristics were obtained through unconfined compression tests. Surprisingly, the compressive strength of PSAS-treated sand was found to be significantly lower than that of OPC-treated sand under similar mixing conditions, despite the relatively similar chemical composition between PSAS and OPC. However, the test results also revealed that the increase in compressive strength with curing time for PSAS-treated sand was more gradual compared to OPC-treated sand. This suggests that PSAS-treated sand is more amenable to re-excavation, potentially providing advantages in certain construction scenarios.

The investigation also extended to analysing the X-ray diffraction profiles of the treated sands. The findings showed that the dominant formation in PSAS-treated sand was calcite, ettringite, and there was a possibility that berlinite might be an additional contributor to the long-term increase in the strength of the PSAS-treated sand. Understanding the mineralogical changes in the treated sand provides valuable insights into the mechanisms responsible for its improved engineering properties.

Moreover, the durability of PSAS-treated sands was scrutinized under dry-wet curing cycles. Cylindrical specimens of the treated sand were subjected to different curing temperatures (40 ℃ and 71 ℃), and the effects of varying numbers of dry-wet curing cycles on the unconfined compressive strength were

investigated. The results showed an initial increase in the unconfined compressive strength of PSAS-treated sand, followed by a subsequent decrease with the progression of the curing process. The influence of confinement on the behaviour of PSAS-treated sand subjected to dry-wet curing cycles was also assessed, revealing its significance in determining the overall durability.

Furthermore, a comparison was made between the results obtained from consolidated triaxial tests and unconfined compression strength data for PSAS-treated sand. The treated sand displayed higher deviator stress and lower volumetric strain compared to untreated Toyoura sand, indicating increased shear strength and reduced compressibility. Additionally, the treated sand exhibited a stronger response to changes in normal stress, as evidenced by the shift of the stress paths. The cohesion and shear resistance of the treated sand were consistently higher than those of Toyoura sand at all relative densities and curing periods. However, an interesting finding was observed, as there were no significant changes in shear strength after 5 days of curing, therefore followed no gradual improvement with further curing time. The comparison between consolidated drained triaxial (CDT) and unconfined compression strength (UCS) test results suggested that the triaxial test provided more realistic stress conditions and was better suited for evaluating the shear strength of PSAS-treated sand in field-like conditions.

The investigation in this thesis expands upon evaluating the liquefaction resistance of the treated sand through cyclic triaxial tests conducted on both Toyoura sand and Paper Sludge Ash (PSAS)-treated sand at different cyclic stress ratios. The liquefaction susceptibility was estimated at a double amplitude of $DA$=5% for untreated Toyoura sand and $DA$=0.1% for PSAS-treated sand. The results provide compelling evidence, confirming that the incorporation of PSAS significantly enhances the liquefaction resistance of the treated sand. Specifically, based on the liquefaction results obtained, which include a $DA$ of 0.1% for PSAS-treated sand and $DA$=0.1%-5% for untreated Toyoura sand, it becomes evident that PSAS-treated sand demonstrates markedly higher resistance to liquefaction compared to its untreated counterpart. Remarkably, the research reveals an intriguing trend - as the duration of curing increases from 4 to 15 days, the resistance of PSAS-treated sand against liquefaction progressively strengthens. This discovery underscores the profound impact of curing duration on the liquefaction resistance of PSAS-treated sand. Consequently, the utilization of PSAS treatment in sand soil emerges as a promising approach to enhance its liquefaction resistance, as evidenced by the discernible increase in cyclic stress ratio. This development holds the potential to significantly bolster soil stability

in regions susceptible to liquefaction, thereby offering a practical solution to mitigate associated risks.

The findings underscore the effectiveness of PSAS as a stabilizing agent, not only in improving the unconfined compressive strength, ($q_u$) and cohesion (c), shear strength ($\phi$) of the sand but also in mitigating liquefaction hazards. This comprehensive study sheds light on the versatile benefits of PSAS in geotechnical engineering applications and provides valuable insights for the construction industry to pursue more sustainable and resilient practices involving treated backfill materials around underground pipes.

# Acknowledgments

I sincerely acknowledge and express my deepest gratitude to my supervisor, Professor Kimitoshi Hayano, for his exceptional guidance, unwavering encouragement, valuable suggestions, and patient mentorship throughout this research endeavour. His enthusiasm and constant support have been instrumental in the completion of this dissertation.

I am also grateful to Dr. Yoshitoshi Mochizuki from the Sustainable Eco Corp. and Dr. Hiromoto Yamauchi from DOMI Environmental Solutions for their valuable comments, insightful discussions, and contributions to the final goals of this study. My heartfelt thanks also go to my co-supervisors, Professor Mamoru Kikumoto and Professor Cui Ying, for their invaluable support and helpful advice during my study.

I extend my appreciation to Professor Hiroshi Tamura from Theory of Steel Structure Design laboratory and Professor Chikako Fujiyama from Concrete Laboratory for their constructive criticism, insightful suggestions, and kind reviews of this dissertation. I am also grateful to Prof. Shungo Kawagata for his enthusiastic support in SEM analysis and Prof. N. Yoshihara for assistance with XRD diffraction tests.

My gratitude extends to the staff and colleagues at the Graduate School of Urban Innovation for their friendship, assistance, and encouragement, which have greatly enriched my study and life in Japan. Special thanks to Ms. Hiromi Goto for her valuable support and contributions to my research works. I am deeply appreciative of the support and guidance provided by Kouki Inasaka, Takanari Ogasawara, Yuki Watanabe, and Liu Yinglong during the experiments.

I am thankful to the Japanese Ministry of Education, Culture, Sports, Science, and Technology (MEXT) for granting me a scholarship that made it possible for me to pursue this study. I also express my gratitude to JICA for granting the ABE initiative program, which allowed me to study in Japan and gain insights into Japan's technology and business development for Africa, including participation in internships at Japanese companies and field trips to construction sites in Japan.

My heartfelt appreciation goes to my parents, my brothers, and my sister Sakinatou Djantchiemo for their kind help and unwavering support. Lastly, I dedicate this research work to my beloved wife and son. Their constant encouragement and moral support have been a driving force behind the completion of this work, and I am deeply grateful for their love and inspiration.

# List of publications

1. Djandjieme M.O., Hayano, K., Mochizuki.Y, Yamauchi, H. (2021): **Fundamental Study on the Mechanical Characteristics of Sand Treated by a PSAS based Improving Material**, *Advances in Sustainable Construction and Resource Management – Proceeding of 1st International Symposium on Construction Resources for Environmentally Sustainable Technologies*, Fukuoka, Japan. (107-116) – *Best presentation award*.

2. Djandjieme M.O., Hayano, K., Mochizuki, K., Yamauchi, H. (2021): **Laboratory observation of volume expansion behavior of PSAS-treated sand premixed at different water content,** *Ground environment and Materials Engineering - The 23rd International Summer Symposium in 2021 (Journal of JSCE), Japan.*

3. Djandjieme, M. O., Hayano, K., Yamauchi, H., & Maqsood, Z. (2022). **Swelling and strength characteristics of sand treated with paper sludge ash-based stabilizer**. Construction and Building Materials, 341, 127849.

4. Djandjieme M.O., Hayano, K., Mochizuki, K., Yamauchi, H. (2021): **Strength characteristics of PSAS-treated sand for application as backfill sand around underground pipes and manholes**, *Ground environment and Materials Engineering - The 24th International Summer Symposium in 2022 (Journal of JSCE), Japan- Best presentation award.*

5. Djandjieme M.O., Hayano, K., Yamauchi, H. (2023): **Effects of dry-wet cycles on the mechanical properties of sand treated with paper sludge ash-based stabiliser**, *environmental land remediation– 9th International Congress on Environmental Geotechnics (9ICEG)*, Chania, Greece. (107-116).

6. Djandjieme M.O., Hayano, K., Yamauchi, H. (2023): **Durability and dynamic assessment of sand treated with paper sludge ash-based stabilizer.** Soils and Foundations (under preparation).

# Table contents

Abstract ..... 1-3
Acknowledgments ..... 1-6
List of publications ..... 1-7
Table contents ..... 1-8
List of figures ..... 1-11
List of tables ..... 1-14
1. Introduction ..... 1-1
1.1 Problem statement ..... 1-1
1.2 Objectives ..... 1-2
1.3 Thesis Organisation ..... 1-3
2. Background (literature review) ..... 2-6
2.1 Overview of Backfilling material ..... 2-6
2.1.1 Types of Backfill materials classified per ASTM D-2321 ..... 2-6
2.1.2 Strength of Backfill material ..... 2-8
2.1.3 Water in backfill material ..... 2-9
2.1.4 Movement of backfill material ..... 2-9
2.2 Overview of backfill stabilised sand ..... 2-10
2.2.1 Types of additives ..... 2-10
2.2.2 Chemical reaction ..... 2-11
2.2.3 Cement stabilized sand ..... 2-12
2.2.4 Potential application of PSAS ..... 2-12
2.2.5 Mechanisms of stabilization ..... 2-13
2.3 Compaction of backfill materials ..... 2-14
2.4 Factors affecting the soil-cement and Paper sludge ash strength development ..... 2-16
2.4.1 water content ..... 2-16
2.4.2 Soil types ..... 2-17
2.4.3 Density requirement ..... 2-17
2.4.4 Strength and deformation characteristic ..... 2-18
2.4.5 Required fly ash content ..... 2-19
2.4.6 Relationship between unconfined compressive strength $q_u$ and the modulus elasticity $E_{50}$ ..... 2-19
2.5 Undrained Monotonic and cyclic loading behaviour of sand ..... 2-20
2.6 Re-excavation ability of backfill material and its importance in underground pipes and manhole. ..... 2-21
2.7 Effects of swelling on backfill material ..... 2-22

2.8 Previous research on the re-excavation ability of backfill material and the effects of stabilisers on these properties. ....2-23
2.9 Dry-wet cycle curing of backfill sand. ....2-24
2.10 Liquefaction study of backfill sand. ....2-25
3. Geotechnical properties of materials used. ....3-29
3.1 Toyoura sand (TS) ....3-29
3.2 Paper sludge ash (PSAS) ....3-29
3.3 Ordinary Portland cement (OPC) ....3-31
3.4 The pH-values of the PSAS and OPC ....3-31
3.5 Investigation of alkalinity of PSAS and OPC-treated sand. ....3-31
3.6 Maximum and minimum density characteristics of treated sands ....3-32
4. Swelling potential of paper sludge ash (PSAS) treated sand. ....4-35
4.1 Effect of swelling of backfill sand around underground pipes and manhole. ....4-35
4.2 Specimen preparation and swelling potential test. ....4-35
4.3 Swelling potential test results. ....4-37
4.4 Isolines of $(\varepsilon_s)_{max}$ determined based on combination of $w$ and $t_p$. ....4-42
5. Deformation and strength development of paper sludge ash treated sand. ....5-44
5.1 Strength characteristics of backfill sand around underground pipes and manholes ....5-44
5.2 specimen preparation of PSAS-treated sand specimen ....5-44
5.3 Unconfined compression test results and strength development of PSAS and OPC-treated sand with $w$=10% and $t_p$= 3d ....5-46
5.4 XRD profiles and hydrates contribution to strength ....5-52
5.5 Deformation characteristics of Backfilled sand around underground pipes and manholes ....5-55
5.6 Shear strength development of PSAS-treated sand ....5-61
5.6.1 Specimen preparation and test program for CD test ....5-62
5.6.3 Experimental set-up for Consolidated drained triaxial test (CDT) ....5-62
5.6.4 Stress-strain and volumetric strain relationship of PSAS-treated sand ....5-63
5.6.5 Effect of curing time on the shear resistance of PSAS-treated sand ....5-69
5.6.6 Effect of confinement pressure on the strength characteristics of PSAS-treated sand ....5-74
6. Effects of dry-wet cycles on the mechanical properties of sand treated with paper sludge ash-based stabilizer ....6-76
6.1 Materials and experiment design of Paper sludge ash (PSAS)-treated sand ....6-76
6.1.1 Specimen preparation for dry-wet curing cycle ....6-76
6.1.2 Experimental design of dry and wet curing cycle ....6-77
6.2 Unconfined compressive strength of treated specimens cured under dry-wet cycle and soaked conditions. ....6-78
6.3 comparison of strength development obtained from cone index test (CIT) and unconfined compressive strength (UCS) ....6-80
6.4 XRD profile of PSAS-treated sand subjected to dry-wet curing. ....6-83

7. Liquefaction evaluation of paper sludge ash treated sand. ..... 7-86
7.1 Preparation of sample ..... 7-86
7.2 Test Procedure ..... 7-86
7.3 Cyclic liquefaction behaviour of untreated sand and PSAS-treated sand ..... 7-88
8. Conclusions and recommendations ..... 8-98
8.1 Conclusions ..... 8-98
8.2 Recommendations ..... 8-100

# List of figures

**Figure 1-1** Failure of underground pipes and manholes ..... 1-2
**Figure 2-1.** Important parameters in the selection of backfilled material ..... 2-8
**Figure 2-2.** Installation of Geotextile Separation Fabrics ..... 2-10
Figure 2-3 Effects of loading rate on the normalized stress–strain relationships of LRMP1(B3)-3Months. ((Z. Maqsood et al., 2020) ..... 2-16
Figure 2-4 Schematic diagram of micromechanics of the rubber-sand mixtures: an effect of rubber fraction on coordination number (Zang et al. 2017) ..... 2-16
**Figure 2-5** Monotonic loading response of saturated Toyoura sand in isotopically consolidated undrained triaxial compression tests: (a) $D_r$=16%, (b) $D_r$=38%, (c) $D_r$=64% (Ishihara et al., 1975) ..... 2-21
**Figure 2-6** Relationships between strength of improved soil and excavation capacity (Hosoya Y et al., n.d.) ..... 2-22
**Figure 2-7** Typical undrained shear response for untreated soil and Fly ash treated SB specimen ((Keramatikerman et al., 2017)) ..... 2-27
**Figure 2-8** CSRs at 10, 15, and 20 cycles (Promputthangkoon & Hyde, 2007) ..... 2-28
**Figure 2-9** Stress-strain relationships ($D_r$=65%) : a) TCr=0% (sands-only), b) TCr= 30% 2-28
**Figure 2-10** Number of loading cycles required for liquefaction of tire chips and sand mixture (T. Uchimura et al., (2007) liquefaction defined at 95% of the initial effective confining pressure. ..... 2-28
**Figure 3-1** Particle size distributions of Toyoura sand and PSAS ..... 3-30
**Figure 3-2** Alkalinity test conditions ..... 3-32
**Figure 3-3**. Change in pH of water in which treated sands with cylindrical moulds were immersed. ..... 3-32
**Figure 3-4.** Maximum and minimum dry densities of PSAS- and OPC-treated sands ..... 3-33
**Figure 3-5.** Maximum and minimum void ratios of PSAS- and OPC-treated sands ..... 3-33
**Figure 4-1.** Process flow from specimen preparation to swelling potential test. ..... 4-37
**Figure 4-2** . Expansion strain of PSAS-treated sand with $A_{PS}$ = 2.5% associated with secondary (soaked) curing period ($D_r$ = 50%). Expansion side is indicated by positive sign. 4-39
**Figure 4-3.** Expansion strain of PSAS-treated sand with $A_{PS}$ = 2.5% associated with secondary (soaked) curing period ($D_r$ = 90%). Expansion side is indicated by positive sign. 4-40
**Figure 4-4.** Formation of needle-like crystals (ettringite) in PSAS ..... 4-41
**Figure 4-5.** Expansion strain of PSAS-treated sand with $A_{PS}$ = 5.0% associated with secondary (soaked) curing period. Expansion side is indicated by positive sign. ..... 4-41
**Figure 4-6.** Relationships between maximum expansion strain of PSAS-treated sand specimens and primary (sealed) curing period. Expansion side is indicated by positive sign. 4-42
**Figure 4-7.** Isolines of $(\varepsilon_s)_{max}$ determined based on combination of w and tp. Expansion side is indicated by positive sign. ..... 4-43
**Figure 5-1.** Relationships between unconfined compressive strength $q_u$ and total curing period $t = t_s + t_p$ ($D_r$ = 50%) ..... 5-48
**Figure 5-2.** Relationships between unconfined compressive strength $q_u$ and total curing period $t = t_s + t_p$ ($D_r$ = 90%) ..... 5-49

**Figure 5-3.** Comparison of unconfined compressive strength of PSAS- and OPC- treated sand with $w = 10\%$ and $t_p = 3$ d. ..... 5-50
**Figure 5-4.** Example of fitting relationship between $q_u$ and $t$ using Eq. (5-1). ..... 5-50
**Figure 5-5.** Comparison of parameters α and β between PSAS- and OPC-treated sands... 5-51
**Figure 5-6** Change in pH of water in which treated sands with cylindrical moulds were immersed. ..... 5-54
**Figure 5-7.** Examples of externally and locally measured axial strains, and evaluation of deformation modulus E0.02% ..... 5-57
**Figure 5-8.** Relationships between deformation modulus E0.02% and unconfined compressive strength $q_u$. ..... 5-57
**Figure 5-9.** Relationships between strength ratio (SR) and total curing period $t = t_s + t_p$ ($D_r$ = 50%). ..... 5-59
**Figure 5-10.** Relationships between strength ratio (SR) and total curing period $t = t_s + t_p$ ($D_r$ = 90%). ..... 5-60
**Figure 5-11** Triaxial testing apparatus. ..... 5-63
**Figure 5-12** Deviator stress-strain and volumetric-strain relationships ($D_r$=50%): (a)-Toyoura sand, (b)-PSAS-treated sand t= 4 days, (c)-PSAS-treated sand t= 8 days, (d)-PSAS-treated sand t= 15 days ..... 5-66
**Figure 5-13** Deviator stress-strain and volumetric-strain relationships ($D_r$=90%): (a)-Toyoura sand, (b)-PSAS-treated sand t= 4 days, (c)-PSAS-treated sand t= 8 days, (d)-PSAS-treated sand t= 15 days. ..... 5-67
**Figure 5-14** Stress paths ($D_r$=50%): (a)- Toyoura sand, (b)-PSAS-treated sand t= 4 days, (c)-PSAS-treated sand t= 8 days, (d)-PSAS-treated sand t= 15 days ..... 5-68
**Figure 5-15** Stress paths ($D_r$=90%): (a)- Toyoura sand, (b)-PSAS-treated sand $t$= 4 days, (c)-PSAS-treated sand $t$= 8 days, (d)-PSAS-treated sand $t$= 15 days ..... 5-69
**Figure 5-16** Mohr Coulomb stress circles ($D_r$=50%): (a)- Toyoura sand, (b)-PSAS-treated sand $t$= 4 days, (c)-PSAS-treated sand $t$= 8 days, (d)-PSAS-treated sand $t$= 15 days ..... 5-72
**Figure 5-17** Mohr Coulomb stress circles ($D_r$=90%): (a)- Toyoura sand, (b)-PSAS-treated sand $t$= 4 days, (c)-PSAS-treated sand $t$= 8 days, (d)-PSAS-treated sand $t$= 15 days ..... 5-73
**Figure 5-18** Shear strength and Cohesion parameters of PSAS-treated sand ..... 5-74
**Figure 5-19** Summary results of $q_u$ of PSAS-treated sand and $q_{cd}$ of PSAS-treated sand .. 5-75
**Figure 5-20** Summary results of Mohr-Coulomb failure envelope ..... 5-75
**Figure 6-1**. Specimen preparation flow for unconfined compression test of treated specimens. ..... 6-77
**Figure 6-2**. Schematic experimental process of the cycling drying-wetting treated specimens. ..... 6-77
**Figure 6-3**. Change in saturation degree of PSAS and OPC-treated sand during dry-wet curing. ..... 6-78
**Figure 6-4.** Relationships between unconfined compressive strength $q_u$ and curing period under dry-wet cycle and soaked conditions for PSAS-treated sand. ..... 6-79
**Figure 6-5.** Relationships between unconfined compressive strength $q_u$ and curing period under dry-wet cycle and soaked conditions for OPC-treated sand. ..... 6-80
**Figure 6-6.** $q_c$ of PSAS-treated sand under dry-wet cycle, T=71℃ ..... 6-82
**Figure 6-7.** $q_c$ of PSAS-treated sand under dry-wet cycle, T=40℃ ..... 6-82
**Figure 6-8** $q_c$ of PSAS-treated sand with the number of dry-wet cycles qc of PSAS-treated sand with the number of dry-wet cycles. ..... 6-83

**Figure 6-9.** XRD Profiles of PSAS-treated sand at each dry-wet cycle conditions..... 6-85
**Figure 7-1** Schematic diagram of triaxial testing machine in the laboratory..... 7-87
**Figure 7-2** Undrained cyclic response of (a)stress-strain relationship of untreated sand (Toyoura sand), (b)stress-strain relationship of PSAS-treated sand ($t_s$=4 days, $D_r$=50%), (c) stress-strain relationship of PSAS-treated sand ($t_s$=8 days, $D_r$=50%), (d) stress-strain relationship of PSAS-treated sand ($t_s$=15 days, $D_r$=50%), for CSR=0.22..... 7-91
**Figure 7-3** Undrained cyclic response of (a)stress-strain relationship of untreated sand (Toyoura sand), (b)stress-strain relationship of PSAS-treated sand ($t_s$=4 days, $D_r$=50%), (c) stress-strain relationship of PSAS-treated sand ($t_s$=8 days, $D_r$=50%), (d) stress-strain relationship of PSAS-treated sand ($t_s$=15 days, $D_r$=50%), for CSR=0.35..... 7-92
**Figure 7-4** Undrained cyclic response of (a)stress-strain relationship of untreated sand (Toyoura sand), ), (b)stress-strain relationship of PSAS-treated sand ($t_s$=4 days, $D_r$=50%), (c) stress-strain relationship of PSAS-treated sand ($t_s$=8 days, $D_r$=50%), (d) stress-strain relationship of PSAS-treated sand ($t_s$=15 days, $D_r$=50%), CSR=0.45..... 7-93
**Figure 7-5** Undrained cyclic response of (a)stress path of untreated sand (Toyoura sand), (b)stress path of PSAS-treated sand ($t_s$=4 days, $D_r$=50%). (c)stress path of PSAS-treated sand ($t_s$=8 days, $D_r$=50%), (d)stress path of PSAS-treated sand ($t_s$=15 days, $D_r$=50%), for CSR=0.22..... 7-94
**Figure 7-6** Undrained cyclic response of (a)stress path of untreated sand (Toyoura sand), (b)stress path of PSAS-treated sand ($t_s$=4 days, $D_r$=50%). (c)stress path of PSAS-treated sand ($t_s$=8 days, $D_r$=50%), (d)stress path of PSAS-treated sand ($t_s$=15 days, $D_r$=50%), for CSR=0.35..... 7-95
**Figure 7-7** Undrained cyclic response of (a)stress path of untreated sand (Toyoura sand), (b)stress path of PSAS-treated sand ($t_s$=4 days, $D_r$=50%). (c)stress path of PSAS-treated sand ($t_s$=8 days, $D_r$=50%), (d)stress path of PSAS-treated sand ($t_s$=15 days, $D_r$=50%), for CSR=0.45..... 7-96
**Figure 7-8** Liquefaction resistance curve of untreated sand and PSAS-treated sand. ..... 7-97

# List of tables

**Table 2-1.** Maximum particle size and pipe size ..... 2-7
**Table 2-2.** Reaction and core agent for different binder types ..... 2-11
**Table 2-3.** The relationship between elastic modulus ($E_{50}$) and UCS ($q_u$) in previous studies 2-20
**Table 3-1.** Component compositions of the PSAS-based improving material. ..... 3-30
**Table 4-1.** Conditions of PSAS-treated specimens for swelling potential tests ..... 4-36
**Table 5-1.** Conditions of treated specimens for unconfined compression tests ..... 5-46
**Table 5-2.** Conditions of PSAS-treated specimen for Drained triaxial test ..... 5-62
**Table 7-1** Experimental Program and mixtures characteristics. ..... 7-88

# CHAPTER 1

## 1. Introduction

### 1.1 Problem statement

The construction of public water supplies, waste acquisition systems, pipelines, and manholes generally require sand backfilling. However, backfilled sand typically exhibit weakness during significant natural events, such as earthquakes. In this context, weakness refers to the liquefaction phenomenon. Liquefaction is a phenomenon where soil loses its strength and stiffness and behaves like a liquid under cyclic loading. This phenomenon can result in damages to underground structures such as pipes and manholes. When backfilled sand around underground pipes and manholes liquefies, it can cause a significant problem as their function is stopped, and they cannot be used during the period of recovery or damage restoration (see figure 1-1). This problem was observed during the Great East Japan earthquake in 2011 (Matsuhashi et al., 2014). According to Matsuhashi et al. (2014), immediately after the earthquake, 48 plants and 79 stations in sewage systems were shut down, and 63 plants and 32 stations were partially damaged. One year later, 2 plants and 12 stations remained shut down, while 12 plants and 25 stations remained partially damaged. Thus, the damage caused by liquefaction to underground pipes and manholes in sewage systems can significantly affect their function, and they cannot be used during the recovery or damage restoration period. To prevent such damage, backfilled sand is often enhanced with other materials to prevent liquefaction.

To date, various additives have been used to improve or stabilize backfilling sand, with conventional cement- and lime-based stabilizers being the most frequently used additives(Mohajerani et al., 2019) (Yuriz et al., 2020). Stabilizers can significantly increase the liquefaction strength of soils(Toyota & Takada, 2023) (Keramatikerman et al., 2017). Most soils treated with cement- or lime-based stabilizers demonstrate significant strength increase, even after 28 days of curing. However, excessive solidification over time may complicate re-excavation. Controlled Low-Strength Material (CLSM) can also be used as a substitute for compacted sand in backfill applications, but it has a limitation in installation, which requires achieving the required density homogeneously (Nataraja & Rao, 2016). In addition, the high alkalinity of cement or lime-soil mixtures is a concern (Imai et al., 2020; Inasaka et al., 2021). Furthermore, significant amounts of CO2 emissions during the production of cement and lime are undesirable.

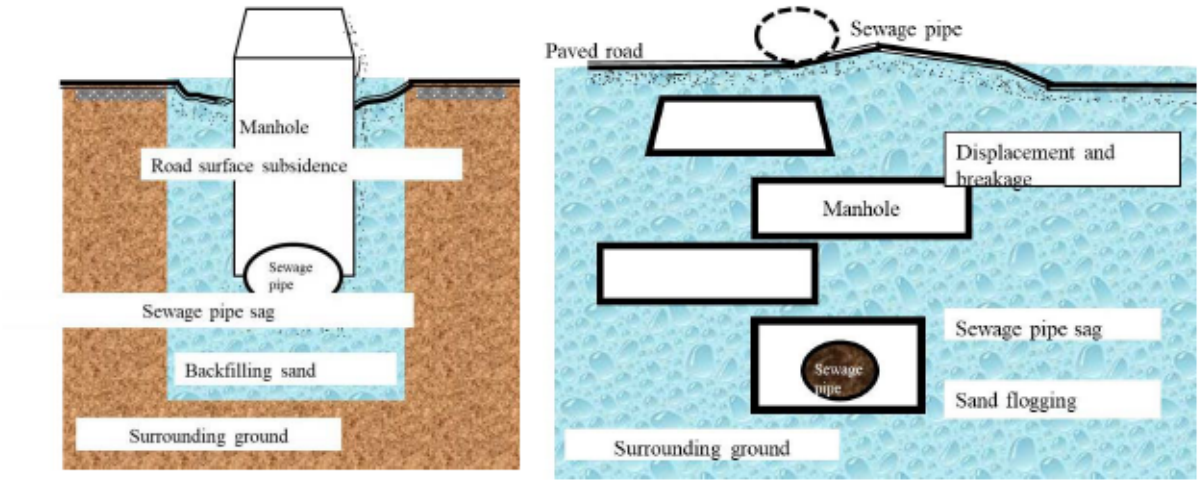


(a) Manhole uplift around sewage pipes

(b) Manhole displacement or breakage in the surrounding area

**Figure 1-1** Failure of underground pipes and manholes

## 1.2 Objectives

The use of stabilisers in backfill materials has been proposed as a solution to mitigate the effects of liquefaction, but their impact on the re-excavation ability of the backfill material is not well understood. Re-excavation ability refers to the ability of backfill material to be easily excavated during maintenance or repair work. This is an important consideration because underground structures such as pipes and manholes require regular maintenance and repairs. If the backfill material is too compacted or difficult to excavate, it can lead to additional damages or safety hazards during excavation work.

This research aims to investigate the re-excavation ability of backfill sand around underground pipes and manholes and their resistance to liquefaction triggering.

The study will focus on analysing the effectiveness of stabilizers in mitigating the effects of liquefaction while also considering their impact on the re-excavation ability of the backfill material. By understanding the relationship between stabilizers-excavation ability and liquefaction triggering, this research can contribute to the development of safer and more effective construction practices for critical infrastructure such as underground structures.

In Details, this research focuses firstly on the investigation of using a PSAS to improve the properties of sand proposed to be used as a backfill material around underground pipes. In this regard, the fundamental properties of sand treated PSASs, such as the swelling potential and strength, are experimentally

investigated by performing a series of laboratory tests. For comparison, similar tests are conducted on sand treated with ordinary Portland cement (OPC). Based on the test results, alterations are performed to control the swelling potential of the PSAS-treated sand and to ensure that the strength does not inhibit re-excavation, secondly on the investigation of long-term durability of Paper sludge ash treated sand by conducting long-term unconfined compression test. However, durability of PSAS-treated sands has not been investigated in detail so far, thirdly on the investigation of the durability of PSAS-treated sands which were subjected to dry-wet curing cycles. Two curing temperature (40°C and 71°C) were adopted for drying cylindrical specimens which were used for unconfined compression tests. In addition to the difference in the drying temperature, the effects of numbers of dry-wet curing cycles on the $q_u$ were examined. Moreover, dry-wet curing cycles were given to cone index specimens to compare the test results with the unconfined compression test results. The effect of the confinement of the PSAS-treated sands on the durability for dry-wet curing cycles is discussed.

In addition, the mechanism causing strength development is discussed based on X-ray diffraction (XRD) analysis results.

Finally, this research investigates the using of PSAS to improve the liquefaction resistance of sand proposed to be used as backfill material around underground pipes and manhole by conduction monotonic and cyclic triaxial laboratory test.

The following section describes how the above objectives will be addressed in this thesis.

## 1.3 Thesis Organisation

Chapter 2 provides a comprehensive overview of backfill materials, their characteristics, and the fundamental properties of soil stabilizers and paper sludge ash within the wide array of materials used in various industries. The chapter delves into the main concept of cement hydration and microstructure development, drawing parallels to a cement, fly ash, gypsum, tyre chips similar material like PSAS employed in this study. Additionally, it establishes the essential concepts of mechanical properties for both backfill materials and the treated material, supported by relevant literature. This comprehensive exploration lays the foundation for understanding the key elements essential to the study of backfill materials and their treatment with paper sludge ash.

Chapter 3 of the thesis is dedicated to exploring fundamental properties of the materials used in the research. Major infrastructure projects often rely on natural materials, some of which are subsequently stabilized using hydraulic binders.

This section provides a comprehensive analysis of the physical properties of both the natural and treated materials. The evaluation encompasses Toyoura sand and Watoru PSAS, aiming to understand their basic parameters. Additionally, the chemical properties of PSAS and Ordinary Portland Cement (OPC) are studied to gain insights into their composition. The research focuses on the soil texture, which is determined by the proportion of sand, silt, and clay-sized particles, along with organic matter. The porous structure of sand allows for efficient drainage and aeration, making it an ideal backfilling material that avoids waterlogging in winter and drought conditions in summer (Batey & McKenzie, 2006). As a result, this investigation centres on backfilling sand using Toyoura sand. The subsequent sections present the particle sand distribution of Toyoura sand and PSAS, as well as the minimum and maximum density of PSAS and cement-treated sand (Ishihara et al., 1975).

Chapter 4 focuses on a preliminary step for the use of treated sand as a backfill material around underground pipes and manholes. The chapter investigates the premix method as a way to reduce the construction period while also ensuring that the treated sand has the necessary cohesive strength. Additionally, the chapter examines the swelling potential of Paper Sludge Ash (PSAS)-treated sand under different water immersion conditions, in order to determine the most suitable conditions for using the treated sand. The investigation of these factors is essential to ensure that the PSAS-treated sand can function effectively as a backfill material and provide sufficient stability for underground structures.

Chapter 5 of this thesis is dedicated to exploring the deformation and strength development of paper sludge ash (PSAS) treated sand. A series of unconfined compression tests were conducted to investigate the short and long-term strength characteristics of both ordinary Portland cement (OPC) and PSAS-treated sands. The focus lies on understanding the behaviour of the treated sand under the effect of traffic load as a subgrade when subbase materials and asphalt mixtures are placed on top of the backfilled PSAS-treated sand. This understanding is crucial for ensuring the stability of underground structures, as traffic load can induce deformation and potentially compromise the integrity of the structure. Additionally, the chapter delves into the investigation of the effect of PSAS on the shear strength characteristics of the treated sand. The aim is to evaluate the enhancements in shear strength parameters, such as cohesion (c) and friction angle (φ), as well as volumetric strain changes resulting from the inclusion of PSAS into the sand matrix. This assessment of changes in shear strength properties is vital for assessing the stability and performance of buried pipes and manholes that utilize PSAS-treated sand as a backfill material. Overall, Chapter 5 provides valuable insights into the mechanical properties of the treated sand,

paving the way for improved design and performance of infrastructure using PSAS as a stabilizing agent.

Chapter 6 focuses on investigating the durability of Paper Sludge Ash (PSAS)-treated sands when subjected to dry-wet curing cycles, which can have a significant impact on the long-term strength and stability of the treated sand. The chapter examines the effects of two different drying temperatures (40°C and 71°C) on cylindrical specimens that are used in unconfined compression tests. Additionally, the chapter investigates the effects of dry-wet curing cycles on the $q_u$ parameter and compares the results with those obtained from the unconfined compression tests. Cone index specimens are also subjected to dry-wet curing cycles to compare their test results with those of the unconfined compression tests. The chapter also explores the impact of confinement on the durability of the PSAS-treated sands during dry-wet curing cycles. Understanding the durability of the treated sands under different conditions is crucial for assessing their long-term performance and potential for use as backfill material around underground pipes and manholes.

Chapter 7 is dedicated to the liquefaction evaluation of Paper Sludge Ash (PSAS)-treated sand using a series of cyclic triaxial tests. The tests are conducted on the treated sand based on the recommended PSAS mixture ratio for re-excavation purposes. The chapter provides important insights into the liquefaction behaviour of the treated sand and evaluates its resistance to cyclic loading under different cyclic stress ratio conditions. The results of the tests are presented and analysed to determine the effects of PSAS treatment on the liquefaction potential and strength characteristics of the sand. Understanding the liquefaction behaviour of the treated sand is crucial for assessing its potential for use as backfill material around underground pipes and manholes, particularly in areas with a high risk of seismic activity.

# CHAPTER 2

## 2. Background (literature review)

### 2.1 Overview of Backfilling material

Backfilling is the process of putting the soil back into a trench or foundation once excavation, and the related work has been completed. The backfill process requires skills and heavy equipment as well as knowledge of the specifications, contract requirements, and soil conditions. Every area of soil has unique characteristics, requiring different construction techniques to ensure optimum performance.

Only soil without stones is capable of being compacted, which must satisfy the same requirements as the covering material, may be used in the region of the pipe zone. If no soil capable of being properly compacted is available, then provision must be made for improving the soil by the addition of non-binding material or by the provision of other suitable soils or materials. In special cases, the pipe can be partly or completely encased with concrete or similar independent of the covering materials used for embedment shall be capable of providing permanent stability and load-bearing capacity for the pipeline buried in the ground. Such materials shall not be detrimental to the pipe or pipe materials or the groundwater. Frozen material shall not be used. Materials used for embedment shall conform to the design requirements. These materials may be either native soil if proved to be suitable or imported materials for bedding shall contain no particles with sizes above 22 mm for DN $\leq$ 200, 40 mm for DN > 200 up to DN $\leq$ 600.

The selection of backfill material is an important aspect of underground construction and requires careful consideration of several factors, including stability, strength, durability, and cost-effectiveness. In this session, we provide an overview of the types of backfill materials commonly used in underground construction and their properties.

#### 2.1.1 Types of Backfill materials classified per ASTM D-2321.

There are several types of backfilling materials commonly used in underground construction, including natural soils, crushed rock, recycled materials, and stabilized soils. Each type has its advantages and disadvantages, and the choice of material depends on the specific project requirements. Backfill material is the material immediately surrounding the pipe, which may be imported, or the material excavated from the trench to make room for the pipe.

Pipe embedment materials have been grouped by ASTM D-2321 into five embedment classes according to their suitability for underground installation of thermoplastic pipes for sewers and other gravity-flow applications. Soil descriptions, classifications, and soil group symbols are referred to for embedment.

Class I and Class II soils provide maximum embedment support and can be blended to resist migration of finer soils into the backfill zone. Class I material is generally manufactured aggregate, while Class II materials consist of clean sands and gravels, and are more likely to be naturally occurring soils such as river deposits. The maximum aggregate size of Class I and Class II materials, when used next to the pipe, should not be larger than those given in Table 2-1. Class III and Class IVA materials provide less supporting stiffness than Class I or II materials for a given density or compaction level, in part because of the increased clay content. Typically, Class IVA material is limited to applications with pressure pipe at the shallow cover. Class IVB and Class V materials offer hardly any support for a buried pipe and are often difficult to properly place and compact.

The properties of the in-situ (or native) soil into which the pipe is placed need not be as demanding as those for the backfill materials. The native soil may experience additional compression and deformation due to the horizontal pressure exerted by the pipe and transferred through the embedment material. This is usually a minor effect, but in some cases, it can result in additional pipe deflection. Therefore, consideration must be given to the in-situ soil to ensure that it has adequate strength.

**Table 2-1.** Maximum particle size and pipe size

| Nominal pipe Size (mm) | Maximum Particle Size (mm) |
|---|---|
| 50.8 mm to 101.6 mm | 12.7 |
| 152.4 mm to 203.2 mm | 19.05 |
| 254 mm to 381 mm | 25.4 mm |
| 406.4 and larger | 38.1 mm |

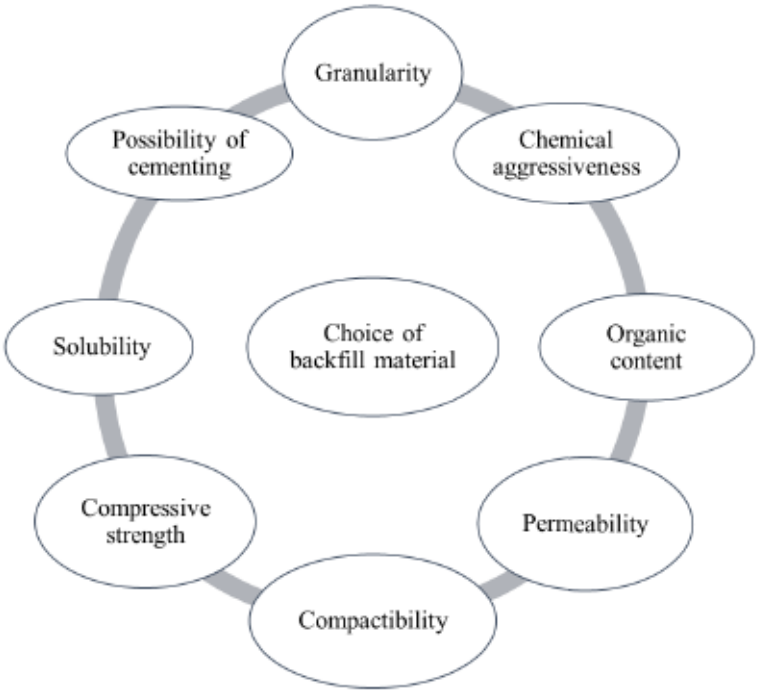


**Figure 2-1.** Important parameters in the selection of backfilled material

### 2.1.2 Strength of Backfill material.

When selecting embedment material, consideration should be given to how the grain size, shape, and distribution will affect its supporting strength (see figure 2-1). The following will help guide the designer or installer in making a choice. In general, soils with large grains such as gravel have the highest stiffness and thus provide the most supporting strengths. Rounded grains tend to roll easier than angular or sharp grains, which tend to interlock and resist shear better. Well graded mixtures of soils (GW, SW), which contain a good representation of grains from a wide range of sizes, tend to offer more resistance than uniformly graded soils (GP, SP).

Aside from the grain characteristics, the density has the most significant effect on embedment's stiffness. For instance, in dense soil, there is a considerable interlocking of grains and a high degree of grain-to-grain contact. Movement within the soil mass is restricted as the volume of the soil along the surface of sliding must expand for the grains to displace. This requires a high degree of energy. In loose soil, movement causes the grains to roll or to slide, which requires far less energy. Thus, loose soil has a lower resistance to change. Loose soil will permit more deflection of pipe for a given load than dense soil.

### 2.1.4 Water in backfill material.

Water in backfill material around underground pipes and manholes is a critical factor that can affect the stability and performance of the structures. The presence of water can increase the weight and hydrostatic pressure on the underground structures, leading to potential instability and deformation (Henshell, 2016). Moreover, water can reduce the strength and stiffness of the backfill material, making it more susceptible to liquefaction, settlement, and erosion. For example, studies by (J. Liu et al., 2020)and (J. Wang & Fu, 2021) have shown that the water content of the backfill material can significantly affect the shear strength and deformation characteristics of the soil. Therefore, it is crucial to consider the water-backfill interaction when selecting and designing the backfill material for underground pipes and manholes. Appropriate drainage systems, such as weep holes and French drains, should be incorporated to prevent the accumulation of water in the backfill material and ensure the long-term stability of the underground structures.

### 2.1.5 Movement of backfill material.

When the pipe is located below the groundwater level, the possibility of soil displacement and loss of side support should be considered. This can occur when finer particles from the trench sidewalls are carried by groundwater into the void spaces of coarser soils. To prevent backfill sand movement, it is important to use non-erodible soils. Typically, erodible soils include fine sand, silts, and dispersive clays. However, most clays exhibit good resistance to dispersion. The situation worsens when there is a significant groundwater gradient from outside to inside the trench, requiring the trench to act as a drain. To minimize migration, it is recommended to use angular and graded granular materials (Class I and II).

To enhance the stability of the backfill, the usage of paper sludge ash as a backfill stabilizer can be considered. Paper sludge ash has been studied as a potential stabilizing agent due to its properties such as water absorption and retention (Kato et al., 2005; Mochizuki, 2016; Kawai et al., 2018). It can granulate and adjust the water content of the sludge, thereby hardening the backfill sand. This can help protect underground pipes and manholes from liquefaction during events like earthquakes. Additionally, incorporating geotextile separation fabrics during the installation process can further improve the effectiveness of the backfill as shown on figure 2-2. Furthermore, to meet the particle size requirements for grading adjacent materials and minimize soil buoyancy, the particle size distribution should be considered. The following requirements are recommended:

a) $D_{15}^{b} < 5D_{85}^{A}$

b) $D_{50}^{b} < 25D_{85}^{A}$

Here, $D_{15}$, $D_{50}$, and $D_{85}$ represent the particle sizes at 15%, 50%, and 85%, respectively, from a particle size distribution plot. The subscript "b" refers to the backfill soil, and "A" refers to the adjacent in-situ soil. Rounded particles tend to flow more easily when there is a significant amount of water, and materials with high void content provide space for particle movement. The Army Corps of Engineers has developed these particle size requirements to accurately grade adjacent materials and minimize soil buoyancy.

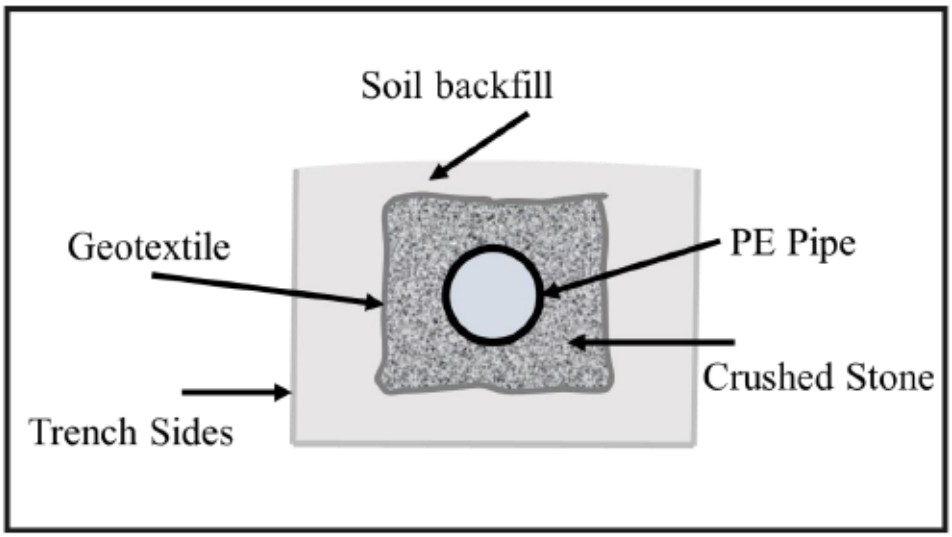


**Figure 2-2.** Installation of Geotextile Separation Fabrics

## 2.2 Overview of backfill stabilised sand.

Generally, soil stabilization is a method of improving soil properties by blending and mixing other materials. Improvements include increasing the dry unit weight, bearing capabilities, volume changes, the performance of in situ subsoils, grains of sand, and other waste materials to strengthen road surfaces and other geotechnical applications in fact to meet an engineering purpose.

### 2.2.1 Types of additives

Various additives may be used to improve or stabilize the sand. Some of them are known such as the common additives named cement, lime or by-products of the industrial process, moreover such as various slags, fly ashes, blast furnace slags, etc. mostly blinders are classified into two types, primary binders related to the hydraulic type of binders and secondary binders related to non-hydraulic one. The

primary binder can be self-curing in contact with water. Consequently, they can be used alone. Meanwhile, the secondary binder needs a catalyst for the reaction to start. The catalyst acts as an activator to initiate the reaction. Awareness of the chemical reactions of binders is considered important to understand the differences between each binder type, which gives the stabilized soil its strength and durability as shown in table 2-2.

**Table 2-2.** Reaction and core agent for different binder types

| **Binder** | **Reaction** | **Core Agent** |
|---|---|---|
| Cement | Hydraulic | Water |
| Lime | Hydraulic | Water + Pozzolanic soil or Pozzolanic additive |
| Granulated Blast furnace slag | Latent hydraulic | Water + $Ca(OH)_2$ |
| Class F fly ash | Pozzolanic | Water + $Ca(OH)_2$ |

### 2.2.2 Chemical reaction

When lime is mixed with clayey material in the presence of water, several chemical reactions take place. They include cation exchange, flocculation-agglomeration, pozzolanic reaction, and carbonation (Taha Jawad et al., 2014). Cation exchange and flocculation-agglomeration are the primary reactions, which take place immediately after mixing. During these reactions, the monovalent cations that are generally associated with clay minerals are replaced by the divalent calcium ions. These reactions contribute to immediate changes in plasticity index, workability, and strength gain. A pozzolanic reaction occurs between lime and the silica and alumina of the clay mineral and produces cementing material, including calcium-silicate-hydrates and calcium alumina hydrates. The basic pozzolanic reactions are as follows:

$$Ca(OH)_2 + SiO_2 \rightarrow CaO - SiO_2 - H_2O \qquad \text{Eq. 2-1}$$

$$Ca(OH)_2 + Al_2O_3 \rightarrow CaO - Al_2O_3 - H_2O \qquad \text{Eq. 2-2}$$

Pozzolanic reactions are time and temperature-dependent and may continue for a long period. The addition of lime to soil increases its pH; studies have shown that when the pH of the soil increases to 12.4, which is the pH of saturated

limewater, the solubility of silica and alumina increases significantly. Therefore, if enough calcium from the lime remains in the mixture, and the pH remains at least 12.4, the pozzolanic reaction will continue. In some instances, lime reacts with carbon dioxide to produce calcium carbonate instead of calcium-silicate-hydrates and calcium alumina hydrates. Such carbonation is an undesirable reaction from the point of soil improvement.

### 2.2.3 Cement stabilized sand

Cement stabilization of soil is a useful method to improve the mechanical behaviors and engineering performance of soils in geotechnical design and construction projects involving weak or liquefiable soils. (Wei & Ku, 2020) investigate the effects of water content and water–cement ratio on the unconfined compressive strength, with good control of the packing density and void ratio of the tested specimens and it was found that The UCS increases with increasing cement content. The efficiency of improvement by adding cement can be affected by dry density and water–cement ratio during compaction. The efficiency increases with increasing dry density and decreasing water–cement ratio.

As defined in the previous session, one special case of Class II material is Cement Stabilized Sand. Cement Stabilized Sand, once cured, is generally considered to give the same or better-supporting strength as compacted Class I material. Cement Stabilized Sand consists of sand mixed with 3 to 5 percent cement (Peterson, 2014). In order to achieve a high density, the material is placed with compaction rather than poured as with concrete. The material must be placed moist (at or near optimum moisture content) and then compacted in lifts as a Class II material (Gerasimova, 2016). (The optimum moisture content is that moisture content at which a material can achieve its highest density for a given level of compaction.) If desired, deflection can be reduced if the cement sand backfill material can cure overnight before placement of backfill to grade. If the trench is backfilled immediately, cement sand will give the same support as a Class II material, but the lag factor will be reduced.

### 2.2.4 Potential application of PSAS

Paper sludge ash (PSAS) is the by-product of paper mills, a cinder generated from the incineration of paper sludge, has been widely an alternative sustainable material in construction industry. The production of paper has stably developed for many years producing a stable amount of paper sludge ash as presented in Fig 1.6 and hence, paper sludge ash has a wide potential for the application. Currently, most PSAS has been disposed of in landfills or used as concrete materials so far

(Kumar et al., 2016; Mochizuki, 2019). Because PSAS particles have a porous microstructure with many complex irregularities and voids, PSAS can absorb and retain excess water in soft soil. Therefore, the application of PSAS to stabilize muds in construction work such as dredging in harbours, rivers, and lakes or excavating tunnels and underground pits has been increasing in practice (Kawasaki & Ishimito, 1992; Mochizuki et al., 2003) like other materials, the application of PSAS in the construction industry needs to satisfy environmental regulations in Japan. Because of the heavy metals in original PSAS may cause harmful impacts on the environment, PSAS was produced as an eco-friendly material by insolubilizing the heavy metals from PSAS. The advantaged characteristics of PSAS in soil treatment such as water absorption and retention performance are remained in PSAS.

Previous studies have focused on the application of PSAS to enhance the strength of surplus soil. However, its potential as a stabilizer for improving backfill sand around underground pipes and manholes has not been explored. PSAS demonstrates water absorption and retention properties (Kato et al., 2005; Mochizuki, 2016; Kawai et al., 2018), enabling it to granulate and adjust sludge water content. This has the potential to harden backfill sand and protect underground pipes and manholes from liquefaction during events like earthquakes. Consequently, it is crucial to investigate the strength development and sand liquefaction resistance of PSAS over time.

### 2.2.5 Mechanisms of stabilization

Little (n.d.) summarized the mechanisms of stabilization using cement, lime, or fly ash as follows:

- Cation exchange: calcium cations from available calcium hydroxide replace sodium, magnesium, and other cations, leading to enhanced soil properties.
- Flocculation and agglomeration: the clay particles' flocculation increases effective grain size, reduces plasticity, and improves matrix strength.
- Pozzolanic reaction: in the high pH environment created by available calcium hydroxide, silicates and aluminates solubilize at the clay surface and react with calcium ions to form primarily calcium silicate hydrates or calcium aluminate hydrates, or both.
- Carbonate cementation: carbon dioxide from the atmosphere reacts with calcium oxide to form calcium carbonate precipitates, which cement soil particles.

- Cementitious hydration reaction: calcium silicates and/or calcium aluminates, which are chemically combined in the production of Portland cement clinker or coal-burning (fly ash) process, hydrate rapidly within a few hours to form calcium silicate hydrates and/or calcium aluminate hydrates.

The chemical reactions during the hydration procedure include but are not limited to the reactions listed below:

- $2C_2S + 6H_2O \rightarrow C_3S_2H_3 + 3Ca(OH)_2$
- $2C_2S + 4H_2O \rightarrow C_3S_2H_3 + Ca(OH)_2$
- $C_3A + 3(CaSO_4 \cdot 2H_2O) \rightarrow 26H_2O \rightarrow C_3A.3CaSO_4.32H_2O$
- $2C_3A + C_3A.3CaSO_4.32H_2O \rightarrow 3[C_3A(CaSO_4.12H_2O)]$
- $C_3S + (Ca(OH)_2 + 12H_2O) \rightarrow C_3A\ [Ca(OH)_2.12H_2O]$
- $C_4AF + 3(CaSO_4 \cdot 2H_2O) \rightarrow 27H_2O \rightarrow C_3(AF).3CaSO_4.32H_2O + Ca(OH)_2$
- $2C_4AF + C_3(AF).3CaSO_4.32H_2O + 6H_2O \rightarrow 3C_3(AF)CaSO_4.12H_2O + 2Ca(OH)_2$
- $C_4AF + 10H_2O + 2Ca(OH)_2 \rightarrow C_3AH_6\text{-}C_3FH_6$ (solid solution)

Le Chatelier's crystalline theory and Taylor's gel theory two popular theories on stabilization mechanisms. These theories have been integrated into a combined gel/crystalline theory that describes the different stages of curing. According to Li et al. (2016), during the hydration process of cement concrete, each cement particle is covered with water and forms a gel-like film if enough moisture is available to ensure complete hydration. The coated cement particles then cover the aggregate or soil particles. At this stage, the cement has not started to set. With the development of hydration, small single crystals form from the reaction between water and cement. As hydration proceeds, the single crystals grow and form a crystalline network.

## 2.3 Segregation, compaction of backfill materials.

In the realm of backfilling around underground structures, a primary hurdle revolves around the challenges of segregation and compaction, particularly when substituting traditional aggregates. The substitution process introduces complexities in achieving uniform compaction when replacing natural aggregates with materials like recycled aggregates or industrial by-products. Segregation, the undesirable separation of finer and coarser particles, poses a significant threat by causing variations in the composition and density of the backfill. This non-uniform distribution jeopardizes the mechanical properties and stability of the backfilled material. Moreover, achieving consistent compaction energy throughout the entire backfill volume becomes intricate during the compaction process. This challenge intensifies when dealing with diverse particle sizes and

shapes, impeding the effective transfer of load-bearing capacity to the surrounding underground structures. Addressing these concerns related to segregation and compaction is pivotal to ensuring the structural integrity and long-term stability of the backfilled material, playing a crucial role in the success of underground construction projects.

The assessment of backfill material for stability, durability, and re-excavation ability stands as a critical aspect of its effective utilization. Figure 2-5 accentuates the intricate relationship between the strength of improved soil and excavation capacity. Notably, re-excavation, particularly using a pick, is capped at 500 kPa. This limitation implies that if the soil layer's strength surpasses 500 kPa, the re-excavation process with a pickaxe becomes challenging (Hosoya Y et al., n.d.). Examining durability in Figure 2-3, which delves into the impact of loading rate on normalized stress-strain relationships of gypsum mixture LRMP1 (B3)-3Months, reveals significant variations at lower loading rates. These variations signal potential challenges in the backfill material's ability to withstand long-term, continuous loading scenarios (Maqsood, Koseki, Ahsan, et al., 2020). Additionally, addressing segregation and compaction concerns, a detailed photograph in the document illustrates non-uniformly shaped and sized shredded rubber tire particles. These irregularities may lead to uneven compaction and segregation issues within the material. Adding complexity, Figure 2-6's schematic diagram delves into the micromechanics of rubber-sand mixtures, emphasizing the influence of the rubber fraction on the coordination number. The figure strongly suggests that incorporating tire chips in sand backfill may result in a reduction in the coordination number, ultimately impacting the stability of the backfill material(Zhang et al., 2018). These multifaceted factors collectively indicate potential limitations in the utilization of tire chips as backfill material, encompassing concerns related to stability, durability under continuous loading, and re-excavation feasibility.

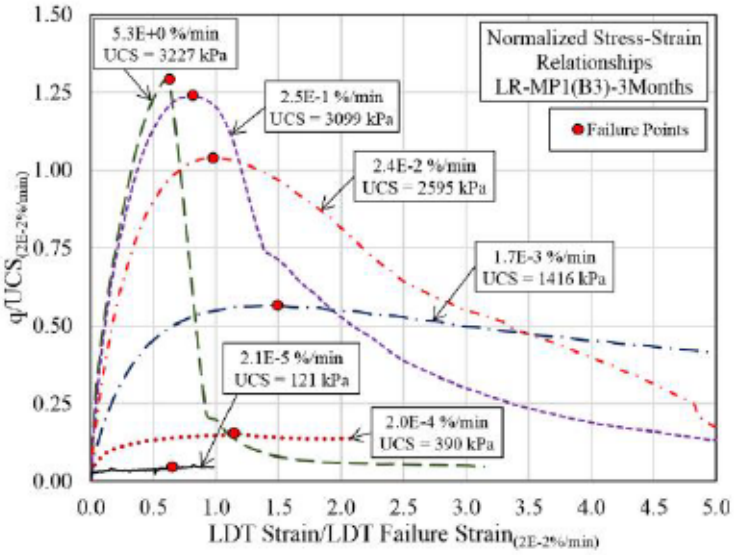


Figure 2-3 Effects of loading rate on the normalized stress–strain relationships of LRMP1(B3)-3Months. ((Z. Maqsood et al., 2020)

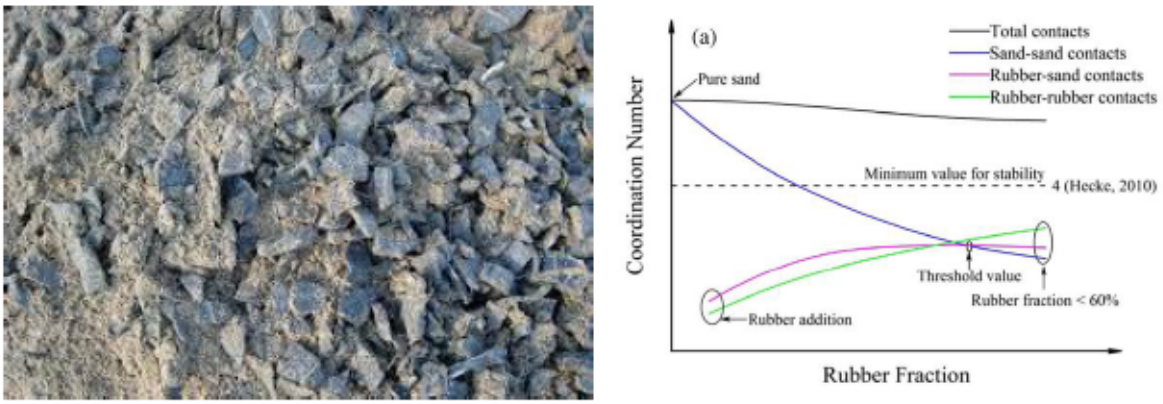


(a) Tyre chips-sand (b) coordination number and rubber fraction

Figure 2-4 Schematic diagram of micromechanics of the rubber-sand mixtures: an effect of rubber fraction on coordination number (Zang et al. 2017).

## 2.4 Factors affecting the soil-cement and Paper sludge ash strength development.

Like cement stabilization, the use of fly ash is common to improve the strength and stiffness of soils, reduce the water content, and decrease soil plasticity. Fly ash is a widely used material to modify soil properties in both the short-term and long-term, and it has been applied to various types of soils, including clay, silt, sand, and gravel (Maher et al., 2005).

### 2.4.1 water content

The water content of soil plays a crucial role in the strength development of cement stabilized soil. During the hydration reaction, cement requires approximately 20 percent of its weight of water to fully react (Sherwood, 1993).

Insufficient water content can hinder the hydration process and result in reduced soil strength. On the other hand, adding high free lime content by-product materials such as class C fly ash to wet soils can effectively reduce the water content. This reduction occurs mainly due to the reaction between the binder and water. Additionally, over time, pozzolanic reactions lead to further drying of the soil (Rossow & Mark, 2003)

### 2.4.2 Soil types

The use of cement and PSAS in soil stabilization is widespread across a range of soil types, both granular and fine-grained. Hydration is the primary reaction mechanism in cement stabilization, which relies on water to form a hydrated compound. The effectiveness of cement stabilization is also dependent on long-term pozzolanic reactions. These reactions are facilitated by the presence of ions and silica in cement and PSAS. Recent studies have shown that cement is more effective in stabilizing well-graded soils than poorly graded ones. Additionally, coarser soils are more effectively stabilized with cement than fine-grained soils. A study by Nontananandh and Yoobanpot (2012) investigated the effect of adding cement on the unconfined compressive strength of various soil types, finding that cement was particularly effective in sandy gravel soil.

### 2.4.3 Density requirement

The designer will determine the necessary degree of compaction for installation based on various factors such as soil properties, height of cover, live loading, and water table elevation. Misra et al. (2005) studied the impact of adding 10% and 20% of class C fly ash on the compaction properties of clayey silt and silty clay. The results indicated that adding class C fly ash led to a decrease in maximum dry density and an increase in optimum moisture content after two hours of mixing. Similarly, Prabakar et al. (2004) found that adding fly ash (ranging from 9% to 46%) decreased the maximum dry density and increased the optimum moisture content of low and high plasticity soils. Kolias et al. (2005) observed that the addition of 5% to 20% of high calcium fly ash to stabilized soil led to a decrease in maximum dry density and an increase in the optimum moisture content. Harichane et al. (2011) reported similar results when adding 5% to 50% of high calcium fly ash to high plasticity soil. Furthermore, Horpibulsuk et al. (2011) investigated the effects of adding 10% of cement and class F fly ash with different replacement ratios on the compaction properties of high plasticity clay. They found that adding cement and class F fly ash increased the maximum dry unit weight without changing the optimum water content after treatment.

### 2.4.4 Strength and deformation characteristic

Various laboratory methods have been used to assess the improvement in soil strength over both short- and long-term periods. The unconfined compressive strength (UCS) and California bearing ratio (CBR) have been identified as easy methods (Mallela et al., 2004). In addition, the triaxial test and direct shear test have been employed to predict soil strength improvement (Little, n.d.). Mitchell (1976) examined the impact of adding different amounts of cement (3% to 16%) on the unconfined compressive strength of fine-grained and coarse-grained soils after 28 days of curing. He found that an increase in cement content led to a linear increase in unconfined compressive strength for both soil types. Coarse-grained soil showed a more pronounced effect, with an increase in soil strength ranging from 80-150 times the cement content. For fine-grained soil, the increase in soil strength varied between 40-80 times the cement content. He also observed that the unconfined compressive strength of cement-stabilized soil increased over time.

The relationship between unconfined compressive strength of cement-stabilized soil and curing time can be expressed as:

$$q_{u_{(d)}} = q_{u_{(d_o)}} + K \times log\left[\frac{d}{d_o}\right] \qquad \text{Eq. 2-3}$$

Where:

$q_{u_{(d)}}$ : Unconfined Compressive strength at age of d days, kPa.

$q_{u_{(d_o)}}$ : Unconfined Compressive strength at the age of $d_o$ days, kPa.

K=70 C for granular soil and 10 C for fine-grained soil, C= cement content, % by mass.

Feda (1998) investigated the effect of adding different cement contents (2% to 8%) on the strength properties of sand. He found that the shear strength and stiffness of sand improved after several treatments with low cement content. Bennert et al. (2000) observed that adding 8% of Portland cement improved the strength characteristics of dredged sediments, making them suitable for structural fill. Chew et al. (2004) investigated the effect of adding various amounts of cement (5% to 50%) on the stress-strain behaviour of soft marine clay after 28 days of curing. They found that as the cement content increased, the peak strength also increased, while the failure strain corresponding to the peak stress decreased. Failure mode changed towards brittle failure with an increase in cement content. Bahar et al. (2004) found similar observations for low plasticity soil stabilized with different cement contents (4% to 20%). Ho et al. (2017) researched the effects of adding 8% cement content on the strength development of two types of soils, namely sand and sand-loam mixtures. They reported that the compressive

strength for both soil types increased during the first 28 days of curing. After that, no further increase in soil strength was observed for the sand, whereas a gradual increase in compressive strength was noted for the sand-loam mixture. This increase in compressive strength was attributed to the pozzolanic reaction between the cement and the clay minerals in the sand-loam mixtures. Zhang et al. (2017) studied the effect of adding various amounts of Portland cement (7%, 9%, and 11%) to stabilize high water content waste mud. Their results showed that both strength and stiffness increased as the cement content was increased.

### 2.4.5 Required fly ash content.

The fly ash content, expressed as a percentage of the weight of fly ash to the dry weight of soil, is influenced by various factors such as soil type, fly ash type, water content, organic content, and targeted soil properties. Generally, the common range for using self-cementing class C fly ashes is between 12% to 16% of dry soil weight, while for low cementing fly ash, a higher amount may be needed with an activator. The reactivity of the binder is affected by the chemical composition of the by-product materials, and the hydration modulus is used to quantify it. This modulus is calculated as the percentage of CaO divided by the sum of the percentages of SiO2, Al2O3, and Fe2O3. To ensure a reaction takes place, Kamon and Nontananandh (1991) recommended that the hydration modulus should exceed 1.7 for various by-product materials. The potential cementing ratio, which is defined as the CaO/SiO2 ratio, is used to evaluate the hydraulic properties of the binder. A higher CaO/SiO2 ratio indicates more hydraulic properties, as suggested by Janz and Johansson (n.d.).

### 2.4.6 Relationship between unconfined compressive strength $q_u$ and the modulus elasticity $E_{50}$

Many investigators have obtained a variable conclusion about the relationship between the unconfined compressive strength ($q_u$) and the elastic modulus ($E_{50}$) for a wide range of soil types stabilized with cement, lime, and fly ash as illustrated in table 2-3.

**Table 2-3.** The relationship between elastic modulus (E50) and UCS (qu) in previous studies

| Material | Upper and Lower range of soil stiffness times | References |
|---|---|---|
| Class F fly ash modified with 4 to 10% lime content | $E_{50} = 55q_u^{0.87}$ | (Ghosh & Subbarao, 2012) |
| Soft clay at high water content stabilized with a mixture of Portland cement (5% to 35%) and class F fly ash (5% to 30%) | $E_{50} = (96 - 129)q_u$ | (Kang et al., 2017) |
| High plasticity Tokuyama marine clay in Japan stabilized with 10 to 30% Portland cement | $E_{50} = (30 - 169)q_u$ | (Yamashita et al., 2020) |
| Marine sediments in France treated with cement (3%-9%) and class F fly ash (3%-9%) | $E_{50} = (60 - 170)q_u$ | (D. Wang et al., 2013) |
| Soft Bangkok clay treated with (10% to 13%) of cement and cement kiln dust with partial replacement of 10 to 20% fly ash | $E_{50} = (99 - 159)q_u$ | (Yoobanpot et al., 2020) |

## 2.5 Undrained Monotonic and cyclic loading behaviour of sand

The behaviour of saturated clean sand under undrained monotonic and cyclic loading have been studied extensively, with the resulting behaviour well described in the literature. the purpose of this section is to provide a complete review behaviour. but rather to draw out some key features that will subsequently provide a useful reference for distinguishing the differences in behaviour between sand-like and clay-like fine-grained soils.

The undrained response of saturated sand to monotonic shear loading is illustrated by the triaxial compression test results in Figure.2-3 for Toyoura sand with DR of 16, 38, and 64% under consolidation stresses ranging from 10 to 3000 kPa (Ishihara et al., 1975). For any given $D_r$, the shape of the stress-strain curves and the stress-paths are affected by the consolidation stress ($\sigma_{3c}'$), but the undrained shear resistance at large strains are relatively independent of $\sigma_{3c}'$. The undrained shear resistance at large strains are, however, very sensitive to $D_r$, as illustrated by the order of magnitude differences in the scales used to present the results for each value of $D_r$. The results of these tests are consistent with critical state concepts, in that the undrained critical state strength is strongly dependent on void ratio (or $D_r$) and essentially independent of initial consolidation stress.

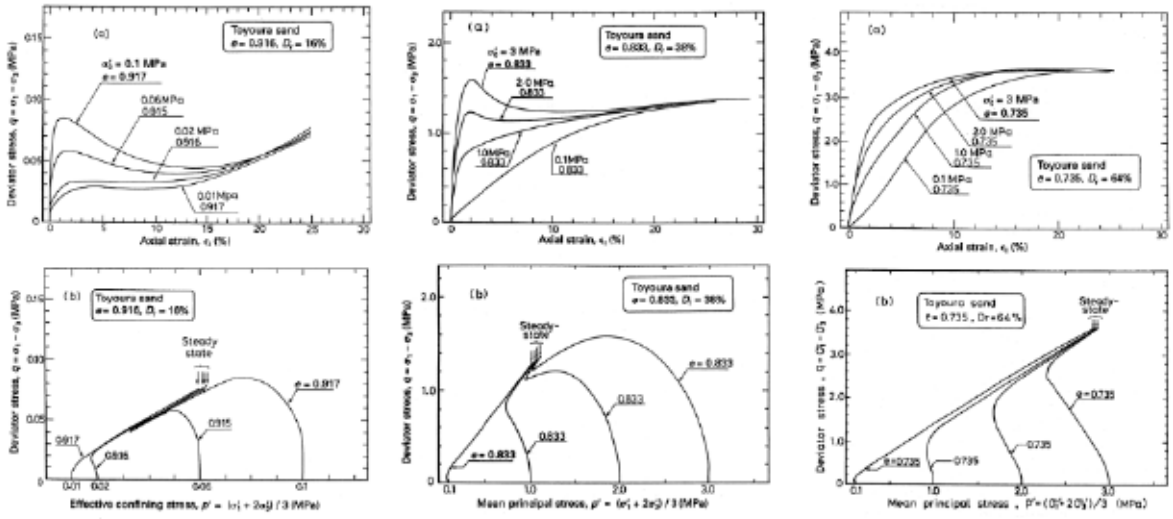

**Figure 2-5** Monotonic loading response of saturated Toyoura sand in isotopically consolidated undrained triaxial compression tests: (a) $D_r$=16%, (b) $D_r$=38%, (c) $D_r$=64% (Ishihara et al., 1975)

## 2.6 Re-excavation ability of backfill material and its importance in underground pipes and manhole.

The importance of backfill materials with good re-excavation ability has been extensively studied in the field of civil engineering. Several studies have investigated the factors that influence the re-excavation ability of backfill materials, including particle size distribution, compaction density, and moisture content (Gupta et al., 2020; Kevern and Li, 2014). It has been observed that backfill materials with a higher percentage of fines (i.e., smaller particle sizes) tend to have better re-excavation ability (Kevern and Li, 2014). In addition, lower compaction densities and higher moisture contents can also improve re-excavation ability (Gupta et al., 2020).

Furthermore, the long-term stability of the backfill material is also an important consideration. Backfill materials that are too loose or have poor stability may shift or settle over time, making future excavations more difficult (Bouasker et al., 2015). Stabilizers have been studied for their potential to improve the re-excavation ability of backfill materials. For example, Bouasker et al. (2015) investigated the effect of adding fly ash and cement on the re-excavation ability of a sandy soil backfill material. They found that the addition of fly ash and cement improved the re-excavation ability of the backfill material. Hosoya et al. (1993) conducted excavation experiments on soil treated with cement and lime at various unconfined compressive strengths $q_u$. As a result, it was demonstrated that

a $q_u$ of 500 kPa or less was desirable for efficient manual excavation without using a pick or breaker Figure 2-4.

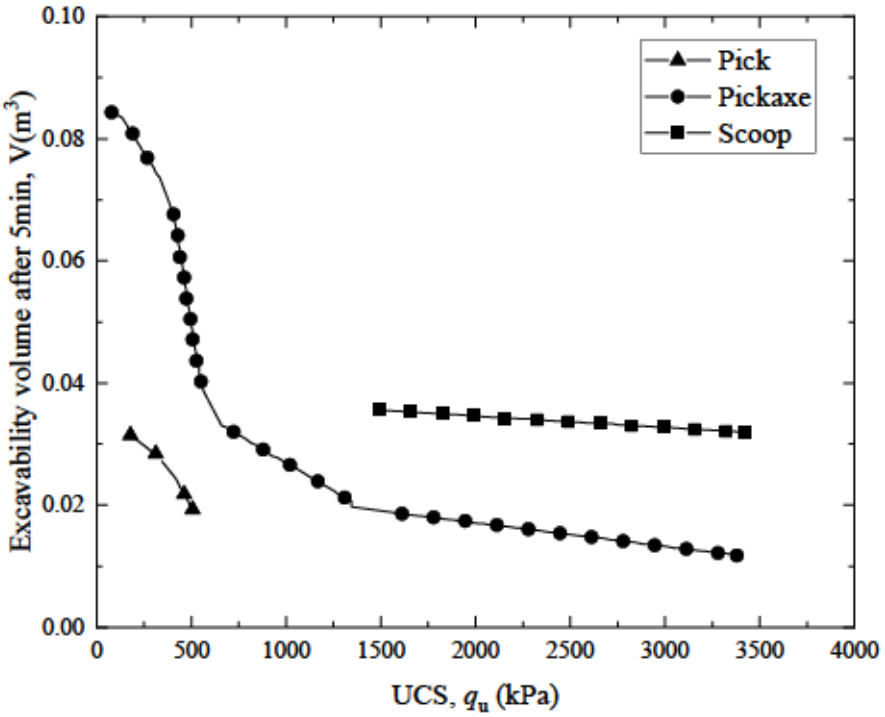


**Figure 2-6** Relationships between strength of improved soil and excavation capacity (Hosoya Y et al., n.d.)

In conclusion, selecting backfill materials with good re-excavation ability is essential for the long-term maintenance and accessibility of underground pipes and manholes. Factors such as particle size distribution, compaction density, moisture content, and long-term stability should be considered in the selection process. Additionally, the use of stabilizers can also improve the re-excavation ability of backfill materials.

## 2.7 Effects of swelling on backfill material.

Several scientific studies have investigated the effects of swelling on backfill material and underground structures. For instance, a study by Hussin et al. (2016) investigated the effect of clay content on the swelling potential of backfill material and found that as the clay content increased, the swelling potential of the backfill material also increased. Similarly, another study by Marzouk and Abdelrahman (2015) found that the type of backfill material significantly affected its swelling potential, with clay-rich materials exhibiting higher swelling potential than well-graded granular materials. In terms of the impact of swelling on underground structures, a study by Abderrahmane et al. (2019) found that the deformation and potential damage caused by swelling can vary depending on the type and

condition of the structure. They also highlighted the importance of selecting appropriate backfill materials and implementing effective drainage systems to mitigate the effects of swelling on underground structures.

To reduce the risk of swelling and its impact on underground structures, various measures have been proposed. For example, a study by Karim et al. (2017) suggested using stabilizers such as lime or cement to improve the stability of backfill material and reduce its potential for swelling. Another study by Hashim and Yusoff (2016) recommended the use of pressure relief valves and flexible joints to accommodate potential deformation caused by swelling. In summary, understanding the effects of swelling on backfill material and underground structures, as well as implementing appropriate measures to mitigate its impact, are critical for ensuring the long-term performance and safety of underground infrastructure.

## 2.8 Previous research on the re-excavation ability of backfill material and the effects of stabilisers on these properties.

Previous research has been conducted on the re-excavation ability of backfill material and the effects of stabilizers on these properties. The use of stabilizers has been investigated to improve the re-excavation ability of backfill materials. A study by Ashour et al. (2016) investigated the effect of using cement and fly ash as stabilizers on the re-excavation ability of backfill material. The results showed that the addition of cement and fly ash improved the re-excavation ability of the backfill material by increasing the compressive strength and reducing the swelling potential. Another study by Al-Tabbaa et al. (2008) investigated the use of different stabilizers, including fly ash, cement, and lime, on the re-excavation ability of backfill material. The results showed that the addition of stabilizers improved the re-excavation ability of the backfill material by increasing the shear strength and reducing the potential for settlement.

Furthermore, a study by Kim et al. (2017) investigated the effect of using different types of stabilizers, including cement, fly ash, and slag, on the re-excavation ability of backfill material. The results showed that the addition of stabilizers improved the re-excavation ability of the backfill material by increasing the strength and reducing the swelling potential. In conclusion, previous research has shown that the use of stabilizers can improve the re-excavation ability of backfill materials by increasing strength and reducing swelling potential. Further research is needed to investigate the optimal type and amount of stabilizer to use for specific types of backfill materials and applications.

## 2.9 Dry-wet cycle curing of backfill sand.

The mechanical behaviour of sand under wetting and drying curing cycles is an important aspect in geotechnical engineering, particularly in the field of soil stabilization and slope stability analysis(Rao, 2011). Understanding the changes in the mechanical properties of sand due to wetting and drying cycles is crucial for the design and construction of infrastructure projects in regions where such cyclic environmental conditions are prevalent. This section presents a comprehensive review of the existing literature on the mechanical behaviour of sand under wetting and drying curing cycles.

The response of sand to wetting and drying cycles can significantly influence its engineering properties, including strength, stiffness, permeability, and volume change characteristics. Several studies have investigated the effects of cyclic wetting and drying on sand and have provided valuable insights into the underlying mechanisms and resulting changes in soil behaviour. One aspect of sand behaviour under wetting and drying cycles that has received considerable attention is the phenomenon of volume change. It is well-established that sand experiences volumetric expansion upon wetting and subsequent contraction upon drying(Li et al., 2020). This volume change can induce significant stress changes within the soil mass, leading to potential instability and deformation(Tang & Shi, 2011).

(J.-J. Wang et al., 2019) (X. Liu et al., 2022) have focused on quantifying the volume change behaviour of sand under cyclic wetting and drying conditions and have proposed various empirical models to predict the associated volumetric strains. In addition to volume change, the strength and stiffness properties of sand can also be affected by wetting and drying cycles. The cyclic variation in moisture content and pore water pressure can alter the interparticle bonding and frictional characteristics, resulting in changes in shear strength and stiffness. (Ishihara et al., 1975) (Kongsukprasert et al., 2007) have conducted laboratory tests, such as triaxial shear tests and direct shear tests, to investigate the influence of wetting and drying cycles on the shear strength parameters of sand. These studies have provided valuable data on the residual strength, cyclic strength degradation, and stress-strain behaviour of sand subjected to wetting and drying cycles.

Furthermore, the permeability of sand can be significantly affected by cyclic wetting and drying. The changes in moisture content and pore water pressure can influence the soil's hydraulic conductivity, affecting the flow of water through the soil mass(Abbas et al., 2023);(Bhaskar et al., 2020). Numerous studies have examined the permeability variations of sand under wetting and drying cycles and have proposed empirical relationships to estimate the permeability changes based

on the number of cycles and other relevant parameters(Ng & Peprah-Manu, 2023);(Yong et al., 2017);.Thus, several factors influence the mechanical behaviour of sand under wetting and drying curing cycles, including the initial state of the soil (e.g., density, grain size distribution), environmental conditions (e.g., temperature, moisture content), and the characteristics of the applied loading. It is important to consider these factors when interpreting the results of various studies and applying the findings to practical engineering applications.

Overall, the literature review highlights the significance of understanding the mechanical behaviour of sand under wetting and drying curing cycles. The findings from previous studies provide valuable insights into the changes in strength, stiffness, permeability, and volume change characteristics of sand subjected to cyclic environmental conditions. The knowledge gained from this review will serve as a foundation for the subsequent chapters of this thesis, where the experimental program, methodology, and analysis will be presented to further investigate the mechanical behaviour of PSAS-treated sand under wetting and drying curing cycles.

## 2.10 Liquefaction study of backfill sand.

Liquefaction of sandy soils is a geotechnical phenomenon that poses significant challenges to the stability and performance of underground structures. Understanding the resistance of sand to liquefaction is crucial for assessing the potential for liquefaction-induced hazards and designing effective mitigation measures. This section provides a comprehensive literature review on the resistance of sand to liquefaction based on laboratory cyclic triaxial testing, focusing on the key parameters such as cyclic stress ratio, double amplitude axial strain, number of loading cycles, and the estimation of liquefaction failure.

Cyclic triaxial testing is a widely used laboratory method for assessing the liquefaction resistance of sandy soils. By subjecting a soil specimen to cyclic loading conditions that simulate earthquake-induced loading, (Wong et al., 1975);(Procter & Khaffaf, 1984) have investigated the response of sands under various seismic loading scenarios.

The cyclic stress ratio (CSR) is a critical parameter in cyclic triaxial testing as it represents the ratio of the cyclic shear stress to the confining stress. Numerous studies have explored the relationship between cyclic stress ratio and the liquefaction resistance of sands. It has been observed that certain cyclic stress ratios are associated with the onset of liquefaction. For instance, Seed and Idriss (1971) reported that cyclic stress ratios in the range of 0.1 to 0.2 are typically associated with the liquefaction failure of sands. Other researchers, such as

Robertson and Wride (1998), have proposed empirical relationships between cyclic stress ratio, double amplitude axial strain, and the number of loading cycles to estimate the potential for liquefaction failure.

The double amplitude axial strain is another critical parameter in cyclic triaxial testing. Several studies have investigated the influence of double amplitude axial strain on the liquefaction resistance of sands. For example, (Ishihara, 1993)Cetin et al. (2004) conducted cyclic triaxial tests on sands and found that for a specific double amplitude axial strain, the number of loading cycles required for liquefaction to occur decreases as the cyclic stress ratio increases. Similarly, Liao et al. (2005)(Silver & Park, 1976) investigated the effects of double amplitude axial strain on the liquefaction resistance of sands and observed that higher double amplitude axial strains require fewer loading cycles to induce liquefaction.

The number of loading cycles is an important factor affecting the liquefaction resistance of sands. Researchers have conducted cyclic triaxial tests with varying numbers of loading cycles to investigate the cyclic mobilization of pore pressures and the resulting liquefaction potential (Erten & Maher, 1995) (Tsukamoto et al., n.d.). Seed and Idriss (1971) found that liquefaction typically occurs after a certain number of loading cycles, which is influenced by factors such as soil type, confining pressure, and the initial state of the soil. The specific number of cycles needed for liquefaction varies depending on the characteristics of the sand being tested. In addition to the number of cycles, researchers have also investigated the cyclic stress ratio required to induce liquefaction for specific double amplitude axial strains or various double amplitude axial strains. For example, Martin et al. (2008) conducted cyclic triaxial tests on treated sands and found that a cyclic stress ratio of 0.2 was sufficient to induce liquefaction for a specific double amplitude axial strain of 5%. In another study, Chen et al. (2012) investigated the effect of different double amplitude axial strains on the liquefaction resistance of sands and proposed a range of cyclic stress ratios (0.1 to 0.3) that can be used to estimate the liquefaction failure for various double amplitude axial strains.

It is important to note that the resistance of sand to liquefaction is influenced by various factors, including grain characteristics, particle size distribution, confining pressure, and initial state of the soil. Different soil types and test conditions can lead to variations in the liquefaction resistance.

In term of the liquefaction resistance of sand treated with sustainable materials such as fly ash , tyre chips , (Keramatikerman et al., 2017) investigated the effect of fly ash on monotonic triaxial test and indicated that fly ash is effective in improving liquefaction behaviour of the soil.

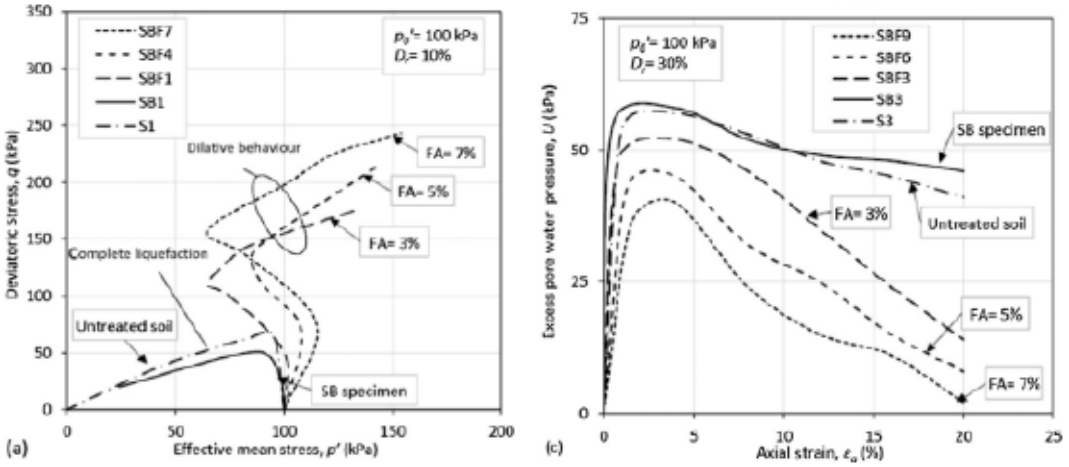


**Figure 2-7** Typical undrained shear response for untreated soil and Fly ash treated SB specimen ((Keramatikerman et al., 2017))

Used tyres have become an increasingly problematic global problem whose disposal is posing dangers to the environment. Thus, recycling needs to be considered imaginatively and the solutions must be sustainable. One method of disposing of tyres is by mixing tyre chips. With soil and using them for landfill purposes. However, the mixtures of sand rubber composites with similar grain sizes for each fraction has demonstrated a more gradual build-up of pore water pressures but actually no sign of increasing the liquefaction strength except for the 99:1 mixture at 10 and 15 cycles Figure 2-6.

(Uchimura et al., 2007) propose to use a mixture of tire chips and sand as backfill material for buried pipes. It was found in the authors' research that a backfill with a mixture of tire chips and sand has higher liquefaction resistance compared to sand-only backfill figure 2-7. This implies that use of such materials for backfilling buried pipes could mitigate floating up damages. The numbers of loading cycles required before the specimens were liquefied are summarized in figure 2-8.

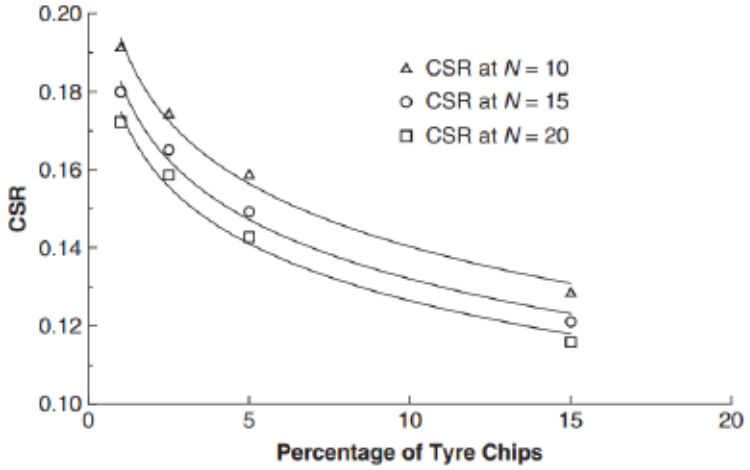


**Figure 2-8** CSRs at 10, 15, and 20 cycles (Promputthangkoon & Hyde, 2007)

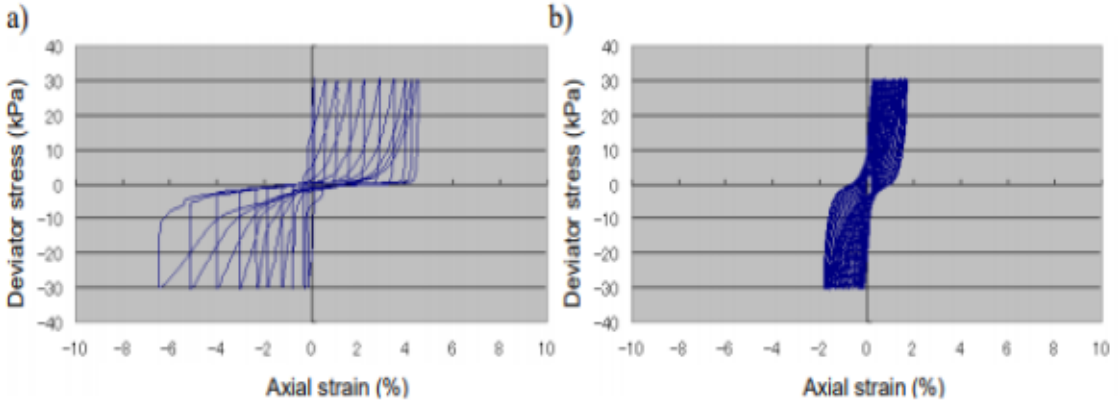


**Figure 2-9** Stress-strain relationships ($D_r$=65%) : a) TCr=0% (sands-only), b) TCr= 30%

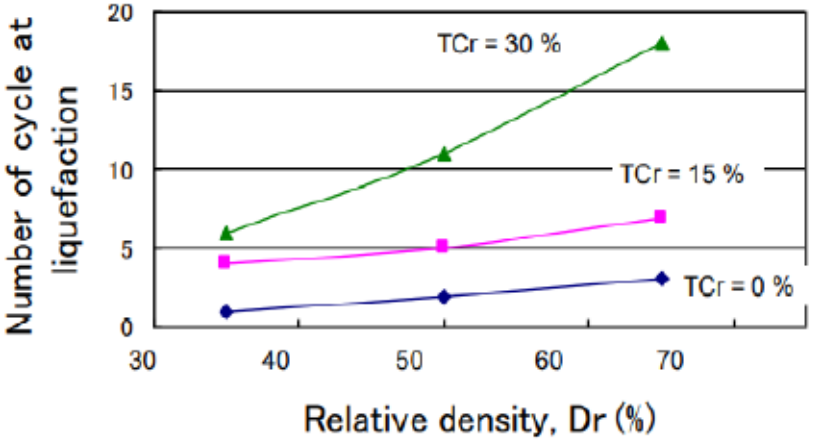


**Figure 2-10** Number of loading cycles required for liquefaction of tire chips and sand mixture (T. Uchimura et al., (2007) liquefaction defined at 95% of the initial effective confining pressure.

# CHAPTER 3

## 3. Fundamental properties of PSAS-treated sand compared with OPC-treated sand.

As major infrastructure projects require a significant number of natural materials, sometimes followed by stabilization using hydraulic binders, this part of the research focuses on providing physical properties of both natural and treated materials. Toyoura sand and Watoru PSAS were used to evaluate their basic parameters. The composition of PSAS and Ordinary Portland Cement (OPC) was studied to better understand their chemical properties. Naturally, soil texture refers to the size particles that make up the soil, which depends on the proportion of sand, silt, and clay-sized particles and organic matter. Sand is used as a backfilling material due to its porous structure, allowing for quick drainage and air to enter the soil. It also doesn't get waterlogged in winter or become drought-prone in summer. Therefore, this research focuses on backfilling sand using Toyoura sand. In the following sections, you will see the particle sand distribution of Toyoura sand and PSAS, as well as the minimum and maximum density of PSAS and cement-treated sand.

### 3.1 Toyoura sand (TS)

Toyoura sand is a commercially available sand that was used in this study for laboratory experiments. It has passed the examination conducted by the Japan Cement Association and is also known as Toyoura silica sand; a rare natural silica sand found in the Toyoura area of Yamaguchi prefecture. Unlike artificially formed sand, Toyoura silica sand has not been ground or modified in any way. It has been washed, kiln-dried, and sifted. The grains of naturally formed sand are typically smoother due to their formation over time by natural elements, which reduces variations in test results. Since Toyoura Silica Sand meets the standard sand test of the Japan Cement Association, it has a stable range of grain distribution, making it ideal for calibration and comparison tests. The unified soil classification system (USCS) classifies Toyoura sand as a poorly graded sand, with a particle density, $\rho_s = 2.641$ g/cm$^3$. The particle size distribution (PSD) of Toyoura sand is shown in Figure 3-1.

### 3.2 Paper sludge ash (PSAS)

The PSAS-based stabilizer used in this study is a commercially available product that can be obtained in Japan. To determine the particle size distribution of the

PSAS-based stabilizer, sedimentation particle size analyses were initially conducted based on the standards set by the Japanese Geotechnical Society (2015a). However, the results were inconclusive due to the hydration reaction of the PSAS. Although the reaction was not as strong as with cement, it still affected the sedimentation process. Kawai et al. (2018) reported that the excess water in muds could be fixed by both water absorption or retention of PS particles and by the hydrated compound, ettringite, during curing. Therefore, in this study, laser diffraction analyses were carried out using alcohol as the medium instead of water to obtain the particle size distribution. Figure 3-1 shows the particle size distribution obtained, with a maximum diameter $D_{max}$ of 0.52 mm and mean diameter $D_{50}$ of 0.074 mm. The chemical components of the PSAS and OPC (%: mass ratio) obtained via X-ray fluorescence analysis are listed in Table 3-1.

**Table 3-1.**Component compositions of the PSAS-based improving material.

| Chemical components of PSAS | | | | | | | |
|---|---|---|---|---|---|---|---|
| CaO | $SiO_2$ | $Al_2O_3$ | $SO_3$ | FeO | MgO | $P_2O_5$ | Others |
| 63.89 | 13.55 | 6.89 | 6.06 | 3.27 | 1.31 | 0.95 | 4.08 |
| Chemical components of OPC | | | | | | | |
| CaO | $SiO_2$ | Al2O3 | $SO_3$ | FeO | MgO | | Others |
| 65.57 | 19.07 | 5.26 | 3.98 | 2.91 | 1.98 | 0.25 | 0.92 |

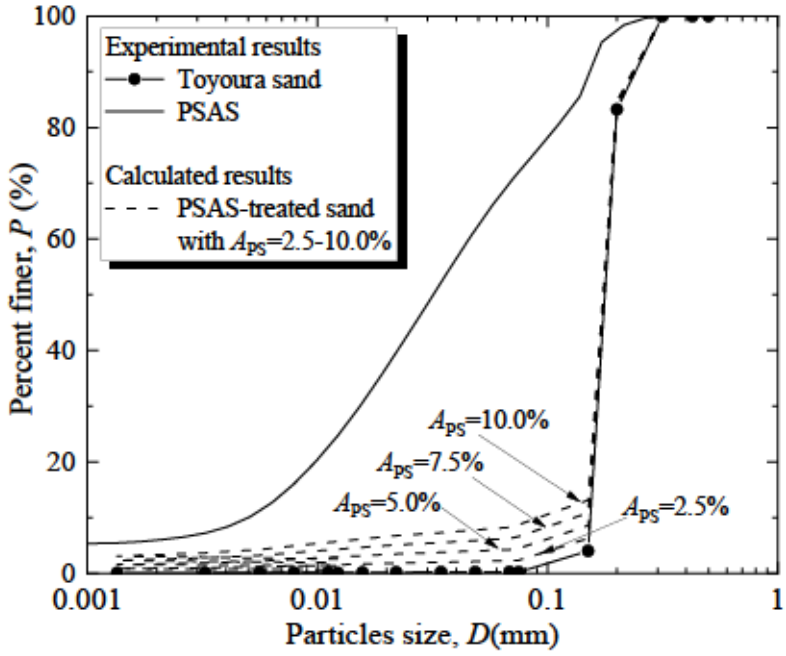


**Figure 3-1** Particle size distributions of Toyoura sand and PSAS

### 3.3 Ordinary Portland cement (OPC)

The Portland cement used in this study is a commercial ordinary Portland cement available elsewhere in Japan. Its particle density is commonly assumed to be 3,150 kg/m$^3$ (3.15 g/cm$^3$). The component composition of the PSAS was similar to that of OPC. The PSAS contains approximately 63.9 % calcium oxide (CaO) by mass.

### 3.4 The pH-values of the PSAS and OPC

Using the PSAS alone is expected to induce a hydration reaction when combined with water, although the reaction is not comparable to that of cement in terms of strength. (Kawai et al., 2018) reported that the excess water in muds is first physically absorbed by the porous structure of the PSAS particles and later chemically absorbed by the hydrated compound ettringite during curing. Additionally, the pH values of the PSAS and OPC were investigated based on the Japanese Geotechnical standards (JGS 0211) (Japanese Geotechnical Society JGS 0211-2020, n.d.) using a glass electrode pH meter placed in suspended water mixed with each stabilizer and distilled water at a mass ratio of 1:5. The PSAS or OPC was immersed in distilled water for 10 min, and the pH was measured for each suspended water. The results show that the pH value of PSAS was 11.7, which was lower than that of OPC (12.7).

### 3.5 Investigation of alkalinity of PSAS and OPC-treated sand.

Alkalinity is an important factor to consider in the construction of treated sand with paper sludge ash and ordinary Portland cement. The high alkalinity of the cement can lead to an increase in pH levels in the soil, which can have negative effects on the surrounding environment. To mitigate these effects, it is important to carefully monitor and control the pH levels during a short and long term for backfill treated sand under the construction process. In this study, the alkalinity of Paper Sludge Ash treated sand (PSAS) and Ordinary Portland Cement (OPC) was investigated at different liquid to solid ratios (L/S) of 3 and <3 to evaluate the impact of curing conditions on strength development over a long period. 5% PSAS and OPC content was mixed with Toyoura sand to prepare a cylindrical mould immersed in water as shown in figure 3-2. The study also aimed to assess the reduction of pH in the PSAS and OPC-treated sand.

In figure.3-3, it was found that the alkalinity of PSAS-treated sand was lower than that of OPC-treated sand. Additionally, specimens cured under L/S = 3 showed a

greater stability in the reduction of pH value after 75 days of curing, compared to those cured at L/S < 3 where the pH value stabilized before 75 days for both PSAS and OPC-treated sample. These findings suggest that the curing condition, as well as the liquid to solid ratio, can have an impact on the alkalinity and pH stability of treated sand with PSAS and OPC. This information is important for the practical application of this material in construction projects, particularly in earthquake-prone areas where the stability and strength of soils are crucial for safety.

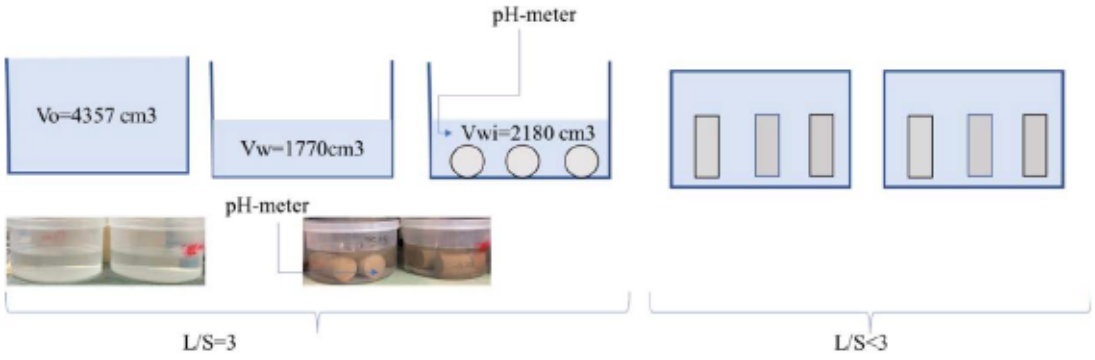


**Figure 3-2** Alkalinity test conditions

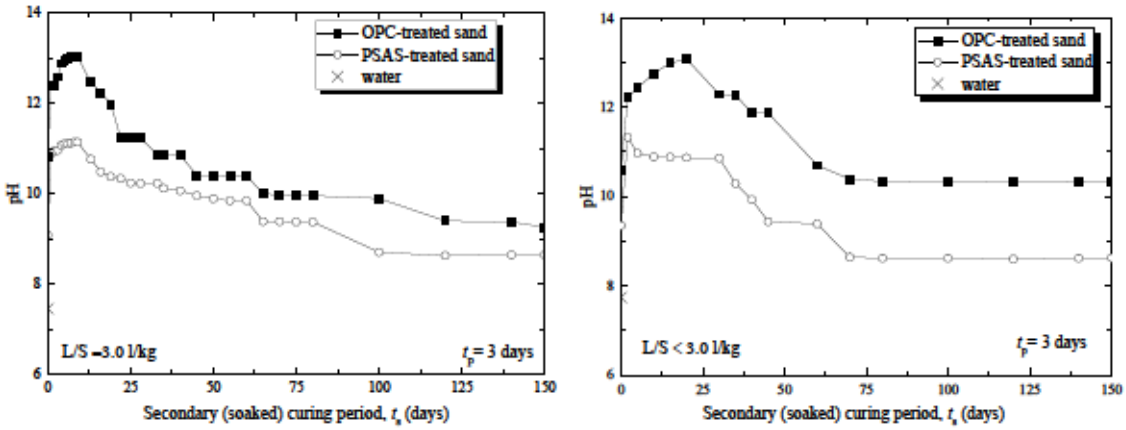


(a) L/S= 3.0 l/kg (b) L/S< 3.0 l/kg

**Figure 3-3**. Change in pH of water in which treated sands with cylindrical moulds were immersed.

## 3.6 Maximum and minimum density characteristics of treated sands

To investigate the potential application of PSAS-treated sand as a backfill material, the maximum and minimum densities of the PSAS-treated sand were compared with those of the OPC-treated sand. The maximum and minimum densities of the PSAS-treated sand with PSAS addition ratios $A_{PS}$ of 2.5%, 5%, 7.5%, and 10% were evaluated based on the Japanese Geotechnical Standard (JGS 0161) (Japanese Geotechnical Society JGS 0161-2009, 2018). $A_{PS}$ is defined

as the dry mass ratio of the PSAS to sand. The PSD of the PSAS-treated sand for each $A_{PS}$ is shown in Figure. 3-1. These PSDs were calculated from the PSDs of the combined PSAS, and sand based on the $A_{PS}$. Additionally, the minimum and maximum densities of the OPC-treated sand samples were evaluated.

To measure the maximum density $\rho_{dmax}$, the sand or treated sand in the dry state was poured into 10 individual layers in the mold. For each layer, 100 blows were applied to the side of the mold by tapping the mold with a wooden hammer to obtain the densest state of the sand or treated sand. No material separation was visually observed in any test. Three tests were conducted on the same sample. To measure the minimum density $\rho_{dmin}$, air pluviation was conducted to obtain the loosest state of the sand or treated sand, which was prepared by slowly pluviation the sand or treated sand into a mold through a long funnel with a small mouth to obtain the minimum dry density. Three tests were conducted on the same sample.

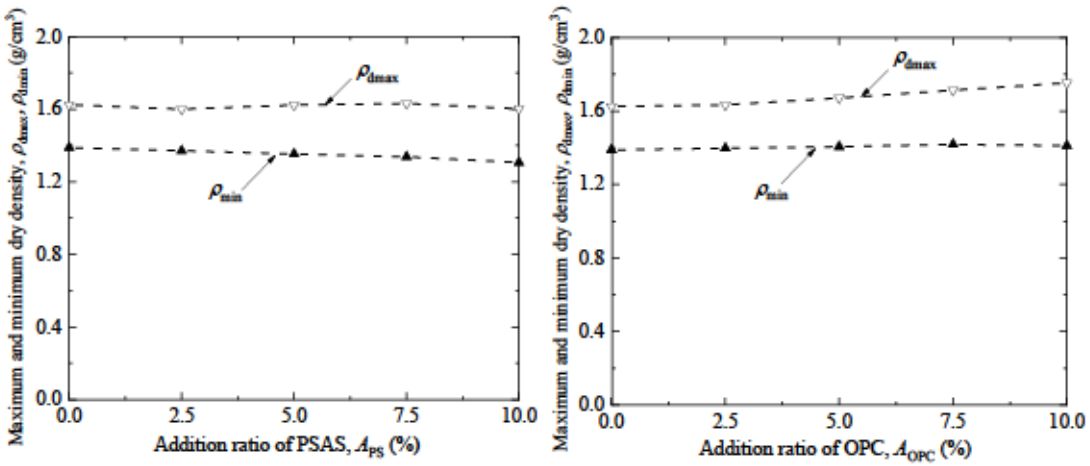


(a) PSAS-treated sand (b) OPC-treated sand

**Figure 3-4.** Maximum and minimum dry densities of PSAS- and OPC-treated sands

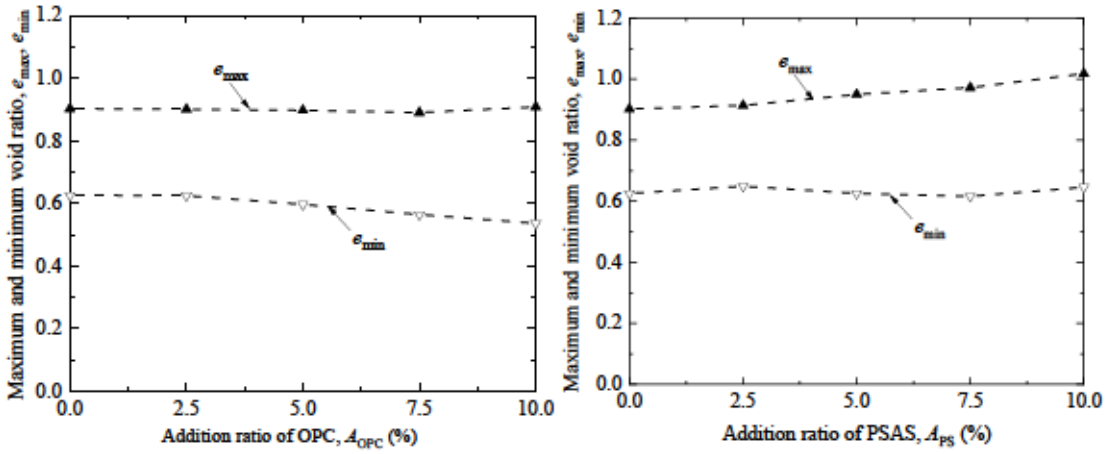


(a) PSAS-treated sand (b) OPC-treated sand

**Figure 3-5.** Maximum and minimum void ratios of PSAS- and OPC-treated sands

The maximum $\rho_{dmax}$ and minimum $\rho_{dmin}$ dry densities plotted against $A_{PS}$ are shown in Figure. 3-3(a). Meanwhile, the $\rho_{dmax}$ and $\rho_{dmin}$ plotted against the addition ratios of OPC, $A_{OPC}$ are shown in Figure. 3-3(b). Here, $A_{OPC}$ is defined as the ratio of OPC to sand in terms of dry weight. The values of $\rho_{dmax}$ and $\rho_{dmin}$ shown in Figure. 3-3 are the averages obtained from three sets of results for the same sample. The maximum standard deviations for the three sets of results are 0.009 g/cm$^3$ for $\rho_{dmax}$ and 0.019 g/cm$^3$ for $\rho_{dmin}$, indicating slight scatter. The larger standard deviation for $\rho_{dmin}$ than for $\rho_{dmax}$ may be due to the greater difficulty in preparing loosest specimens than densest specimens. In addition, no correlation is observed between the variation degree and stabilizer type or addition ratio. As shown in Figure. 3-3, the weight of the PSAS-treated sand is slightly lower than that of the OPC-treated sand when the addition ratios $A_{PS}$ and $A_{OPC}$ are increased, as shown in Figures. 3-3(a) and (b), respectively.

The maximum void ratio $e_{max}$ and minimum void ratio $e_{min}$ are calculated based on $\rho_{dmin}$ and $\rho_{dmax}$ shown in Figure. 3-3, as well as the soil particle density $\rho_s$. The soil particle density of the treated sand is determined using the particle density and mixing ratio of Toyoura sand and the stabilizer. The $e_{max}$ and $e_{min}$ of the PSAS- and OPC-treated sands plotted against $A_{PS}$ and $A_{OPC}$ are shown in Figures. 3-4(a) and (b), respectively. The $e_{max}$ and $e_{min}$ for the Toyoura sand-only cases are similar to those of previous studies (Toyota et al., 2004) .Furthermore, the $e_{min}$ of the PSAS-treated sand changes slightly as $A_{PS}$ increases, whereas $e_{max}$ increases gradually, as shown in Fig. 3-4(a). Therefore, the difference $e_{max} - e_{min}$ increases with $A_{PS}$. The increase in $e_{max} - e_{min}$ with $A_{PS}$ suggest that the compaction of the PSAS-treated sand as a backfill material around the manholes and underground pipes will be successful. Meanwhile, the $e_{max}$ of the OPC-treated sand changes only slightly, and the $e_{min}$ decreases as $A_{PS}$ increases. The reason contributing to the difference in trends between the PSAS- and OPC-treated sands is yet to be determined. However, the difference might be caused by the relative magnitude relationship between the $\rho_s$ of the two types of stabilizers and the $\rho_s$ of the sand.

# CHAPTER 4

## 4. Swelling potential of paper sludge ash (PSAS) treated sand.

This chapter explores the swelling potential of paper sludge ash (PSAS)-treated sand, building upon the geotechnical properties investigated in Chapter 3. The decision to conduct swelling tests on PSAS-treated sand was motivated by the notable expansion observed when dry sand and PSAS were mixed with water. This phenomenon raised concerns about the potential impact on the behaviour of treated sand. The chapter aims to provide insights into the swelling characteristics of PSAS-treated sand, offering a comprehensive understanding of its behaviour under varying conditions.

### 4.1 Effect of swelling of backfill sand around underground pipes and manhole.

The swelling of backfill soils can affect the surrounding structures over time, such as underground pipes and manholes. Therefore, in the second step of this study, the swelling potential of PSAS-treated sand associated with water immersion was investigated to determine the suitable conditions for using the treated sand as a backfill material. To control the swelling potential of the PSAS-treated sand, the water content and primary curing were adjusted during specimen preparation. The specimen preparation method and test results are presented in Sections 4.2 and 4.3, respectively.

### 4.2 Specimen preparation and swelling potential test.

The swelling potential test was performed to measure the deformation or strain resulting from swelling and the stress or pressure required to prevent deformation due to swelling. The method used in this study involved the complete immersion of a test specimen in water to measure the change in the height of the specimen while restraining the specimen sides with a mold. The specimens subjected to this test method were permitted to swell immediately after immersion. This test was performed to measure the expansion strain of PSAS-treated sand without any external overburden pressure when it was submerged in water. In fact, such tests have also been conducted in the previously published studies to determine the one-dimensional swelling potential of various types of treated soils [31-34].

To prepare specimens for the swelling potential tests, dry Toyoura sand was first mixed with the PSAS with $A_{PS}$ = 2.5% or 5.0%, as shown in Figure. 4-1. Immediately after mixing, the water content $w$ of the treated sand was adjusted to 0%, 10%, 15%, or 20%, as shown in Table 4-1. Subsequently, the specimens were cured in plastic bags under sealed conditions for 0–7 d, as shown in Table 4-1.

After the primary curing, the specimens were poured into cylindrical plastic molds with a diameter of 5 cm and a height of 10 cm. Next, they were compacted using the wet tamping method based on JGS 0821 (Japanese Geotechnical Society JGS 0821-2020, n.d.) to achieve a relative density $D_r$ of 50% or 90%. Finally, the molds containing the specimens were immersed in water for secondary curing, with the top surface of each specimen exposed for 0 to 4 d, as shown in Table 4-1. Each specimen was removed from the water container after a predetermined secondary curing period $t_s$, and the change in the maximum height was measured to calculate the expansion strain $\varepsilon_s$.

Similarly, swelling potential tests were conducted on the OPC-treated sand for comparison. To prepare the specimens, OPC was added to Toyoura sand at an $A_{OPC}$ of 2.5% and 5.0%. Subsequently, the specimens with a water content of 0% were immediately immersed in water (i.e., the primary curing period $t_p$ was 0 d), and the expansion strain $\varepsilon_s$ was measured after the soaked secondary curing.

**Table 4-1.** Conditions of PSAS-treated specimens for swelling potential tests

| Addition ratio of PSAS, $A_{PS}$ (%) | Adjusted water content $w$ (%) | Primary curing period under sealed condition $t_p$ (d) | Relative density, $D_r$ (%) | Secondary curing period under soaked condition $t_s$ (d) |
|---|---|---|---|---|
| 2.5 | 0, 10, 15, 20 | 0, 1, 2, 3, 4, 5, 6, 7 (0 for $w$ = 0%) | 50, 90 | 0, 1, 2, 3, 4 |
| 5.0 | 0, 20 | 0, 1, 2, 3, 4, 5, 6, 7 (0 for $w$ = 0%) | 50, 90 | 0, 1, 2, 3, 4 |

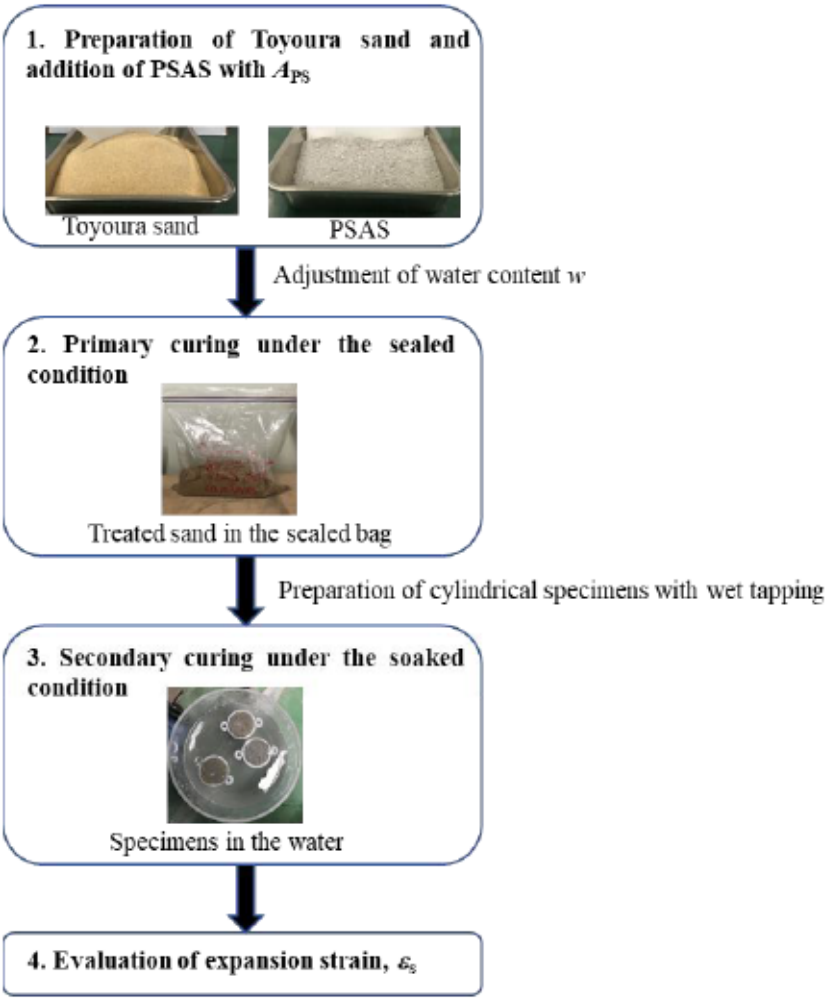


**Figure 4-1.** Process flow from specimen preparation to swelling potential test.

## 4.3 Swelling potential test results.

The relationships between the secondary curing period $t_s$ and expansion strain $\varepsilon_s$ of each specimen of the PSAS- and OPC-treated sands with an $A_{PS}$ of 2.5% and $A_{OPC}$ of 2.5% are shown in Figures. 4-2 and 4-3, respectively. The $\varepsilon_s$ of the specimens with $D_r$ = 50% and 90% are shown in Figures. 4-2 and 4-3, respectively. The results for the specimens with $w$ = 10%, 15%, and 20% are shown in Figures. 4-2 and 4.3(a), (b), and (c), respectively. The expansion side is indicated by the positive sign. In each figure, the results for the specimen with $w$ = 0% are shown for comparison. The figures show that the OPC- and PSAS-treated sands expanded when soaked in water, where the most significant expansion occurred when $w$ = 0%. The expansion was particularly evident in the early stages of soaking, whereas it became milder as the secondary curing period $t_s$ continued. However, the rapid expansion of the PSAS-treated sand in the early stage of soaking can be suppressed by adjusting $w$ to some extent prior to soaking. The abovementioned findings were observed regardless of the relative densities of the specimens.

The relationships between the $t_s$ and $\varepsilon_s$ of each specimen of the PSAS- and OPC-treated sands with an $A_{PS}$ of 5.0% and $A_{OPC}$ of 5.0% are shown in Figure. 4-5. Similarly, to the results in Fig.4.3, the figures indicate that the OPC- and PSAS-treated sands expanded when soaked in water, where the most significant expansion occurred at $w$ = 0%. However, adjusting $w$ to 20% resulted in an $\varepsilon_s$ of less than 1% for $D_r$ = 50% and 90%, similar to the results shown in Figs. 4.2(c) and 4.3(c).

This expansion is attributable the formation of ettringite via the following reaction:

$$CaO + H_2O \rightarrow Ca(OH)_2 \quad (1)$$

$$3Ca(OH)_2 + Al_2O_3 + 3CaSO_4 + 29H_2O \rightarrow 3CaO{\cdot}Al_2O_3{\cdot}3CaSO_4{\cdot}32H_2O \quad (2)$$

Based on the chemical compositions listed in Table 3-1, the PSAS and OPC contain both CaO and $Al_2O_3$. An analysis of the hydrated PSAS via scanning electron microscopy indicates the formation of needle-like crystals, as shown in Figure.4-4. These needle-like crystals are ettringite, which is speculated to expand the volume of the treated sands. In general, ettringite is formed in the early stages of hydration, which is consistent with the significant expansion that occurs in the early stages of hydration of the treated sands. The higher the amount of unreacted CaO, the higher is the amount of ettringite formed during soaking, which is consistent with the greater expansion under $w$ = 0%. Mixing at a higher initial water content resulted in less unreacted CaO, which reduced the amount of ettringite formed after soaking, and hence less expansion of the treated sand volume.

The maximum expansion strain that occurred in each specimen during soaking $(\varepsilon_s)_{max}$ was determined from the results shown in Figures.4-2, 4-3, and 4-5. The relationship between the obtained $(\varepsilon_s)_{max}$ and primary (sealed) curing period $t_p$ for each PSAS-treated sand specimen is shown in Figure. 4.6. The results for the specimens with $A_{PS}$ = 2.5% and $w$ = 10%, 15%, and 20% are shown in Figs. 4-6(a), (b), and (c), respectively. The results for the specimens with $A_{PS}$ = 5.0% and $w$ = 20% are shown in Figure. 4-6(d). Regardless of the mixture conditions of the specimens, the $(\varepsilon_s)_{max}$ of the PSAS-treated sands decreases as $t_p$ increases. However, the rate of change of $(\varepsilon_s)_{max}$ decreases with $t_p$ as $w$ increases. Furthermore, the difference in the magnitude of $(\varepsilon_s)_{max}$ between $D_r$ = 50% and 90% is negligible as $w$ increases.

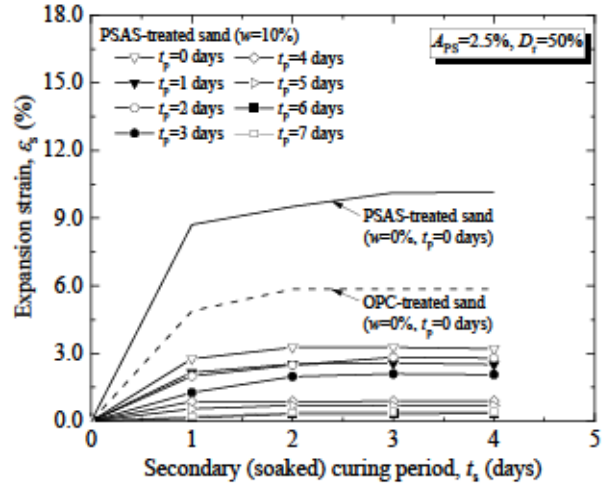


(a) $A_{PS} = 2.5\%$, $w = 10\%$

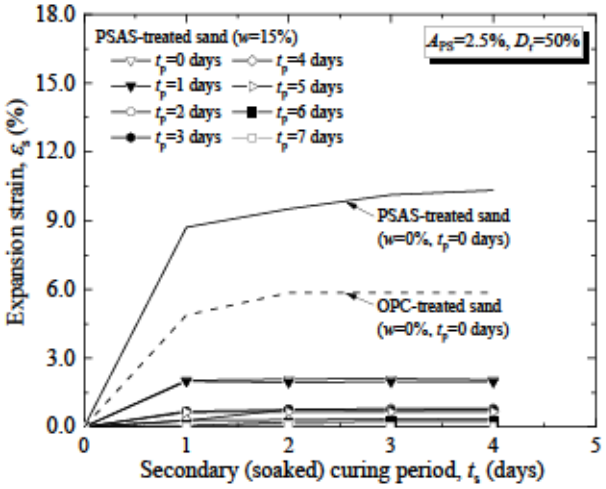


(b) $A_{PS} = 2.5\%$, $w = 15\%$

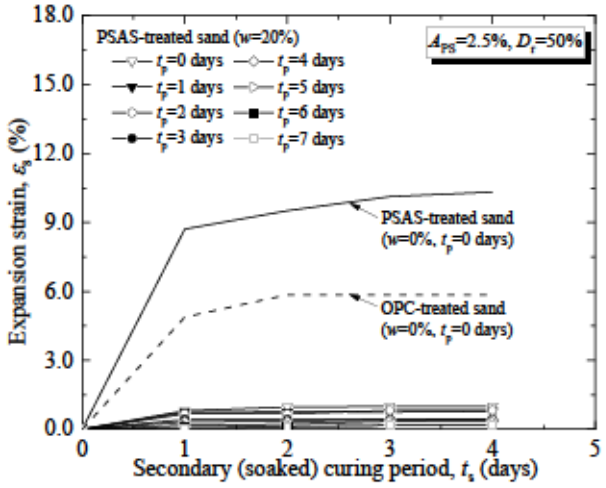


(c) $A_{PS} = 2.5\%$, $w = 20\%$

**Figure 4-2** . Expansion strain of PSAS-treated sand with $A_{PS} = 2.5\%$ associated with secondary (soaked) curing period ($D_r = 50\%$). Expansion side is indicated by positive sign.

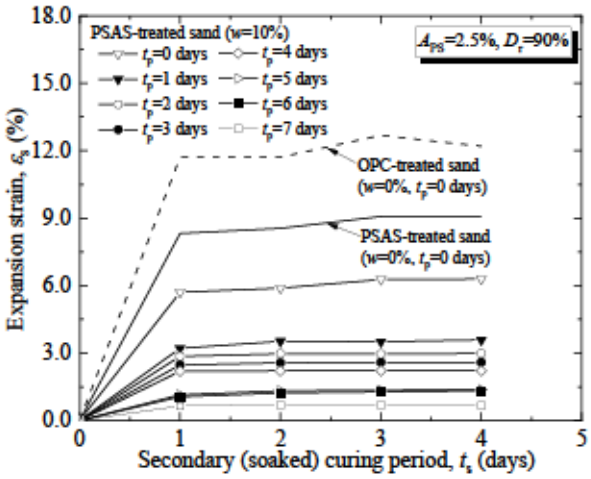


(a) $A_{PS} = 2.5\%$, $w = 10\%$

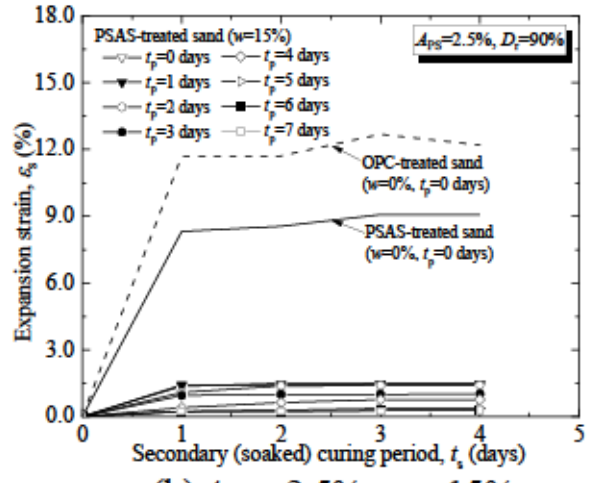


(b) $A_{PS} = 2.5\%$, $w = 15\%$

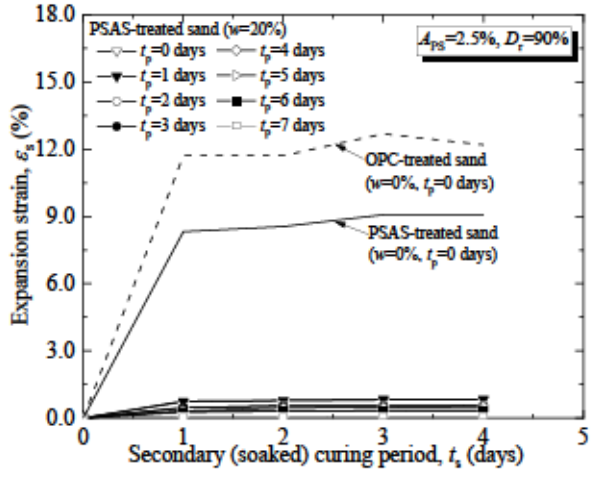


(c) $A_{PS} = 2.5\%$, $w = 20\%$

**Figure 4-3.** Expansion strain of PSAS-treated sand with $A_{PS} = 2.5\%$ associated with secondary (soaked) curing period ($D_r = 90\%$). Expansion side is indicated by positive sign.

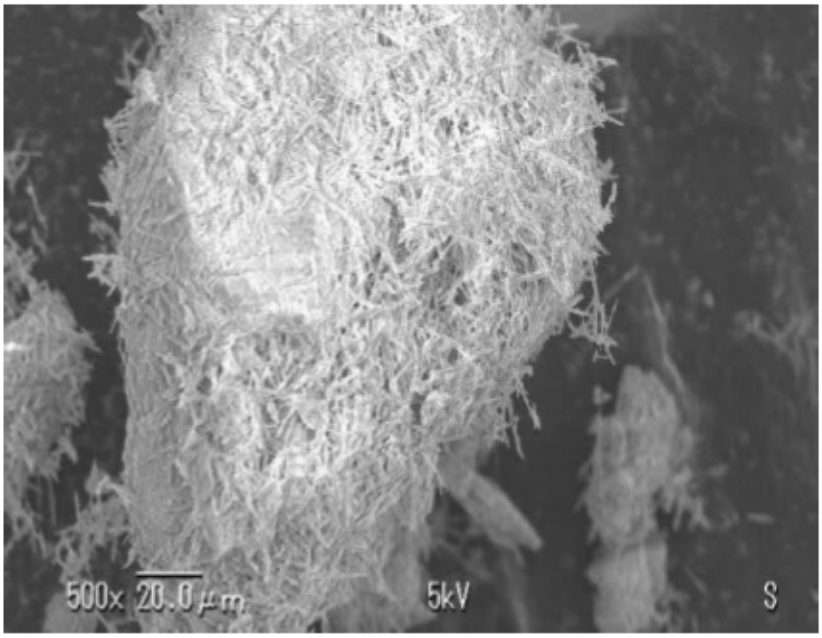


**Figure 4-4.** Formation of needle-like crystals (ettringite) in PSAS

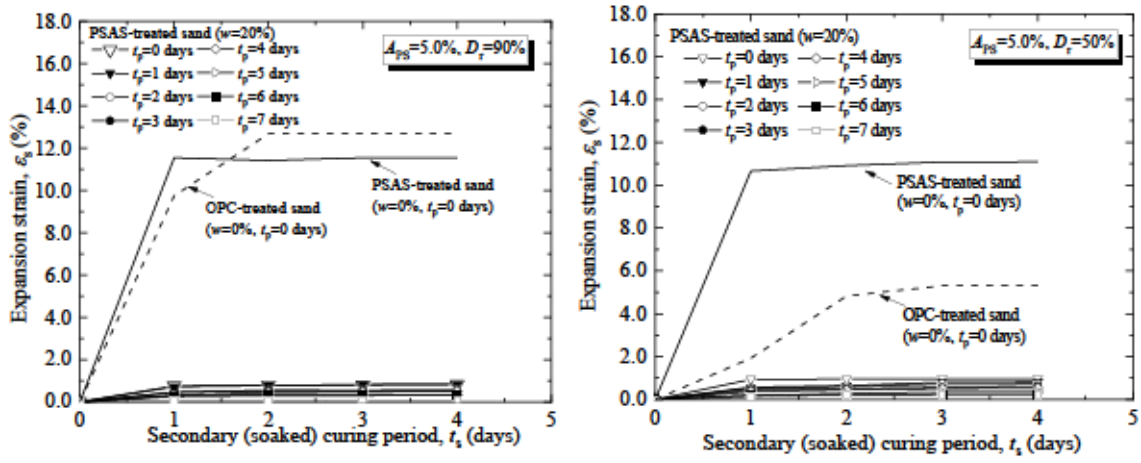


(a) $D_r = 50\%$ (b) $D_r = 90\%$

**Figure 4-5.** Expansion strain of PSAS-treated sand with $A_{PS}$ = 5.0% associated with secondary (soaked) curing period. Expansion side is indicated by positive sign.

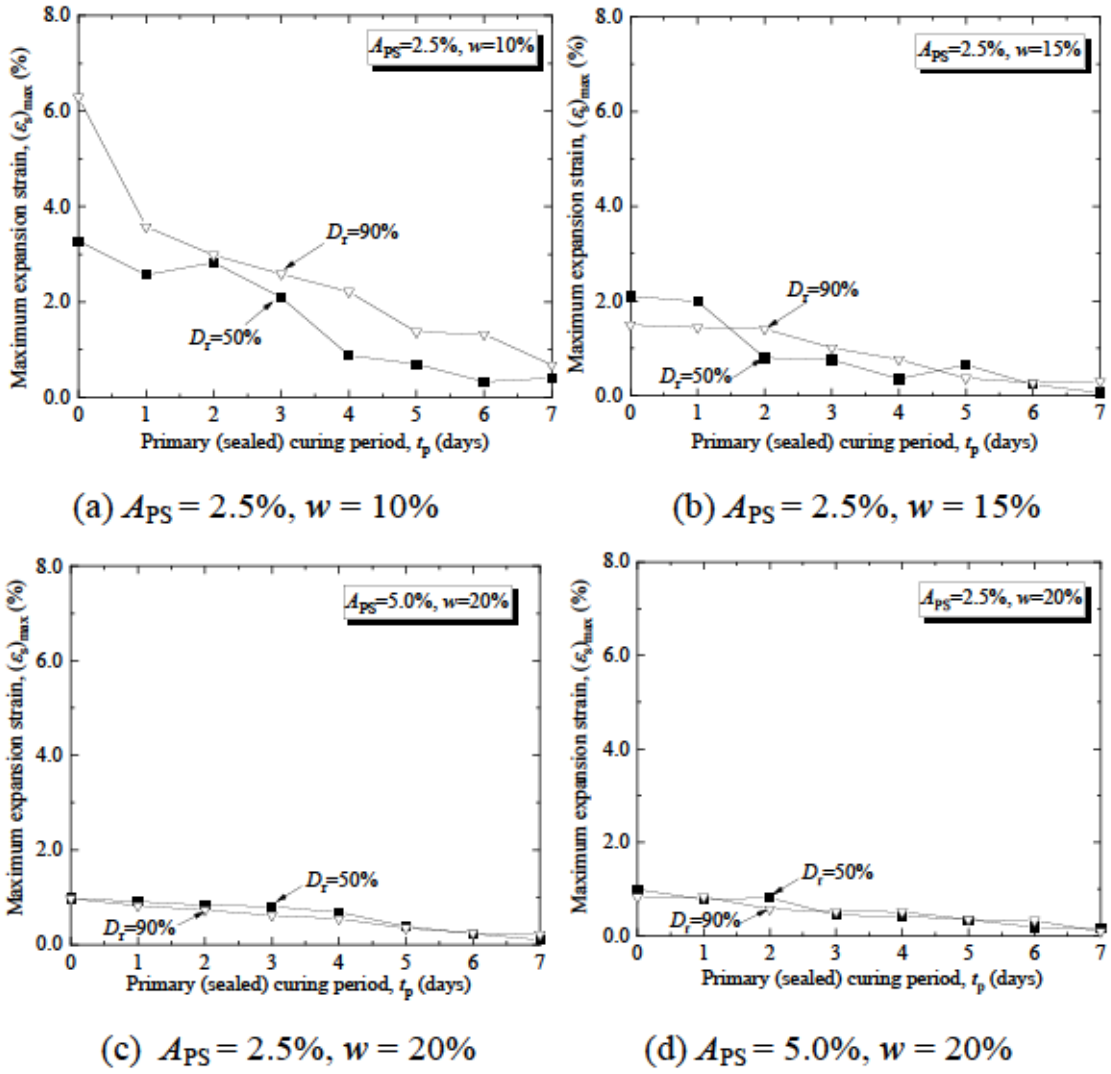


**Figure 4-6.** Relationships between maximum expansion strain of PSAS-treated sand specimens and primary (sealed) curing period. Expansion side is indicated by positive sign.

### 4.4 Isolines of $(\varepsilon_s)_{max}$ determined based on combination of $w$ and $t_p$.

According to the results presented in Figs. 4-6(a), (b), and (c), it has been found that there is no significant difference in the maximum swelling $(\varepsilon_s)_{max}$ between the specimens with $A_{PS}$ values of 2.5% and 5.0% when the moisture content ($w$) is fixed at 20%. To further understand the relationship between $(\varepsilon_s)_{max}$ and the combination of $w$ and the temporary placement duration ($t_p$), the isolines of $(\varepsilon_s)_{max}$ have been determined and are shown in Figures.4-7(a) and (b). The term "isoline" refers to the pattern of maximum expansion $(\varepsilon_s)_{max}$ and its relationship with the moisture content ($w$). The findings of this study suggest that an appropriate level of moisture content in the sand treated with PSAS can help reduce the potential for expansion, depending on the duration of its temporary

placement at the construction site. This information is essential for engineers and construction professionals in designing and constructing underground structures using PSAS-treated sand to ensure their long-term performance and stability.

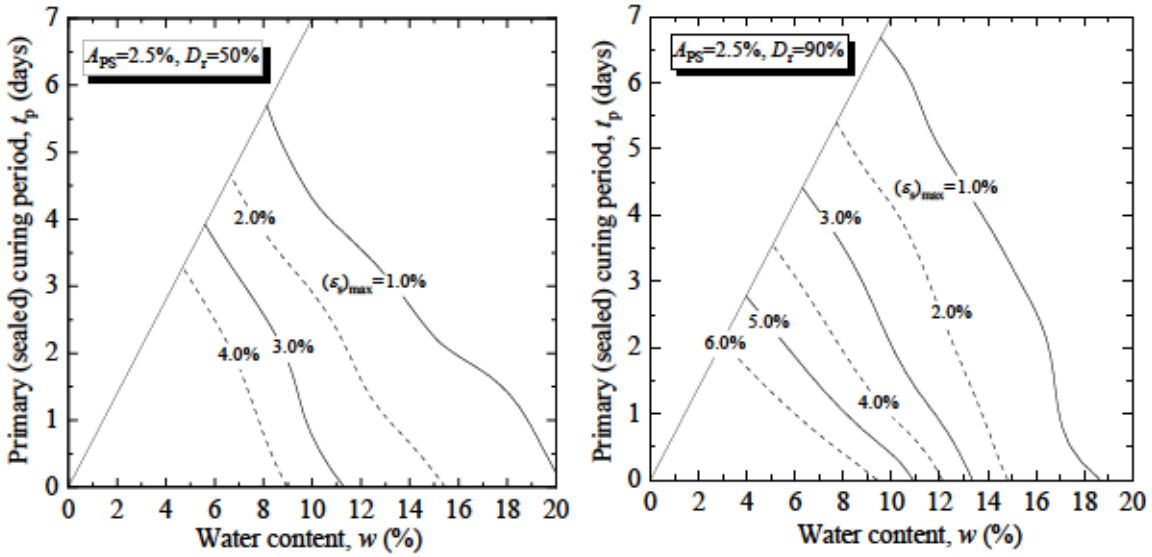


(a) $A_{PS}$ = 2.5%, $D_r$ = 50% (b) $A_{PS}$ = 2.5%, $D_r$ = 90%

**Figure 4-7.** Isolines of $(\varepsilon_s)_{max}$ determined based on combination of w and tp. Expansion side is indicated by positive sign.

# CHAPTER 5

## 5. Deformation and strength development of paper sludge ash treated sand.

This chapter focuses on the deformation and strength development of paper sludge ash (PSAS) treated sand, achieved through unconfined compression tests to assess short and long-term strength characteristics of both ordinary Portland cement (OPC) and PSAS-treated sands. A key aspect of this investigation is understanding the behaviour of the treated sand as a subgrade under traffic load, considering subbase materials and asphalt mixtures placed on top of the backfilled PSAS-treated sand. This understanding is vital to ensure the stability of underground structures, as traffic load can cause deformation and potentially compromise structural integrity. Additionally, the evaluation examines the re-excavation ability of PSAS-treated sand as a backfill material around underground pipes and manholes during maintenance works. Furthermore, the chapter explores the impact of PSAS on shear strength properties, including cohesion ($c$) and friction angle ($\phi$), as well as changes in volumetric strain resulting from PSAS inclusion in the sand matrix. This assessment is crucial for evaluating the stability and performance of buried pipes and manholes that utilize PSAS-treated sand as a backfill material. Overall, Chapter 5 offers valuable insights into the mechanical properties of the treated sand, paving the way for improved infrastructure design and performance through the use of PSAS as a stabilizing agent.

## 5.1 Strength characteristics of backfill sand around underground pipes and manholes.

A series of unconfined compression tests was conducted to investigate the strength characteristics of the OPC- and PSAS-treated sands.

### 5.2 specimen preparation of PSAS-treated sand specimen

The mixtures and curing conditions used to prepare the specimens for the unconfined compression tests are listed in Table 5-1. PSAS-treated sand specimens were prepared with and without primary curing. Based on the results presented in Section 4-3, the appropriate mixture conditions were selected to prevent the excessive expansion of treated sands and an overly high-water content, regardless of whether primary curing was performed.

To prepare the specimens for primary curing, the PSAS was mixed with Toyoura sand at $A_{PS}$ = 2.5%, 5.0%, 7.5%, and 10.0%, and the water content $w$ was adjusted to 10%. Subsequently, the mixtures were placed into cylindrical plastic molds (50 mm in diameter and 100 mm in height) and compacted to achieve $D_r$ = 50% and 90%; the molds were sealed for 3 d for primary curing. The specimens in the molds were cured in water for specified periods after the primary curing, as shown in Table 5-1. For comparison, OPC-treated sand specimens with $A_{OPC}$ = 2.5%, 5.0%, 7.5%, and 10.0% were prepared under the same conditions. The PSAS was mixed with Toyoura sand at $A_{PS}$ = 2.5%, 5.0%, 7.5%, and 10.0%, and the water content was adjusted to 20% to prepare specimens without primary curing. Subsequently, the mixtures were placed in molds and compacted to achieve $D_r$ = 50% and 90%; next, they were cured in water for specified periods, as listed in Table 5-1. Three specimens were prepared for each treatment.

In the case of PSAS-treated sand with $A_{PS}$ = 2.5%, the maximum expansion strain $(\varepsilon_s)_{max}$ was less than 3% when $w$ = 10% and $t_p$ = 3 d, as shown in Figure. 4-7. Meanwhile, the $(\varepsilon_s)_{max}$ of the PSAS-treated sand with an $A_{PS}$ of 2.5% was approximately 1% when $w$ = 20% and $t_p$ = 0 d. According to Japanese standards and laboratory tests of geomaterials associated with JGS 0721 (Japanese Geotechnical Society JGS 0721-2009, n.d.), a California bearing ratio (CBR) test specimen is generally under normal conditions as a subgrade if its expansion ratio is less than 3%, and in good condition if it is less than 1%. The conditions in Table 5-1 were determined to avoid poor subgrade conditions by referring to the thresholds above, even though the CBR test conditions were different from those of the swelling potential tests, and the test results were limited to $A_{PS}$ = 2.5% and 5.0%, as shown in Figure. 4-6. In the CBR test, the water immersion expansion of the specimen was evaluated by placing a weight on the top surface of the specimen and applying overburden pressure. However, the specimens were not subjected to overburden pressure during the swelling potential tests in this study. The mixing and curing conditions based on the results of the swelling potential tests were considered acceptable (not a risk-side evaluation) because the application of overburden pressure suppresses water immersion expansion more effectively as compared with the absence of applied pressure.

**Table 5-1.** Conditions of treated specimens for unconfined compression tests

| Addition ratio of PSAS, $A_{PS}$ (%) | Addition ratio of OPC, $A_{OPC}$ (%) | Adjusted water content, $w$ (%) | Relative density, $D_r$ (%) | Primary curing period under sealed condition, $t_p$ (d) | Secondary curing period under soaked condition, $t_s$ (d) | Total curing days, $t$ (d) |
|---|---|---|---|---|---|---|
| 2.5, 5.0, 7.5, 10.0 | 0 | 10 | 50, 90 | 3 | 0, 4, 11, 25, 57, 87,177,357 | 3, 7, 14, 28, 60, 90,180,360 |
| | | 20 | | 0 | 3, 7, 14, 28, 60, 90,180,360 | |
| 0 | 2.5, 5.0, 7.5, 10.0 | 10 | | 3 | 0, 4, 11, 25, 57, 87,177,360 | |

## 5.3 Unconfined compression test results and strength development of PSAS and OPC-treated sand with $w$=10% and $t_p$= 3d

The average unconfined compressive strength $q_u$ of the three specimens against the total curing days $t$ for each treatment condition is shown in Figures.5-1 and 5-2. Here, the values of $q_u$ are plotted on a log scale to ease the comparison of $q_u$ of the PSAS-and OPC-treated sands. The results for the specimens with $D_r$ = 50% and 90% are shown in Figures. 5-1 and 5-2, respectively. In each figure, (a) shows the results for OPC-treated sands with $w$ = 10% and $t_p$ = 3 d, (b) shows the results for PSAS-treated sands with $w$ = 10% and $t_p$ = 3 d, and (c) shows the results for PSAS-treated sands with $w$ = 20% and $t_p$ = 0 d. The $q_u$ of the specimens of PSAS- and OPC-treated sands increases with $t$. However, the $q_u$ of the OPC-treated sand is significantly higher than that of the PSAS-treated sand under the same mixing conditions.

The $q_u$ of the PSAS-treated sand with $w$ = 20% and $t_p$ = 0 d is lower than that of PSAS-treated sand with $w$ = 10% and $t_p$ = 3 d, as shown in Figs. 5-1 and 5-2. This trend is more pronounced at $D_r$ = 50%, which suggests that the concentration of the PSAS in water during compaction may affect the strength of the PSAS-treated sand. This is similar to the effect of cement paste concentration on concrete strength.

The $q_u$ of the OPC-treated sands with $w$ = 10% and $t_p$ = 3 d is compared with that of the PSAS-treated sands with $w$ = 10% and $t_p$ = 3 and 0 d, as shown in Figure. 5-3(a). Similarly, the $q_u$ of the OPC-treated sands with $w$ = 10% and $t_p$ = 3 d is compared with that of the PSAS-treated sands with $w$ = 20% and $t_p$ = 0 d, as shown

in Figure. 5-3(b). The $q_u$ of the OPC-treated sands is approximately 7.4 to 14.1 times larger than that of the PSAS-treated sands.

In his chapter (Kohata, 2006) regarding liquefied stabilized soils, Kohata stated that when liquefied stabilized soils are used as backfill for open-cut tunnels, the unconfined compressive strength is often set to 490 kPa or less because of the possibility of re-excavation. Meanwhile, in a previous study (Hosoya Y et al., n.d.), excavation experiments on soils treated with cement and lime were conducted at various unconfined compressive strengths $q_u$. Consequently, a $q_u$ of 500 kPa or less is shown to be desirable for efficient manual excavation without using a pick or breaker. The $q_u$ values at 500 kPa are shown as dashed lines in Figures.5-3 and 5-4. The $q_u$ of the OPC-treated sand with $A_{OPC}$ = 5% either exceeded 500 kPa from the beginning (Fig. 5-2(a)) or exceeded 500 kPa in the middle of curing (Figure. 5-2(b). Conversely, the $q_u$ of the PSAS-treated samples with $A_{PSAS}$ = 5% barely exceeded 500 kPa during 90 d of curing. This indicates that the PSAS-treated sand may be more easily re-excavated than the OPC-treated sand. An addition rate of 5% was applied because the minimum addition ratio of OPC and PSAS in most practical cases is 50 kg/m$^3$ in consideration of mixing homogeneity, which corresponds to an addition rate of approximately 3.3%.

The relationship between $q_u$ and $t$ was investigated to determine the characteristics of the strength development of the PSAS-treated sand during curing, as shown in Figures.5-1 and 5-2. The value of $q_u$ is approximated as follows:

$$q_u\,(kPa) = 10^{\alpha+\beta\cdot t} \quad (3 \le t(d) \le 90), \qquad \text{Eq. 5-1}$$

$$q_u\,(kPa) = 10^{\alpha} \quad (90 \le t(d) \le 360)\ where\ \beta = 0 \qquad \text{Eq. 5-2}$$

where $\alpha$ represents the degree of initial strength, and $\beta$ the degree of strength increases after curing. The approximation results are shown in Figure. 5-4.

The relationship between $q_u$ and $t$ for the OPC-treated sand was approximated for comparison using Eq. (5-1). Parameters $\alpha$ and $\beta$ in Eq. (5-1) were obtained from the approximation and plotted against $A_{PS}$ and $A_{OPC}$ in Figures. 5-5(a) and (b), respectively. The PSAS-treated sand shows lower values of $\beta$ and $\alpha$ than the OPC-treated sand at the same addition rate. The PSAS-treated sand shows a lower value $\beta$ than the OPC-treated sand for the same value of $\alpha$, as shown in Fig. 19(c). For example, when the initial strength of the PSAS- and OPC-treated sands is approximately $q_u = 10^{2.0}$ kPa (i.e., $\alpha$ = 2.0), the increase in strength with subsequent curing is more gradual in the PSAS-treated sand than in the OPC-treated sand. This suggests that the PSAS-treated sand is easier to re-excavate than the OPC-treated sand because of the slower increase in strength.

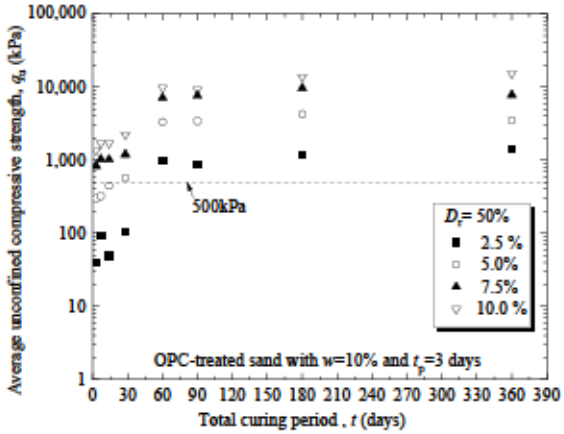


(a) OPC-treated sand with $w$ = 10% and $t_p$ = 3 d

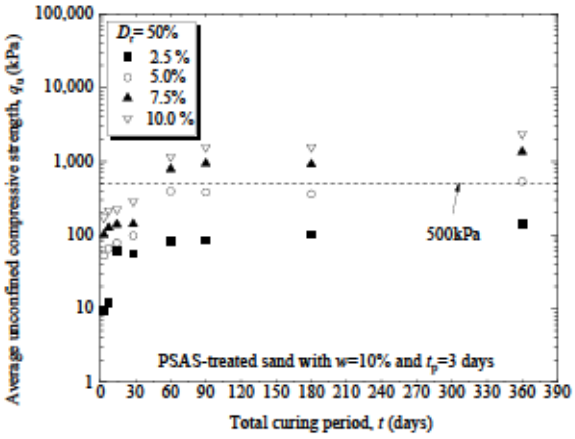


(b) PSAS-treated sand with w = 10% and $t_p$ = 3 d

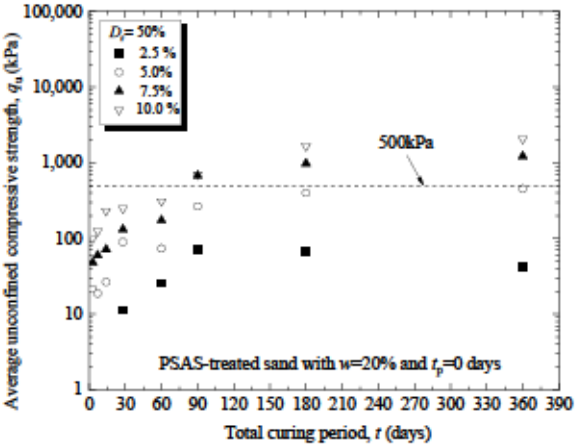


(c) PSAS-treated sand with $w$ = 20% and $t_p$ = 0 d

**Figure 5-1.** Relationships between unconfined compressive strength $q_u$ and total curing period $t = t_s + t_p$ ($D_r$ = 50%)

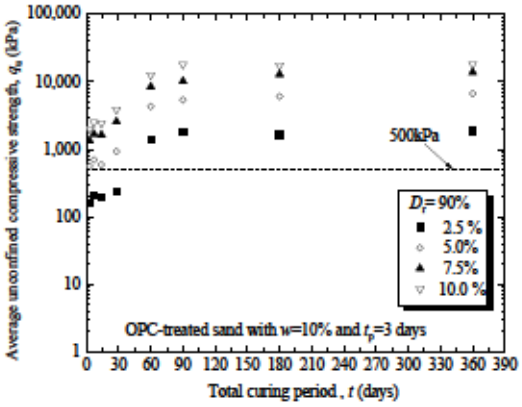


(a) OPC-treated sand with $w$ = 10% and $t_p$ = 3 d

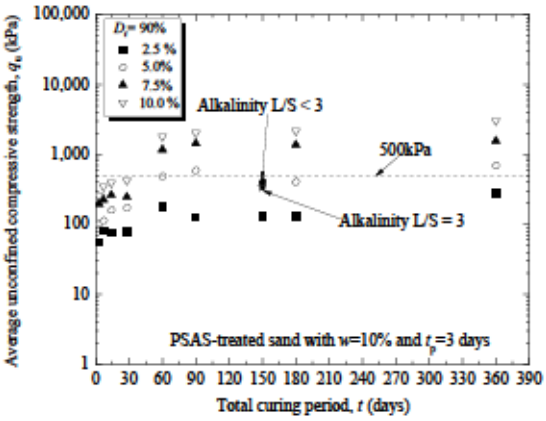


(b) PSAS-treated sand with w = 10% and $t_p$ = 3 d

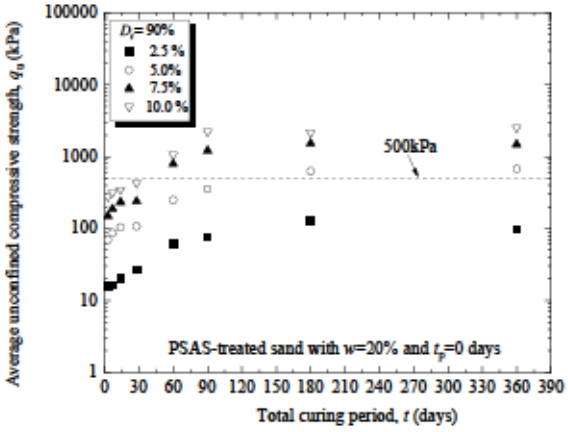


(c) PSAS-treated sand with $w$ = 20% and $t_p$ = 0 d

**Figure 5-2.** Relationships between unconfined compressive strength $q_u$ and total curing period $t = t_s + t_p$ ($D_r$ = 90%)

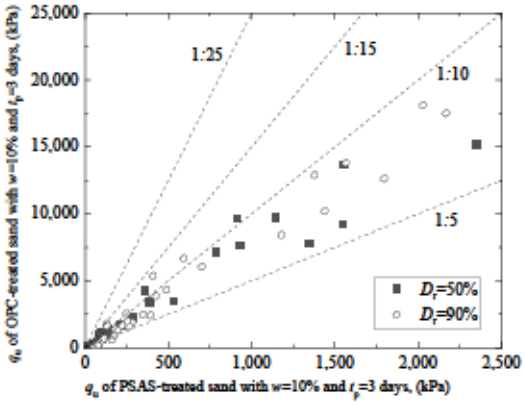


(b) PSAS-treated sand with $w$ = 10% and $t_p$ = 3 d

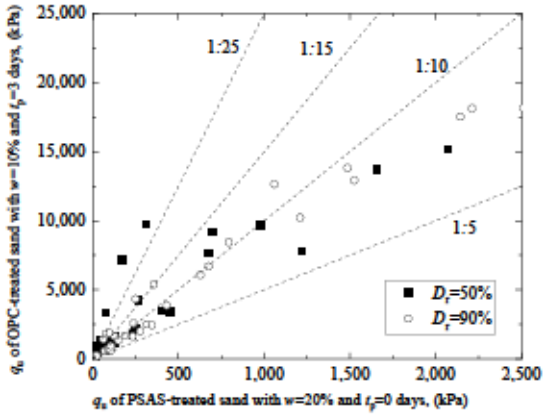


(c) PSAS-treated sand w = 20% and tp = 0 d

**Figure 5-3.** Comparison of unconfined compressive strength of PSAS- and OPC- treated sand with $w$ = 10% and $t_p$ = 3 d.

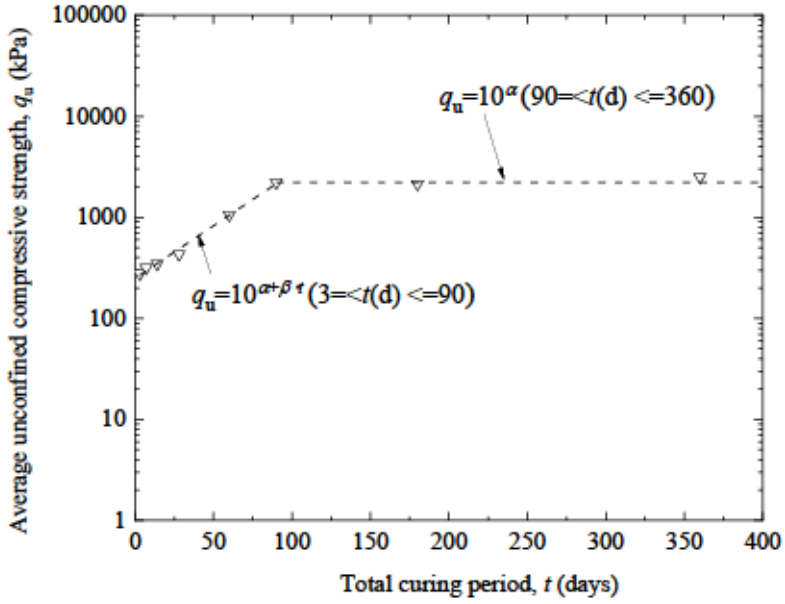


**Figure 5-4.** Example of fitting relationship between $q_u$ and $t$ using Eq. (5-1).

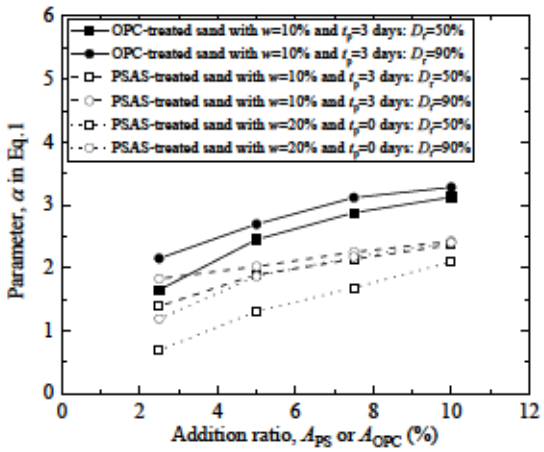


(a) Changes in parameter $\alpha$ as a function of $A_{PS}$ or $A_{OPC}$

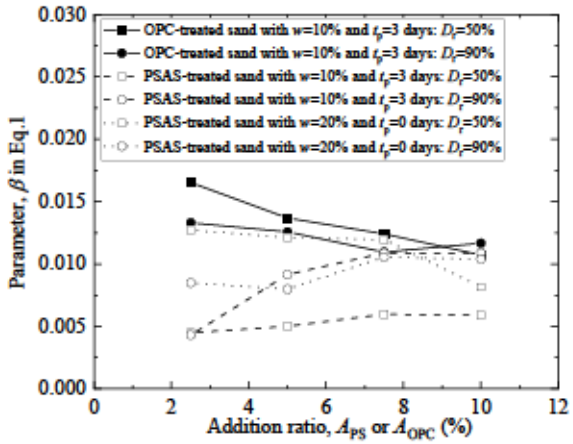


(b) Change in parameter $\beta$ as a function of $A_{PS}$ or $A_{OPC}$

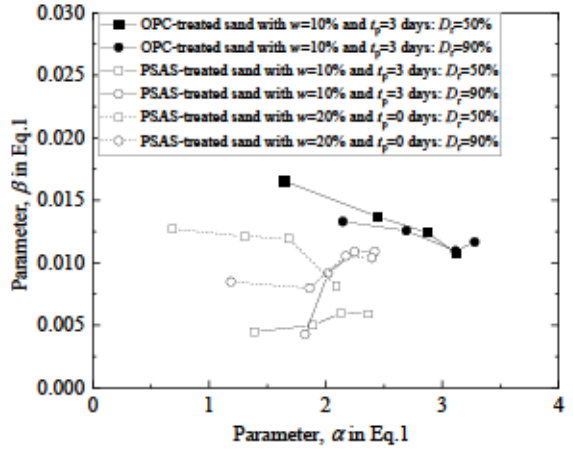


(c) $\alpha$–$\beta$ relationships

**Figure 5-5.** Comparison of parameters α and β between PSAS- and OPC-treated sands

## 5.4 XRD profiles and hydrates contribution to strength

The strength of the PSAS-treated sand increased gradually with age, as described in the previous section. XRD tests were conducted on PSAS-treated sand prepared by mixing the PSAS with Toyoura sand with an $A_{PS}$ of 10% to investigate the hydrates contributing to the strength increase with time. The water content of the mixture was adjusted to 20%. Subsequently, the mixtures were placed in molds and compacted to achieve $D_r = 90\%$; subsequently, they were cured in water for 7, 28, 90, and 180 d.

After the prescribed curing, the PSAS-treated sand was crushed in a ceramic mortar using a pestle and soaked in iso-propanol for 2 h. Next, vacuum filtration was performed to remove the alcohol, and the sample was placed in a vacuum oven set to 40 °C for 1 d. Immersing treated sand in alcohol halted the hydration reaction. The treated sand was passed through a 0.075 mm sieve, and XRD analysis was conducted on the resulting powders.

The XRD results are shown in Figure. 5-6. The XRD pattern shows that the formation of calcite ($CaCO_3$) was dominant in the PSAS-treated sand at curing periods of 7, 28, 90, and 180 d. By performing soaked curing, some of the Ca $(OH)_2$ that can be formed based on the reaction shown in Eq. (1) are expected to react with $CO_2$ dissolved in water to produce $CaCO_3$, as shown in the following reaction:

$$Ca(OH)_2 + CO_2 \rightarrow CaCO_3 + H_2O \quad (4)$$

Similarly, the ettringite produced via the reaction shown in Eq. (2) are expected to produce $CaCO_3$ as follows:

$$3CaCO_3 + 2Al(OH)_3 + 3CaSO_4 + 29H_2O \rightarrow 3CaO{\cdot}Al_2O_3{\cdot}3CaSO_4{\cdot}32H_2O + 3CO_2 \quad (5)$$

Subsequently, the generation of $CaCO_3$ is expected to reduce the pH of the treated sands. Therefore, the change in pH of the water in which the PSAS-treated sand with cylindrical molds was immersed was investigated. The same investigation was conducted on the OPC-treated sand specimens for comparison. The results are shown in Fig. 5-7. Although the pH of the PSAS-treated sand was not directly measured, the pH of the water surrounding the PSAS-treated sand decreased over time, based on observation.

A detailed analysis of the results in Figure 5.7 indicates that, in addition to $CaCO_3$, berlinite ($AlPO_4$) may contribute additionally to the increase in strength of the PSAS-treated sand in the long term. In fact, this was observed previously in soils treated with coal ash (Ayob et al., 2014) (Zhou et al., 2019).

Moreover, the primary contributor to the strength development in PSAS-treated sand is the pozzolanic reaction. PSAS, like other pozzolanic materials, contains reactive silica and alumina compounds. During curing, water molecules penetrate the PSAS particles, initiating a chemical reaction with the calcium hydroxide (Ca (OH)2) released from cement hydration (Eq.5). This reaction forms additional calcium silicate hydrate (C-S-H) gel and calcium aluminate hydrate (C-A-H) phases, which act as binding agents within the sand particles (see SEM figure 5-9)(Kitazume & Okamura, 2010),(Stavridakis, 2005), (Yao & Sun, 2012) This continuous pozzolanic reaction contributes to the long-term strength of the treated sand.

As shown in SEM images (fig 5-8), Together with the microstructure refinement Over an extended curing period, the pozzolanic reaction leads to the formation of a denser microstructure within the treated sand matrix. The new crystalline phases fill the voids and pores between sand particles, resulting in a more compact and interlocked structure. This microstructure refinement enhances the sand's cohesion and reduces its porosity, which are critical factors for maintaining strength.

Finally, unlike conventional cementitious materials, where the majority of strength gain occurs rapidly during the early stages of curing (Ramaji, 2012),(Subramanian et al., 2019) PSAS-treated sand exhibits a more gradual strength development. This characteristic is advantageous because it allows the sand to continue gaining strength over time. The slower rate of strength development indicates that PSAS-treated sand is less prone to early-age cracking and damage in an environment where the temperature changes is not important, making it a robust choice for long-term applications.

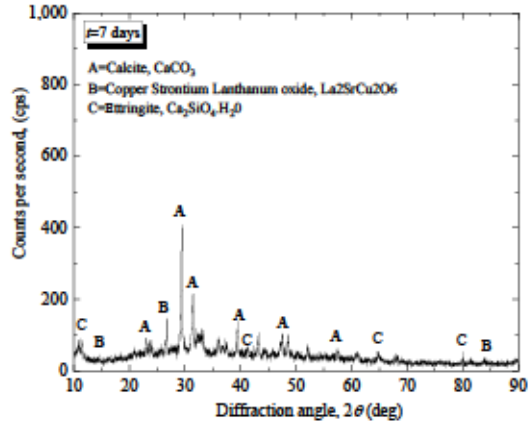


(a) $t = 7$ days

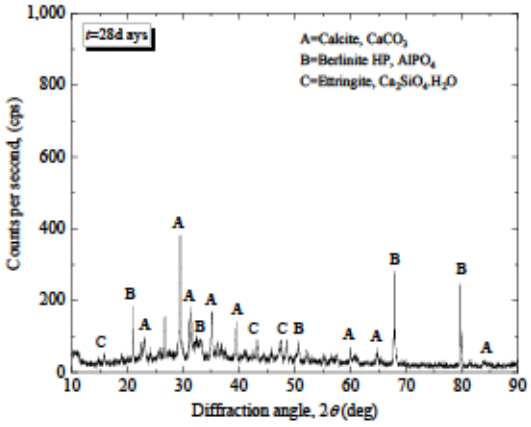


(b) $t = 28$ days

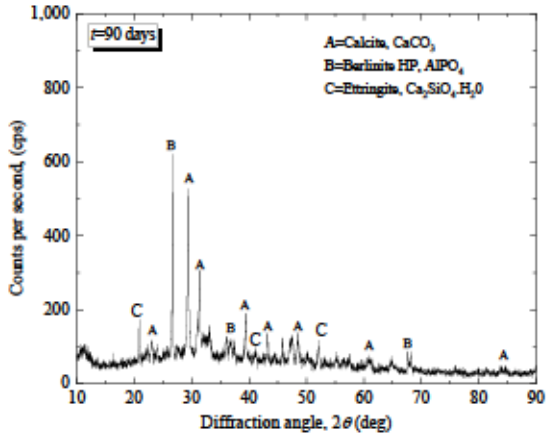


**(c) $t = 90$ d**

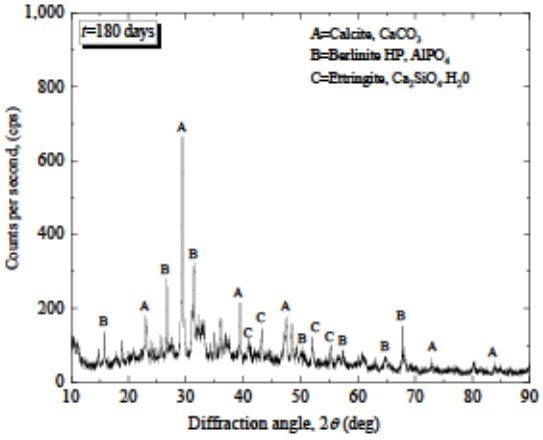


**(d) $t = 180$ d**

**Figure 5-6**. XRD profiles of PSAS-treated sand with w = 20% and tp = 0 d

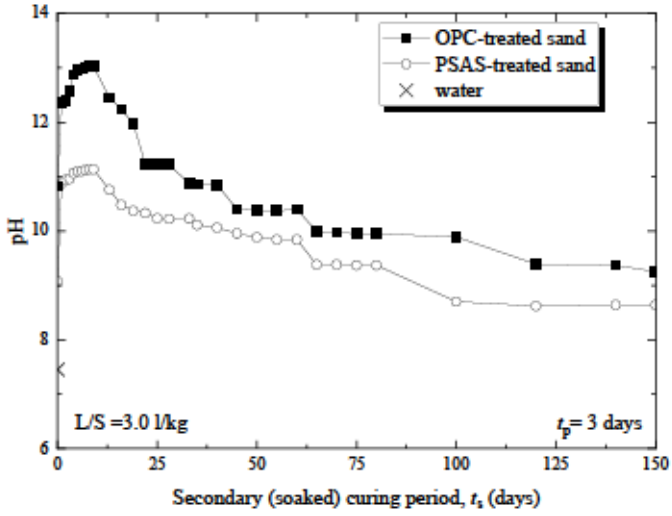


**Figure 5-6** Change in pH of water in which treated sands with cylindrical moulds were immersed.

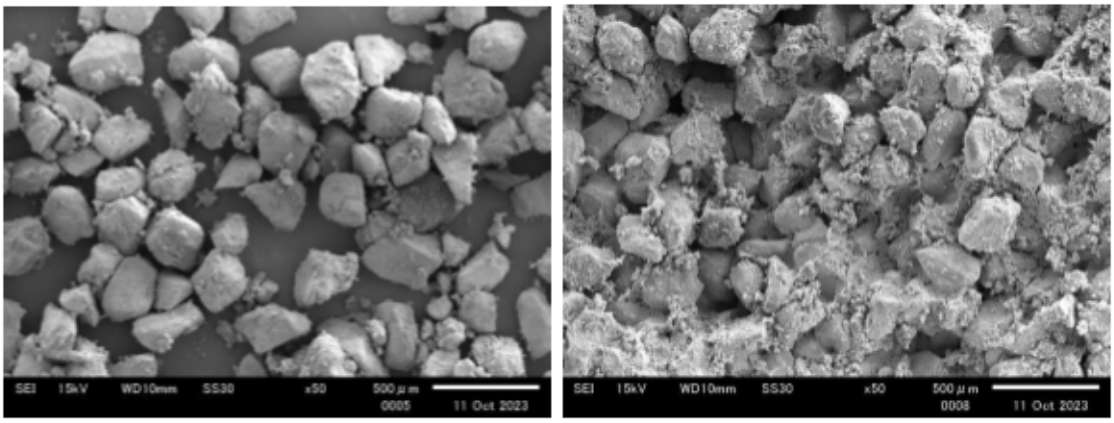

(a) Without Soaking (b) With soaking

**Figure. 5-8** SEM images of PSAS-treated sand with and without soaking

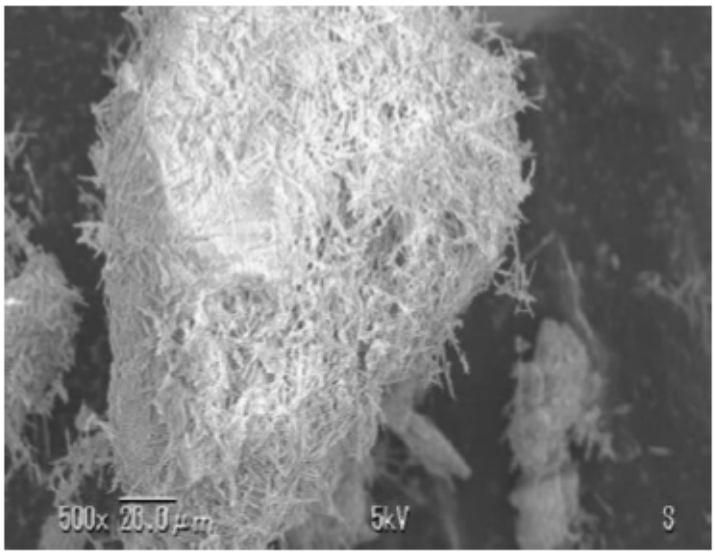


**Figure.5-9** Formation of needle-like crystals (ettringite) in PSAS.

## 5.5 Deformation characteristics of Backfilled sand around underground pipes and manholes

Subbase materials and asphalt mixtures can be arranged on top of the PSAS-treated sand and accessed by traffic after backfilling is performed around a buried pipe. In this case, the PSAS-treated sand becomes deformed under the effect of traffic load as a subgrade. The stress–strain relationships obtained from the unconfined compression tests for evaluating the deformation modulus of the PSAS-treated sand are presented in this section.

Bedding errors caused by loose layers of the upper and lower ends of a specimen can be problematic when evaluating the deformation modulus of cement-treated sand specimens based on the stress–strain relationship (Tatsuoka et al., 1997). Therefore, in the unconfined compression tests, a pair of linear variable differential transformers was installed on the lateral sides of the cylindrical

specimens (50 mm diameter and 100 mm height) to directly measure the axial strain (Maqsood, Koseki, Ahsan, et al., 2020) (Maqsood, Koseki, Miyashita, et al., 2020). The test specimens were prepared using PSAS-treated sand with $w$ = 20% and $t_p$ = 0 d, as listed in Table 5-1. Three specimens were prepared for each treatment.

The stress–strain curves obtained from the unconfined compression tests of the PSAS-treated sand with $D_r$ = 90% are shown in Figure. 5-8(a). In the figure, axial strains measured directly on the lateral sides of the specimens are denoted as "local measurement," and axial strains measured from the displacements of the loading rod are denoted as "external measurement." (Maqsood, Koseki, Ahsan, et al., 2020) (Maqsood, Koseki, Miyashita, et al., 2020) The externally measured axial strain is higher than that of the local measurement, regardless of the $A_{PS}$, thereby confirming the effect of the bending error on the externally measured axial strain. Therefore, the deformation modulus is evaluated using locally measured axial strain, as shown in Figure. 5-8(b). The secant deformation modulus $E_{0.02\%}$ at an axial strain of 0.02% is evaluated because the strain in a subgrade owing to traffic loads is often approximately 0.01% (Puppala et al., 2009), as shown in Figure. 5-8. The relationship between $E_{0.02\%}$ and $q_u$ is illustrated in Figure. 5-9. The values of $E_{0.02\%}$ and $q_u$ are shown in Figure. 5-9 are the averages values of the three sets of results obtained for the same sample. The value of $E_{0.02\%}$ is approximately $q_u \times 3000$.

regardless of the difference in $D_r$. However, it decreases by 3000 times when $q_u$ is below 100 kPa.

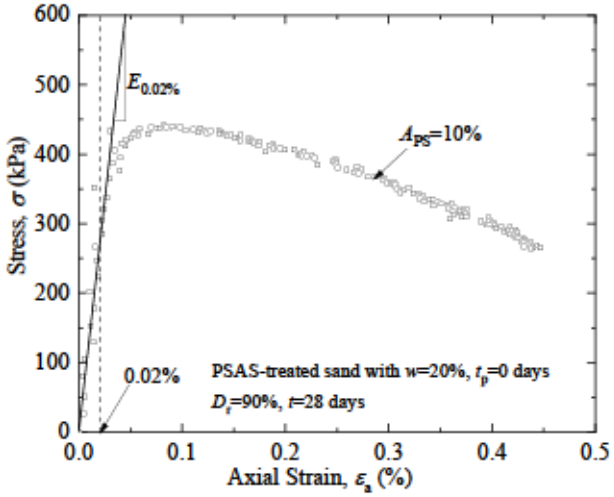


(a) External and locally measured axial strains

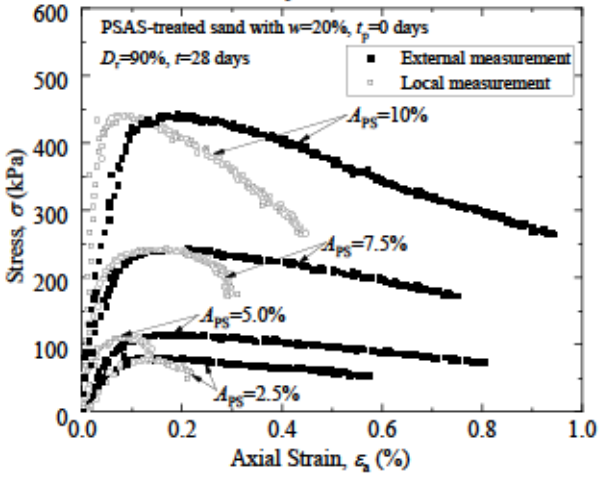


(b) Evaluation of deformation modulus $E_{0.02\%}$

**Figure 5-7.** Examples of externally and locally measured axial strains, and evaluation of deformation modulus E0.02%

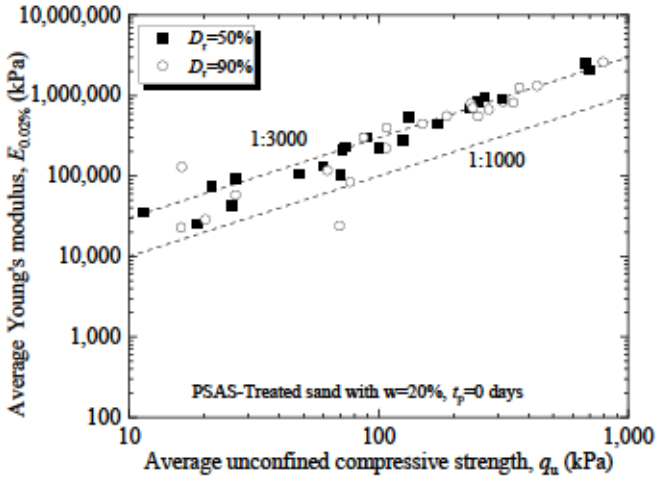


**Figure 5-8.** Relationships between deformation modulus E0.02% and unconfined compressive strength $q_u$.

### 5.6 Strength increases ratio with curing period.

The assessment of backfill treated sand's improvement using the strength increase ratio offers several advantages over a direct measurement of compressive strength at various curing periods. Primarily, the strength increase ratio facilitates a comparative analysis of treated sand strength at different curing periods ($t$=7, 14, 28, 60, 90, 180, and 360 days) against the strength at $t$=3 days. This method effectively gauges the efficacy of PSAS in contrast to OPC treatment in enhancing sand strength over time, aiding in the identification of the most effective treatment for stabilizing backfill sand strength in the viewpoint of its re-excavation ability. Secondly, utilizing a normalized strength increase ratio ensures a consistent and reliable comparison among different types of treated sand. By referencing the unconfined compressive strength at 3 days curing period, variations in the strength increase ratio can be attributed to differences in treatment methods rather than variances in initial sand strength.

In Figure 5-9, depicting the relationships between the strength ratio ($SR$) and total curing periods for OPC-treated sand ($w$ = 10%, $t_p$ = 3 days), PSAS-treated sand ($w$ = 10%, $t_p$ = 3 days), and PSAS-treated sand ($w$ = 20%, $t_p$ = 0 days), an upward trend in the strength ratio with increasing curing periods is evident. Interestingly, the PSAS-treated sand with 20% water content and no premixing ($t_p$ = 0 days) consistently exhibits the highest strength ratio compared to PSAS-treated sand at $t_p$=3 days, $w$=10%, and OPC-treated sand $t_p$=3 days, $w$=10%. This observation contrasts with its strength stabilization characteristics discussed in the preceding section. This study emphasizes the re-excavation ability of PSAS-treated sand due to limitations in strength development when the PSAS ratio $A_{PS}$=2.5%-5% to 500 kPa. oreover, Figure 5-10 extends these observations to a higher degree of saturation ($D_r$ = 90%) for the same types of sand. Similar to Figure 5-9, an increase in strength ratio is noted with prolonged curing periods. The PSAS-treated sand with 20% water content and $t_p$ = 0 days continues to exhibit the highest $SR$ at all curing periods. Importantly, the values of $SR$ are generally higher in Figure 5-10 due to the higher $D_r$ value ($D_r$=90%).

Overall, Figure 5-10 reinforces the efficacy of PSAS treatment, particularly with higher water content and no premixing. It underscores that enhancing the degree of saturation further improves treated sand strength. This practical insight from Figure 5-10 aids specialists and engineers in determining the optimal treatment combination (sand type, water content, premixing) and curing period to achieve the desired strength ratio, enhancing the stability and safety of structures on backfill. In conclusion, the strength increase ratio proves to be a vital tool for measuring and comparing the effectiveness of various backfill treated sands in

enhancing sand strength—an essential aspect for ensuring the stability and safety of structures built on backfill.

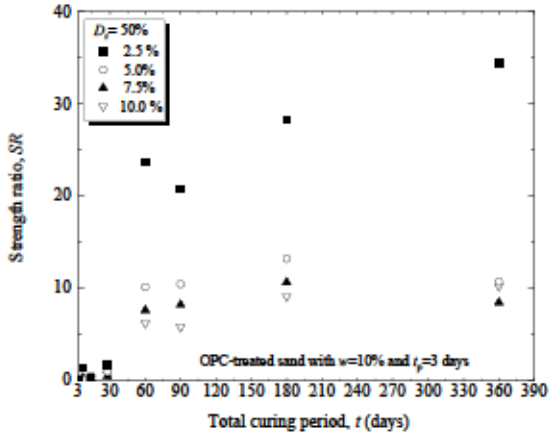


(a) OPC-treated sand with $w = 10\%$ and $t_p = 3$ d

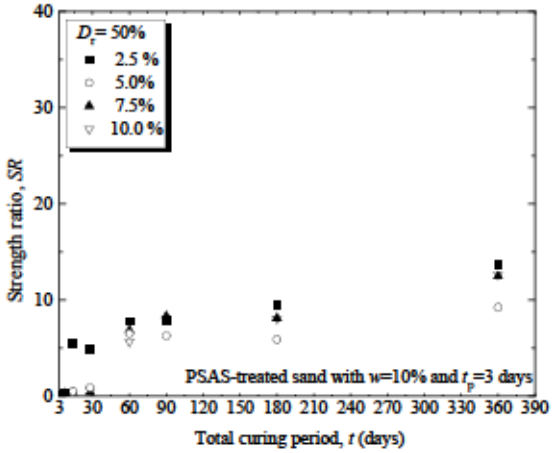


(b) PSAS-treated sand with $w = 10\%$ and $t_p = 3$ d

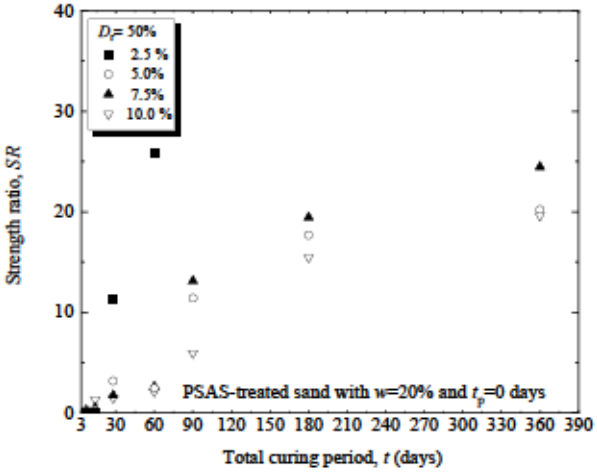


(c) PSAS-treated sand with $w = 20\%$ and $t_p = 0$ d

**Figure 5-9.** Relationships between strength ratio (SR) and total curing period $t = t_s + t_p$ ($D_r = 50\%$).

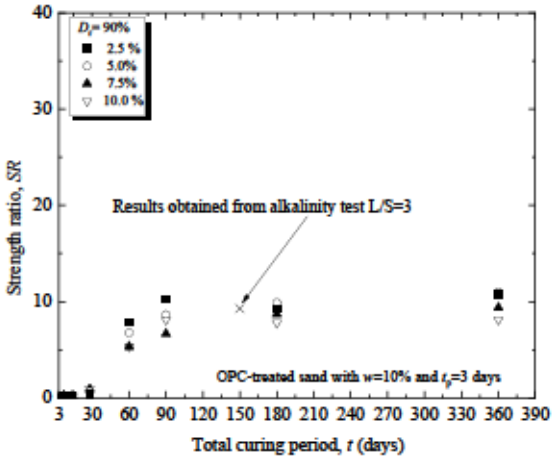


(a) OPC-treated sand with $w$ = 10% and $t_p$ = 3 d

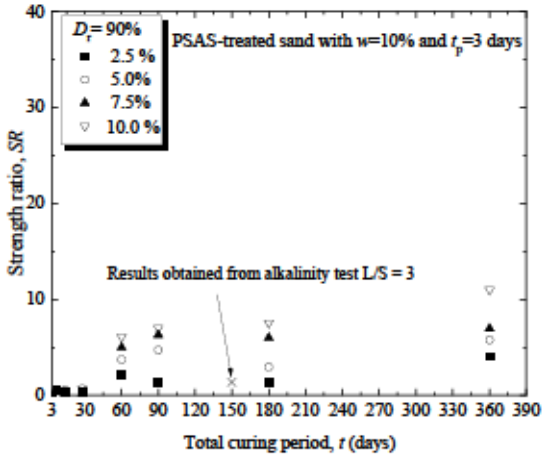


(b) PSAS-treated sand with $w$ = 10% and $t_p$ = 3 d

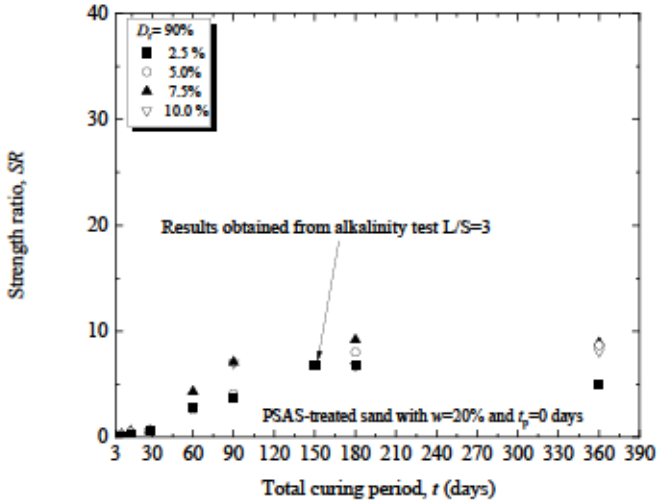


(c) PSAS-treated sand with $w$ = 20% and $t_p$ = 0 d

**Figure 5-10.** Relationships between strength ratio (SR) and total curing period $t = t_s + t_p$ ($D_r$ = 90%).

## 5.7 Shear strength development of PSAS-treated sand

The uses of PSAS in treating sand has shown promising results in improving of strength and overall performance of the treated soil (Mochizuki et al., 2003), (Kawai et al., 2018). PSAS is derived from the in solubilization of heavy metals in paper sludge ash, which is a waste product generated during the incineration of paper sludge. This eco-friendly stabilizer offers several advantages, including its potential to reduce $CO_2$ emissions compared to conventional cement- or lime-based stabilizers (Imai et al., 2020) (Trung et al., 2021).

This section focuses on investigating the effect of PSAS on the shear strength characteristics of PSAS-treated sand. The aim is to evaluate the improvements in shear strength parameters, such as cohesion ($c$) and friction angle ($\phi$), resulting from the incorporation of PSAS into the sand matrix. Understanding the changes in shear strength properties is crucial for assessing the stability and performance of buried pipes and manhole that utilize PSAS-treated sand as a backfill material.

To achieve this objective, a comprehensive experimental program involving consolidated drained triaxial tests was conducted. The triaxial tests allowed for the measurement of shear strength parameters under controlled laboratory conditions. The results obtained from these tests provide valuable insights into the shear strength behaviour of PSAS-treated sand and contribute to the existing knowledge in the field of Backfill material.

The triaxial test device was used to subject the treated sand samples to varying levels of effective stress, including $\sigma_c' = 50$ kPa, 100 kPa, and 200 kPa. The consolidated drained triaxial test was conducted to simulate the behavior of the treated sand under realistic field conditions. By subjecting the treated sand samples to different levels of effective stress, the study aimed to assess the influence of PSAS treatment on the shear strength development of the sand. The results of the triaxial tests were analyzed to determine the impact of the treatment on the shear strength parameters of the sand, such as the cohesion and internal friction angle.

In the following sections, the experimental setup, testing procedures, and the results of the consolidated drained triaxial tests will be presented and discussed in detail. The implications of the findings and their significance for geotechnical practice will be highlighted, followed by suggestions for future research in this area.

**Table 5-2.** Conditions of PSAS-treated specimen for Drained triaxial test

| Consolidation stress, $\sigma_c$' (kPa) | Addition ratio of PSAS, $A_{PS}$ (%) | Adjusted water content, $w$ (%) | Relative density, $D_r$ (%) | Primary curing period under sealed condition, $t_p$ (d) | Secondary curing period under soaked condition, $t_s$ (d) | Total curing days, $t$ (d) |
|---|---|---|---|---|---|---|
| Toyoura sand | | | | | | |
| 50,100, 200 | 0 | 20 | 50, 90 | 0 | 0 | 0 |
| PSAS-treated sand | | | | | | |
| 50,100, 200 | 5.0 | 20 | 50, 90 | 1 | 3, 7, 14 | 4, 8, 15 |

### 5.6.1 Specimen preparation and test program for CD test

For consolidated drained triaxial (CDT) test specimen preparation, the sample preparation technique suggested by Ladd (Dobry & Ladd, 1980) was adopted. Dry Toyoura sand was first mixed with the PSAS with $A_{PS}$ = 5.0% The $A_{PS}$ was the dry mass ratio of PSAS to Toyoura sand. Immediately after mixing, the water content $w$ of the treated sand was adjusted to 20% as appropriate mixture conditions to prevent the excessive expansion of treated sand and an overly high water content (Djandjieme et al., 2022).Thus, the mixtures were placed into cylindrical plastic molds (50 mm in diameter and 100 mm in height) and compacted to achieve $D_r$= 50% and 90%; the molds were exposed to air-precuring for $t_p$=1 days before it is remolded for triaxial compression tests. The specimens in the molds were cured in water for specified periods after the primary curing, as shown in Table 5-2.

### 5.6.3 Experimental set-up for Consolidated drained triaxial test (CDT)

In accordance with the Japan Geotechnical Society standards 0520-0524, consolidated (CD) triaxial tests were conducted on both traditional Toyoura sand and treated PSAS sand obtained from remoulded cylindrical specimens, as described in Section 5.6.1. For the CD test on Toyoura sand, the wet tamping method was employed for sample preparation. Oven-dried soil was mixed with distilled water in a weight proportion of 20% and compacted in three layers to achieve the desired relative densities of 50% and 90% (as presented in Table 5-2). The $D_r$=50% represent the loosest state of treated sand and the $D_r$=90% the

densest state of treated sand. Regarding the treated PSAS sand, after the specific curing period each specimen was remoulded, it was placed in a triaxial test pressure chamber and sealed using a rubber sleeve, as depicted in Figure 5-12. After detaching the mould, the cell was installed, and water was introduced to fill the cell while simultaneously removing the vacuum. A double vacuum pump was used to aid saturation. De-aired water was then flushed through the sample, and a prescribed back pressure was applied to achieve a saturation level of 95% or higher. Consolidation stress of $\sigma_c' = 50$ kPa, 100 kPa, and 200 kPa were applied for the consolidated drained tests. The drainage water-pressure measurement route was left open to ensure a drained condition within the specimen. To prevent pore pressure from developing within the composite structure, the specimens were subjected to slow shearing at a rate of 0.074 mm/minute. Throughout the experiment, the values of deviator stress and axial strains and volumetric strain were continuously recorded. The experiment was concluded upon reaching 15% axial strain.

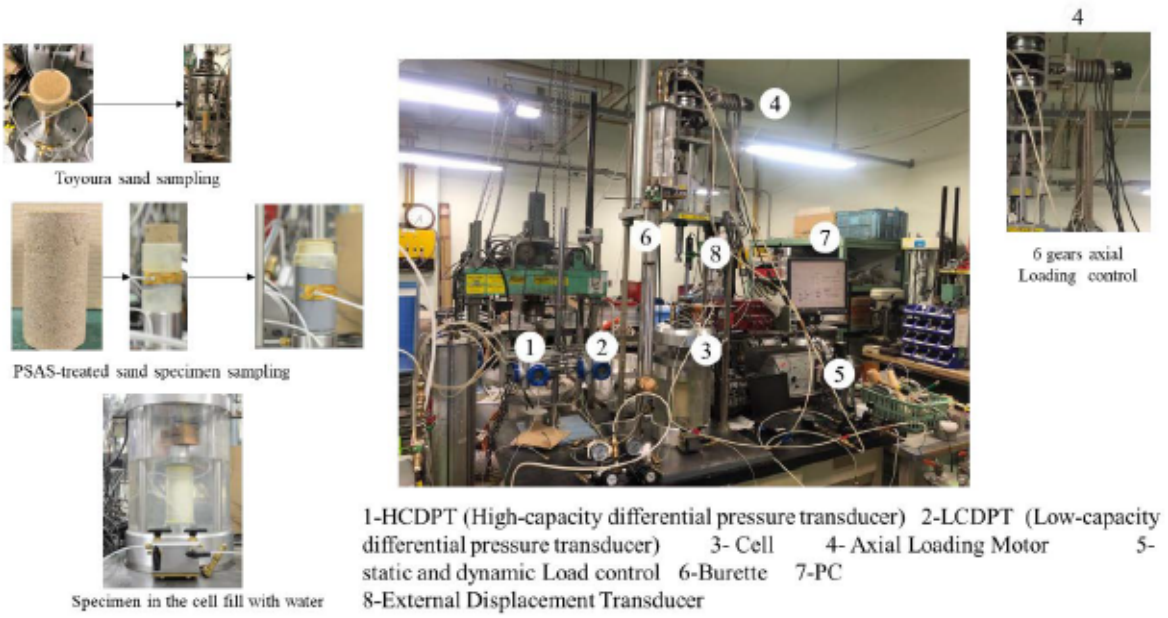


**Figure 5-11** Triaxial testing apparatus.

### 5.6.4 Stress-strain and volumetric strain relationship of PSAS-treated sand

Figures 5-11&5-12 show the deviator stress-strain and volumetric strain relationship for PSAS-treated sand compacted at $D_r$=50% (looses-state of sand) and $D_r$=90% (densest-state of sand), respectively.

The dilation behaviour refers to the increase in volume of the treated sand under shear deformation, while the contraction behaviour refers to the decrease in

volume of the treated sand under shear deformation. Increase in confining pressure increased initial contraction and decreased the residual dilation.

Looking at figure 5-13 where Deviator stress-strain and volumetric-strain relationships ($D_r$=50%) are plotted for (a)- Toyoura sand, (b)-PSAS-treated sand t= 4 days, (c)-PSAS-treated sand $t$= 8 days, (d)-PSAS-treated sand $t$= 15 days, we see that the deviator stress of Toyoura sand and PSAS-treated sand increases gradually as the axial strain increases. Besides, it was found that there was a significant increase in the maximum deviatoric stress with an increase in the confining pressure. However, the deviator stress of PSAS-treated sand is consistently higher than that of Toyoura sand. Additionally, the treated sand showed a dilation behaviour as evidenced by the negative volumetric strain curve. The higher shear strength of the treated sand can lead to a more pronounced dilation behaviour, as the treated sand can withstand higher shear stresses before undergoing significant deformation.

In figure 5-14, Deviator stress-strain and volumetric-strain relationships ($D_r$=90%) are plotted for, (a)- Toyoura sand, (b)-PSAS-treated sand $t$= 4 days, (c)-PSAS-treated sand $t$= 8 days, (d)-PSAS-treated sand $t$= 15 days. We see that the deviator stress-strain relationship for PSAS-treated sand compacted at $D_r$=90% is also higher than that of Toyoura sand. The slope of the stress-strain curve is steep at the beginning of the test (low axial strain) but decreases as the axial strain increases. Thus, the PSAS-treated sand has a lower volumetric strain compared to Toyoura sand at the same axial strain level. This indicates that the PSAS-treated sand has a lower compressibility than Toyoura sand alone. The lower compressibility of the treated sand can lead to a more pronounced dilation behaviour, as the treated sand can withstand higher axial stresses before undergoing significant deformation.

Figure 5-15 and Figure 5-16 show the effect of the effective stress on the effective stress path of PSAS-treated sand and Toyoura sand. Figure 5-15 shows the stress paths for Toyoura sand and PSAS-treated sand compacted at $D_r$=50%. As the applied stress increased from $\sigma_c' =$ 100 kPa to 200 kPa, the stress paths for both materials shifted further to the right on the deviator stress axis. The stress paths also became steeper. However, it is notable that the stress paths for the PSAS-treated sand are higher than those for Toyoura sand at all stress levels, indicating a higher shear strength for the treated sand compared to Toyoura sand. The effective stress path refers to the path followed by the effective stress during shear deformation of the treated sand. The effective stress is the stress that is transmitted between the sand particles, and it is related to the shear strength of the treated sand.

Figure 5-16 shows that the effective stress path of the PSAS-treated sand compacted at $D_r$=90% is more linear compared to the effective stress path of Toyoura sand. This indicates that the PSAS-treated sand undergoes less deformation under shear stress compared to Toyoura sand. The less pronounced deformation behaviour of the treated sand can be attributed to the lower compressibility of the treated sand, which allows it to withstand higher axial stresses before undergoing significant deformation. The effect of the applied stress on the effective stress paths is similar to that observed for the smaller relative density.

The results from Figures 5-15 and 5-16 indicate that PSAS-treated sand has a higher shear strength and is capable of carrying a higher load than Toyoura sand. Additionally, when treated with PSAS, the sand shows a stronger response to changes in normal stress, as evidenced by the shift of the stress paths to the right as the applied stress increases.

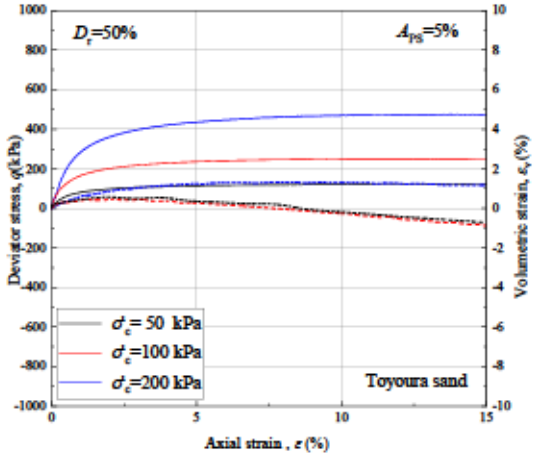


(a) Toyoura sand

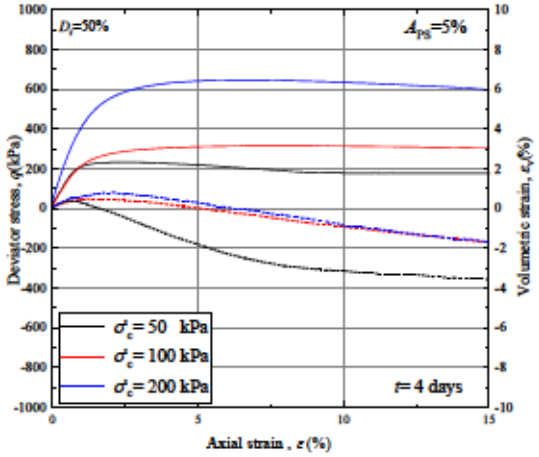


(b) $t_p$=4 days

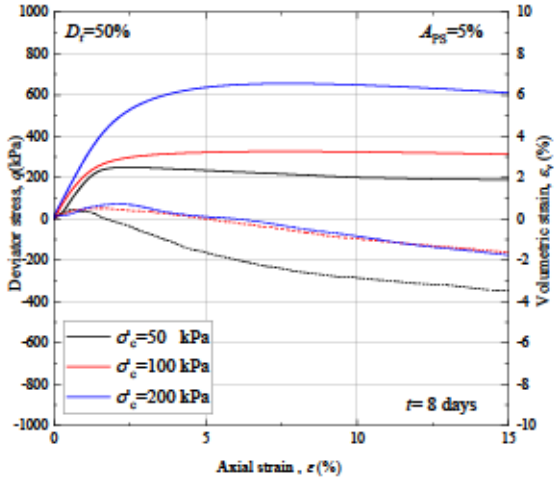


(c) $t_p$=8 days

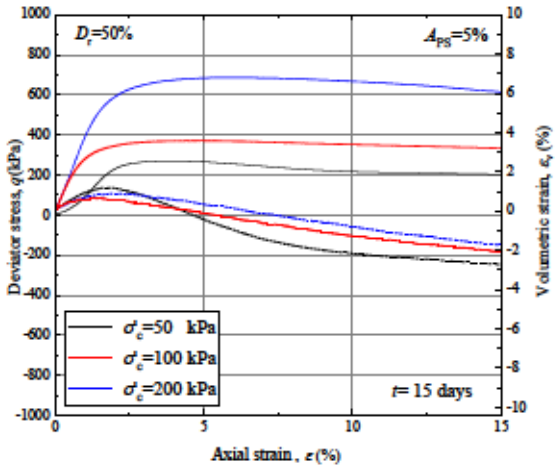


(d) $t_p$=15 days

**Figure 5-12** Deviator stress-strain and volumetric-strain relationships ($D_r$=50%): (a)-Toyoura sand, (b)-PSAS-treated sand $t$= 4 days, (c)-PSAS-treated sand $t$= 8 days, (d)-PSAS-treated sand $t$= 15 days

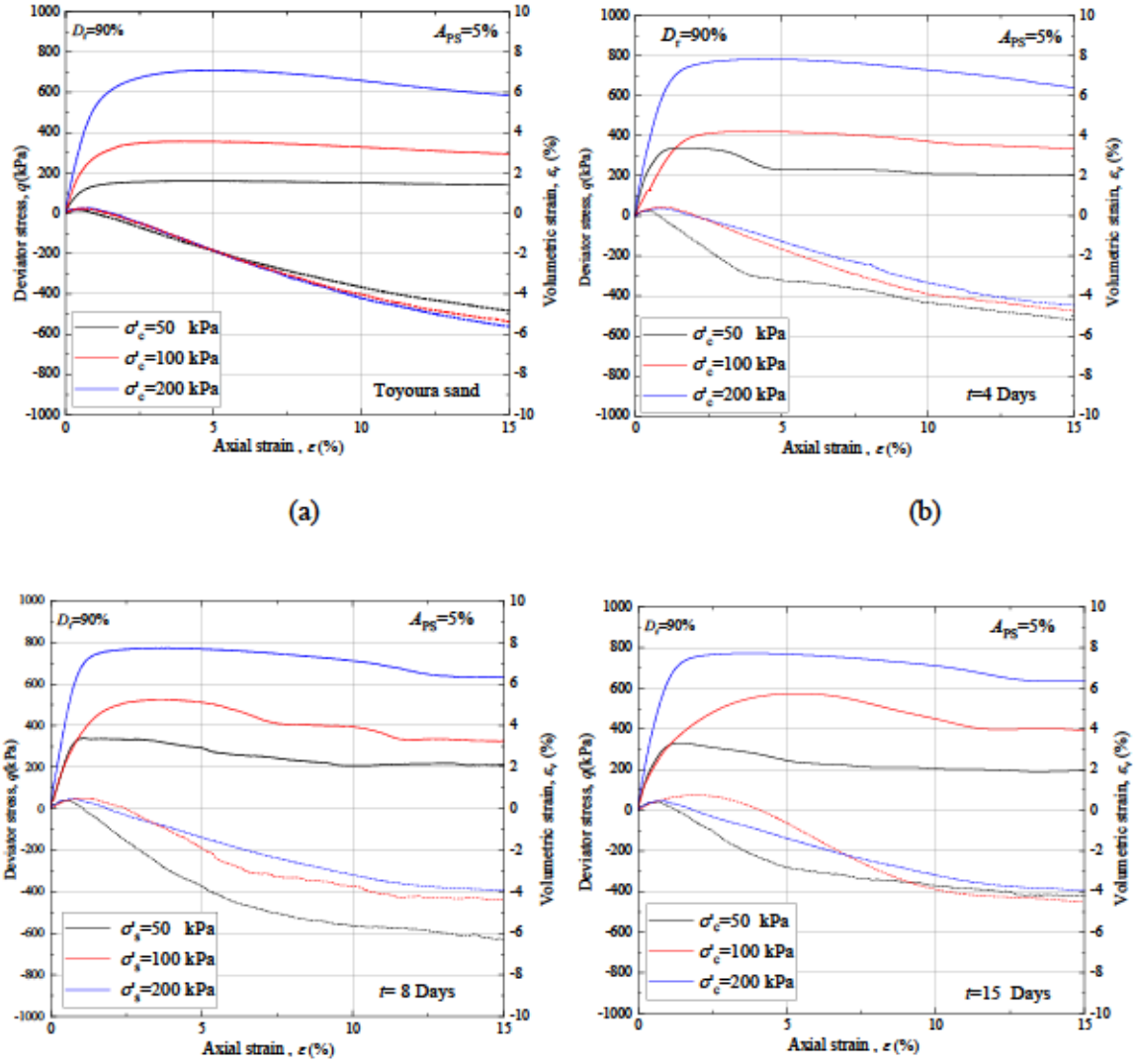


**Figure 5-13** Deviator stress-strain and volumetric-strain relationships ($D_r$=90%): (a)-Toyoura sand, (b)-PSAS-treated sand $t$= 4 days, (c)-PSAS-treated sand $t$= 8 days, (d)-PSAS-treated sand $t$= 15 days.

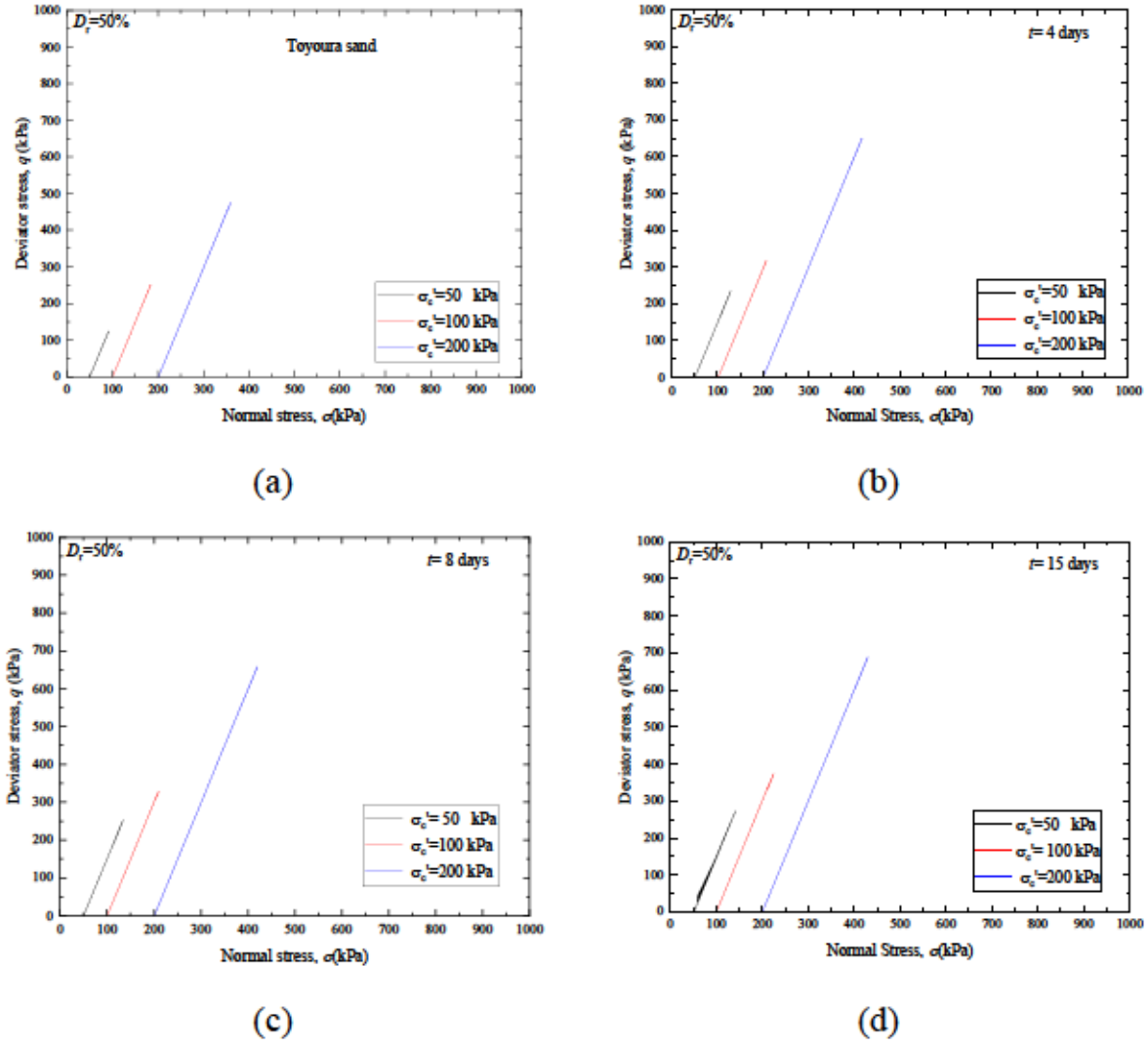


**Figure 5-14** Stress paths ($D_r$=50%): (a)- Toyoura sand, (b)-PSAS-treated sand $t$= 4 days, (c)-PSAS-treated sand $t$= 8 days, (d)-PSAS-treated sand $t$= 15 days

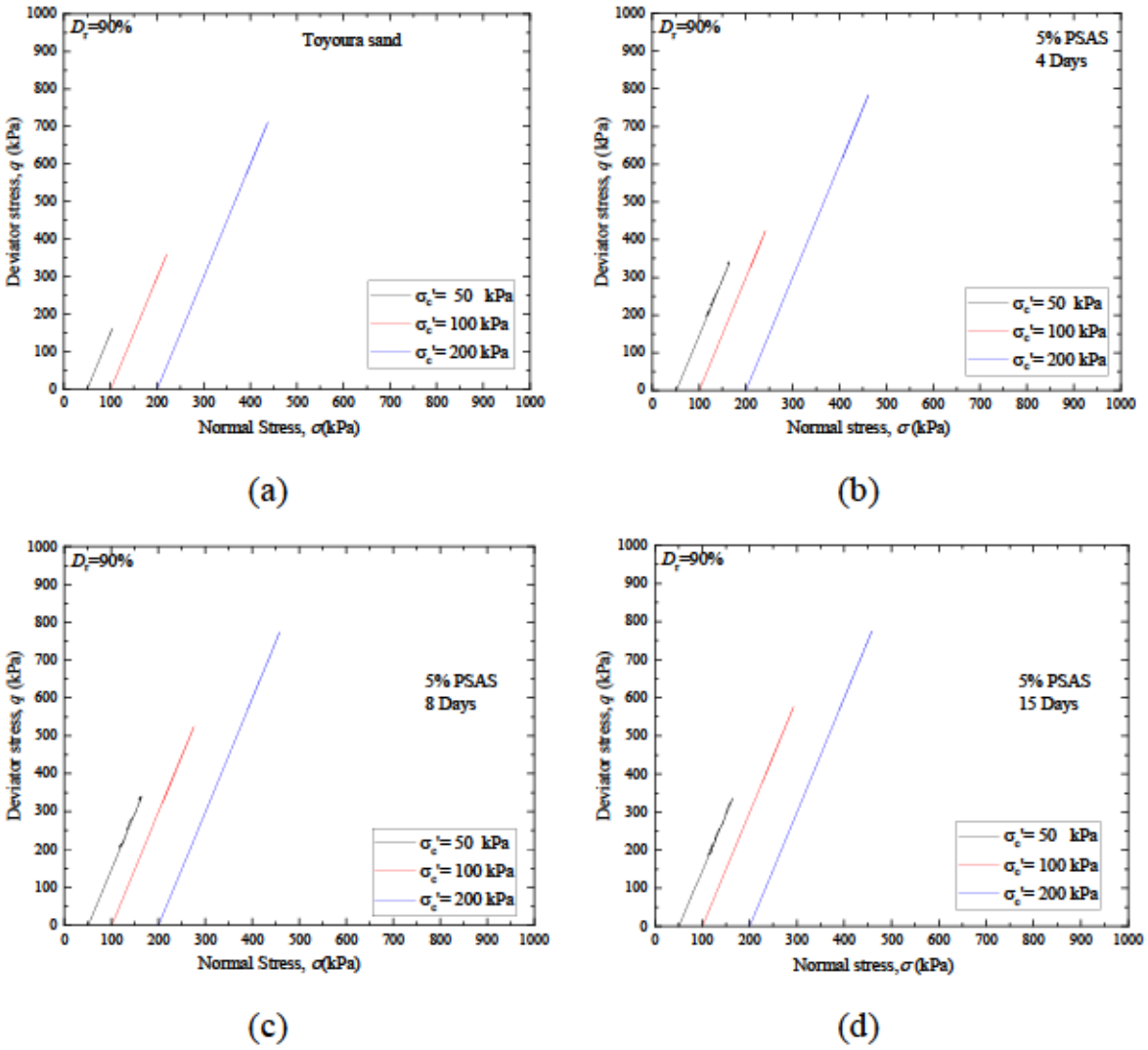


**Figure 5-15** Stress paths ($D_r$=90%): (a)- Toyoura sand, (b)-PSAS-treated sand $t$= 4 days, (c)-PSAS-treated sand $t$= 8 days, (d)-PSAS-treated sand $t$= 15 days

### 5.6.5 Effect of curing time on the shear resistance of PSAS-treated sand

Figures 5-17&5-18 show Mohr Coulomb stress circles of (a)- Toyoura sand, (b)-PSAS-treated sand $t$= 4 days, (c)-PSAS-treated sand $t$= 8 days, (d)-PSAS-treated sand $t$= 15 days at $D_r$=50% and $D_r$=90%. Figures shows the increase in cohesion and shear resistance of PSAS-treated sand when compared to untreated Toyoura sand.

Figure 5-17 shows the variations of the cohesion c of Toyoura sand and PSAS-treated sand compacted at $D_r$=50% and cured for $t$= 4days, 8 days and 15 days. The results indicate a clear increase in cohesion ($c$) of the treated sand compared to the untreated sand. As the curing period increased from 4 to 15 days, the cohesion for both Toyoura sand and PSAS-treated sand showed an increasing trend. However, the cohesion of treated sand was always higher than that of

Toyoura sand at all relative densities and curing periods, indicating the effectiveness of PSAS in increasing the cohesion of the sand.

Figure 5-16 shows the variations of the shear resistance (ϕ) of Toyoura sand and PSAS-treated sand compacted at $D_r$=90% and subjected to various curing periods. Similar to Figure 5-17, the results indicate an increase in shear resistance of PSAS-treated sand compared to Toyoura sand. As the curing period increased from 4 to 15 days, the shear resistance for both materials showed an increasing trend. However, the shear resistance of PSAS-treated sand was always higher than that of Toyoura sand at all relative densities, however for as the curing periods increases no significance increase of shear strength could be obtained this behaviour was also observed for tyre chips sand as aggregate substitution solution (Mashiri et al., 2015), (Zhang et al., 2018),

It is reported in previous studies that, in triaxial CD tests on sands with the same void ratio but different effective confining pressures, the peak points of the stress paths in the p'–q plane can be connected using a straight line that goes through the original point, as illustrated in Figure. 5-20a&b. This line is defined as the failure line in the p'–q plane expressed as Mohr-coulomb failure line obtained from Mohr circle(Gao et al., 2019).

Thus, it can be concluded that PSAS treatment has a significant effect in increasing the cohesion but no significant for shear resistance of the sand. This result is advantageous for applications in geotechnical engineering where materials with higher shear strength are required to resist sliding along internal planes or surfaces when subjected to shear forces.

Figure 5-18a shows the variation of shear strength with curing time for PSAS-treated sand compacted at $D_r$=90%. The graph shows a slight decrease in shear strength after 5 days of curing, followed by a stability in shear strength with further curing time. The decrease in shear strength after 5 days of curing can be attributed to the initial reaction between PSAS and sand particles, which leads to the formation of a weak bond between them. This weak bond reduces the shear strength of the treated sand (Xu et al., 2021), (Allam & Sridharan, 1981). Moreover, the decrease in shear resistance for the sand compacted at $D_r$=90% can be attributed to the contraction behaviour observed in the deviator stress-strain and volumetric strain relationships, as shown in Figures 5-13 and 5-14 of the documents. These figures indicate that, for the sand compacted at $D_r$=90%, there is a significant reduction in the volumetric strain during shearing when compared to PSAS-treated sand. The reduction in the volumetric strain could be due to the initial high relative density of the treated sand, which caused significant compression during the shearing process (Patel & Singh, 2019), (Alshameri et al.,

2017). This contraction behaviour could have resulted in the stability of the shear resistance of the sand.

However, with further curing time, the reaction between PSAS and sand particles continues, leading to the formation of a stronger bond between them. This stronger bond increases the shear strength of the treated sand, which explains the gradual increase or stability from $t$=8-15 days in shear strength with further curing time.

The variations observed in Figure 5-18a can be extended to the analysis of Figure 5-18b, which shows the variation of cohesion with curing time for the PSAS-treated sand compacted at two different relative densities. The results show that the PSAS treatment is effective in enhancing the cohesion of the sand, and increasing the $D_r$ led to an increase in cohesion.

Therefore, the behaviour observed in Figures 5-18a and 5-18b indicates that the compaction method and curing periods play an important role in the shear resistance ($\phi$) and cohesion ($c$) behaviour of the treated sand. Overall, the PSAS treatment is effective in enhancing the cohesion of sand but does not have a strong effect on the shear resistance.

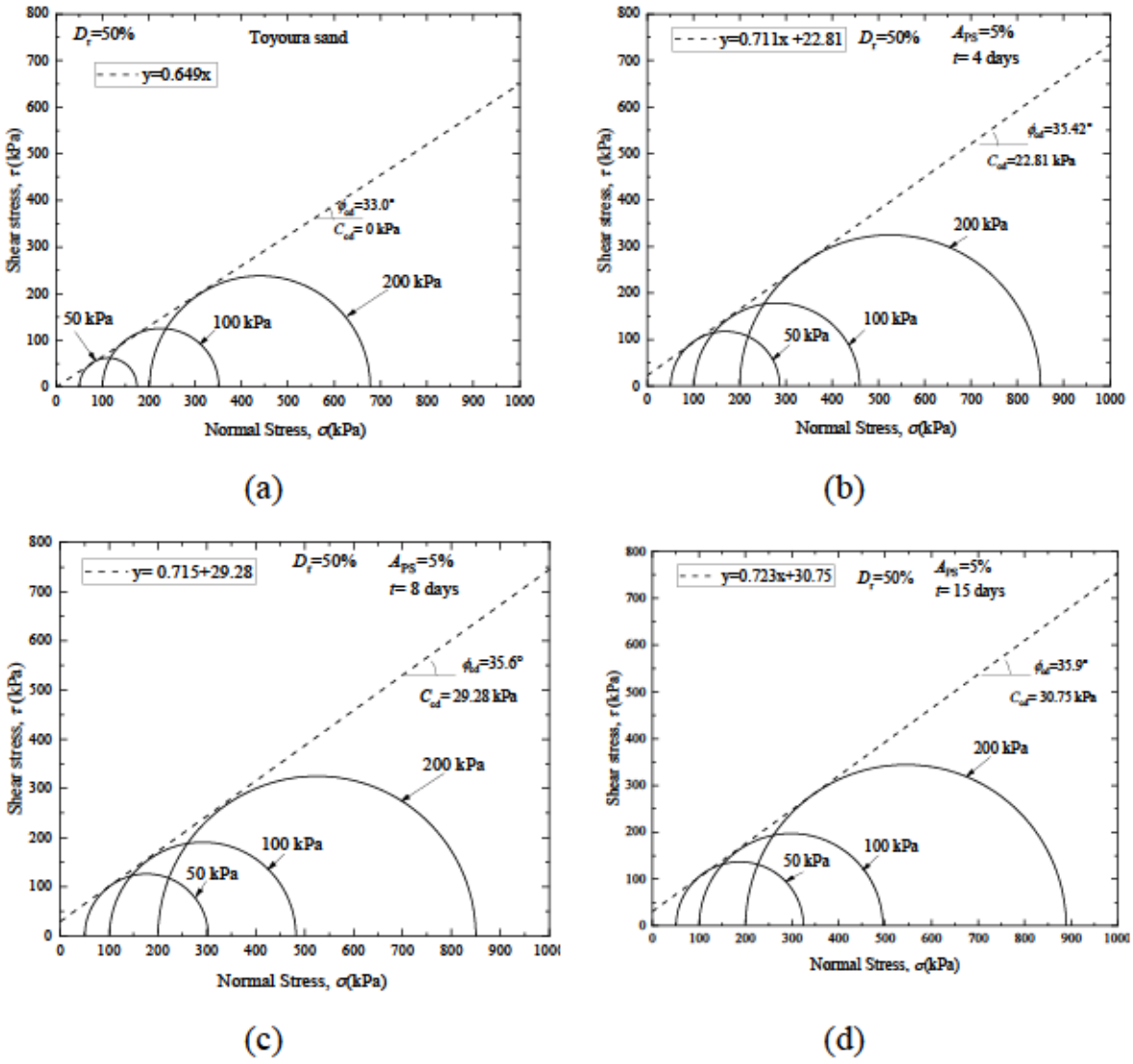


**Figure 5-16** Mohr Coulomb stress circles ($D_r$=50%): (a)- Toyoura sand, (b)- PSAS-treated sand $t$= 4 days, (c)-PSAS-treated sand $t$= 8 days, (d)-PSAS-treated sand $t$= 15 days

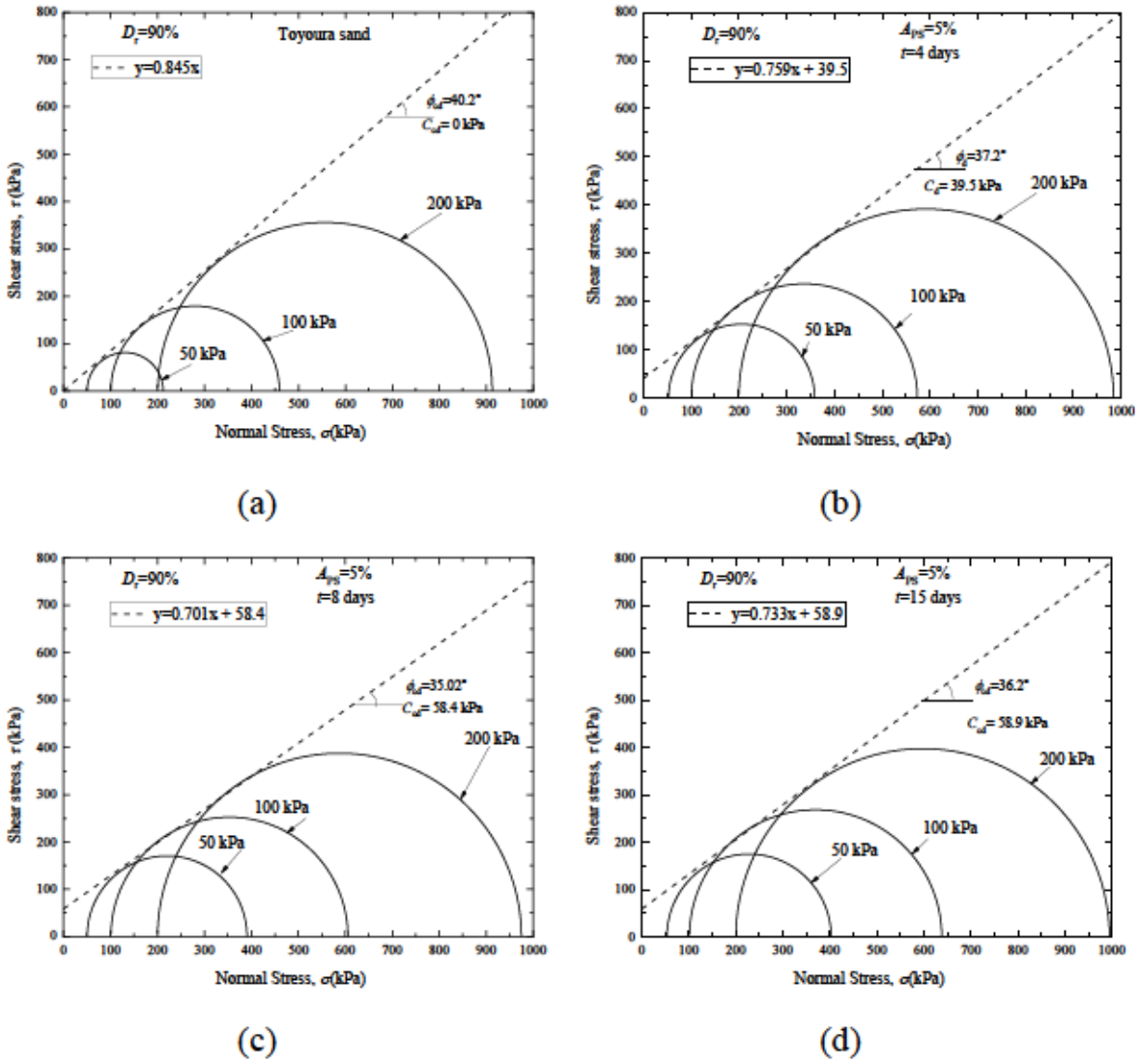


**Figure 5-17** Mohr Coulomb stress circles ($D_r$=90%): (a)- Toyoura sand, (b)-PSAS-treated sand $t$= 4 days, (c)-PSAS-treated sand $t$= 8 days, (d)-PSAS-treated sand $t$= 15 days

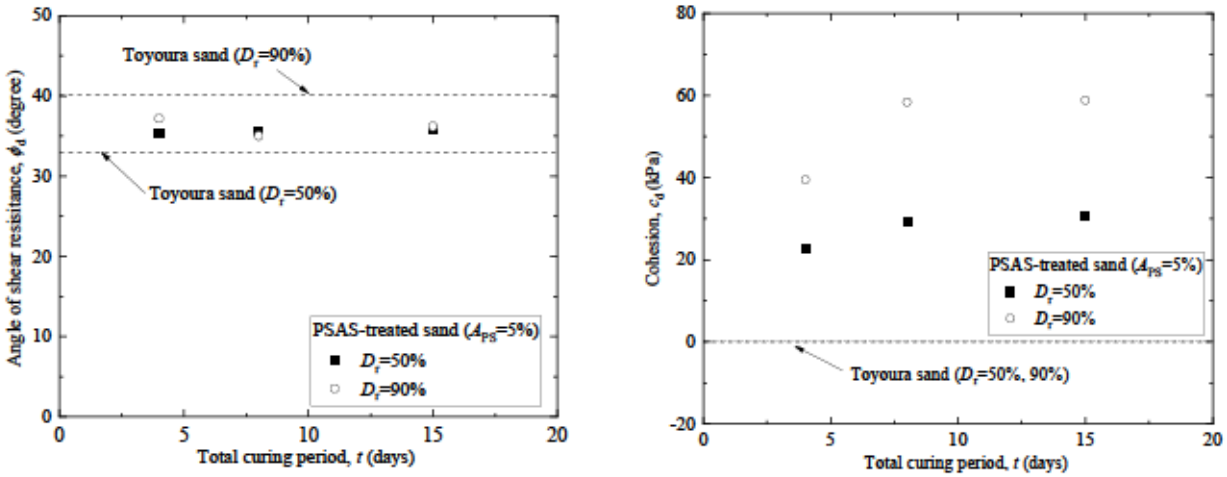


**Figure 5-18** Shear strength and Cohesion parameters of PSAS-treated sand

### 5.6.6 Effect of confinement pressure on the strength characteristics of PSAS-treated sand

Figure 5-20 shows a comparison of the results obtained from consolidated drained (CDT) tests at $\sigma_c' = 50$ kPa, 100 kPa, and 200 kPa consolidation stress with the results obtained from unconfined compression tests (UCS). The figure indicates that for both relative densities of treated sand, the results of the unconfined compression test are lower compared to the one obtained from the triaxial test.

This difference in results can be attributed to the difference in stress conditions between the two tests. In the unconfined compression test, the sample is subjected to a uniaxial stress condition, where the stress is applied in one direction only. In contrast, in the triaxial test, the sample is subjected to a multiaxial stress condition, where the stress is applied in three directions. The multiaxial stress condition in the triaxial test leads to a more realistic representation of the stress conditions that the treated sand would experience in the field. This is because the stress conditions in the field are rarely uniaxial and are more likely to be multiaxial. Therefore, the results obtained from the triaxial test are more representative of the actual behaviour of the treated sand in the field.

It is also important to note that the tests were carried out at relatively low consolidation stress, and the behaviour of the treated sand at higher consolidation stress could be different. However, the results obtained from the tests indicate that confining pressure plays an important role in the shear strength behaviour of the treated sand.

Overall, the results suggest that the triaxial test is a more appropriate test method for evaluating the shear strength of PSAS-treated sand, as it provides a more

realistic representation of the stress conditions that the treated sand would experience in the field.

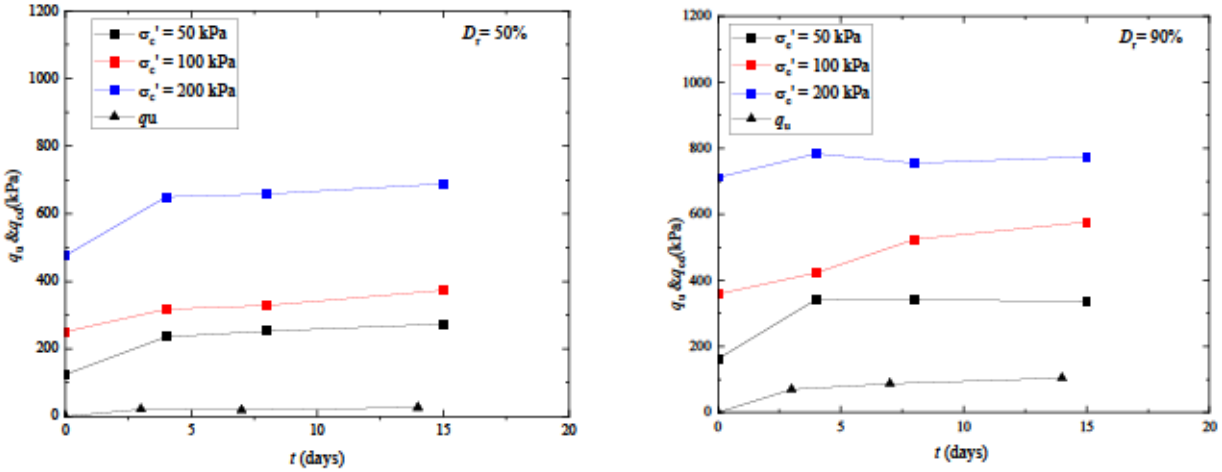


**Figure 5-19** Summary results of $q_u$ of PSAS-treated sand and $q_{cd}$ of PSAS-treated sand

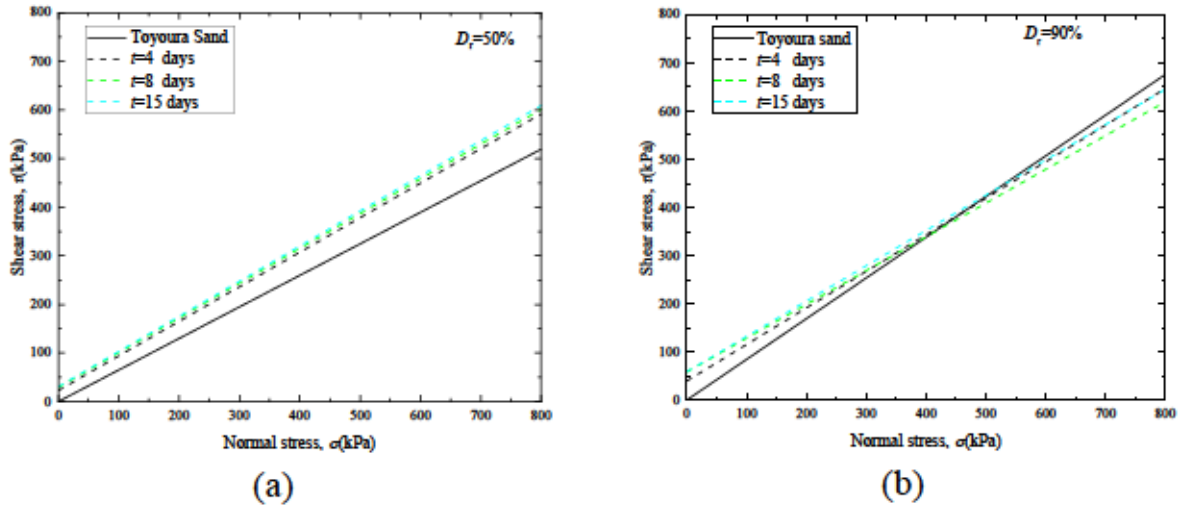


**Figure 5-20** Summary results of Mohr-Coulomb failure envelope

# CHAPTER 6

## 6. Effects of dry-wet cycles on the mechanical properties of sand treated with paper sludge ash-based stabilizer.

Backfill sand mixed with various additives changes the engineering properties during long-term variations in meteorological and hydrological conditions. Therefore, this chapter aims to investigate the durability of Paper Sludge Ash-Based Stabilizer (PSAS)-treated sands subjected to dry-wet curing cycles. Two curing temperatures (40°C and 71°C) were adopted for drying cylindrical specimens which were used for unconfined compression tests. In addition to the difference in the drying temperature, the effects of a number of dry-wet curing cycles on the unconfined compressive strength $q_u$ were examined. The results showed an increase in the $q_u$ of Paper sludge ash-treated sand at the early stage of the curing followed by a decrease in $q_u$ with the curing process. However, the comparison of the unconfined compression test results with the cone index test results show that the confinement of the PSAS-treated sand can be an essential parameter for investigating the durability of PSAS-treated sands which were subjected.

### 6.1 Materials and experiment design of Paper sludge ash (PSAS)-treated sand

#### 6.1.1 Specimen preparation for dry-wet curing cycle

For unconfined compression test specimen preparation, dry Toyoura sand was first mixed with the PSAS with $A_{PS}$ = 5.0% The $A_{PS}$ was the dry mass ratio of PSAS to Toyoura sand. Immediately after mixing, the water content $w$ of the treated sand was adjusted to 20% as appropriate mixture conditions to prevent the excessive expansion of treated sand and an overly high water content (Djandjieme et al., 2022).Thus, the mixtures were placed into cylindrical plastic molds (50 mm in diameter and 100 mm in height) and compacted to achieve $D_r$ = 50% and 90%; the molds were exposed to air-precuring for $t_p$=1 days before it is remolded for dry-wet cycle process shown in Figure 6-1. For comparison, OPC-treated sand specimens with $A_{OPC}$ = 5.0% were prepared under the same condition. The $A_{OPC}$ was the dry mass ratio of OPC to Toyoura sand.

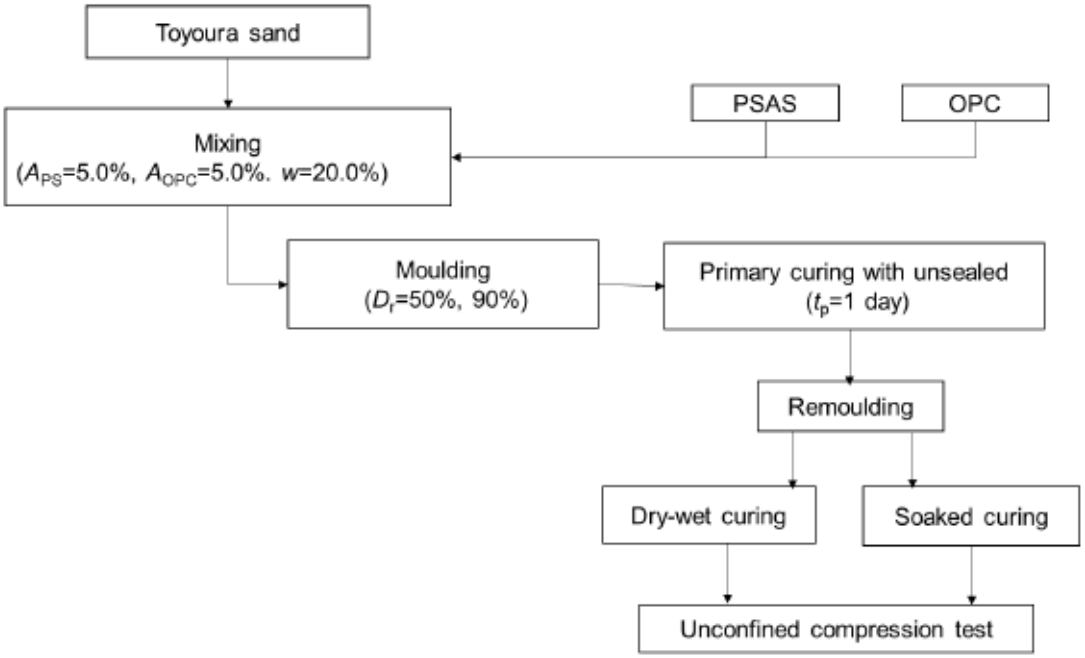


**Figure 6-1**. Specimen preparation flow for unconfined compression test of treated specimens.

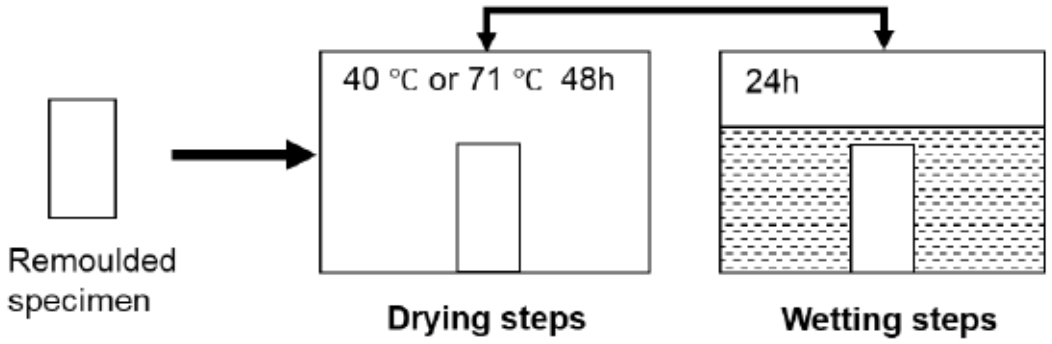


**Figure 6-2**. Schematic experimental process of the cycling drying-wetting treated specimens.

### 6.1.2 Experimental design of dry and wet curing cycle

The presence of dry-wet curing cycles is considered as one of the aggressive environmental conditions experienced by soils. In this study, the indoor dry and wet cycle environment was simulated as shown in Figure 6-2. The PSAS- and OPC-treated sand specimens were dried for 48h in an oven at temperature of 40°C or 71°C. Subsequently, they were immersed in the water and left for 24h in the room temperature. The drying and wetting process was repeated. The mass of each specimen was measured associated with the drying and wetting curing cycles, and the change in the saturation degree was calculated. Figure 6-3 shows the examples of the change in the saturation degree with cycles. Finally, unconfined

compression tests were carried out on the treated sand specimens with 1,2,3,4,5,6 and 7 cycles.

### 6.2 Unconfined compressive strength of treated specimens cured under dry-wet cycle and soaked conditions.

Unconfined compressive strength $q_u$ of PSAS-treated specimens is shown in Figure. 6-4. The $q_u$ of PSAS-treated specimens subjected to continuous soaked curing increased with the curing period. However, the $q_u$ of PSAS-treated specimens subjected to dry-wet curing cycles increased at the initial stage of the curing, and then, the $q_u$ decreased towards zero after several cycles of dry-wet curing. In Figure 6-5 where $q_u$ of OPC-treated sand at 5% mixture ratio is plotted against the curing period, the $q_u$ of treated specimen increased from the 1st to 7th cycle for each curing condition. The $q_u$ of OPC-treated sand specimens demonstrates the importance of considering higher temperature during the curing process under dry-wet cycles. When specimens were cured at $T$=40°C, Figure 6-5 clearly shows that the $q_u$ of OPC-treated sand under soaked conditions was lower than the $q_u$ obtained under dry-wet cycles. At $T$=71°C, there was a disruption in the $q_u$ value obtained when number of the dry-wet curing cycles increased. This might be because moderately high temperatures accelerated the hydration reaction, whereas excessively high temperatures might also cause loss of hydrates.

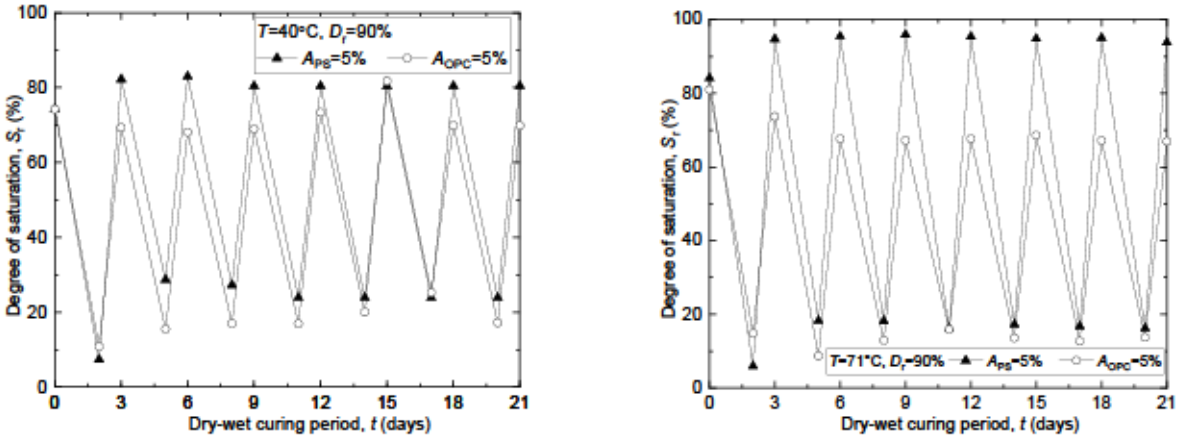


(a) $T$=40°C (b) $T$=71°C

**Figure 6-3**. Change in saturation degree of PSAS and OPC-treated sand during dry-wet curing.

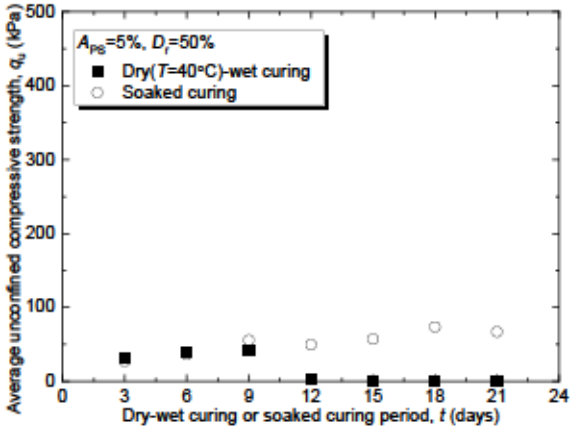


(a) PSAS-treated sand at $D_r$=50%, $T$=40°C

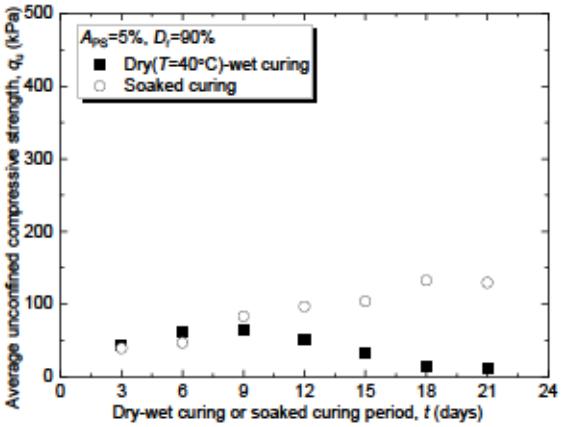


(b) PSAS-treated sand at $D_r$=90%, $T$=40°C

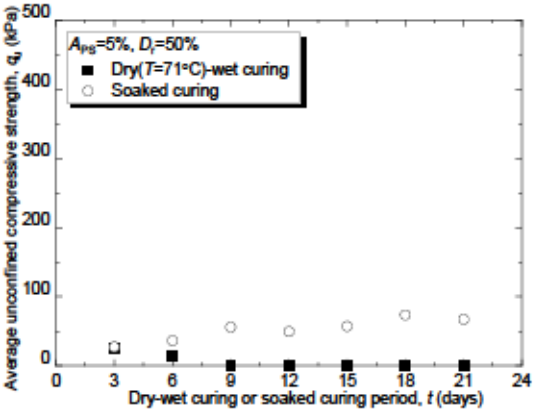


(c) PSAS-treated sand at $D_r$=50%, $T$=71°C

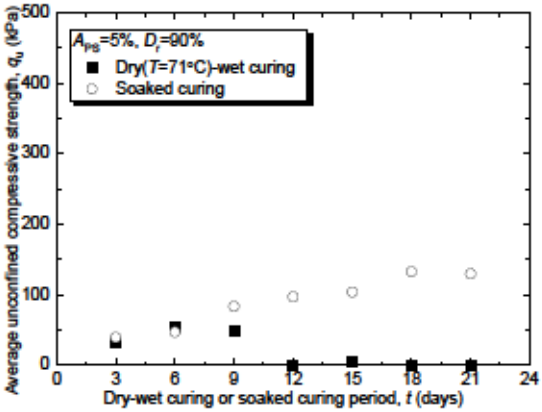


(d) PSAS-treated sand at $D_r$=90%, $T$=71°C

**Figure 6-4.** Relationships between unconfined compressive strength $q_u$ and curing period under dry-wet cycle and soaked conditions for PSAS-treated sand.

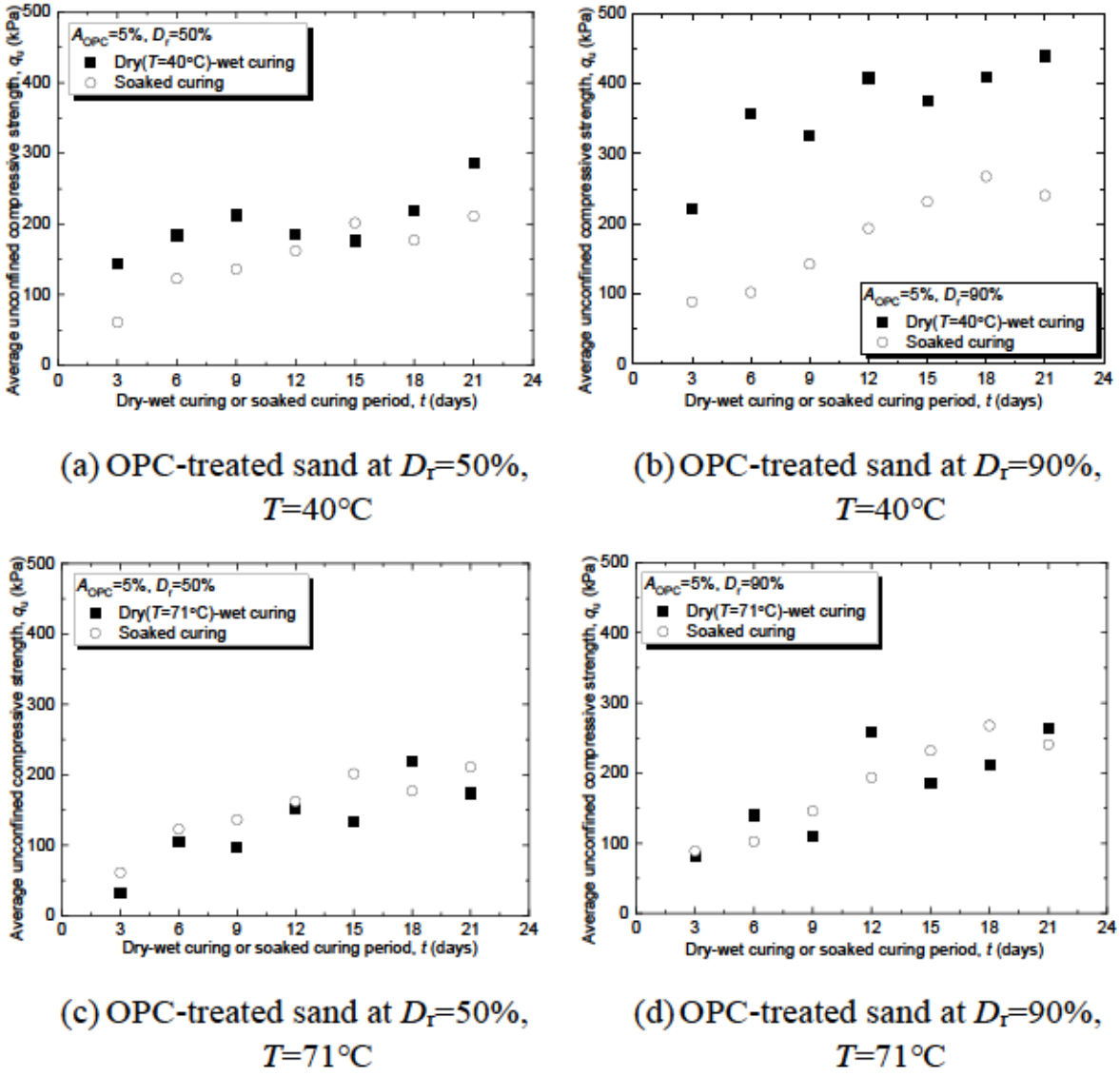


(a) OPC-treated sand at $D_r$=50%, $T$=40°C

(b) OPC-treated sand at $D_r$=90%, $T$=40°C

(c) OPC-treated sand at $D_r$=50%, $T$=71°C

(d) OPC-treated sand at $D_r$=90%, $T$=71°C

**Figure 6-5.** Relationships between unconfined compressive strength $q_u$ and curing period under dry-wet cycle and soaked conditions for OPC-treated sand.

## 6.3 comparison of strength development obtained from cone index test (CIT) and unconfined compressive strength (UCS)

The Cone index test is a widely used method in Japan for determining the cone index of compacted treated soils. This test involves the use of a cone penetrometer equipped with a tip cone, a rod, a jack for penetrating, and a load cell. To obtain the cone index value, the average force acting on the cone is divided by the bottom area of the tip cone when it has penetrated 5 cm, 7.5 cm, and 10 cm from the top surface of the specimen. In this study, cone index tests were performed on PSAS-treated samples cured under dry-wet cycles, and the results were compared with those of unconfined compression tests to investigate the effect of confinement on the strength development. The specimen for the cone index test was prepared

following the Japanese geotechnical society standard for cone index test on compacted soil (JGS 0716 & 0711). The dry and wet cycle environment were simulated such that the specimen was dried for 48h in an oven at temperature of 71°C and soaked in water for one day.

Figure 6-6(a) shows the change in the saturation degree with the dry-wet curing cycle. Figure 6-6(b) shows the relationship between the cone penetration resistance and the cone penetration of each specimen at $T$=71°C. The cone penetration resistance increased from the 1$^{st}$ to the 3$^{rd}$ cycle. Followingly, the cone penetration resistance decreased with the increase in the number of dry-wet curing cycle. However, the cone penetration resistance obtained at the 7$^{th}$ cycle was significantly higher than that of untreated specimen. The test results suggested that the confinement was essential to precisely assess the durability of the PSAS-treated sands subjected to dry-wet curing.

Moreover, Figure 6-7 (a) shows the change in the saturation degree with the dry-wet curing cycle. Figure 6-7 (b) shows the cone penetration resistance ($q_c$) of PSAS-treated sand under dry-wet cycle at a temperature of 40°C. The results in this figure indicate that $q_c$ increased from the first to the 6$^{th}$ dry-wet curing cycle and then decreased with an increase in the number of dry-wet curing cycles. However, $q_c$ of the PSA-treated sand at the 7$^{th}$ cycle was still significantly higher than that of the untreated specimen. This indicates that the PSAS treatment has effectively enhanced the durability and strength of the sand even after undergoing harsh environmental cycles including seven dry-wet cycles moulded specimen. This figure supports the discussion for figure 6-6 (b) that suggests that the confinement during the experiment was essential for accurately assessing the durability of the PSAS-treated sand under dry-wet curing cycles. Also, the alternative strength development method using the Cone Index Test (CIT) was an effective strength characterization method for PSAS-treated sand.

In conclusion, Figure 6-8 shows the relationship between the cone penetration resistance and the number of dry-wet cycles for PSAS-treated sand at a temperature of both 40°C and 71°C. The figure suggests that as the number of dry-wet cycles increases, the cone penetration resistance decreases for both temperatures. However, the results show that PSAS-treated sand can still retain higher penetration resistance than the untreated sand even after undergoing harsh environmental cycles including seven dry-wet cycles. It can be concluded that the confinement during the experiment was essential for accurately assessing the durability of the PSAS-treated sand under dry-wet curing cycles, and the alternative strength development method using the Cone Index Test (CIT) proved to be an effective strength characterization method for PSAS-treated sand.

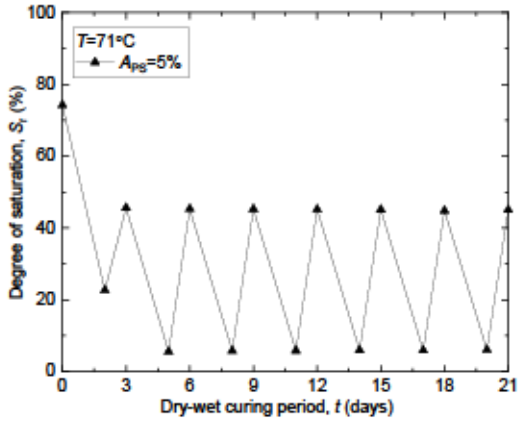


**(a)** Saturation table of PSAS-treated sand under dry-wet cycle

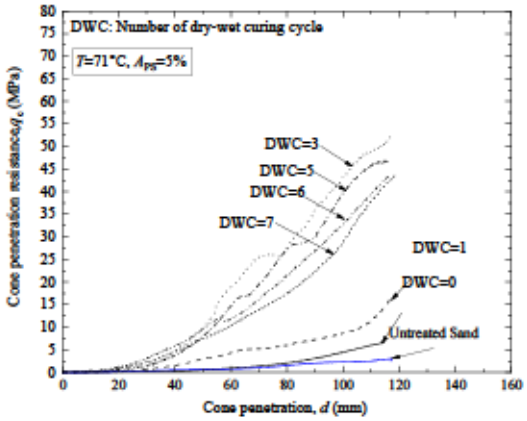


**(b)** Cone index test of PSAS-treated sand under dry-wet cycle

**Figure 6-6.** $q_c$ of PSAS-treated sand under dry-wet cycle, $T$=71°C

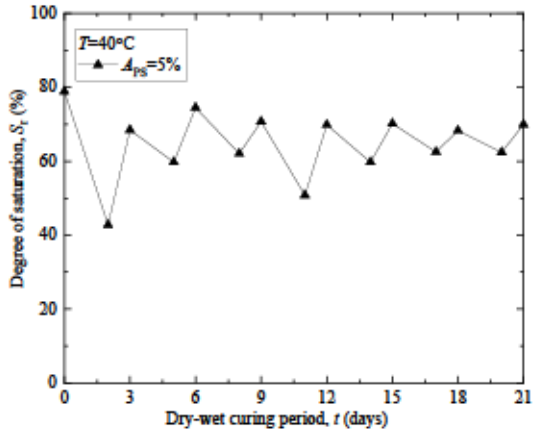


**(a)** Saturation table of PSAS-treated sand under dry-wet cycle

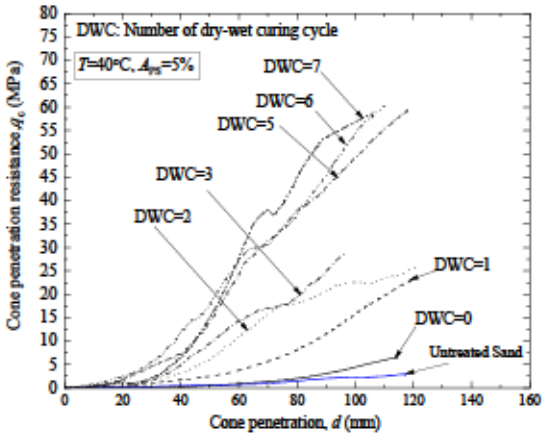


**(b)** Cone index test of PSAS-treated sand under dry-wet cycle

**Figure 6-7.** $q_c$ of PSAS-treated sand under dry-wet cycle, $T$=40°C

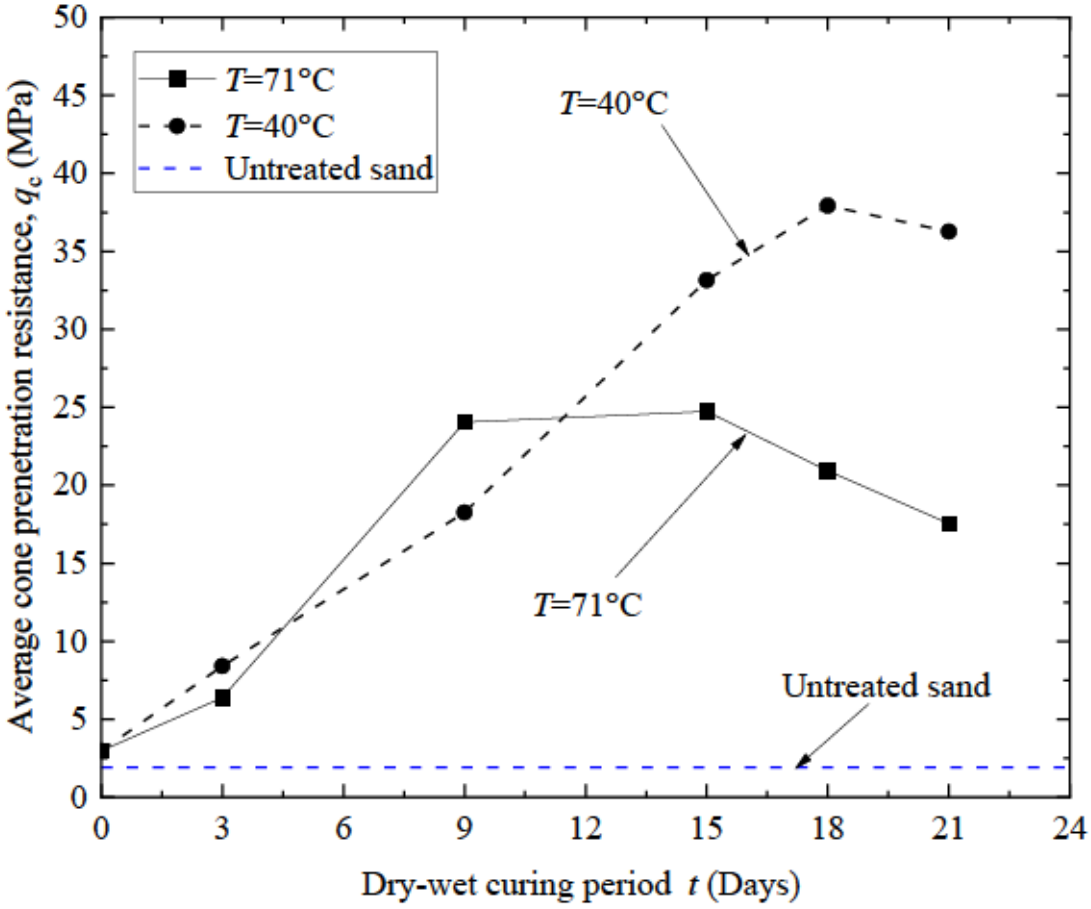


**Figure 6-8** $q_c$ of PSAS-treated sand with the number of dry-wet cycles qc of PSAS-treated sand with the number of dry-wet cycles.

### 6.4 XRD profile of PSAS-treated sand subjected to dry-wet curing.

The $q_u$ of the PSAS-treated sand increased gradually at the initial stage of the curing and then decreased as number of the dry-wet curing cycles increased, as described in the previous section. Then, the investigation of the crystalline substance was conducted to understand the hydration process during the dry-wet cycle by conducting XRD diffraction tests. XRD analyses were conducted on PSAS-treated sands after the 1st, 3rd and 5th cycle (C1, C3 and C5) of dry-wet curing (see table 6-1). The PSAS-treated sands were dried for 48h in an oven-dry at temperature of 71°C. Subsequently, they were immersed below the water surface and left for 24h in the room temperature. After the prescribed dry-wet cycle curing at C1, C3, and C5, PSAS-treated sand was crushed in a ceramic mortar using a pestle and soaked in iso-propanol for 2h. Next, vacuum filtration was performed to remove the alcohol, and the sample was placed in a vacuum oven set to 40°C for 1 day. Immersing treated sand in alcohol halted the hydration reaction. The treated sand was passed through a 0.075 mm sieve and was used for X-ray powder diffraction in a Rigaku Ultima IV D-5000 Diffractometer using Cu

K-alpha radiation. The diffractometer was collected in the range of 0-80° 2θ Scale, with a step size of 0.005°/sec.

The X-ray Diffraction (XRD) profiles detailing the impact of dry-wet cycles on PSAS-treated sand are elucidated in Figure 6-9. Simultaneously, the XRD profiles of PSAS prior to hydration are provided for reference in the same figure. Notably, the presence of Ettringite is evident at C1, with a subsequent decrease in counts observed at C3 and C5 as dry-wet cycles progress. This alteration in Ettringite counts is presumed to influence the observed variation in unconfined compression strength ($q_u$) of PSAS-treated sands. At elevated temperatures $T$=71°C, a component of Ettringite transforms into monosulphate during the early stages of hydration (Nanayakkara, 2011), akin to concrete. Consequently, Figure 6-9 illustrates a noticeable decrease in the Ettringite peak after the fourth cycle, a phenomenon attributed to the instability of Ettringite at high temperatures (>70°C). Detailed analysis further reveals an increased presence of quartz and Calcium oxide components after the fourth cycle, indicating the presence of Calcium sulfate resulting from the reaction between calcite ($CaCO_3$) and Sodium sulfate ($Na_2SO_4$).

The XRD profile chart in Figure 6-9a&b, provides a comprehensive view of the hydrate content variations in treated PSAS-sand under distinct dry-wet cycles, denoted as cycle 1 (C1), cycle 2 (C2), and cycle 3 (C3). The alterations in hydrate products are depicted by the relative intensity of each peak, calculated by dividing the absolute intensity of every peak by the absolute intensity of the most intense peak and converting it to a percentage(Speakman, 2013), (Takayama et al., 2018). The outcomes of this analysis reveal a consistent decrease in hydrate content with an increasing number of dry-wet cycles. This trend is evident for both temperatures studied ($T$=71°C and $T$=40°C) and is visually represented in Figure 6-9c&d, illustrating the percentage of hydrate content during each dry-wet cycle. These results strongly imply that prolonged exposure to dry-wet cycles adversely affects the retention of hydrates in treated sand. However, further research is warranted to elucidate the underlying factors contributing to the reduction in hydrate content during extended dry-wet cycling.

**Table 6.1** XRD test conditions

| Temperature | Dry-wet cycles | comparison |
|---|---|---|
| $T$=71 | C1, C3 | $t_p$ |
| $T$=40 | C3, C5 | |

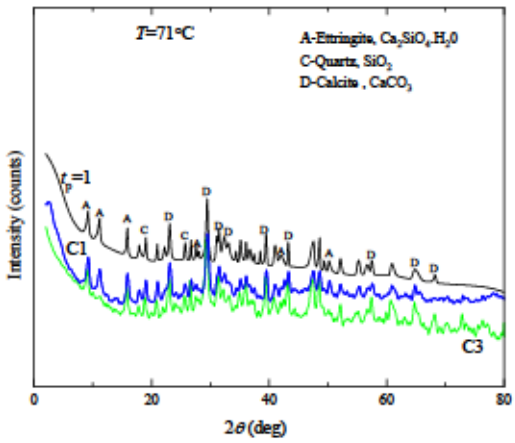


(a) XRD profile, $T$=71°C, $t_p$=1, C1, C3

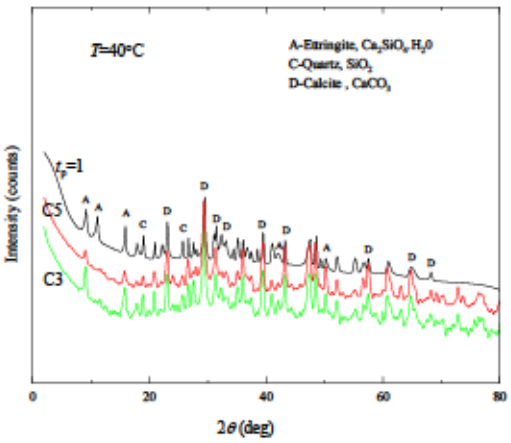


(b) XRD profile , $T$=40°C, $t_p$=1, C3, C5

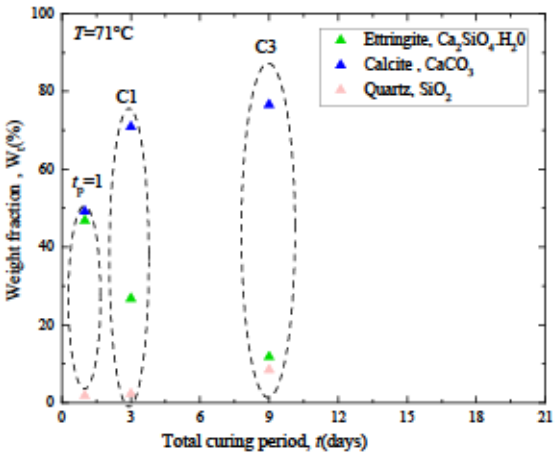


(b) Weight fraction of i$^{th}$ phases, $T$=71°C, (d)Weight fraction of i$^{th}$ phases, T=40°C,

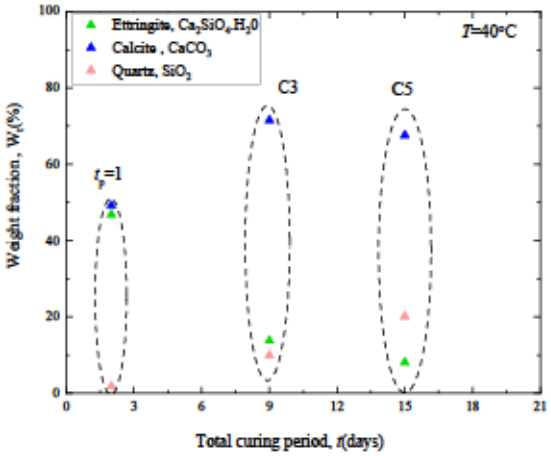


**Figure 6-9.** XRD Profiles of PSAS-treated sand at each dry-wet cycle conditions.

# CHAPTER 7

## 7. Liquefaction evaluation of paper sludge ash treated sand.

In previous chapters, preliminary tests including unconfined compression strength (UCS) and isotopically consolidated monotonic drained triaxial tests were conducted on PSAS-treated sand specimens to evaluate the effect of treatment on the monotonic strength properties. The results indicated that the curing period significantly influenced the cohesion, friction angle, and overall strength development of the PSAS-treated sand.

To further investigate the behaviour of PSAS-treated samples under cyclic loading, a series of cyclic triaxial tests were conducted. These tests encompassed a wide range of cyclic stress levels (*CSR*), relative densities ($D_r$), and consolidation stress ($\sigma_c$'). The relative density of the PSAS-treated sand specimens used in the testing was $D_r$=50%, and the tests were carried out under a confining stress of 100 kPa.

### 7.1 Preparation of sample

In this chapter the sample preparation technique was used as the one explained in section 5.6.1.

### 7.2 Test Procedure

The experimental setup for the cyclic triaxial tests in this thesis adhered to the standard requirements specified for the test equipment (JGS 0541-2009). The triaxial apparatus consisted of a triaxial pressure cell, a cell pressure and back pressure supply device, an axial loading device, and various measuring and recording devices. The apparatus was designed to accommodate the maximum cell pressure, back pressure, and axial load on the specimen, ensuring sufficient capacity and load resistance. To induce a triaxial extensile stress state, a rigidly connected triaxial cell with a load piston and cap was employed. The specimen was carefully prepared and covered with a cap, pedestal, and rubber sleeve, enabling the application of cell pressure, back pressure, and axial load. The volume change of the pore water pressure measurement line was minimized, and the cap and pedestal diameters matched those of the specimen. During the tests, continuous application of the required cell pressure, back pressure, and axial stress within specified ranges was ensured for isotropic consolidation and cyclic loading phases.

Notably, for cyclic loading, a controlled load amplitude approach is employed, where the cyclic axial load is controlled within predetermined maximum and minimum stress limits. This allows for precise control and measurement of the cyclic axial load during the test. The equipment has been specifically designed to accommodate this controlled load amplitude approach, ensuring that the cyclic axial load remains within the specified stress limits throughout the test. Additionally, the apparatus enables continuous measurement of pore water pressure, cyclic axial load, axial displacement, and, if necessary, the cell pressure, providing comprehensive data for analysis and evaluation

The cyclic loading in the triaxial compression tests was characterized by the cyclic stress ratio (*CSR*), which represents the ratio of the maximum cyclic shear stress ($\tau_{cyc}$) to the initial Consolidation stress ($\sigma_c^{'}$). In this study, cyclic tests were conducted with *CSR* values of 0.22, 0.30, 0.34, and 0.45 (see table 7-1). In all the cyclic tests performed in this study, a cyclic shear strain of single amplitude ($\varepsilon_{SA}$) of 5.0% was used as the liquefaction criterion, as suggested by criterion (Du & Chian, 2015) (Zhu et al., 2021) (JGS 0541-2009). This criterion served as an indicator of the potential liquefaction behaviour of the PSAS-treated sand specimens during the cyclic loading.

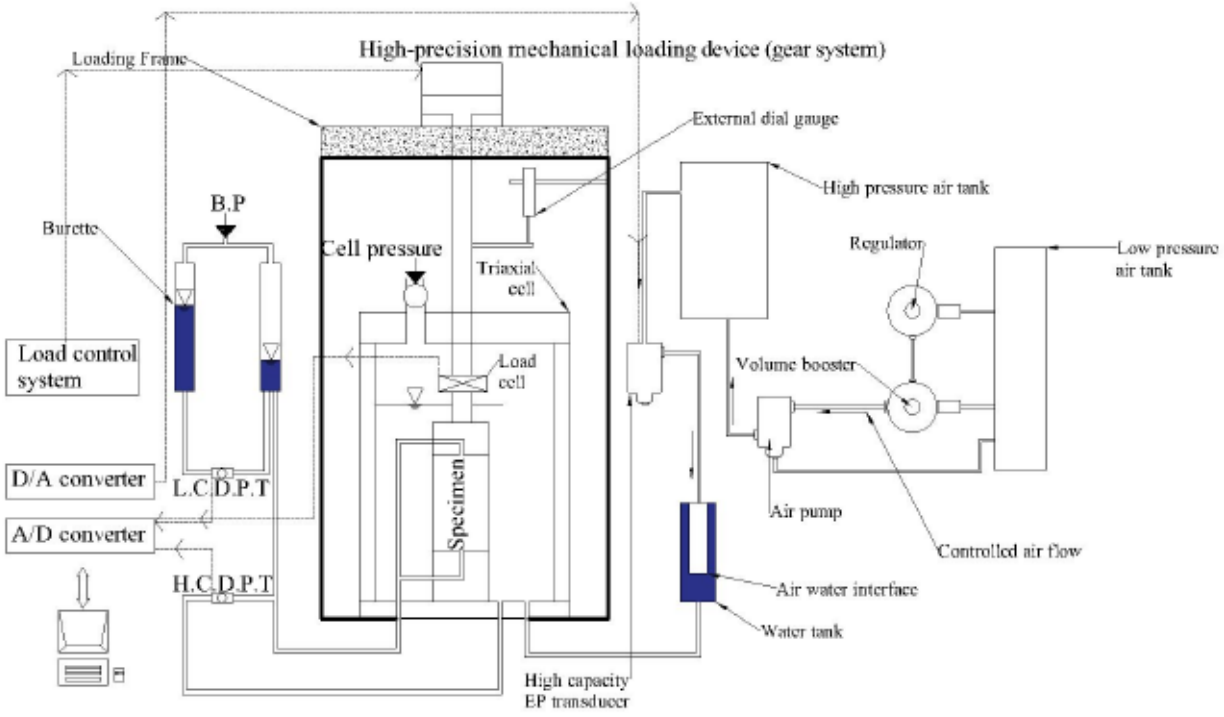


**Figure 7-1** Schematic diagram of triaxial testing machine in the laboratory.

**Table 7-1** Experimental Program and mixtures characteristics.

| Addition ratio of PSAS, $A_{PS}$ (%) | Adjusted water content, $w$ (%) | Relative density, $D_r$ (%) | Primary curing period under sealed condition, $t_p$ (d) | Secondary curing period under soaked condition, $t_s$ (d | Total curing days, $t$ (d) | Consolidated stress $\sigma_c'$ (kPa) | Cyclic stress ratio $CSR = \frac{\sigma_d}{2\sigma_0'}$ |
|---|---|---|---|---|---|---|---|
| | Toyoura Sand | | | | | | |
| 0 | 20 | 50% | 0 | 0 | 0 | 100 kPa | 0.45 |
| | | | | | | | 0.35 |
| | | | | | | | 0.22 |
| | PSAS-treated sand | | | | | | |
| 5% | 20 | 50% | 1 | 3, 7, 14 | 4,8,15 | 100 kPa | 0.45 |
| | | | | | | | 0.35 |
| | | | | | | | 0.22 |

## 7.3 Cyclic liquefaction behaviour of untreated sand and PSAS-treated sand

The undrained cyclic triaxial tests were conducted to evaluate the liquefaction behaviour of PSAS-treated sand specimens compacted at $D_r$=50% under different cyclic stress ratios. the stress-strain response for different cyclic stress results obtained from the tests are presented in Figures 7-2, 7-3, and 7-4.in each figure, (a) shows the results for untreated Toyoura sand, (b) shows the results for PSAS-treated sands at $t$ =4 days, (c) shows the results for PSAS-treated sand at $t$ =8days, and (d) shows the results for PSAS-treated sand at $t$=15days.

The stress-strain relationship illustrated in the figures shows that the PSAS-treated sand exhibits lower strain at a given cyclic stress, indicating a more stable and liquefaction-resistant soil compared to Toyoura sand. The stiffer sand structure developed through PSAS treatment allowed it to withstand cyclic loading without undergoing significant deformations that may lead to liquefaction. The major difference between the two curves is that the PSAS-treated sand exhibits a more linear relationship between the stress and strain. This indicates that the soil is more stable and may not liquefy even under seismic loading conditions.

Figure 7-2 shows the stress-strain response of Toyoura sand (untreated) and PSAS-treated sand specimen for $CSR$=0.22 at $D_r$=50%. The plot illustrates that the PSAS-treated sand exhibits lower strain at a given cyclic stress, indicating a more stable and liquefaction-resistant soil compared to Toyoura sand. The stiffer sand structure developed through PSAS treatment allowed it to withstand cyclic

loading without undergoing significant volumetric straining that may lead to liquefaction.

Figure 7-3 & Figure7- 4 show the stress-strain response of PSAS-treated sand specimens with different *CSR* = 0.35 and 0.45. A comparison with the Toyoura sand stress-strain plots in Figure 7-2 shows that, under identical *CSR* values, PSAS-treated sands have a significantly lower strain compared to untreated sand, indicating a more stable and liquefaction-resistant soil under cyclic loading.

Figures 7-5, 7-6, and 7-7 show cyclic stress path responses of the untreated Toyoura sand specimens under different cyclic stress ratios (*CSR*) and PSAS-treated specimen. in each figure, (a) shows the results for untreated Toyoura sand, (b) shows the results for PSAS-treated sands at $t$ =4 days, (c) shows the results for PSAS-treated sand at $t$ =8days, and (d) shows the results for PSAS-treated sand at $t$=15days.

Figure 7-5 presents the stress path responses of untreated Toyoura sand and PSAS-treated sand specimens with $D_r$=50% under *CSR*=0.22. The stress path curve of PSAS-treated sand is distinctly different from that of untreated Toyoura sand, with the PSAS-treated sand specimens exhibiting a lower strain at a given cyclic stress compared to the untreated sand.

Figure 6 shows the stress-path responses of PSAS-treated sand specimens with different curing periods ($t$=4, 8, and 15 days) and *CSR*=0.35. Similar to Figure 7-5, the PSAS-treated sand specimens exhibit lower strain and more linear stress paths compared to untreated Toyoura sand under the same *CSR*. As the curing time of the PSAS-treated sand increases, the stress paths become closer to vertical, indicating even less plastic deformation and hysteresis.

Figure 7-7 shows the stress-strain responses of PSAS-treated sand specimens with different curing periods ($t$=4, 8, and 15 days) and *CSR*=0.45. The stress-strain plots of the PSAS-treated sand specimens again show lower strain at a given cyclic stress and more linear stress paths compared to untreated Toyoura sand. Furthermore, as the curing time increases, the stress paths become even closer to vertical.

Figure 7-8 shows the liquefaction resistance curves for untreated Toyoura sand and PSAS-treated sand at double amplitudes of *DA*=5% and *DA*=0.1%, respectively. The horizontal axis represents the cyclic stress ratio (*CSR*), while the vertical axis represents the number of cycles the specimen can withstand before liquefaction.

For Toyoura sand, the plot shows that the number of cycles to liquefaction decreases as the *CSR* increases. At *CSR*=0.22, Toyoura sand can withstand

approximately $N_c$=226 cycles before liquefaction occurs at *DA*=5%, and at *CSR*=0.45, it can withstand only about $N_c$ =2 cycles. This behaviour is consistent with the typical trend observed in liquefaction resistance curves for sandy soils (Toyota & Takada, 2023).

In contrast, the liquefaction resistance curve for PSAS-treated sand exhibits a different pattern. As shown in Figure 8, the PSAS-treated sand specimens with *t*=15 days and *DA*=0.1% exhibit the highest number of cycles values among all curves. At this double amplitude and with a curing time of 15 days, the PSAS-treated sand can withstand cycles up to $N_c$=220 at a *CSR* = 0.22 before liquefaction occurs.

For the same *CSR*=0.45 for PSAS-treated sand the number of cycles before liquefaction increase to $N_c$= 11 for *DA*=0.1% compared to natural Toyoura sand at *DA*=5% with $N_c$=2. This higher resistance to liquefaction highlights the effectiveness of the PSAS treatment in improving the cyclic behaviour of the sand.

In conclusion, PSAS treatment served to significantly improve the liquefaction resistance of treated sand, even with low double amplitudes, when compared to untreated Toyoura sand.

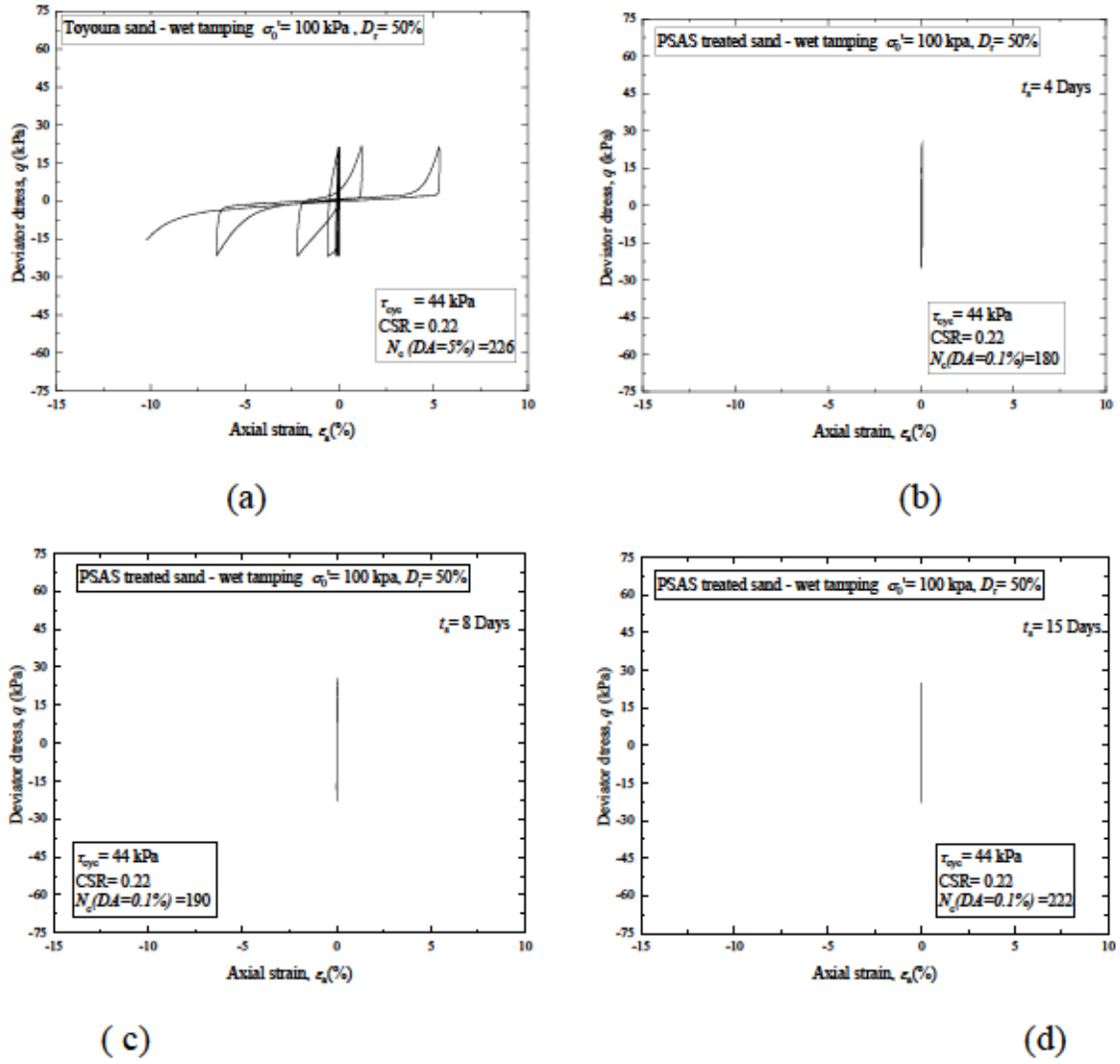


**Figure** 7-2 Undrained cyclic response of (a)stress-strain relationship of untreated sand (Toyoura sand), (b)stress-strain relationship of PSAS-treated sand ($t_s$=4 days, $D_r$=50%), (c) stress-strain relationship of PSAS-treated sand ($t_s$=8 days, $D_r$=50%), (d) stress-strain relationship of PSAS-treated sand ($t_s$=15 days, $D_r$=50%), for *CSR*=0.22

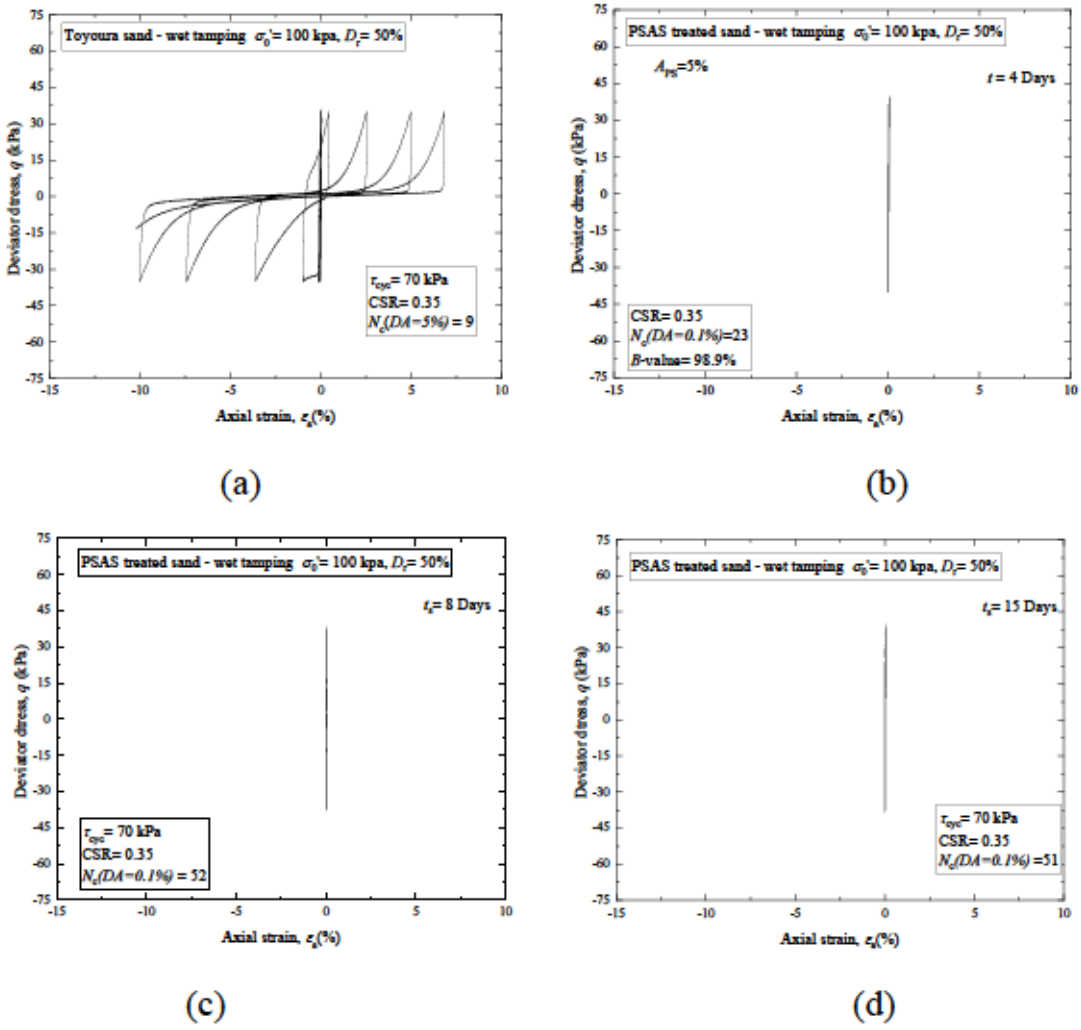


**Figure 7-3** Undrained cyclic response of (a)stress-strain relationship of untreated sand (Toyoura sand), (b)stress-strain relationship of PSAS-treated sand ($t_s$=4 days, $D_r$=50%), (c) stress-strain relationship of PSAS-treated sand ($t_s$=8 days, $D_r$=50%), (d) stress-strain relationship of PSAS-treated sand ($t_s$=15 days, $D_r$=50%), for *CSR*=0.35

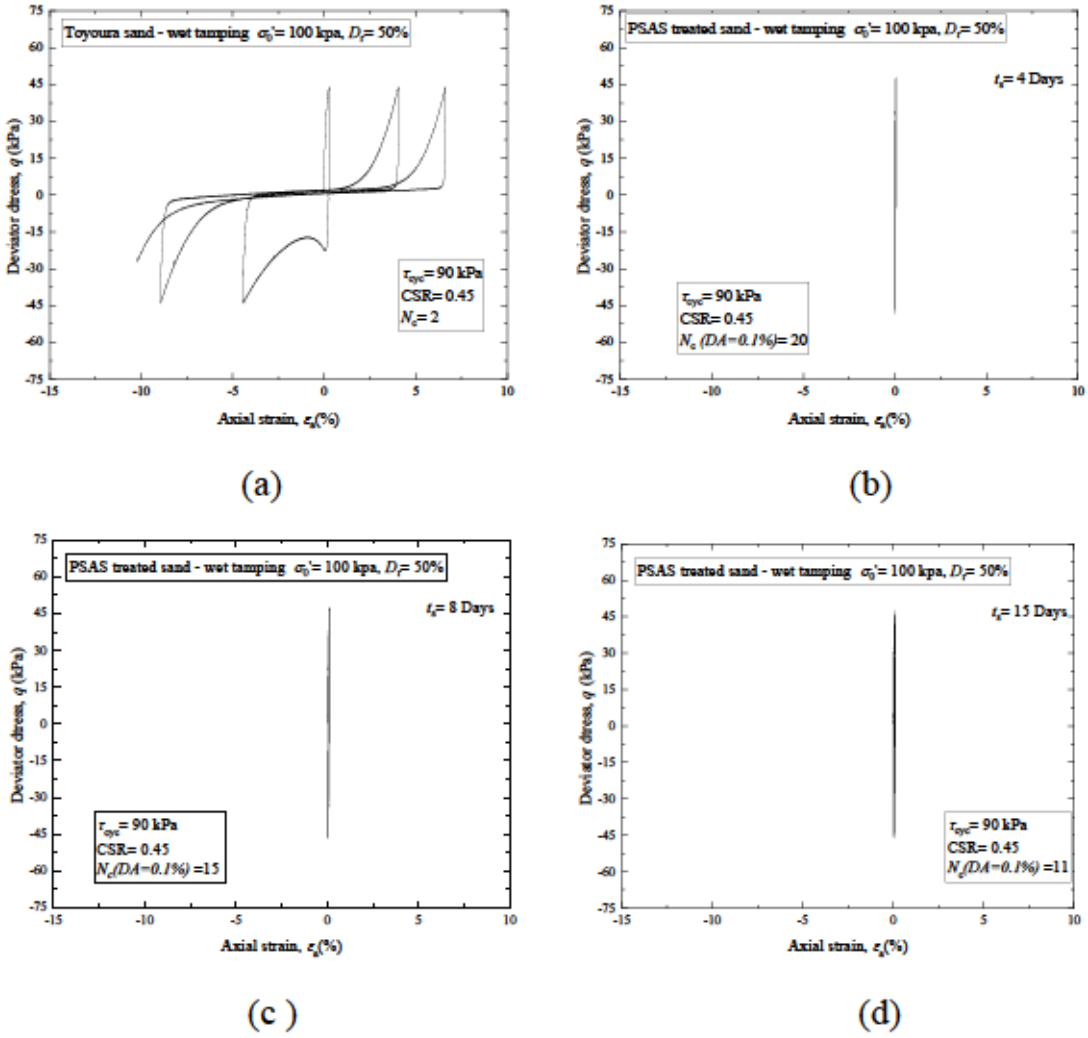


**Figure 7-4** Undrained cyclic response of (a)stress-strain relationship of untreated sand (Toyoura sand), ), (b)stress-strain relationship of PSAS-treated sand ($t_s$=4 days, $D_r$=50%), (c) stress-strain relationship of PSAS-treated sand ($t_s$=8 days, $D_r$=50%), (d) stress-strain relationship of PSAS-treated sand ($t_s$=15 days, $D_r$=50%), *CSR*=0.45

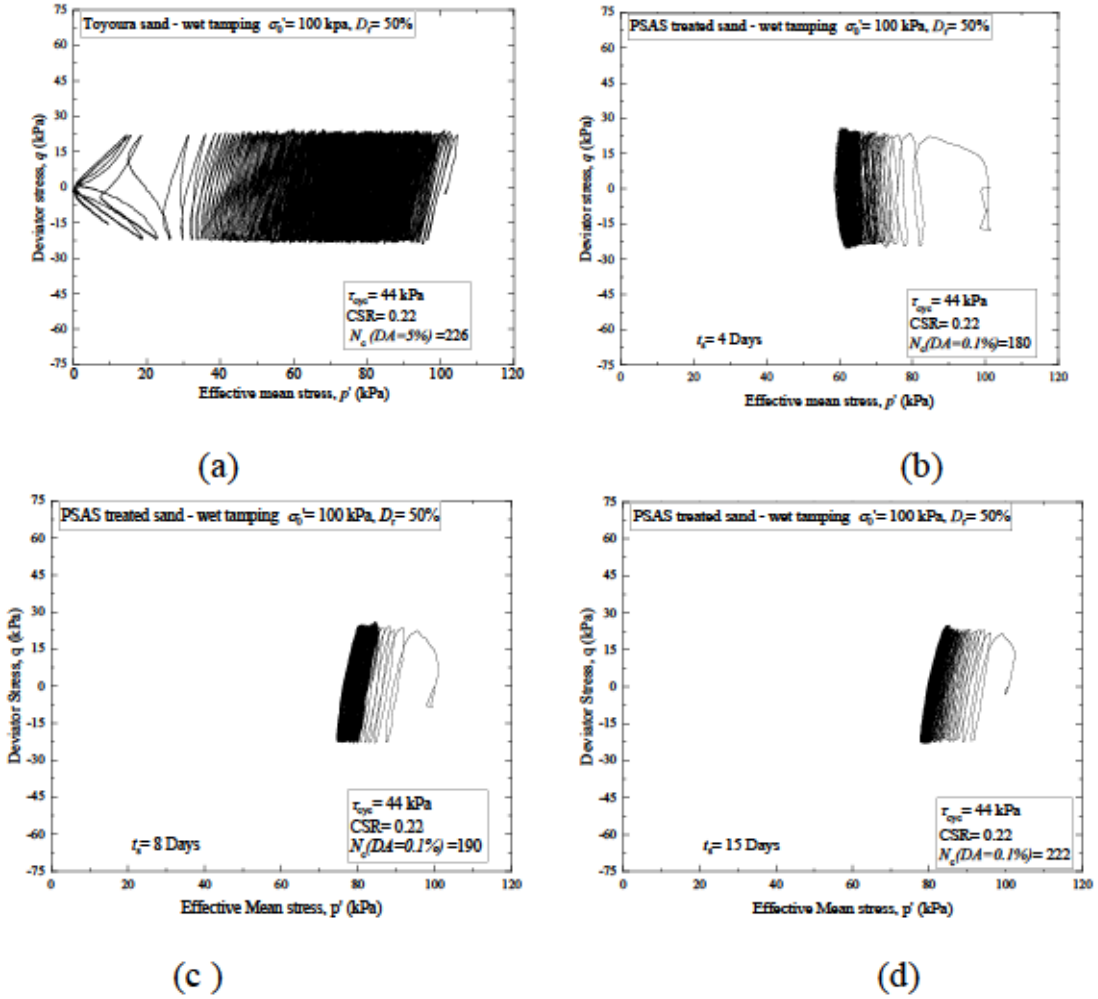


**Figure 7-5** Undrained cyclic response of (a)stress path of untreated sand (Toyoura sand), (b)stress path of PSAS-treated sand ($t_s$=4 days, $D_r$=50%). (c)stress path of PSAS-treated sand ($t_s$=8 days, $D_r$=50%), (d)stress path of PSAS-treated sand ($t_s$=15 days, $D_r$=50%), for *CSR*=0.22.

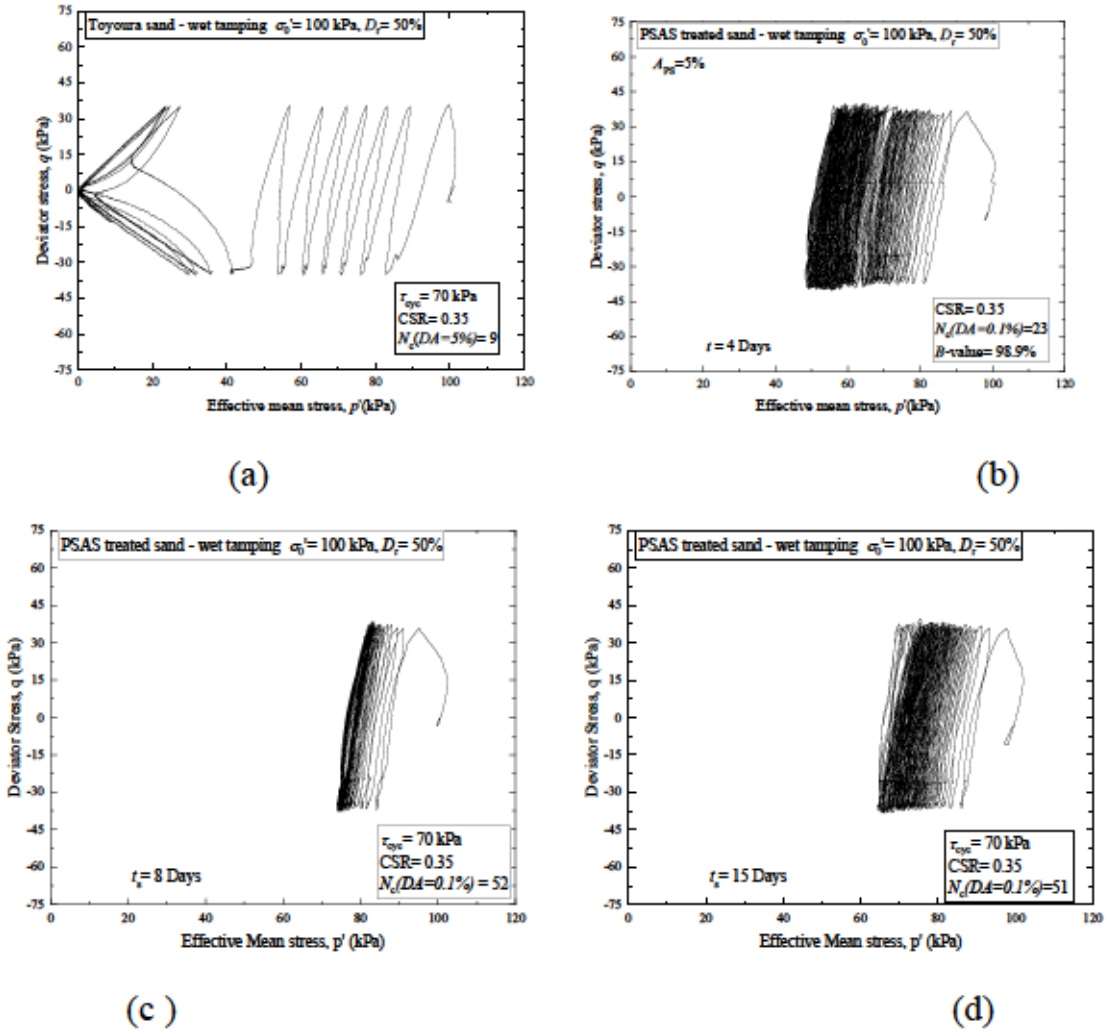


**Figure 7-6** Undrained cyclic response of (a)stress path of untreated sand (Toyoura sand), (b)stress path of PSAS-treated sand ($t_s$=4 days, $D_r$=50%). (c)stress path of PSAS-treated sand ($t_s$=8 days, $D_r$=50%), (d)stress path of PSAS-treated sand ($t_s$=15 days, $D_r$=50%), for *CSR*=0.35.

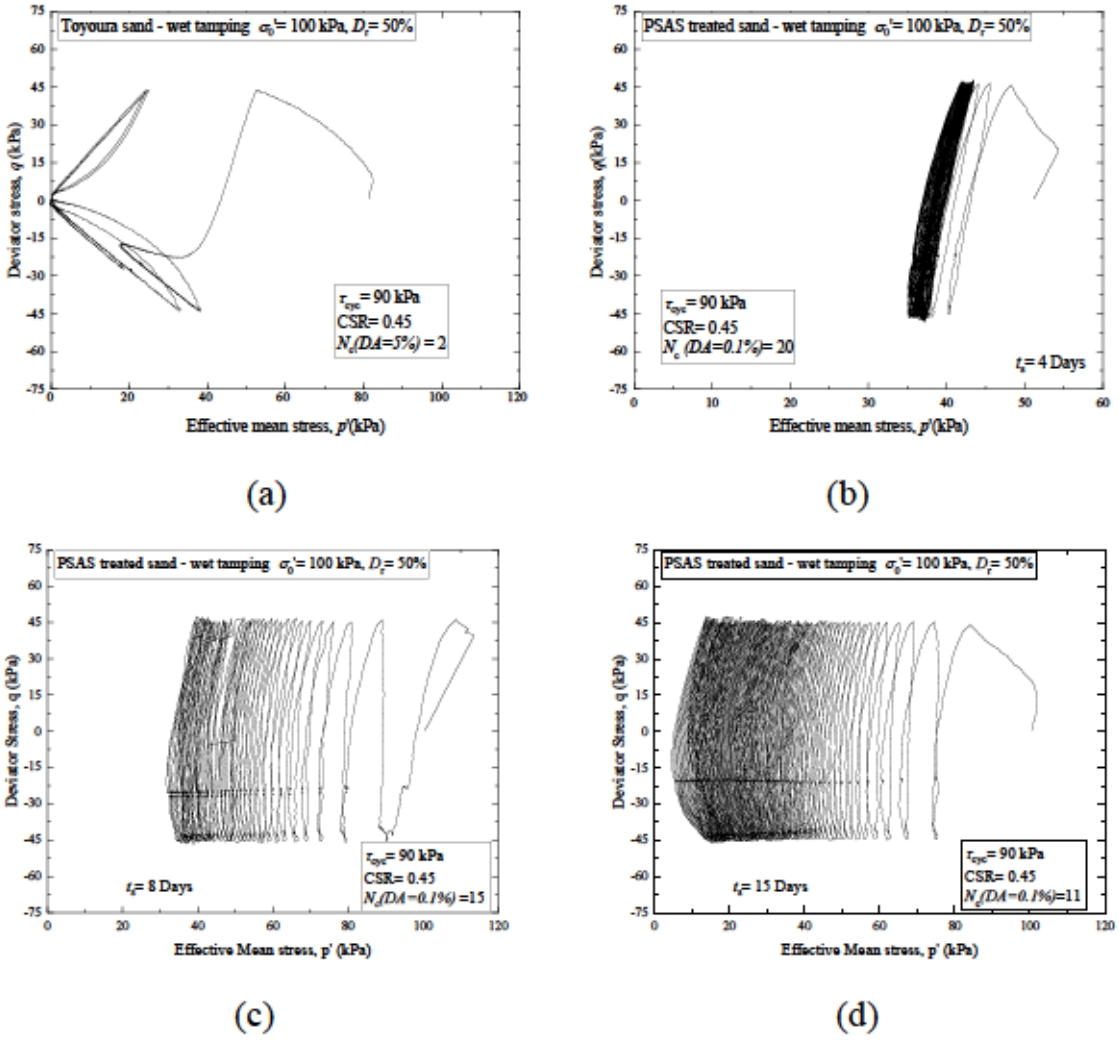


**Figure** 7-7 Undrained cyclic response of (a)stress path of untreated sand (Toyoura sand), (b)stress path of PSAS-treated sand ($t_s$=4 days, $D_r$=50%). (c)stress path of PSAS-treated sand ($t_s$=8 days, $D_r$=50%), (d)stress path of PSAS-treated sand ($t_s$=15 days, $D_r$=50%), for *CSR*=0.45.

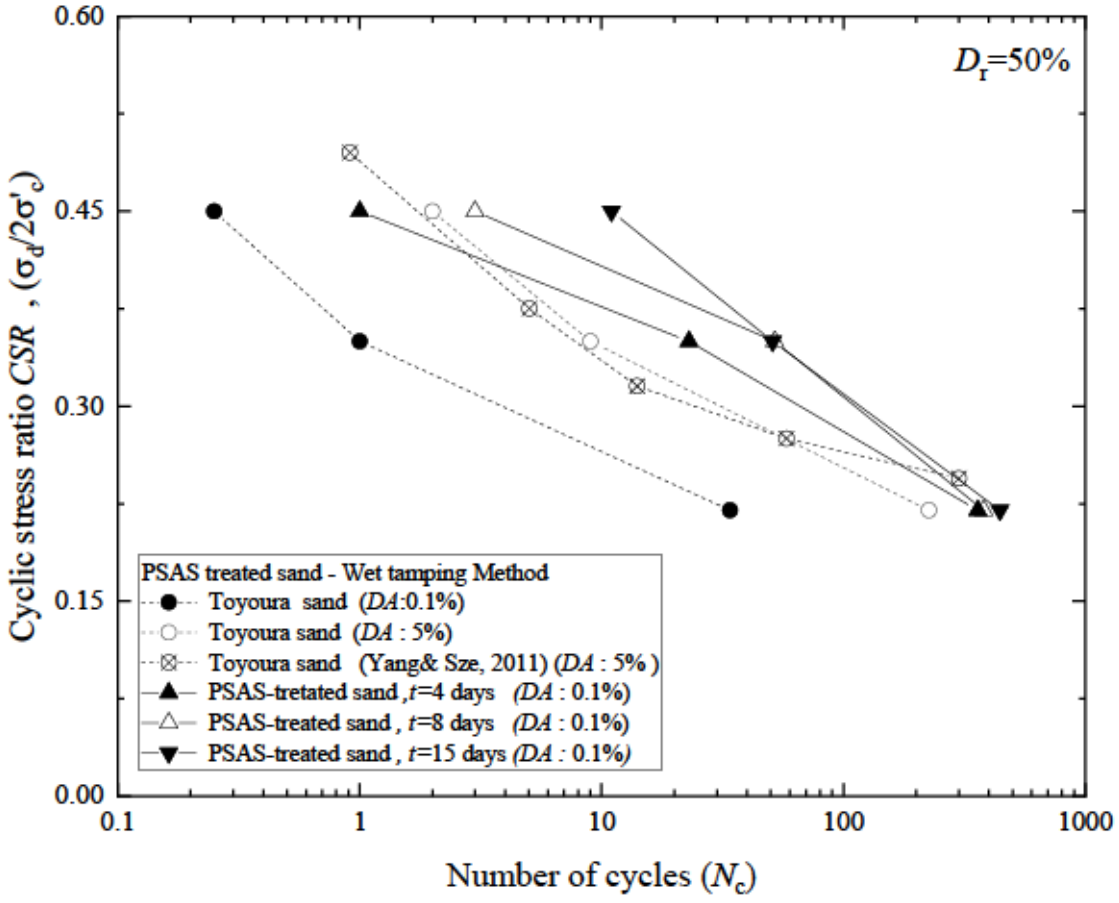


**Figure 7-8** Liquefaction resistance curve of untreated sand and PSAS-treated sand.

CHAPTER 8

# 8. Conclusions and recommendations

## 8.1 Conclusions

Throughout this comprehensive thesis, a detailed investigation into the geotechnical properties of Toyoura sand and Paper Sludge Ash-Based Stabilizer (PSAS) has been conducted with the aim of assessing their suitability for backfilling materials around underground pipes and structures. The research focused on understanding the deformation and strength characteristics of the treated sand to ensure the stability and integrity of buried pipes, particularly under the influence of traffic loads and cyclic loading. The results obtained from a wide range of laboratory tests have provided valuable insights into the behaviour of PSAS-treated sand in comparison to untreated sand, paving the way for potential engineering applications. The key findings and implications from each chapter can be summarized as follows:

**(a) Fundamental properties and swelling potential of PSAS-treated sand:**

- The results from maximum and minimum density tests showcased that the incorporation of PSAS increased the difference between $e_{max}$ and $e_{min}$, which has practical implications for achieving more effective compaction of PSAS-treated sand as a backfill material around underground pipes.
- Swelling potential tests unveiled that PSAS-treated sand with a specific water content ($w$=0%) displayed significant expansion during soaking, akin to OPC-treated sand.
- However, the test results also revealed that the appropriate $w$ of the PSAS-treated sand reduced its expansion potential, depending on the duration of its temporary placement at the construction site.

**(b) Deformation and strength development of PSAS-treated sand:**

- The comprehensive unconfined compression tests conducted on PSAS-treated sands revealed intriguing results. While the compressive strength ($q_u$) of PSAS-treated sands was comparatively lower than that of OPC-treated sands under similar mixing conditions, it was observed that the $q_u$ increased gradually with curing time, signifying the ease of re-excavation for PSAS-treated sands.
- The X-ray Diffraction (XRD) profiles further deepened our understanding, indicating the presence of $CaCO_3$ , Ettringite $Ca_6Al_2(SO_4)3(OH)_{12}\cdot 26H_2O$ and $AlPO_4$, which contributed to the long-term enhancement of the treated sand's strength.

- Comparison of external and local measurements of axial strain indicated bedding errors in both the PSAS- and cement-treated sands. The deformation modulus of the PSAS-treated sand at 0.002% axial strain was determined via local measurement while considering the strain level in the subgrade, and it was discovered to be approximately 3000 times the value of $q_u$.
- The treated sand exhibits higher deviator stress and lower volumetric strain compared to Toyoura sand, indicating increased shear strength and reduced compressibility. Additionally, the treated sand shows a stronger response to changes in normal stress, as evidenced by the shift of the stress paths.
- The cohesion of the PSAS treated sand is consistently higher than those of Toyoura sand at all relative densities ($D_r$=50% and $D_r$=90%) and curing periods. However, the shear resistance increased remain limited after curing period after 5 days of curing, followed by no significant improvement with further curing time.
- The comparison between CDT and UCS results indicates that the triaxial test provides more realistic stress conditions and is better suited for evaluating the shear strength of PSAS-treated sand in field-like conditions.

**(c) Effects of dry-wet cycles on the mechanical properties of sand treated with paper sludge ash-based stabiliser:**

- The durability of PSAS-treated sands subjected to dry-wet cycles was investigated for backfilling purposes. The $q_u$ of PSAS-treated specimens initially increased with curing and then decreased towards zero after several dry-wet cycles.
- Confinement played a crucial role in assessing the durability of PSAS-treated sands subjected to dry-wet curing.
- XRD profiles demonstrated the changes in ettringite content under varying dry-wet cycles, indicating the instability of ettringite at high temperatures.

**(d) Liquefaction evaluation of PSAS-treated sand:**

- Cyclic triaxial tests revealed distinctive stress paths for Toyoura sand and PSAS-treated sand. The figure-eight shapes of stress paths for Toyoura sand indicated significant plastic deformation and hysteresis during cyclic loading, while PSAS-treated sand exhibited more linear paths, suggesting minimal plastic deformation.
- Moreover, with increasing curing time, the stress paths of PSAS-treated sand became closer to vertical, indicating reduced plastic deformation. These results clearly demonstrate the effectiveness of PSAS treatment

in improving the cyclic shear behaviour of sandy soil and its potential for providing a more stable and less plastic response to applied stresses, making it a reliable and liquefaction-resistant soil for civil engineering applications.

Throughout this comprehensive thesis, a detailed investigation into the geotechnical properties of Toyoura sand and Paper Sludge Ash-Based Stabilizer (PSAS) has been conducted with the aim of assessing their suitability for backfilling materials around underground pipes and structures. The research focused on understanding the deformation and strength characteristics of the treated sand to ensure the stability and integrity of buried pipes, particularly under the influence of traffic loads and cyclic loading. The results obtained from a wide range of laboratory tests have provided valuable insights into the behaviour of PSAS-treated sand in comparison to untreated sand, paving the way for potential engineering applications.

## 8.2 Recommendations

Building upon the findings of this research, the adoption of Paper Sludge Ash-Based Stabilizer (PSAS) as a backfill material around underground pipes is highly recommended.

- The substantial enhancement of cohesion and shear resistance observed in PSAS-treated sand makes it an appealing and promising option for geotechnical engineering applications. The ability of PSAS-treated sand to resist liquefaction and exhibit improved cyclic performance under varying stress conditions reinforces its potential as a reliable and durable material.
- In addition to the aforementioned recommendations, there is a need for further research to investigate the hysteric deformation behaviour of PSAS-treated sand for its suitability in liquefaction resistance. Understanding how PSAS treatment impacts the cyclic loading response and hysteresis of the treated sand is crucial for assessing its performance in seismic-prone regions. Conducting cyclic triaxial tests with varying stress amplitudes and loading frequencies will enable a more comprehensive evaluation of the liquefaction resistance of PSAS-treated sand under realistic seismic conditions.
- Furthermore, to optimize the implementation of PSAS treatment in geotechnical projects, it is essential to conduct field-scale studies. Assessing the long-term performance of PSAS-treated sand in actual construction scenarios will provide practical insights into its behaviour

under real-world conditions, considering factors like weathering, moisture changes, and traffic loading.

- Finally, collaborative efforts between researchers, civil engineers, and environmental experts are necessary to develop guidelines and standards for the implementation of PSAS-treated sand in geotechnical engineering projects. Establishing clear protocols for mixture design, compaction procedures, and quality control will ensure consistent and reliable outcomes in various applications.

# References

Abbas, M. F., Shaker, A. A., & Al-Shamrani, M. A. (2023). Hydraulic and volume change behaviors of compacted highly expansive soil under cyclic wetting and drying. *Journal of Rock Mechanics and Geotechnical Engineering*, *15*(2), 486–499. https://doi.org/10.1016/j.jrmge.2022.05.015

Allam, M. M., & Sridharan, A. (1981). Effect of Wetting and Drying on Shear Strength. *Journal of the Geotechnical Engineering Division*, *107*(4), 421–438. https://doi.org/10.1061/AJGEB6.0001117

Alshameri, B., Madun, A., & Hj. Bakar, I. (2017). Comparison of the effect of fine content and density towards the shear strength parameters. *Geotechnical Engineering*, *48*, 104–111.

Ayob, A., Zahid, M., Mohammad, M. F., & Yunus, N. M. (2014). Physical, morphological and strength properties of Jana Manjung coal ash mixture for geotechnical applications. *Advances in Environmental Biology*, 25–30.

Batey, T., & McKenzie, D. C. (2006). Soil compaction: Identification directly in the field. *Soil Use and Management*, *22*(2), 123–131. https://doi.org/10.1111/j.1475-2743.2006.00017.x

Bhaskar, P., Boluk, B., Mosadegh, L., Banerjee, A., & Puppala, A. (2020). *Effect of Fines on Hysteretic Hydraulic Conductivity of Unsaturated Soil* (p. 339). https://doi.org/10.1061/9780784482827.037

Dobry, R., & Ladd, R. S. (1980). Discussion of "Soil Liquefaction and Cyclic Mobility Evaluation for Level Ground during Earthquakes and Liquefaction Potential: Science Versus Practice". *Journal of the Geotechnical Engineering Division*, *106*(6), 720–724. https://doi.org/10.1061/AJGEB6.0000984

Du, S., & Chian, S. C. (2015). Cyclic response of liquefiable sand under stress-controlled and strain-controlled triaxial testing. In *Geotechnical Engineering for Infrastructure and Development* (Vols 1–7, pp. 2135–2140). ICE Publishing. https://doi.org/10.1680/ecsmge.60678.vol4.324

Erten, D., & Maher, M. H. (1995). Cyclic undrained behavior of silty sand. *Soil Dynamics and Earthquake Engineering*, *14*(2), 115–123. https://doi.org/10.1016/0267-7261(94)00035-F

Gao, Y., Hang, L., He, J., & Chu, J. (2019). Mechanical behaviour of biocemented sands at various treatment levels and relative densities. *Acta Geotechnica*, *14*(3), 697–707. https://doi.org/10.1007/s11440-018-0729-3

Gerasimova, V. (2016). Underground engineering and trenchless technologies at the defense of environment. *Procedia Engineering*, *165*, 1395–1401.

Ghosh, A., & Subbarao, C. (2012). Deformation Modulus of Fly Ash Modified with Lime and Gypsum. *Geotechnical and Geological Engineering*, *30*(2), 299–311. https://doi.org/10.1007/s10706-011-9468-z

Henshell, J. (2016). Negative-side waterproofing. In *The Manual of Below-Grade Waterproofing* (2nd ed.). Routledge.

Hosoya Y et al. (n.d.). *Studies on Soil Improvement Controlled at Low Strenght for Excavtion of Ground treated by Deep mixing Method*. *Part 3*(1993). https://doi.org/1993_046_11

Imai, K., Hayano, K., & Yamauchi, H. (2020). Fundamental study on the acceleration of the neutralization of alkaline construction sludge using a CO2 incubator. *Soils and Foundations*, *60*(4), 800–810.

Ishihara, K. (1993). Liquefaction and flow failure during earthquakes. *Géotechnique*, *43*(3), 351–451. https://doi.org/10.1680/geot.1993.43.3.351

Ishihara, K., Tatsuoka, F., & Yasuda, S. (1975). Undrained Deformation and Liquefaction of Sand Under Cyclic Stresses. *Soils and Foundations*, *15*(1), 29–44. https://doi.org/10.3208/sandf1972.15.29

Japanese Geotechnical Society JGS 0161-2009. (2018). *Test method for minimum and maximum desnities of sands* (Vol. 1). Japanese Geotechnical Society.

Japanese Geotechnical Society JGS 0211-2020. (n.d.). *Test Method for pH of suspended soils* (Vol. 3). Japanese Geotechnical Society.

Japanese Geotechnical Society JGS 0721-2009. (n.d.). *Test method for the California Bearing Ratio (CBR) of soils in laboratory* (Vol. 2). Japanese Geotechnical Society.

Japanese Geotechnical Society JGS 0821-2020. (n.d.). *Practice for making and curing stabilized soil specimens without compaction* (Vol. 2). Japanese Geotechnical Society.

Kang, G., Tsuchida, T., & Kim, Y. (2017). Strength and stiffness of cement-treated marine dredged clay at various curing stages. *Construction and Building Materials*, *132*, 71–84. https://doi.org/10.1016/j.conbuildmat.2016.11.124

Kawai, S., Hayano, K., & Yamauchi, H. (2018). Fundamental Study on Curing Effect and its Mechanism on the Strength Characteristics of PS Ash-Based Improved Soil. *Journal of Japan Society of Civil Engineers, Ser. C (Geosphere Engineering)*, *74*(3), 306–317.

Keramatikerman, M., Chegenizadeh, A., & Nikraz, H. (2017). Experimental study on effect of fly ash on liquefaction resistance of sand. *Soil Dynamics and Earthquake Engineering*, *93*, 1–6. https://doi.org/10.1016/j.soildyn.2016.11.012

Kitazume, M., & Okamura, M. (2010). Contributions to "Soils and Foundations": Ground Improvement. *Soils and Foundations*, *50*(6), 965–975. https://doi.org/10.3208/sandf.50.965

Kohata, Y. (2006). Mechanical property of liquefied stabilized soil and future issues. *Doboku Gakkai Ronbunshuu, F*, *62*(4), 618–627.

Kongsukprasert, L., Tatsuoka, F., & Takahashi, H. (2007). Effects of curing period and stress conditions on the strength and deformation characteristics of cement-mixed soil. *Soils and Foundations*, *47*(3), 577–596.

Li, Y., Zhang, W., He, S., & Aydin, A. (2020). Wetting-driven formation of present-day loess structure. *Geoderma*, *377*, 114564. https://doi.org/10.1016/j.geoderma.2020.114564

Liu, J., Sui, W., Zhang, D., & Zhao, Q. (2020). Durability of water-affected paste backfill material and its clean use in coal mining. *Journal of Cleaner Production*, *250*, 119576. https://doi.org/10.1016/j.jclepro.2019.119576

Liu, X., Li, S., Yin, J., & Li, T. (2022). The effect of drying and wetting cycles on the mechanical properties and particle breakage of carbonate sand. *Acta Geotechnica*, *17*(10), 4641–4654.

Maqsood, Z., Koseki, J., Ahsan, M. K., Shaikh, M., & Kyokawa, H. (2020). Experimental study on hardening characteristics and loading rate dependent mechanical behaviour of gypsum mixed sand. *Construction and Building Materials*, *262*, 119992.

Maqsood, Z., Koseki, J., Miyashita, Y., Xie, J., & Kyokawa, H. (2020). Experimental study on the mechanical behaviour of bounded geomaterials under creep and cyclic loading considering effects of instantaneous strain rates. *Engineering Geology*, *276*, 105774.

Mashiri, M. S., Vinod, J. S., Sheikh, M. N., & Tsang, H.-H. (2015). Shear strength and dilatancy behaviour of sand–tyre chip mixtures. *Soils and Foundations*, *55*(3), 517–528. https://doi.org/10.1016/j.sandf.2015.04.004

Mochizuki, Y., Yoshino, H., Saito, E., & Ogata, T. (2003). Effects of soil improvement due to mixing with paper sludge ash. *Proceeding of China-Japan Geotechnical Symposium*, 1–8.

Mohajerani, A., Hui, S.-Q., Mirzababaei, M., Arulrajah, A., Horpibulsuk, S., Abdul Kadir, A., Rahman, M. T., & Maghool, F. (2019). Amazing Types, Properties, and Applications of Fibres in Construction Materials. *Materials*, *12*(16), Article 16. https://doi.org/10.3390/ma12162513

Mohamed, A. E. M. K. (2013). Improvement of swelling clay properties using hay fibers. *Construction and Building Materials*, *38*, 242–247. https://doi.org/10.1016/j.conbuildmat.2012.08.031

Ng, C. W. W., & Peprah-Manu, D. (2023). Pore structure effects on the water retention behaviour of a compacted silty sand soil subjected to drying-wetting cycles. *Engineering Geology*, *313*, 106963. https://doi.org/10.1016/j.enggeo.2022.106963

Patel, S. K., & Singh, B. (2019). Shear strength response of glass fibre-reinforced sand with varying compacted relative density. *International Journal of Geotechnical Engineering*, *13*(4), 339–351. https://doi.org/10.1080/19386362.2017.1352157

Peterson, K. (2014). Underground piping systems. *ASHRAE Journal*, *56*(9), 54–58.

Prabakar, J., Dendorkar, N., & Morchhale, R. K. (2004). Influence of fly ash on strength behavior of typical soils. *Construction and Building Materials*, *18*(4), 263–267.

Procter, D. C., & Khaffaf, J. H. (1984). Cyclic Triaxial Tests on Remoulded Clays. *Journal of Geotechnical Engineering*, *110*(10), 1431–1445. https://doi.org/10.1061/(ASCE)0733-9410(1984)110:10(1431)

Promputthangkoon, P., & Hyde, A. (2007). Compressibility and liquefaction potential of rubber composite soils. *Proc. of the Int. Workshop on Scrap Tire Derived Geometricals Â€“Opportunities and Challenges*, 161–170.

Puppala, A. J., Saride, S., & Chomtid, S. (2009). Experimental and Modeling Studies of Permanent Strains of Subgrade Soils. *Journal of Geotechnical and Geoenvironmental Engineering*, *135*(10), 1379–1389.

Ramaji, A. E. (2012). A review on the soil stabilization using low-cost methods. *Journal of Applied Sciences Research*, *8*(4), 2193–2196.

Rao, S. (2011). Wetting and Drying, Effect on Soil Physical Properties. In *Encyclopedia of Earth Sciences Series* (pp. 992–996). https://doi.org/10.1007/978-90-481-3585-1_189

Silver, M. L., & Park, T. K. (1976). Liquefaction Potential Evaluated from Cyclic Strain-Controlled Properties Tests on Sands. *Soils and Foundations*, *16*(3), 51–65. https://doi.org/10.3208/sandf1972.16.3_51

Speakman, S. A. (2013). Introduction to x-ray powder diffraction data analysis. *Center for Materials Science and Engineering at MIT*.

Stavridakis, E. I. (2005). Evaluation of engineering and cement–stabilization parameters of clayey–sand mixtures under soaked conditions. *Geotechnical & Geological Engineering*, *23*(6), 635–655.

Subramanian, S., Khan, Q., & Ku, T. (2019). Strength development and prediction of calcium sulfoaluminate treated sand with optimized gypsum for replacing OPC in ground improvement. *Construction and Building Materials*, *202*, 308–318. https://doi.org/10.1016/j.conbuildmat.2018.12.121

Taha Jawad, I., Raihan Taha, M., Hameed Majeed, Z., & A. Khan, T. (2014). Soil Stabilization Using Lime: Advantages, Disadvantages and Proposing a Potential Alternative. *Research Journal of Applied Sciences, Engineering and Technology*, *8*(4), 510–520. https://doi.org/10.19026/rjaset.8.1000

Takayama, T., Murao, R., & Kimura, M. (2018). Quantitative Analysis of Mineral Phases in Iron-ore Sinter by the Rietveld Method of X-ray Diffraction Patterns. *ISIJ International*, *58*(6), 1069–1078. https://doi.org/10.2355/isijinternational.ISIJINT-2017-717

Tang, C.-S., & Shi, B. (2011). Swelling and shrinkage behaviour of expansive soil during wetting-drying cycles. *Yantu Gongcheng Xuebao/Chinese Journal of Geotechnical Engineering*, *33*, 1376–1384.

Tatsuoka, F., Uchida, K., Imai, K., Ouchi, T., & Kohata, Y. (1997). Properties of cement-treated soils in Trans-Tokyo Bay Highway project. *Proceedings of the Institution of Civil Engineers - Ground Improvement*, *1*(1), 37–57. https://doi.org/10.1680/gi.1997.010105

Toyota, H., Nakamura, K., & Kazama, M. (2004). Shear and Liquefaction Characteristics of Sandy Soils in Triaxial Tests. *Soils and Foundations*, *44*(2), 117–126. https://doi.org/10.3208/sandf.44.2_117

Toyota, H., & Takada, S. (2023). Aging effects on liquefaction resistance of sand estimated from laboratory investigation. *Soils and Foundations*, *63*(3), 101318. https://doi.org/10.1016/j.sandf.2023.101318

Trung, N. D., Ogasawara, T., Hayano, K., & Yamauchi, H. (2021). Accelerated carbonation of alkaline construction sludge by paper sludge ash-based stabilizer and carbon dioxide. *Soils and Foundations*, *61*(5), 1273–1286. https://doi.org/10.1016/j.sandf.2021.06.012

Tsukamoto, Y., Nebuya, Y., & Noda, S. (n.d.). *Effects of ageing and stress history on liquefaction resistance of soils*.

Uchimura, T., Chi, N., Nirmalan, S., Sato, T., Meidani, M., & Towhata, I. (2007). Shaking table tests on effect of tire chips and sand mixture in increasing liquefaction resistance and mitigating uplift of pipe. *Proceedings, International Workshop on Scrap Tire Derived Geomaterials—Opportunities and Challenges, Yokosuka, Japan*, 179–186.

Wang, D., Abriak, N. E., & Zentar, R. (2013). Strength and deformation properties of solidified marine sediments with cement, lime and fly ash. *Engineering Geology*, *166*, 90–99.

Wang, J., & Fu, J. (2021). *Influence of water saturation on the strength characteristics and deformation behavior of hardened cement paste backfill*. https://doi.org/10.21203/rs.3.rs-351748/v1

Wang, J.-J., Zhou, Y.-F., Wu, X., & Zhang, H.-P. (2019). Effects of soaking and cyclic wet-dry actions on shear strength of an artificially mixed sand. *KSCE Journal of Civil Engineering*, *23*, 1617–1625.

Wei, X., & Ku, T. (2020). New design chart for geotechnical ground improvement: Characterizing cement-stabilized sand. *Acta Geotechnica*, *15*, 999–1011.

Wong, R. T., Seed, H. B., & Chan, C. K. (1975). CYCLIC LOADING LIQUEFACTION OF GRAVELLY SOILS. *Journal of Geotechnical and Geoenvironmental Engineering*, *101*(GT6), Article ASCE #11396 Proceeding. https://trid.trb.org/view/39487

Xu, X., Shao, L., Huang, J., Xu, X., Liu, D., Xian, Z., & Jian, W. (2021). Effect of wet-dry cycles on shear strength of residual soil. *Soils and Foundations*, *61*(3), 782–797. https://doi.org/10.1016/j.sandf.2021.03.001

Yamashita, E., Aristo Cikmit, A., Tsuchida, T., & Hashimoto, R. (2020). Strength estimation of cement-treated marine clay with wide ranges of sand and initial water contents. *Soils and Foundations*, *60*(5), 1065–1083. https://doi.org/10.1016/j.sandf.2020.05.002

Yao, Y., & Sun, H. (2012). A novel silica alumina-based backfill material composed of coal refuse and fly ash. *Journal of Hazardous Materials*, *213–214*, 71–82. https://doi.org/10.1016/j.jhazmat.2012.01.059

Yong, he, Cui, Y.-J., Ye, W.-M., & Conil, N. (2017). Effects of wetting-drying cycles on the air permeability of compacted Téguline clay. *Engineering Geology*, *228*. https://doi.org/10.1016/j.enggeo.2017.08.015

Yoobanpot, N., Jamsawang, P., Krairan, K., Jongpradist, P., & Likitlersuang, S. (2020). Laboratory investigation of the properties of cement fly ash gravel for use as a column-supported embankment. *Construction and Building Materials*, *257*, 119493.

Yuriz, Y., Ismail, T. N. H. T., & Hassan, N. N. M. (2020). An Overview of Waste Materials for Sustainable Road Construction. *International Journal of Sustainable Construction Engineering and Technology*, *11*(1), 215–229.

Zhang, T., Cai, G., & Duan, W. (2018). Strength and microstructure characteristics of the recycled rubber tire-sand mixtures as lightweight backfill. *Environmental Science and Pollution Research*, *25*(4), 3872–3883. https://doi.org/10.1007/s11356-017-0742-3

Zhou, S., Zhou, D., Zhang, Y., & Wang, W. (2019). Study on Physical-Mechanical Properties and Microstructure of Expansive Soil Stabilized with Fly Ash and Lime. *Advances in Civil Engineering*, *2019*, e4693757. https://doi.org/10.1155/2019/4693757

Zhu, Z., Zhang, F., Peng, Q., Dupla, J.-C., Canou, J., Cumunel, G., & Foerster, E. (2021). Effect of the loading frequency on the sand liquefaction behaviour in cyclic triaxial tests. *Soil Dynamics and Earthquake Engineering*, *147*, 106779. https://doi.org/10.1016/j.soildyn.2021.106779

# APPENDIX

# A Contents


**A APPENDIX–I Geotechnical properties of materials used. 7**

A.1 Density of soil Particles 7

A.1.1 Equipment 7

A.1.2 Particle density Test methods 7

A.1.3 Toyoura Sand Particle Density 8

A.2 Particles size distribution test (PSD) 8

A.2.1 PSD Test sequence 8

A.2.2 Equipment for PSD 8

A.2.3 PSD test Results 10

A.3 Minimum and maximum density tests 11

A.3.1 Minimum and maximum test results 13

A.3.2 Calculation of void ratio of each treated specimen 16

A.3.3 Mixture method of Treated sand 17

**B APPENDIX–II Swelling potential of paper sludge ash (PSAS) treated sand. 18**

B.1 Swelling potential measurement set up. 18

B.2 Swelling test results obtained using a comparator. 18

**C APPENDIX -III Deformation and strength development of paper sludge ash treated sand. 20**

C.1 Unconfined compression test of treated specimen 20

C.1.1 Test record for unconfined compression test 20

C.2 Unconfined compression test Results 22

C.2.1 Stress-strain relationship of PSAS treated sand for w=10%, tp=3 days, $D_r$=50% 22

C.2.2 Stress-strain relationship of PSAS treated sand for $w$=10%, tp=3 days, $D_r$=90% 26

C.2.3 Stress-strain relationship of PSAS treated sand for $w$=20%, $t$p=0 days, $D_r$=50% 30

C.2.4 Stress-strain relationship of PSAS treated sand for $w$=20%, tp=0 days, $D_r$=90% 37

C.2.5 Stress-strain relationship of OPC-treated sand for w=10%, tp=3 days, Dr=50% 44

C.2.6 Stress-strain relationship of OPC-treated sand for w=10%, tp=3 days, Dr=90% 48

C.3 Monotonic triaxial tests 52

C.3.1 Normative references 52

C.3.2 Triaxial test apparatus and setting. 52

C.3.3 Terms and definitions 54

C.3.4 Types of triaxial test 54

C.3.5 Equipment conditions in the laboratory 55

C.3.6 Negative pressure method used for sample preparation 56

C.3.7 Method used to fill the mould with sample material. JGS 0520 56

C.3.8 Saturation of specimen 57

C.3.9 Consolidation process 57

C.3.10 Axial compression process 58

C.3.11 Data record for Triaxial test 58

C.4 Method for cyclic undrained triaxial test on soils-Japanese geotechnical society standard (JGS 0541 -2009) 60

C.4.1 Scope....60
C.4.2 Cyclic deviator stress....60
C.4.3 Cyclic stress amplitude ratio....60
C.4.4 Equipment for cyclic triaxial test....61
C.4.5 5.3 Consolidation process....64
C.4.6 5.5 tests with cyclic loading amplitude varied....64
C.4.7 Typical Undrained cyclic result obtained....64
**D APPENDIX- IV. Effects of dry-wet cycles on the mechanical properties of sand treated with paper sludge ash-based stabilizer....65**
D.1 Specimen Test Procedure and measurement condition....65
D.2 Unconfined compression test results for specimen cured under dry-wet cycle process....65
D.2.1 T=40℃ Dry-wet cycle Stress-strain relationship of PSAS treated sand for w=20%, tp=1 days, Dr=50% 65
D.2.2 T=40℃ Dry-wet cycle Stress-strain relationship of PSAS treated sand for w=20%, tp=1 days, Dr=90% 66

## List of Appendix figures

Figure A-1 Sieve setting and Mass measurement....10
Figure A-2 Minimum and maximum test setting up and Measurement....12
Figure A-3 Mixing condition of PSAS-treated sand....17
Figure B-1 Swelling measurement using CBR test setting....18
Figure C-1 UCT apparatus setting....20
Figure C-2 Specimen preparation flow....21
Figure C-3 Typical UCT stress-strain relationship of PSAS-treated sand for w=10%, tp=3days, $D_r$=50% (a) t= 3days, (b) t= 7 days....22
Figure C-4 Typical UCT stress-strain relationship of PSAS-treated sand for w=10%, tp=3 days, $D_r$=50%: (c) t= 14days, (d) t= 28 days....23
Figure C-5 Typical UCT stress-strain relationship of PSAS-treated sand for w=10%, tp=3days, $D_r$=50% (e) t= 60 days, (f) t= 90 days....24
Figure C-6 Typical UCT stress-strain relationship of PSAS-treated sand for w=10%, tp=3days, $D_r$=50%: (g) t= 180days, (h) t= 360 days....25
Figure C-7 Typical UCT stress-strain relationship of PSAS-treated sand for w=10%, tp=3days, $D_r$=90%: (a) t= 3days, (b) t= 7 days....26
Figure C-8 Typical UCT stress-strain relationship of PSAS-treated sand for w=10%, tp=3days, Dr=90%: (c) t= 14days, (d) t= 28 days....27

Figure C-9 Typical UCT stress-strain relationship of PSAS-treated sand for w=10%, tp=3days, Dr=90%: (e) t= 60days, (f) t= 90days....28
Figure C-10 Typical UCT stress-strain relationship of PSAS-treated sand for w=10%, tp=3days, Dr=90%: (e) t= 180days, (f) t= 360days....29
Figure C-11 Typical UCT stress-strain relationship of PSAS-treated sand for w=20%, tp=0days, Dr=50%, t= 3days: (a) ESM, (b) LSM....30
Figure C-12 Typical UCT stress-strain relationship of PSAS-treated sand for w=20%, tp=0days, Dr=50%, t= 7days: (a) ESM (b) LSM....31
Figure C-13 Typical UCT stress-strain relationship of PSAS-treated sand for w=20%, tp=0days, Dr=50%, t= 14days: (a) ESM (b) LSM....32
Figure C-14 Typical UCT stress-strain relationship of PSAS-treated sand for w=20%, tp=0days, Dr=50%, t= 28 days: (a) ESM (b) LSM....33
Figure C-15 Typical UCT stress-strain relationship of PSAS-treated sand for w=20%, tp=0days, Dr=50%, t= 60 days: (a) ESM (b) LSM....34
Figure C-16 Typical UCT stress-strain relationship of PSAS-treated sand for w=20%, tp=0days, Dr=50%, t= 90 days: (a) ESM (b) LSM....35
Figure C-17 Typical UCT stress-strain relationship of PSAS-treated sand for w=20%, tp=3days, Dr=50%: (a) t= 180 days, (b) t= 360 days....36
Figure C-18 Typical UCT stress-strain relationship of PSAS-treated sand for w=20%, tp=0days, Dr=90%, t= 3days: (a) ESM, (b) LSM....37
Figure C-19 Typical UCT stress-strain relationship of PSAS-treated sand for w=20%, tp=0days, Dr=90%, t= 7days: (a) ESM, (b) LSM....38
Figure C-20 Typical UCT stress-strain relationship of PSAS-treated sand for w=20%, tp=0days, Dr=90%, t= 17days: (a) ESM, (b) LSM....39
Figure C-21 Typical UCT stress-strain relationship of PSAS-treated sand for w=20%, tp=0days, $D_r$=90%, t= 28 days: (a) ESM, (b) LSM....40
Figure C-22 Typical UCT stress-strain relationship of PSAS-treated sand for w=20%, tp=0days, Dr=90%, t= 60 days: (a) ESM, (b) LSM....41
Figure C-23 Typical UCT stress-strain relationship of PSAS-treated sand for w=20%, tp=0days, Dr=90%, t= 90 days: (a) ESM, (b) LSM....42
Figure C-24 Typical UCT stress-strain relationship of PSAS-treated sand for w=20%, tp=0days, Dr=90%: (a) t= 180 days, (b) t= 360 days....43
Figure C-25 Typical UCT stress-strain relationship of OPC-treated sand for w=10%, tp=3days, Dr=50%: (a) t= 3 days, (b) t= 7 days....44
Figure C-26 Typical UCT stress-strain relationship of OPC-treated sand for w=10%, tp=3days, Dr=50%: (c) t= 14 days, (d) t= 28 days....45
Figure C-27 Typical UCT stress-strain relationship of OPC-treated sand for w=10%, tp=3days, Dr=50%: (e) t= 60 days, (f) t= 90 days....46
Figure C-28 Typical UCT stress-strain relationship of OPC-treated sand for w=10%, tp=3days, Dr=50%: (g) t= 180 days, (h) t= 360 days....47
Figure C-29 Typical UCT stress-strain relationship of OPC-treated sand for w=10%, tp=3days, Dr=90%: (g) t= 3 days, (h) t= 7 days....48
Figure C-30 Typical UCT stress-strain relationship of OPC-treated sand for w=10%, tp=3days, Dr=90%: (c) t= 14 days, (d) t= 28 days....49
Figure C-31 Typical UCT stress-strain relationship of OPC-treated sand for w=10%, tp=3days, $D_r$=90%: (e) t= 60 days, (f) t= 90 days....50
Figure C-32 Typical UCT stress-strain relationship of OPC-treated sand for w=10%, tp=3days, Dr=90%: (e) t= 180 days, (f) t= 360 days....51
Figure C-33 Stress condition in a typical triaxial test....52
Figure C-34 Schematic illustration of triaxial apparatus....53
Figure C-35 Sample preparation equipment-Sample setup....57
Figure D-1 test program for each specimen....65
Figure D-2 T=40℃ Typical UCT stress-strain relationship of PSAS-treated sand for w=20%, tp=1days, Dr=50%, $A_{PS}$=5%: (a) C1, (b) C2, (c)= C3, and (d)=C4 ....65
Figure D-3 T=40℃ Typical UCT stress-strain relationship of PSAS-treated sand for w=20%, tp=1days, Dr=90%, $A_{PS}$=5%: (a) C1, (b) C2, (c)= C3, and (d)=C4 ....66

## List of appendix tables

Table A-a soil Particles density results of Toyoura sand....8
Table A-b particles size distribution test results of Toyoura sand....10
Table A-c Results of Minimum and a maximum density of Toyoura sand, PSAS, 2.5% PSAS treated sand....13
Table A-d Results of Minimum and the maximum density of 5%, 7.5%, 10% PSAS treated sand....14
Table A-e Results of Minimum and maximum density of Toyoura sand, OPC 2.5% cement, treated sand. 15
Table A-f Results of Minimum and maximum density of 5%,7.5%, 10% OPC-treated sand....16
Table A-g summary of Physical properties of the materials used....17
Table B-a Height measure and variation for Specimen at $D_r$=50....18
Table B-b Expansion of specimen expressed in mm for specimen compacted at $D_r$=50% ....18
Table B-c Expansion of specimen expressed in % for specimen compacted at $D_r$=50%....19
Table B-d Height measure and variation for Specimen at $D_r$=90 ....19
Table B-e Expansion of specimen expressed in mm for specimen compacted at $D_r$=90%....19
Table B-f Expansion of specimen expressed in % for specimen compacted at $D_r$=90%....19
Table C-a UCT data record for PSAS-treated sand for w=10%, tp=3days, Dr=50% at t= 3days,....22
Table C-b UCT data record for PSAS-treated sand for w=10%, tp=3days, Dr=50% at t= 7days ....22
Table C-c UCT data record for PSAS-treated sand for w=10%, tp=3days, Dr=50% at t= 14 days....23
Table C-d UCT data record for PSAS-treated sand for w=10%, tp=3days, Dr=50% at t= 28 days ....23
Table C-e UCT data record for PSAS-treated sand for w=10%, tp=3days, Dr=50% at t= 60 days....24

Table C-f UCT data record for PSAS-treated sand for w=10%, tp=3days, Dr=50% at t= 90 days .....24
Table C-g UCT data record for PSAS-treated sand for w=10%, tp=3days, Dr=50% at t= 180days .....25
Table C-h UCT data record for PSAS-treated sand for w=10%, tp=3days, Dr=50% at t= 360days .....25
Table C-i UCT data record for PSAS-treated sand for w=10%, tp=3days, Dr=90% at t= 3days .....26
Table C-j UCT data record for PSAS-treated sand for w=10%, tp=3days, Dr=90% at t= 7days .....26
Table C-k UCT data record for PSAS-treated sand for w=10%, tp=3days, Dr=90% at t= 14days .....27
Table C-l UCT data record for PSAS-treated sand for w=10%, tp=3days, Dr=90% at t= 28days .....27
Table C-m UCT data record for PSAS-treated sand for w=10%, tp=3days, Dr=90% at t= 60days .....28
Table C-n UCT data record for PSAS-treated sand for w=10%, tp=3days, Dr=90% at t= 90days .....28
Table C-o UCT data record for PSAS-treated sand for w=10%, tp=3days, Dr=90% at t= 180days .....29
Table C-p UCT data record for PSAS-treated sand for w=10%, tp=3days, Dr=90% at t= 360days .....29
Table C-q UCT data record for PSAS-treated sand for w=20%, tp=0days, Dr=50% at t= 3days .....30
Table C-r UCT data record for PSAS-treated sand for w=20%, tp=0days, Dr=50% at t= 7days .....31
Table C-s UCT data record for PSAS-treated sand for w=20%, tp=0days, Dr=50% at t= 14days.....32
Table C-t UCT data record for PSAS-treated sand for w=20%, tp=0days, Dr=50% at t= 28days .....33
Table C-u UCT data record for PSAS-treated sand for w=20%, tp=0days, Dr=50% at t= 60days .....34
Table C-v UCT data record for PSAS-treated sand for w=20%, tp=0days, Dr=50% at t= 90days .....35
Table C-w UCT data record for PSAS-treated sand for w=20%, tp=0days, Dr=50% at t= 180days.....36
Table C-x UCT data record for PSAS-treated sand for w=20%, tp=0days, Dr=50% at t= 360days .....36
Table C-y UCT data record for PSAS-treated sand for w=20%, tp=0days, Dr=90% at t= 3days .....37
Table C-z UCT data record for PSAS-treated sand for w=20%, tp=0days, Dr=90% at t= 7days.....38
Table C-aa UCT data record for PSAS-treated sand for w=20%, tp=0days, Dr=90% at t= 14days.....39
Table C-bb UCT data record for PSAS-treated sand for w=20%, tp=0days, Dr=90% at t= 28days .....40
Table C-cc UCT data record for PSAS-treated sand for w=20%, tp=0days, Dr=90% at t= 60days.....41
Table C-dd UCT data record for PSAS-treated sand for w=20%, tp=0days, Dr=90% at t= 90days .....42
Table C-ee UCT data record for PSAS-treated sand for w=20%, tp=0days, Dr=90% at t= 180days.....43
Table C-ff UCT data record for PSAS-treated sand for w=20%, tp=0days, Dr=90% at t= 360 days.....43
Table C-gg UCT data record for OPC-treated sand for w=10%, tp=3days, Dr=50% at t= 3 days .....44
Table C-hh UCT data record for OPC-treated sand for w=10%, tp=3days, Dr=50% at t= 7 days .....44
Table C-ii UCT data record for OPC-treated sand for w=10%, tp=3days, Dr=50% at t= 14days.....45
Table C-jj UCT data record for OPC-treated sand for w=10%, tp=3days, Dr=50% at t= 28 days.....45
Table C-kk UCT data record for OPC-treated sand for w=10%, tp=3days, Dr=50% at t= 60 days .....46
Table C-ll UCT data record for OPC-treated sand for w=10%, tp=3days, Dr=50% at t= 90 days.....46
Table C-mm UCT data record for OPC-treated sand for w=10%, tp=3days, Dr=50% at t= 180 days.....47
Table C-nn UCT data record for OPC-treated sand for w=10%, tp=3days, Dr=90% at t= 3 days .....48
Table C-oo UCT data record for OPC-treated sand for w=10%, tp=3days, Dr=90% at t= 7 days .....48
Table C-pp UCT data record for OPC-treated sand for w=10%, tp=3days, Dr=90% at t= 14 days .....49
Table C-qq UCT data record for OPC-treated sand for w=10%, tp=3days, Dr=90% at t= 28 days .....49
Table C-rr UCT data record for OPC-treated sand for w=10%, tp=3days, Dr=90% at t= 60 days.....50
Table C-ss UCT data record for OPC-treated sand for w=10%, tp=3days, Dr=90% at t= 90 days .....50
Table C-tt UCT data record for OPC-treated sand for w=10%, tp=3days, Dr=90% at t= 180 days .....51
Table C-uu UCT data record for OPC-treated sand for w=10%, tp=3days, Dr=90% at t= 360 days .....51
Table D-aUCT data record for PSAS-treated sand for w=20%, tp=1days, Dr=90% at C1 .....66
Table D-bUCT data record for PSAS-treated sand for w=20%, tp=1days, Dr=90% at C2 .....66
Table D-cUCT data record for PSAS-treated sand for w=20%, tp=1days, Dr=90% at C3 .....66
Table D-dUCT data record for PSAS-treated sand for w=20%, tp=1days, Dr=90% at C4 .....66

# A APPENDIX–I Geotechnical properties of materials used.

This first part of the appendix presents the geotechnical properties of materials used.

## A.1 Density of soil Particles

The density of soil particle is the mass per unit volume of the sold part of the soil.

### A.1.1 Equipment

- Pycnometer
- Thermometer
- Constant - Temperature drying oven
- Dessiccation
- Apparatus for separating soil particles and for crushing
- Boiling water bath
- Distilled water

### A.1.2 Particle density Test methods

The main objective of the tests is to calculate the volume of water displaced inside the pycnometer.

First, the mass is calculated following this formula:

$$M_{wd} = M_{\rho w} + M_s - M_{psw}$$

To find out the mass in the laboratory experiment the following steps has been achieved:

Steps 1: Measure 5-10 g of oven-dried soil sample passing BS 2mm sieve for pycnometer of 100ml.

Steps 2: markdown density bottle and stopper numbers.

Steps 3: weight the mass of the bottle including one of the stoppers.

Steps 4: add distilled water about half to three-four of the density bottle.

Steps 5: after distilled water was added, the bottle (without stopper) and its content were placed in the vacuum desiccator to remove the air inside the total volume. After placing it was left for at least one hour until no further loss of air is apparent.

Steps 6: after one hour in the desiccator, the bottle was shacked carefully and then added distilled water to make it filled, then left for an hour at room temperature.

Steps 7: after one hour in the room temperature place stopper and wipe dry the bottle, then weight together with the content and stopper W3

Steps 8: remove content, clean and refill with distilled water.

Steps 9: Leave about one hour tapping up the water if necessary.

Steps 10: Weight together with its content and stopper.

### A.1.3 Toyoura Sand Particle Density

Tableau 1

Table A-a soil Particles density results of Toyoura sand

| Soil particle Density ds (g/cm3) | | | | |
|---|---|---|---|---|
| (sample + distilled water + bicnometer) mass W1 | | 96.48 | 87.52 | 87.8 |
| the temperature of content when mass is measured | | 20.5 | 20.5 | 20.5 |
| density of distilled water at (T) | | 0.99818 | 0.99818 | 0.99818 |
| Distille water + pycnometer Wo | | 90.28 | 81.38 | 81.89 |
| mass of sample from oven-dried | pycnometer Number No. | 61 | 2 | 50 |
| | sample + pycnometer (g) | 45.39 | 38.08 | 37.72 |
| | pycnometer weigth (g) | 35.39 | 28.19 | 28.16 |
| | Ms (g) | 10 | 9.89 | 9.56 |
| mass of water displaced (g) | | 3.8 | 3.75 | 3.65 |
| volume of water displaced (g) | | 3.806929 | 3.756837 | 3.656655 |
| soil particle density ds (g/cm3) | | 2.626789 | 2.632533 | 2.614411 |
| Average | | 2.624578013 | | |

## A.2 Particles size distribution test (PSD)

### A.2.1 PSD Test sequence

The test was conducted according to the following sequence.

1. Sieving of a soil sample using a sieve with an aperture width of 2 mm.
2. Sieving analysis of the portion passing a sieve width an aperture width of 2 mm.

### A.2.2 Equipment for PSD

The test apparatus was as follows.

1. Sieves: A series of sieves, of metal wire cloth, with the following aperture widths specified in JIS Z 8801-1: 75μm, 106μm, 250μm, 425μm, 850μm, 2mm, 4.75mm, 9.5 mm, 19 mm, 26.5mm, 37.5mm, 53mm, and 75mm.

- Sieving of soil sample

The sample was sieved as follows.

1. Firstly, the Toyoura sand was Sieved the oven-dried sample through the

sieves with an aperture width of 75mm, 53mm, 37.5mm, 26.5mm, 19 mm, 9.5mm, and 4.75mm. it was continuously for one minute until portion passing the sieve becomes approximately 1% or less of the portion remaining on the sieve. During the sieve operation, the sieve was laterally and vertically while vibrating the sieve to keep the sample moving continuously over the surface of the sieve.

2. Secondly, the mass of the sample remaining on each sieve was weighed and taken, the mass of the sample remaining on the sieve with an aperture width of di as m(di) (g). Further, the mass of the sample passing the sieve with an aperture width of 4.75 mm and the mass of the sample remaining on the sieve with an aperture width of 2mm as m (2mm) (g) was taken on each sieve.

- Particles size accumulation curve

Particle size accumulation curve shall be determined as follows.

1. From the particles size accumulation curve, it was ridden the particle size D(mm) when the mass percentage passing is 10%, 30%,50%, and 60% and had taken them as particle size at 10% passing by mass D10 (mm), the particles size at 30% passing by mass D30 (mm), the particles size at 50 % passing by mass D50(mm) and the particles size at 60% passing mass D60 (mm), respectively.
2. From the particle size accumulation curve, the percentages passing at particle sizes 2mm, 0.425mm, and 0.075mm was ridden.
3. From the particle size accumulation curve, the mass percentage passing of the following samples was ridden.

Series of sieves

Sieving Vibration apparatus

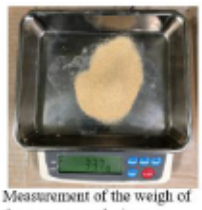

Measurement of the weigh of the mass on each sieve

Oven-dried Toyoura sand

Figure A-1 Sieve setting and Mass measurement.

### A.2.3 PSD test Results

Table A-b particles size distribution test results of Toyoura sand.

| Modules AFNOR | Sieve Diameter (mm) | Partial refusal | Cumulative refusals | % Cumulative refusal | % smaller | Observations |
|---|---|---|---|---|---|---|
| 50 | 80 | | | | | Cobble |
| 49 | 63 | | | | | |
| 48 | 50 | | | | | |
| 47 | 40 | | | | | |
| 46 | 31.5 | | | | | |
| 45 | 25 | | | | | Gravel |
| 44 | 20 | | | | | |
| 43 | 16 | | | | | |
| 42 | 12.5 | | | | | |
| 41 | 10 | | | | | |
| 40 | 8 | | | | | |
| 39 | 6.3 | | | | | |
| 38 | 5 | | | | | sand |
| 37 | 4 | | | | | |
| 36 | 3.15 | | | | | |
| 35 | 2.5 | | | | | |
| 34 | 2 | | | | | |
| 33 | 1.6 | | | | | |
| 32 | 1.25 | | | | | |
| 31 | 1 | | | | | |
| 30 | 0.8 | | | | | |
| 29 | 0.63 | | | | | |
| 28 | 0.5 | | | | | |
| 27 | 0.425 | 0.14 g | 0.1 | 0.0% | 100.00% | |
| 26 | 0.315 | | 0.1 | 0.0% | 100.00% | |
| 25 | 0.25 | 77.76 g | 77.9 | 16.8% | 83.27% | |
| 24 | 0.2 | | 77.9 | 16.8% | 83.27% | |
| 23 | 0.15 | 368.43 g | 446.3 | 96.0% | 4.00% | |
| 22 | 0.125 | | 446.3 | 96.0% | 4.00% | |
| 21 | 0.106 | 15.14 g | 461.5 | 99.3% | 0.75% | |
| 20 | 0.075 | 2.42 g | 463.9 | 99.8% | 0.22% | |
| 19 | 0.063 | | 463.9 | 99.8% | 0.22% | |
| 18 | 0.053 | 1 g | 464.9 | 100.0% | 0.00% | |
| 17 | 0.040 | | | | | |

- **Minimum density**

For each sample, the test was repeated three times with the same sample of sand as the following steps.

1. In the beginning, the mass of the mould was measured then after we placed the funnel in the center of the bottom of the mould and poured the sample throughout the funnel. During the pouring of the sand, the sample was poured through the funnel with care so that the sample for each grain size is not separated. After the material was poured in the funnel was lifted at a constant rate. The most important point in this step was to pay close attention so that the bottom end of the funnel was in constant with the top of the sand in the mould and the flow of the sample does not stop.
2. Secondly, the knife was placed on the top edges of the mould and quickly used to level the top edge of the mold. During the sweeping of the sand on the top edge of the mould the knife was placed so that the centre of the bounce preventing plate attached to the knife passed there. At that time, prevent the Mould to be impacted. At the end of the recommended steps, the mass of the specimen and $m_1$ (g) was weighed.

- **maximum density Test**

For each sample, the maximum density test was repeated three times with the same sample of sand as the following steps.

1. Firstly, the collar was placed on the mould, the sample was divided into nearly equal 10 parts, and the sample was poured into 10 layers. in each layer, 100 impacts are applied to the side of the mould while rotating the mould to compact the sample. After completing the compaction in the $9^{th}$ layers, the sand was filled nearly to the top of the mould and overfilled above the top edge of the mould in the final $10^{th}$ layer. During the rounded compaction, one hand was held against the collar and mould and the wood

hammer was sided along the table to strike the side of the mould. Secondly, we stroke the same point on the side of the mould 5 times in about 1 second, with about 5cm stroke of the hammer. After striking 5 times, rotate the mould 45-90 degree and repeat the operation. At the end of compaction, the collar and trim the sand were removed and levelled with the top edge of the mould with the knife.

2. In the end, the mass of the specimen and mould $m_2$ (g) is weighed.

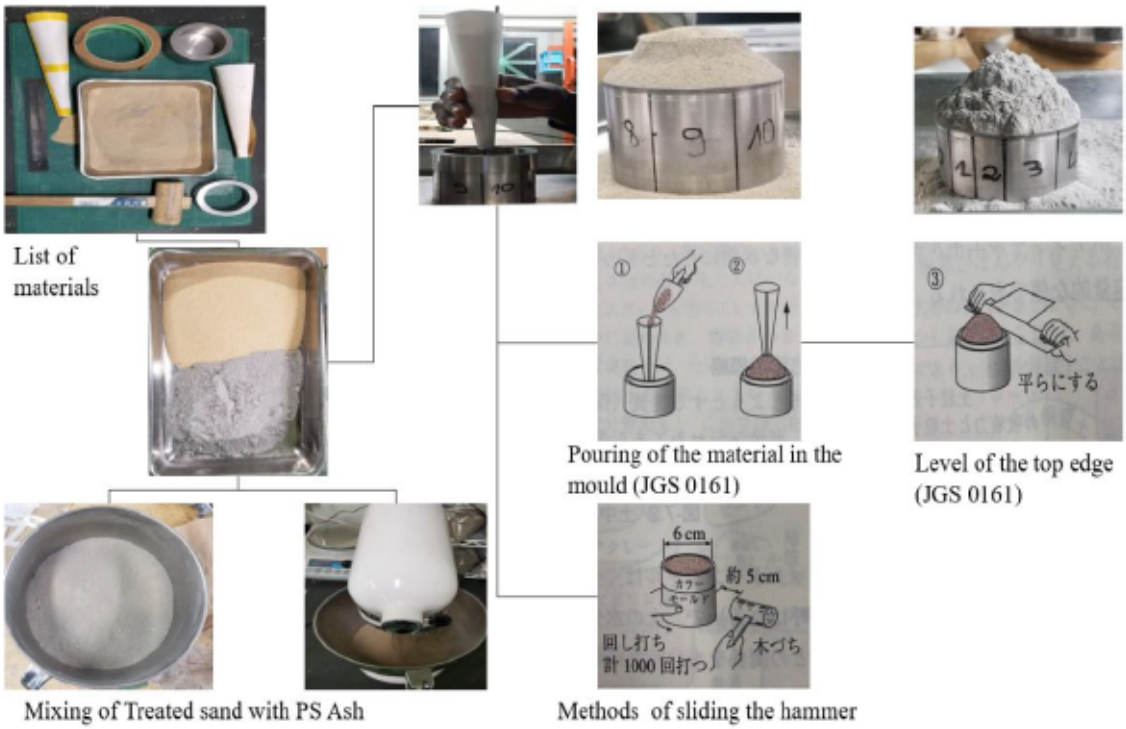


Figure A-2 Minimum and maximum test setting up and Measurement.

### A.3.1 Minimum and maximum test results

- PSAS treated sand.

Table A-c Results of Minimum and a maximum density of Toyoura sand, PSAS, 2.5% PSAS treated sand.

| TOYOURA SAND | | | | | | | | | | |
|---|---|---|---|---|---|---|---|---|---|---|
| | | TEST 1 | TEST 2 | TEST 3 | | | | TEST 1 | TEST 2 | TEST 3 | |
| minimum Density | mass of specimen and mould (g) | 985.240 | 984.250 | 984.350 | Average | maximum Density | mass of specimen and mould (g) | 1011.680 | 1011.070 | 1011.200 | Average |
| | mass of the mould (g) | 827.580 | 827.580 | 827.580 | | | mass of the mould (g) | 827.580 | 827.580 | 827.580 | |
| | weight net g) | 157.660 | 156.670 | 156.770 | | | weight net (g) | 184.100 | 183.490 | 183.620 | |
| | the volume of the mould | 113.100 | 113.100 | 113.100 | | | the volume of the mould | 113.100 | 113.100 | 113.100 | |
| minimum density (g/cm3): | | 1.394 | 1.385 | 1.386 | 1.388 | maximum density g (g/cm3): | | 1.628 | 1.622 | 1.624 | 1.625 |
| PSAS | | | | | | | | | | | |
| | | TEST 1 | TEST 2 | TEST 3 | | | | TEST 1 | TEST 2 | TEST 3 | |
| minimum Density | mass of specimen and mould (g) | 902.180 | 901.500 | 901.720 | Average | maximum Density | mass of specimen and mould (g) | 933.340 | 932.350 | 931.970 | Average |
| | mass of the mould (g) | 827.580 | 827.580 | 827.580 | | | mass of the mould (g) | 827.580 | 827.580 | 827.580 | |
| | weight net g) | 74.600 | 73.920 | 74.140 | | | weight net g) | 105.760 | 104.770 | 104.390 | |
| | volume of the mould | 113.100 | 113.100 | 113.100 | | | volume of the mould | 113.100 | 113.100 | 113.100 | |
| minimum density (g/cm3): | | 0.660 | 0.654 | 0.656 | 0.656 | maximum density (g/cm3): | | 0.935 | 0.926 | 0.923 | 0.928 |
| TOYOURA SAND + 2.5% PSAS | | | | | | | | | | | |
| | | TEST 1 | TEST 2 | TEST 3 | | | | TEST 1 | TEST 2 | TEST 3 | |
| minimum Density | mass of specimen and mould (g) | 984.135 | 981.490 | 982.310 | Average | maximum Density | mass of specimen and mould (g) | 1008.710 | 1008.530 | 1008.600 | Average |
| | mass of the mould (g) | 827.580 | 827.580 | 827.580 | | | mass of the mould (g) | 827.580 | 827.580 | 827.580 | |
| | weight net (g) | 156.555 | 153.910 | 154.730 | | | weight net (g) | 181.130 | 180.950 | 181.020 | |
| | volume of the mould | 113.100 | 113.100 | 113.100 | | | volume of the mould | 113.100 | 113.100 | 113.100 | |
| minimum density (g/cm3): | | 1.384 | 1.361 | 1.368 | 1.371 | maximum density (g/cm3): | | 1.602 | 1.600 | 1.601 | 1.601 |

Table A-d Results of Minimum and the maximum density of 5%, 7.5%, 10% PSAS treated sand.

| TOYOURA SAND + 5% PSAS | | | | | | | | | | | |
|---|---|---|---|---|---|---|---|---|---|---|---|
| | | TEST 1 | TEST 2 | TEST 3 | | | | TEST 1 | TEST 2 | TEST 3 | |
| minimum Density | mass of specimen and mould (g) | 983.030 | 978.730 | 980.270 | Average | maximum Density | mass of specimen and mould (g) | 1011.010 | 1010.440 | 1012.070 | Average |
| | mass of the mould (g) | 827.580 | 827.580 | 827.580 | | | mass of the mould (g) | 827.580 | 827.580 | 827.580 | |
| | weight net g) | 155.450 | 151.150 | 152.690 | | | weight net g) | 183.430 | 182.860 | 184.490 | |
| | the volume of the mould | 113.100 | 113.100 | 113.100 | | | the volume of the mould | 113.100 | 113.100 | 113.100 | |
| minimum density g (g/cm3) : | | 1.374 | 1.336 | 1.350 | 1.354 | maximum density g (g/cm3): | | 1.622 | 1.617 | 1.631 | 1.623 |
| TOYOURA + 7.5% PSAS | | | | | | | | | | | |
| | | TEST 1 | TEST 2 | TEST 3 | | | | TEST 1 | TEST 2 | TEST 3 | |
| minimum Density | mass of specimen and mould (g) | 979.510 | 980.160 | 976.990 | Average | maximum Density | mass of specimen and mould (g) | 1011.680 | 1012.710 | 1012.140 | Average |
| | mass of the mould (g) | 827.580 | 827.580 | 827.580 | | | mass of the mould (g) | 827.580 | 827.580 | 827.580 | |
| | weight net g) | 151.930 | 152.580 | 149.410 | | | weight net g) | 184.100 | 185.130 | 184.560 | |
| | volume of the mould | 113.100 | 113.100 | 113.100 | | | volume of the mould | 113.100 | 113.100 | 113.100 | |
| minimum density g (g/cm3) : | | 1.343 | 1.349 | 1.321 | 1.338 | maximum density g (g/cm3): | | 1.628 | 1.637 | 1.632 | 1.632 |
| TOYOURA + 10% PSAS | | | | | | | | | | | |
| | | TEST 1 | TEST 2 | TEST 3 | | | | TEST 1 | TEST 2 | TEST 3 | |
| minimum Density | mass of specimen and mould (g) | 976.460 | 974.890 | 974.850 | Average | maximum Density | mass of specimen and mould (g) | 1008.640 | 1009.930 | 1007.860 | Average |
| | mass of the mould (g) | 827.580 | 827.580 | 827.580 | | | mass of the mould (g) | 827.580 | 827.580 | 827.580 | |
| | weight net g) | 148.880 | 147.310 | 147.270 | | | weight net g) | 181.060 | 182.350 | 180.280 | |
| | volume of the mould | 113.100 | 113.100 | 113.100 | | | volume of the mould | 113.100 | 113.100 | 113.100 | |
| minimum density g (g/cm3): | | 1.316 | 1.302 | 1.302 | 1.307 | maximum density g (g/cm3) : | | 1.601 | 1.612 | 1.594 | 1.602 |

- Cement-treated sand

Table A-e Results of Minimum and maximum density of Toyoura sand, OPC 2.5% cement, treated sand.

| TOYOURA SAND | | | | | | | | | | |
|---|---|---|---|---|---|---|---|---|---|---|
| | | TEST 1 | TEST 2 | TEST 3 | | | | TEST 1 | TEST 2 | TEST 3 | |
| minimum Density | mass of specimen and mould (g) | 985.240 | 984.250 | 984.350 | Average | maximum Density | mass of specimen and mould (g) | 1011.680 | 1011.070 | 1011.200 | Average |
| | mass of the mould (g) | 827.580 | 827.580 | 827.580 | | | mass of the mould (g) | 827.580 | 827.580 | 827.580 | |
| | weight net g) | 157.660 | 156.670 | 156.770 | | | weight net g) | 184.100 | 183.490 | 183.620 | |
| | volume of the mould | 113.100 | 113.100 | 113.100 | | | volume of the mould | 113.100 | 113.100 | 113.100 | |
| minimum density (g/cm3): | | 1.394 | 1.385 | 1.386 | 1.388 | maximum density (g/cm3): | | 1.628 | 1.622 | 1.624 | 1.625 |
| PORTLAND CEMENT | | | | | | | | | | |
| | | TEST 1 | TEST 2 | TEST 3 | | | | TEST 1 | TEST 2 | TEST 3 | |
| minimum Density | mass of specimen and mould (g) | 933.890 | 931.740 | 931.960 | Average | maximum Density | mass of specimen and mould (g) | 1004.850 | 1005.720 | 1001.300 | Average |
| | mass of the mould (g) | 827.580 | 827.580 | 827.580 | | | mass of the mould (g) | 827.580 | 827.580 | 827.580 | |
| | weight net g) | 106.310 | 104.160 | 104.380 | | | weight net g) | 177.270 | 178.140 | 173.720 | |
| | volume of the mould | 113.100 | 113.100 | 113.100 | | | volume of the mould | 113.100 | 113.100 | 113.100 | |
| minimum density (g/cm3) : | | 0.940 | 0.921 | 0.923 | 0.928 | maximum density (g/cm3): | | 1.567 | 1.575 | 1.536 | 1.559 |
| TOYOURA SAND + 2.5% CEMENT | | | | | | | | | | |
| | | TEST 1 | TEST 2 | TEST 3 | | | | TEST 1 | TEST 2 | TEST 3 | |
| minimum Density | mass of specimen and mould (g) | 985.200 | 986.000 | 985.400 | Average | maximum Density | mass of specimen and mould (g) | 1011.700 | 1012.400 | 1012.900 | Average |
| | mass of the mould (g) | 827.580 | 827.580 | 827.580 | | | mass of the mould (g) | 827.580 | 827.580 | 827.580 | |
| | weight net g) | 157.620 | 158.420 | 157.820 | | | weight net g) | 184.120 | 184.820 | 185.320 | |
| | volume of the mould | 113.100 | 113.100 | 113.100 | | | volume of the mould | 113.100 | 113.100 | 113.100 | |
| minimum density (g/cm3): | | 1.394 | 1.401 | 1.395 | 1.397 | maximum density (g/cm3) : | | 1.628 | 1.634 | 1.639 | 1.634 |

Table A-f Results of Minimum and maximum density of 5%,7.5%, 10% OPC-treated sand

| TOYOURA SAND + 5% CEMENT | | | | | | | | | | |
|---|---|---|---|---|---|---|---|---|---|---|
| | | TEST 1 | TEST 2 | TEST 3 | | | | TEST 1 | TEST 2 | TEST 3 | |
| minimum Density | mass of specimen and mould (g) | 986.000 | 986.600 | 987.100 | Average | maximum Density | mass of specimen and mould (g) | 1017.900 | 1015.600 | 1016.000 | Average |
| | mass of the mould (g) | 827.580 | 827.580 | 827.580 | | | mass of the mould (g) | 827.580 | 827.580 | 827.580 | |
| | weight net g) | 158.420 | 159.020 | 159.520 | | | weight net g) | 190.320 | 188.020 | 188.420 | |
| | volume of the mould | 113.100 | 113.100 | 113.100 | | | volume of the mould | 113.100 | 113.100 | 113.100 | |
| minimum density g (g/cm3): | | 1.401 | 1.406 | 1.410 | 1.406 | maximum density g (g/cm3): | | 1.683 | 1.662 | 1.666 | 1.670 |
| TOYOURA SAND + 7.5% CEMENT | | | | | | | | | | | |
| | | TEST 1 | TEST 2 | TEST 3 | | | | TEST 1 | TEST 2 | TEST 3 | |
| minimum Density | mass of specimen and mould (g) | 988.000 | 987.800 | 987.900 | Average | maximum Density | mass of specimen and mould (g) | 1022.200 | 1020.100 | 1021.600 | Average |
| | mass of the mould (g) | 827.580 | 827.580 | 827.580 | | | mass of the mould (g) | 827.580 | 827.580 | 827.580 | |
| | weight net g) | 160.420 | 160.220 | 160.320 | | | weight net g) | 194.620 | 192.520 | 194.020 | |
| | volume of the mold | 113.100 | 113.100 | 113.100 | | | volume of the Mold | 113.100 | 113.100 | 113.100 | |
| minimum density (g/cm3) : | | 1.418 | 1.417 | 1.418 | 1.418 | maximum density (g/cm3): | | 1.721 | 1.702 | 1.715 | 1.713 |
| TOYOURA SAND + 10% CEMENT | | | | | | | | | | | |
| | | TEST 1 | TEST 2 | TEST 3 | | | | TEST 1 | TEST 2 | TEST 3 | |
| minimum Density | mass of specimen and mould (g) | 988.400 | 987.100 | 986.000 | Average | maximum Density | mass of specimen and mould (g) | 1024.500 | 1025.600 | 1027.400 | Average |
| | mass of the mould (g) | 827.580 | 827.580 | 827.580 | | | mass of the mould (g) | 827.580 | 827.580 | 827.580 | |
| | weight net g) | 160.820 | 159.520 | 158.420 | | | weight net g) | 196.920 | 198.020 | 199.820 | |
| | volume of the mold | 113.100 | 113.100 | 113.100 | | | volume of the mold | 113.100 | 113.100 | 113.100 | |
| minimum density (g/cm3) : | | 1.422 | 1.410 | 1.401 | 1.411 | maximum density (g/cm3) : | | 1.741 | 1.751 | 1.767 | 1.753 |

### A.3.2 Calculation of void ratio of each treated specimen

Void ratio is calculated from the value of dry density using equation. However, the density index is calculated directly from the maximum, minimum and in-situ of dry density, avoiding the need to know the value of $G_s$.

Equation A-a void ratio

$$\rho_d \left(\frac{g}{cm^3}\right) = \frac{G_s}{1+e}\rho_s$$

Table A-g summary of Physical properties of the materials used.

| Material | Gs | $\rho_{max}$ | $\rho_{min}$ | $e_{max}$ | $e_{min}$ | Cu | $D_{50}$ (mm) |
|---|---|---|---|---|---|---|---|
| PSAS | 2.603 | 0.930 | 0.654 | 2.979 | 1.800 | | |
| Cement | 3.150 | 1.559 | 0.928 | 2.395 | 1.020 | | |
| Toyoura Sand | 2.641 | 1.625 | 1.388 | 0.874 | 0.596 | 1.470 | 0.160 |
| PSAS-Treated sand | | | | | | | |
| 2.5% PSAS | 2.640 | 1.601 | 1.371 | 0.926 | 0.649 | | |
| 5% PSAS | 2.639 | 1.623 | 1.354 | 0.950 | 0.626 | | |
| 7.5% PSAS | 2.638 | 1.632 | 1.338 | 0.972 | 0.616 | | |
| 10% PSAS | 2.637 | 1.602 | 1.307 | 1.018 | 0.646 | | |
| OPC-Treated sand | | | | | | | |
| 2.5% Cement | 2.654 | 1.634 | 1.397 | 0.900 | 0.625 | | |
| 5% Cement | 2.666 | 1.670 | 1.406 | 0.897 | 0.596 | | |
| 7.5% Cement | 2.679 | 1.713 | 1.418 | 0.890 | 0.564 | | |
| 10% Cement | 2.692 | 1.753 | 1.411 | 0.908 | 0.536 | | |

### A.3.3 Mixture method of Treated sand

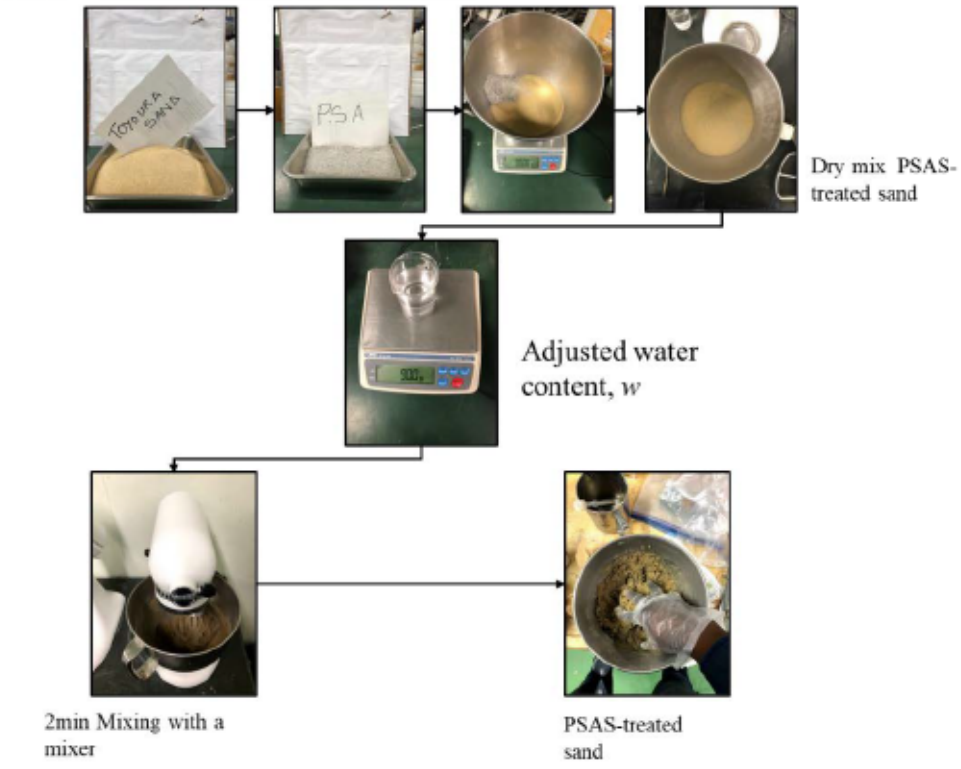


Figure A-3 Mixing condition of PSAS-treated sand.

# B APPENDIX–II Swelling potential of paper sludge ash (PSAS) treated sand.

This second part of the appendix presents the swelling potential of paper sludge ash (PSAS) treated sand.

B.1 Swelling potential measurement set up.

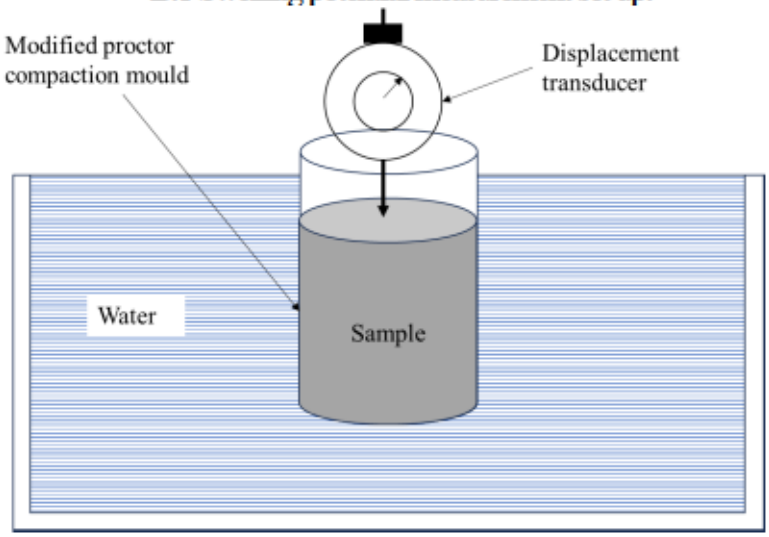


Figure B-1 Swelling measurement using CBR test setting.

Equation B-a Expansion measurement equation

$$Expansion(\%) = \frac{L_i - L_0}{L_0} \times 100$$

B.2 Swelling test results obtained using a comparator.

Table B-a Height measure and variation for Specimen at $D_r$=50

| Measured height of the specimen | | | | | | | | | |
|---|---|---|---|---|---|---|---|---|---|
| DAYS | W=0 PRE-MIXING 0DAYS | 0 DAYS | 1 DAYS | 2 DAYS | 3 DAYS | 4 DAYS | 5 DAYS | 6 DAYS | 7 DAYS |
| | | **2.5% PSA DR50%** | **2.5% PSA DR50%** | **2.5% PSA DR50%** | **2.5% PSA DR50%** | **2.5% PSA DR90%** | **2.5% PSA DR50%** | **2.5% PSA DR90%** | **2.5% PSA DR90%** |
| 0 | 103.485 | 103.36 | 103.485 | 103.395 | 102.955 | 103.015 | 103.165 | 103.61 | 102.875 |
| 1 | 114.515 | 103.975 | 104.05 | 103.715 | 103.26 | 103.185 | 103.325 | 103.665 | 102.885 |
| 2 | 114.78 | 104.15 | 104.09 | 103.885 | 103.38 | 103.32 | 103.385 | 103.72 | 102.925 |
| 3 | 114.955 | 104.21 | 104.24 | 103.93 | 103.4 | 103.39 | 103.485 | 103.735 | 102.95 |
| 4 | 114.965 | 104.265 | 104.255 | 103.95 | 103.405 | 103.395 | 103.525 | 103.755 | 102.95 |

Table B-b Expansion of specimen expressed in mm for specimen compacted at $D_r$=50%

| Expansion (mm) | | | | | | | | | |
|---|---|---|---|---|---|---|---|---|---|
| DAYS | W=0 PRE-MIXING 0DAYS | 0 DAYS | 1 DAYS | 2 DAYS | 3 DAYS | 4 DAYS | 5 DAYS | 6 DAYS | 7 DAYS |
| | | **2.5% PSA DR50%** | **2.5% PSA DR50%** | **2.5% PSA DR50%** | **2.5% PSA DR50%** | **2.5% PSA DR50%** | **2.5% PSA DR50%** | **2.5% PSA DR50%** | **2.5% PSA DR50%** |
| 0 | 0 | 0 | 0 | 0 | 0 | 0 | 0 | 0 | 0 |
| 1 | 11.03 | 0.615 | 0.565 | 0.32 | 0.305 | 0.17 | 0.16 | 0.055 | 0.01 |
| 2 | 11.295 | 0.79 | 0.605 | 0.49 | 0.425 | 0.305 | 0.22 | 0.11 | 0.05 |
| 3 | 11.47 | 0.85 | 0.755 | 0.535 | 0.445 | 0.375 | 0.32 | 0.125 | 0.075 |
| 4 | 11.48 | 0.905 | 0.77 | 0.555 | 0.45 | 0.38 | 0.36 | 0.145 | 0.075 |

Table B-c Expansion of specimen expressed in % for specimen compacted at $D_r$=50%

| Expansion (%) | | | | | | | | | |
|---|---|---|---|---|---|---|---|---|---|
| DAYS Dr50% | | 0 DAYS | 1 DAYS | 2 DAYS | 3 DAYS | 4 DAYS | 5 DAYS | 6 DAYS | 7 DAYS |
| | | 2.5% PSA DR50% | 2.5% PSA DR50% | 2.5% PSA DR50% | 2.5% PSA DR50% | 2.5% PSA DR50% | 2.5% PSA DR50% | 2.5% PSA DR50% | 2.5% PSA DR50% |
| 0 | 0.00% | 0.00% | 0.00% | 0.00% | 0.00% | 0.00% | 0.00% | 0.00% | 0.00% |
| 1 | 10.66% | 0.60% | 0.55% | 0.31% | 0.30% | 0.17% | 0.16% | 0.05% | 0.01% |
| 2 | 10.91% | 0.76% | 0.58% | 0.47% | 0.41% | 0.30% | 0.21% | 0.11% | 0.05% |
| 3 | 11.08% | 0.82% | 0.73% | 0.52% | 0.43% | 0.36% | 0.31% | 0.12% | 0.07% |
| 4 | 11.09% | 0.87% | 0.74% | 0.54% | 0.44% | 0.37% | 0.35% | 0.14% | 0.07% |
| **Max (Exp)** | **11.09%** | **0.87%** | **0.74%** | **0.54%** | **0.44%** | **0.37%** | **0.35%** | **0.14%** | **0.07%** |

Table B-d Height measure and variation for Specimen at $D_r$=90

| Measured height of the specimen | | | | | | | | | |
|---|---|---|---|---|---|---|---|---|---|
| DAYS | W=0 PRE-MIXING 0DAYS | 0 DAYS | 1 DAYS | 2 DAYS | 3 DAYS | 4 DAYS | 5 DAYS | 6 DAYS | 7 DAYS |
| | | 2.5% PSA DR90% | 2.5% PSA DR90% | 2.5% PSA DR90% | 2.5% PSA DR90% | 2.5% PSA DR90% | 2.5% PSA DR90% | 2.5% PSA DR90% | 2.5% PSA DR90% |
| 0 | 103.165 | 102.95 | 104.225 | 103.25 | 103.155 | 103.125 | 103.63 | 103.395 | 103.16 |
| 1 | 115.085 | 103.73 | 104.755 | 103.745 | 103.49 | 103.445 | 103.685 | 103.63 | 103.16 |
| 2 | 114.95 | 103.755 | 104.95 | 103.78 | 103.585 | 103.47 | 103.745 | 103.66 | 103.255 |
| 3 | 115.085 | 103.78 | 104.93 | 103.79 | 103.64 | 103.48 | 103.9 | 103.665 | 103.255 |
| 4 | 115.095 | 103.8 | 104.995 | 103.825 | 103.655 | 103.48 | 103.96 | 103.67 | 103.26 |

Table B-e Expansion of specimen expressed in mm for specimen compacted at $D_r$=90%

| Expansion (mm) | | | | | | | | | |
|---|---|---|---|---|---|---|---|---|---|
| DAYS | W=0 PRE-MIXING 0DAYS | 0 DAYS | 1 DAYS | 2 DAYS | 3 DAYS | 4 DAYS | 5 DAYS | 6 DAYS | 7 DAYS |
| | | 2.5% PSA DR90% | 2.5% PSA DR90% | 2.5% PSA DR90% | 2.5% PSA DR90% | 2.5% PSA DR90% | 2.5% PSA DR90% | 2.5% PSA DR90% | 2.5% PSA DR90% |
| 0 | 0 | 0 | 0 | 0 | 0 | 0 | 0 | 0 | 0 |
| 1 | 11.92 | 0.78 | 0.53 | 0.495 | 0.335 | 0.32 | 0.055 | 0.235 | 0 |
| 2 | 11.785 | 0.805 | 0.725 | 0.53 | 0.43 | 0.345 | 0.115 | 0.265 | 0.095 |
| 3 | 11.92 | 0.83 | 0.705 | 0.54 | 0.485 | 0.355 | 0.27 | 0.27 | 0.095 |
| 4 | 11.93 | 0.85 | 0.77 | 0.575 | 0.5 | 0.355 | 0.33 | 0.275 | 0.1 |

Table B-f Expansion of specimen expressed in % for specimen compacted at $D_r$=90%

| Expansion (%) | | | | | | | | | |
|---|---|---|---|---|---|---|---|---|---|
| DAYS Dr50% | W=0 PRE-MIXING 0DAYS | 0 DAYS | 1 DAYS | 2 DAYS | 3 DAYS | 4 DAYS | 5 DAYS | 6 DAYS | 7 DAYS |
| | | 2.5% PSA DR90% | 2.5% PSA DR90% | 2.5% PSA DR90% | 2.5% PSA DR90% | 2.5% PSA DR90% | 2.5% PSA DR90% | 2.5% PSA DR90% | 2.5% PSA DR90% |
| 0 | 0.00% | 0.00% | 0.00% | 0.00% | 0.00% | 0.00% | 0.00% | 0.00% | 0.00% |
| 1 | 11.55% | 0.76% | 0.51% | 0.48% | 0.32% | 0.31% | 0.05% | 0.23% | 0.00% |
| 2 | 11.42% | 0.78% | 0.70% | 0.51% | 0.42% | 0.33% | 0.11% | 0.26% | 0.09% |
| 3 | 11.55% | 0.81% | 0.68% | 0.52% | 0.47% | 0.34% | 0.26% | 0.26% | 0.09% |
| 4 | 11.56% | 0.83% | 0.74% | 0.56% | 0.48% | 0.34% | 0.32% | 0.27% | 0.10% |
| **Max(Exp)** | **11.56%** | **0.83%** | **0.74%** | **0.56%** | **0.48%** | **0.34%** | **0.32%** | **0.27%** | **0.10%** |

# C APPENDIX -III Deformation and strength development of paper sludge ash treated sand.

## C.1 Unconfined compression test of treated specimen

The test is done using the following steps. The test starts promptly after preparing the specimen.

- Step 1 is set up in the unconfined compression test apparatus. place the specimen in the center of the lower pressure plate and bring the upper-pressure plate into contact with the top while avoiding any compression on the specimen before the test itself. Once the specimen is in place, adjust the origin of the displacement gauge and load cell.
- In step 2 we apply continuous compression to the specimen at a basic compressive strain rate of 1% per minute.
- During the test, the required apparatus measures the amount of compression, ΔH (cm), and the compressive force, P (N). Measurement of compression and force is taken at intervals small enough to allow a smooth stress-strain curve to be drawn.
- Stop the compression either when the increase in strain exceeds 2% after the point of the maximum compressive force, or the compressive force reading has fallen 2/3 of its maximum value, or a compressive strain of 15% has been reached.
- Observe and record the deformed shape and failure mode of the specimen as well as other observations. Observations must be done from the most characteristic direction of the specimen. Also, if a slip surface is found, it might be observed from the direction in which the steepest slope is determined. It must be recorded such that the angle of the steepest slope can be approximately read. Any heterogeneity in the specimen and the presence of foreign matter shall be observed and recorded.

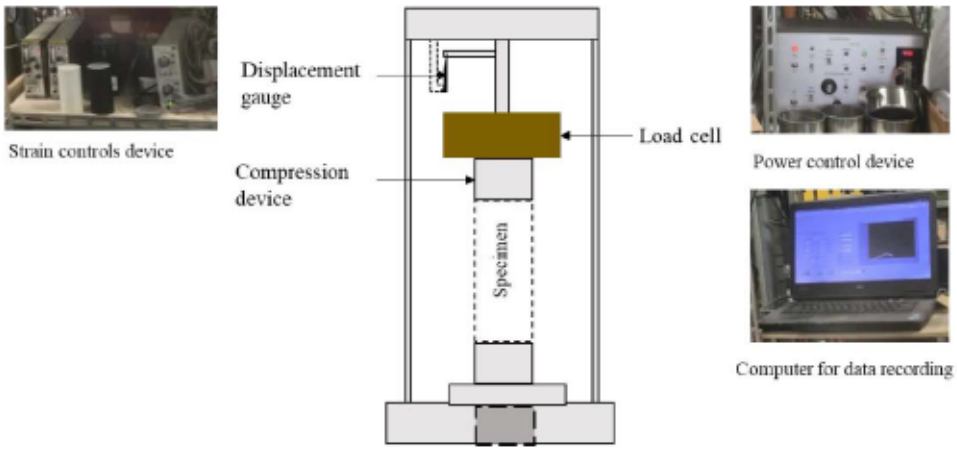


Figure C-1 UCT apparatus setting

### C.1.1 Test record for unconfined compression test

The calculation was performed as follows:

- The compressive strain of the specimen was calculated using the following equation:

Equation C-a compressive axial strain

$$\varepsilon = \frac{\Delta H}{H_0} \times 100$$

- The compressive stress at compressive strain ε was calculated using the following equation.

Equation C-b Compressive stress

$$\sigma = \frac{P}{A_0} \times \left[1 - \frac{\varepsilon}{100}\right] \times 10$$

- Draw a stress-strain curve with compressive strain on the horizontal axis versus compressive stress on the vertical axis.
- Using the stress-curve, obtain the maximum value of compressive stress before the point where the compressive strain reaches 15%. Establish this value as the unconfined compressive strength $q_u$ (kN/m$^2$) and establish the strain at this point as strain at failure (%). In case there an inflection point in the initial phase of the stress-strain curve, the straight section after the inflection point was extended and the point at which the extended line crossed the horizontal axis shall be established as the point of origin for correction pf the strain calculation.

The method used to calculate the deformation modulus, $E_{50}$(kN/m$^2$) is explained as follows.

Equation C-c Deformation modulus, $E_{50}$

$$E_{50} = \frac{\frac{q_u}{2}}{\varepsilon_{50}}$$

Where:

$E_{50}$ : deformation modulus (kN/m$^2$)

$q_u$: unconfined compressive strength (kN/m$^2$)

$\varepsilon_{50}$ : compressive strain (%) at compressive stress $\sigma = \frac{q_u}{2}$. If there is a presence of an inflection point in the initial phase of the stress-strain curve, a correction is done in the same manner.

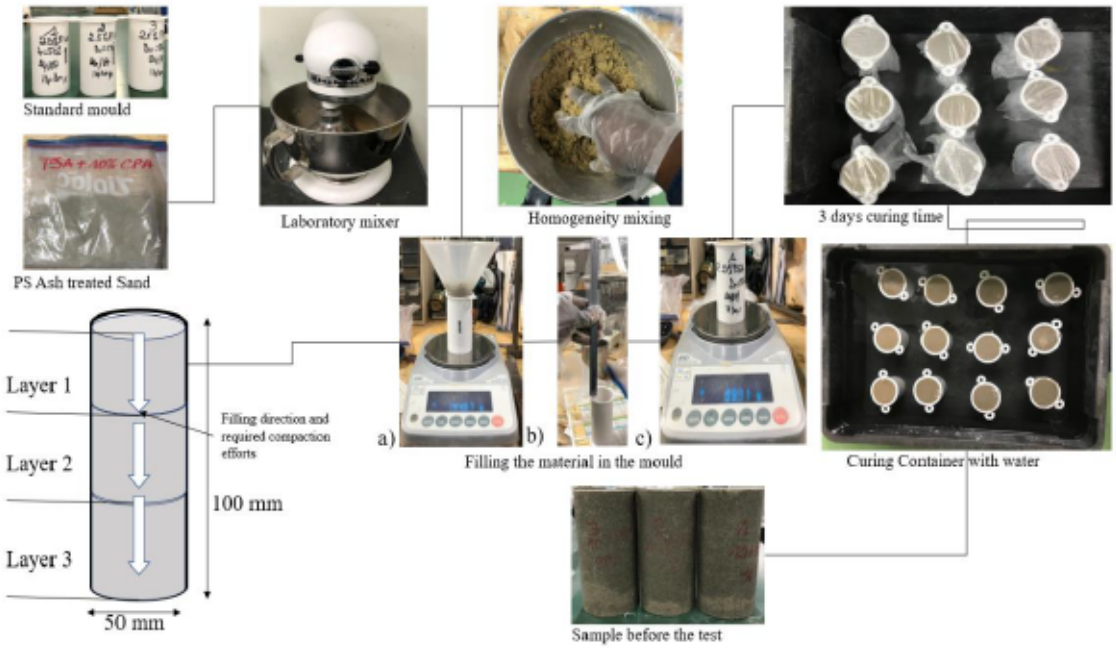


Figure C-2 Specimen preparation flow

## C.2 Unconfined compression test Results

### C.2.1 Stress-strain relationship of PSAS treated sand for w=10%, tp=3 days, $D_r$=50%

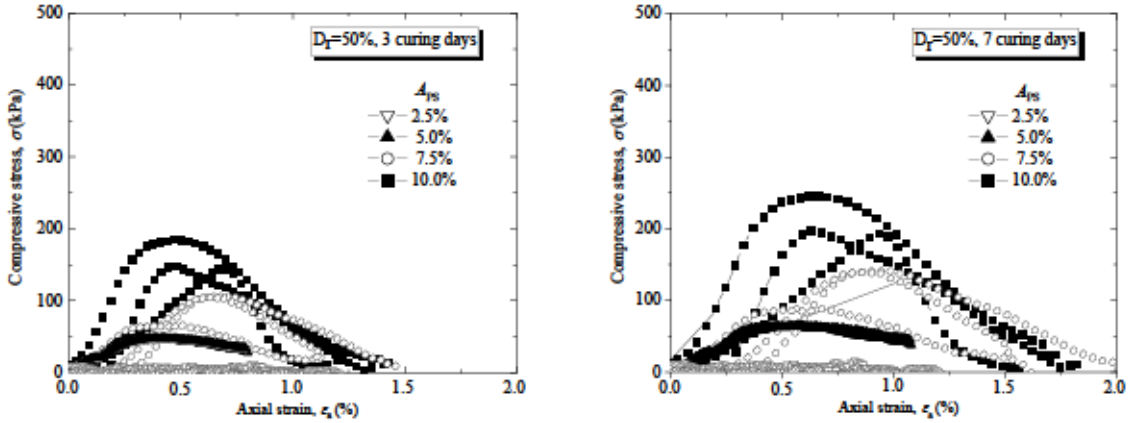


Figure C-3 Typical UCT stress-strain relationship of PSAS-treated sand for $w$=10%, $tp$=3days, $D_r$=50% (a) $t$= 3days, (b) $t$= 7 days

Table C-a UCT data record for PSAS-treated sand for w=10%, tp=3days, Dr=50% at t= 3days,

| Specimen No. | $A_{PS}$(%) | Modifier Batch | Curing days, $t$ | $q_u$ (kN/m²) | $\varepsilon_f$ (%) | $E_{50}$ (kN/m²) | $\gamma_d$ (g/cm³) | $e$ | $w$ (%) | $D_r$ (%) |
|---|---|---|---|---|---|---|---|---|---|---|
| 1 | 2.5 | *Batch A* | 3 Days | 12.9 | 0.768 | 600 | 1.48 | 0.787 | 20.38% | 50.12% |
| 2 | 2.5 | *Batch A* | 3 Days | 0 | 0 | 0 | 1.48 | 0.787 | 22.89% | 50.21% |
| 3 | 2.5 | *Batch A* | 3 Days | 5.8 | 0.609 | 660 | 1.48 | 0.785 | 19.25% | 50.82% |
| 1 | 5 | *Batch A* | 3 Days | 54.9 | 0.25 | 23760 | 1.48 | 0.785 | 23.58% | 50.89% |
| 2 | 5 | *Batch A* | 3 Days | 0 | 0 | 14420 | 1.48 | 0.785 | 21.14% | 50.95% |
| 3 | 5 | *Batch A* | 3 Days | 47.4 | 0.276 | 13980 | 1.48 | 0.782 | 23.03% | 51.91% |
| 1 | 7.5 | *Batch A* | 3 Days | 106.5 | 0.646 | 25880 | 1.47 | 0.796 | 23.55% | 49.60% |
| 2 | 7.5 | *Batch A* | 3 Days | 105.9 | 0.558 | 24720 | 1.47 | 0.792 | 22.09% | 50.57% |
| 3 | 7.5 | *Batch A* | 3 Days | 65.9 | 0.275 | 25250 | 1.47 | 0.793 | 21.83% | 50.43% |
| 1 | 10 | *Batch A* | 3 Days | 185.2 | 0.594 | 19750 | 1.44 | 0.829 | 25.05% | 50.73% |
| 2 | 10 | *Batch A* | 3 Days | 147.5 | 0.451 | 59280 | 1.44 | 0.831 | 25.69% | 50.13% |
| 3 | 10 | *Batch A* | 3 Days | 144.9 | 0.304 | 40930 | 1.44 | 0.829 | 25.55% | 50.69% |

Table C-b UCT data record for PSAS-treated sand for w=10%, tp=3days, Dr=50% at t= 7days

| Specimen No. | $A_{PS}$(%) | Modifier Batch | Curing days, $t$ | $q_u$ (kN/m²) | $\varepsilon_f$ (%) | $E_{50}$ (kN/m²) | $\rho_d$ (g/cm³) | $e$ | $w$ (%) | $D_r$ (%) |
|---|---|---|---|---|---|---|---|---|---|---|
| 1 | 2.5 | *Batch A* | 7 Days | 15.79 | 0.768 | 600 | 1.48 | 0.787 | 20.38% | 50.12% |
| 2 | 2.5 | *Batch A* | 7 Days | 0 | 0 | | | | | |
| 3 | 2.5 | *Batch A* | 7 Days | 8.1 | 0.609 | 660 | 1.48 | 0.787 | 20.36% | 50.20% |
| 1 | 5 | *Batch A* | 7 Days | 65.11 | 0.25 | 23760 | 1.48 | 0.785 | 23.58% | 50.89% |
| 2 | 5 | *Batch A* | 7 Days | 65.8 | 0.276 | 14420 | 1.48 | 0.784 | 23.48% | 51.35% |
| 3 | 5 | *Batch A* | 7 Days | 64.6 | 0.276 | 13980 | 1.48 | 0.784 | 23.49% | 51.30% |
| 1 | 7.5 | *Batch A* | 7 Days | 143.4 | 0.646 | 25880 | 1.47 | 0.789 | 23.09% | 51.47% |
| 2 | 7.5 | *Batch A* | 7 Days | 141.4 | 0.558 | 24720 | 1.47 | 0.794 | 23.46% | 49.99% |
| 3 | 7.5 | *Batch A* | 7 Days | 90.4 | 0.275 | 25250 | 1.47 | 0.790 | 23.18% | 51.10% |
| 1 | 10 | *Batch A* | 7 Days | 196.3 | 0.594 | 19750 | 1.44 | 0.829 | 25.05% | 50.73% |
| 2 | 10 | *Batch A* | 7 Days | 200.4 | 0.451 | 59280 | 1.45 | 0.825 | 24.73% | 51.95% |
| 3 | 10 | *Batch A* | 7 Days | 248.9 | 0.304 | 40930 | 1.44 | 0.829 | 25.07% | 50.64% |

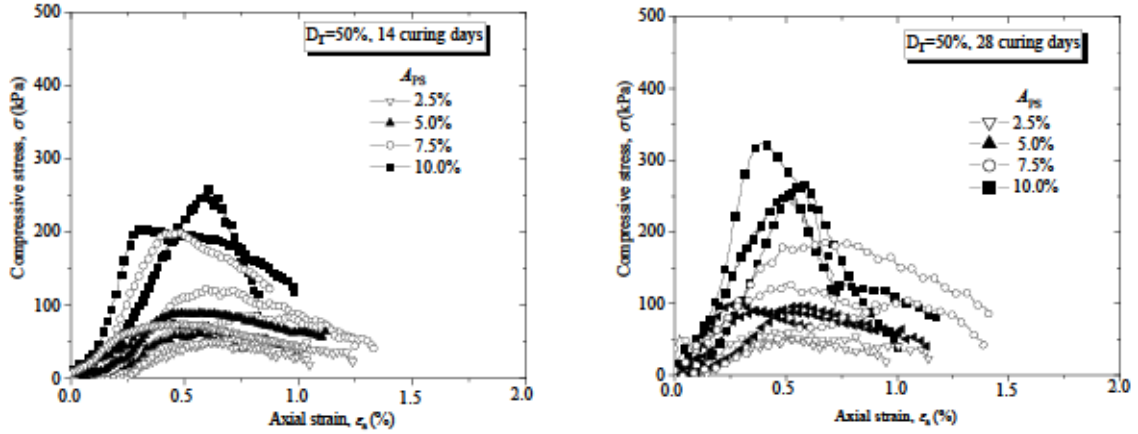


Figure C-4 Typical UCT stress-strain relationship of PSAS-treated sand for $w$=10%, $tp$=3 days, $D_r$=50%: (c) $t$= 14days, (d) $t$= 28 days.

Table C-c UCT data record for PSAS-treated sand for w=10%, tp=3days, Dr=50% at t= 14 days

| Specimen No. | $A_{PS}$ (%) | Modifier Batch | Curing days, t | $q_u$ (kN/m2) | $\varepsilon_f$ (%) | $E_{50}$ (kN/m2) | $\rho_d$ (g/cm3) | e | $w$ (%) | $D_r$ (%) |
|---|---|---|---|---|---|---|---|---|---|---|
| 1 | 2.5 | Batch A | 14 Days | 54.9 | 0.533 | 12760 | 1.48 | 0.783 | 21.62% | 51.79% |
| 2 | 2.5 | Batch A | 14 Days | 52.1 | 0.384 | 25790 | 1.48 | 0.787 | 18.94% | 50.27% |
| 3 | 2.5 | Batch A | 14 Days | 75.9 | 0.551 | 19970 | 1.48 | 0.787 | 20.66% | 50.15% |
| 1 | 5 | Batch A | 14 Days | 63.13 | 0.623 | 21400 | 1.48 | 0.784 | 20.87% | 51.20% |
| 2 | 5 | Batch A | 14 Days | 90.8 | 0.559 | 21010 | 1.48 | 0.785 | 19.74% | 50.92% |
| 3 | 5 | Batch A | 14 Days | 77.6 | 0.5 | 21500 | 1.48 | 0.787 | 19.93% | 50.53% |
| 1 | 7.5 | Batch A | 14 Days | 201.9 | 0.497 | 34100 | 1.47 | 0.791 | 23.47% | 50.77% |
| 2 | 7.5 | Batch A | 14 Days | 125.1 | 0.5 | 27670 | 1.47 | 0.793 | 22.48% | 50.24% |
| 3 | 7.5 | Batch A | 14 Days | 89.7 | 0.582 | 37060 | 1.47 | 0.792 | 21.46% | 50.74% |
| 1 | 10 | Batch A | 14 Days | 207.4 | 0.369 | 44120 | 1.44 | 0.828 | 21.65% | 50.99% |
| 2 | 10 | Batch A | 14 Days | 261.6 | 0.522 | 49350 | 1.44 | 0.831 | 23.77% | 50.15% |
| 3 | 10 | Batch A | 14 Days | 196.9 | 0.464 | 80040 | 1.44 | 0.829 | 24.00% | 50.75% |

Table C-d UCT data record for PSAS-treated sand for w=10%, tp=3days, Dr=50% at t= 28 days

| Specimen No. | $A_{PS}$(%) | Modifier Batch | Curing days, $t$ | $q_u$ (kN/m$^2$) | $\varepsilon_f$ (%) | $E_{50}$ (kN/m$^2$) | $\rho_d$ (g/cm$^3$) | $e$ | $w$ (%) | $D_r$ (%) |
|---|---|---|---|---|---|---|---|---|---|---|
| 1 | 2.5 | *Batch A* | 28 Days | 53.6 | 0.494 | 16750 | 1.48 | 0.786 | 24.61% | 50.56% |
| 2 | 2.5 | *Batch A* | 28 Days | 51 | 0.381 | 26280 | 1.48 | 0.786 | 23.16% | 50.45% |
| 3 | 2.5 | *Batch A* | 28 Days | 62.3 | 0.402 | 24920 | 1.48 | 0.787 | 23.04% | 50.27% |
| 1 | 5 | *Batch A* | 28 Days | 99.96 | 0.538 | 16720 | 1.48 | 0.785 | 24.61% | 50.94% |
| 2 | 5 | *Batch A* | 28 Days | 100.3 | 0.444 | 40120 | 1.48 | 0.786 | 23.16% | 50.85% |
| 3 | 5 | *Batch A* | 28 Days | 91.68 | 0.227 | 28830 | 1.48 | 0.786 | 23.04% | 50.70% |
| 1 | 7.5 | *Batch A* | 28 Days | 186.9 | 0.657 | 36930 | 1.47 | 0.793 | 23.51% | 50.28% |
| 2 | 7.5 | *Batch A* | 28 Days | 105.5 | 0.968 | 13150 | 1.47 | 0.793 | 25.44% | 50.33% |
| 3 | 7.5 | *Batch A* | 28 Days | 128.1 | 0.448 | 41050 | 1.47 | 0.791 | 24.51% | 50.80% |
| 1 | 10 | *Batch A* | 28 Days | 260.6 | 0.651 | 49920 | 1.44 | 0.831 | 24.41% | 50.20% |
| 2 | 10 | *Batch A* | 28 Days | 325.8 | 0.534 | 51710 | 1.44 | 0.833 | 27.11% | 49.70% |
| 3 | 10 | *Batch A* | 28 Days | 267.4 | 0.717 | 49800 | 1.44 | 0.826 | 27.28% | 51.60% |

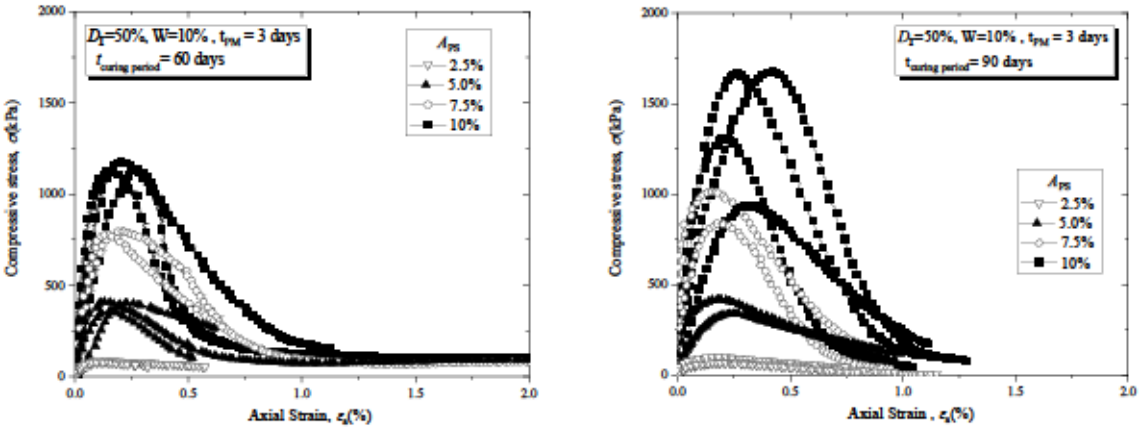


(e) (f)

Figure C-5 Typical UCT stress-strain relationship of PSAS-treated sand for *w*=10%, *tp*=3days, $D_r$=50% (e) *t*= 60 days, (f) *t*= 90 days.

Table C-e UCT data record for PSAS-treated sand for w=10%, tp=3days, Dr=50% at t= 60 days

| Specimen No. | $A_{PS}$(%) | Modifier Batch | Curing days, *t* | $q_u$ (kN/m²) | $\varepsilon_f$ (%) | $E_{50}$ (kN/m²) | $E_{0.02}$ (kN/m²) | $\rho_d$ (g/cm³) | *e* | *w* (%) | $D_r$ (%) |
|---|---|---|---|---|---|---|---|---|---|---|---|
| 1 | 2.5 | *Batch A* | 60 Days | 79.99 | 0.261 | 114200 | 266367 | 1.48 | 0.787 | 23.02% | 50.01% |
| 2 | 2.5 | *Batch A* | 60 Days | 77.29 | 0.257 | 200200 | 257633 | 1.48 | 0.786 | 23.24% | 50.61% |
| 3 | 2.5 | *Batch A* | 60 Days | 86.5 | 0.0962 | 254400 | 285615 | 1.48 | 0.788 | 22.89% | 49.85% |
| 1 | 5.0 | *Batch A* | 60 Days | 411.030 | 0.122 | 604400 | 1356050 | 1.48 | 0.788 | 26.86% | 50.03% |
| 2 | 5.0 | *Batch A* | 60 Days | 404.49 | 0.0231 | 227200 | 1333000 | 1.48 | 0.786 | 26.51% | 50.68% |
| 3 | 5.0 | *Batch A* | 60 Days | 357.750 | 0.139 | 458600 | 1192000 | 1.48 | 0.788 | 26.41% | 50.25% |
| 1 | 7.5 | *Batch A* | 60 Days | 776.88 | 0.132 | 1253000 | 2563665 | 1.47 | 0.792 | 27.51% | 50.68% |
| 2 | 7.5 | *Batch A* | 60 Days | 776.88 | 0.135 | 1253000 | 2563704 | 1.47 | 0.792 | 26.16% | 50.48% |
| 3 | 7.5 | *Batch A* | 60 Days | 795.72 | 0.191 | 828800 | 2627500 | 1.47 | 0.791 | 28.95% | 50.83% |
| 1 | 10 | *Batch A* | 60 Days | 1139.01 | 0.27 | 654600 | 3769000 | 1.44 | 0.830 | 28.91% | 50.41% |
| 2 | 10 | *Batch A* | 60 Days | 1174.55 | 0.199 | 995300 | 3998300 | 1.44 | 0.829 | 31.61% | 50.64% |
| 3 | 10 | *Batch A* | 60 Days | 1125.55 | 0.138 | 1825400 | 3709700 | 1.44 | 0.829 | 30.89% | 50.73% |

Table C-f UCT data record for PSAS-treated sand for w=10%, tp=3days, Dr=50% at t= 90 days

| Specimen No. | $A_{PS}$(%) | Modifier Batch | Curing days, *t* | $q_u$ (kN/m²) | $e_f$ (%) | $E_{50}$ (kN/m²) | $E_{0.02}$ (kN/m²) | $r_d$ (g/cm³) | *e* | *w* (%) | $D_r$ (%) |
|---|---|---|---|---|---|---|---|---|---|---|---|
| 1 | 2.5 | *Batch A* | 90 Days | 99.84 | 0.185 | 554667 | 333050 | 1.48 | 0.781 | 23.02% | 52.19% |
| 2 | 2.5 | *Batch A* | 90 Days | 67.4 | 0.186 | 140417 | 224667 | 1.48 | 0.789 | 23.24% | 49.31% |
| 3 | 2.5 | *Batch A* | 90 Days | 68.85 | 0.231 | 93041 | 226650 | 1.48 | 0.786 | 22.89% | 50.57% |
| 1 | 5.0 | *Batch A* | 90 Days | 339.550 | 0.236 | 273831 | 1122650 | 1.48 | 0.788 | 26.86% | 50.03% |
| 2 | 5.0 | *Batch A* | 90 Days | 419.2 | 0.177 | 235506 | 1383700 | 1.48 | 0.787 | 26.51% | 50.33% |
| 3 | 5.0 | *Batch A* | 90 Days | 383.600 | 0.191 | 639333 | 1192000 | 1.48 | 0.788 | 26.41% | 50.25% |
| 1 | 7.5 | *Batch A* | 90 Days | 1014.91 | 0.145 | 3903500 | 2561000 | 1.47 | 0.792 | 27.51% | 50.68% |
| 2 | 7.5 | *Batch A* | 90 Days | 936.793 | 0.312 | 493049 | 3093000 | 1.47 | 0.792 | 26.16% | 50.48% |
| 3 | 7.5 | *Batch A* | 90 Days | 840.17 | 0.183 | 2 | 2773000 | 1.47 | 0.791 | 28.95% | 50.94% |
| 1 | 10 | *Batch A* | 90 Days | 1676.79 | 0.421 | 716577 | 5539000 | 1.44 | 0.830 | 28.91% | 50.41% |
| 2 | 10 | *Batch A* | 90 Days | 1665.81 | 0.261 | 1140966 | 5486000 | 1.44 | 0.829 | 31.61% | 50.85% |
| 3 | 10 | *Batch A* | 90 Days | 1307.95 | 0.202 | 1676859 | 4315200 | 1.44 | 0.829 | 30.89% | 50.73% |

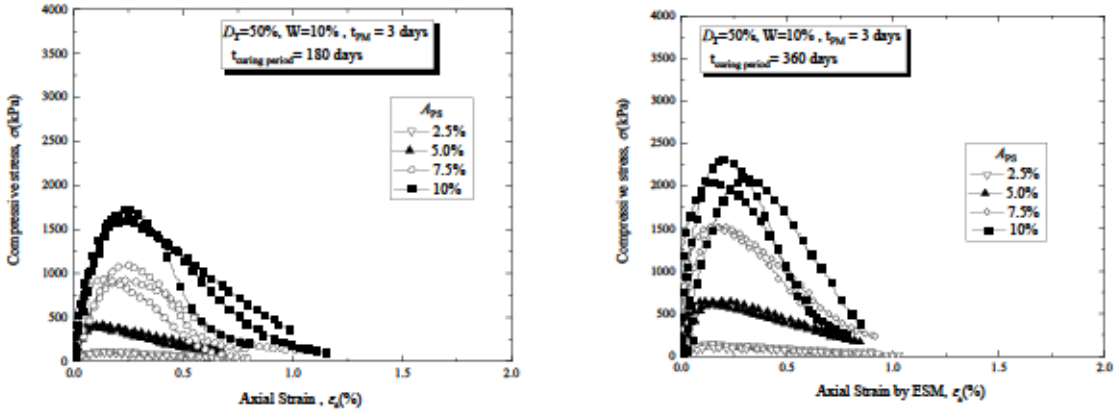


(g) (h)

Figure C-6 Typical UCT stress-strain relationship of PSAS-treated sand for $w$=10%, $t$p=3days, $D_r$=50%: (g) $t$= 180days, (h) $t$= 360 days.

Table C-g UCT data record for PSAS-treated sand for w=10%, tp=3days, Dr=50% at t= 180days

| Specimen No. | $A_{PS}$(%) | Modifier Batch | Curing days, $t$ | $q_u$ (kN/m²) | $\varepsilon_f$ (%) | $E_{50}$ (kN/m²) | $E_{0.02}$ (kN/m²) | $\rho_d$ (g/cm³) | $e$ | $w$ (%) | $D_r$ (%) |
|---|---|---|---|---|---|---|---|---|---|---|---|
| 1 | 2.5 | *BATCH B* | 180 Days | 107.6 | 0.205 | 137949 | 197000 | 1.48 | 0.785 | 24.29% | 50.93% |
| 2 | 2.5 | *BATCH B* | 180 Days | 93.44 | 0.159 | 194667 | 128150 | 1.48 | 0.785 | 24.67% | 50.92% |
| 3 | 2.5 | *BATCH B* | 180 Days | 92.44 | 0.182 | 154067 | 250500 | 1.48 | 0.788 | 24.75% | 49.91% |
| 1 | 5.0 | *BATCH B* | 180 Days | 363.800 | 0.167 | 757917 | 1297500 | 1.48 | 0.787 | 24.68% | 50.39% |
| 2 | 5.0 | *BATCH B* | 180 Days | 370.4 | 0.177 | 771667 | 742000 | 1.48 | 0.788 | 27.00% | 50.22% |
| 3 | 5.0 | *BATCH B* | 180 Days | 343.000 | 0.191 | 571667 | 1009500 | 1.48 | 0.786 | 24.35% | 50.84% |
| 1 | 7.5 | *BATCH B* | 180 Days | 870.8 | 0.237 | 691111 | 2116500 | 1.47 | 0.793 | 25.92% | 50.24% |
| 2 | 7.5 | *BATCH B* | 180 Days | 1004.3 | 0.247 | 865776 | 3138500 | 1.47 | 0.791 | 25.06% | 50.98% |
| 3 | 7.5 | *BATCH B* | 180 Days | 855.9 | 0.161 | 713250 | 2084500 | 1.47 | 0.792 | 26.99% | 50.54% |
| 1 | 10 | *BATCH B* | 180 Days | 1554.9 | 0.236 | 1619688 | 2542500 | 1.44 | 0.830 | 24.04% | 50.38% |
| 2 | 10 | *BATCH B* | 180 Days | 1512.8 | 0.237 | 1483137 | 3187500 | 1.44 | 0.829 | 22.42% | 50.74% |
| 3 | 10 | *BATCH B* | 180 Days | 1597.1 | 0.202 | 1330917 | 5462500 | 1.44 | 0.831 | 23.77% | 50.19% |

Table C-h UCT data record for PSAS-treated sand for w=10%, tp=3days, Dr=50% at t= 360days

| Specimen No. | $A_{PS}$(%) | Modifier Batch | Curing days, $t$ | $q_u$ (kN/m²) | $\varepsilon_f$ (%) | $E_{50}$ (kN/m²) | $E_{0.02}$ (kN/m²) | $\rho_d$ (g/cm³) | $e$ | $w$ (%) | $D_r$ (%) |
|---|---|---|---|---|---|---|---|---|---|---|---|
| 1 | 2.5 | *BATCH B* | 360 Days | 251.6 | 0.205 | 46593 | 197000 | 1.48 | 0.787 | 23.02% | 50.01% |
| 2 | 2.5 | *BATCH B* | 360 Days | 293.8 | 0.159 | 36725 | 128150 | 1.48 | 0.787 | 23.24% | 50.03% |
| 3 | 2.5 | *BATCH B* | 360 Days | 301.8 | 0.182 | 60360 | 250500 | 1.48 | 0.787 | 22.89% | 50.21% |
| 1 | 5 | *BATCH B* | 360 Days | 891.4 | 0.167 | 108707 | 1297500 | 1.48 | 0.788 | 26.86% | 50.17% |
| 2 | 5 | *BATCH B* | 360 Days | 589.2 | 0.177 | 56654 | 742000 | 1.48 | 0.785 | 26.51% | 50.92% |
| 3 | 5 | *BATCH B* | 360 Days | 754.9 | 0.191 | 99329 | 1009500 | 1.48 | 0.788 | 26.41% | 50.25% |
| 1 | 7.5 | *BATCH B* | 360 Days | 1474.3 | 0.237 | 122858 | 2116500 | 1.47 | 0.793 | 27.51% | 50.26% |
| 2 | 7.5 | *BATCH B* | 360 Days | 1626 | 0.247 | 159412 | 3138500 | 1.47 | 0.792 | 26.16% | 50.48% |
| 3 | 7.5 | *BATCH B* | 360 Days | 1592.5 | 0.161 | 220568 | 2084500 | 1.47 | 0.793 | 28.95% | 50.19% |
| 1 | 10 | *BATCH B* | 360 Days | 3037.3 | 0.236 | 446662 | 2542500 | 1.44 | 0.830 | 28.91% | 50.41% |
| 2 | 10 | *BATCH B* | 360 Days | 2735 | 0 | 0 | 3187500 | 1.44 | 0.829 | 31.61% | 50.85% |
| 3 | 10 | *BATCH B* | 360 Days | 2223 | 0.202 | 241630 | 5462500 | 1.44 | 0.829 | 30.89% | 50.73% |

### C.2.2 Stress-strain relationship of PSAS treated sand for $w$=10%, tp=3 days, $D_r$=90%

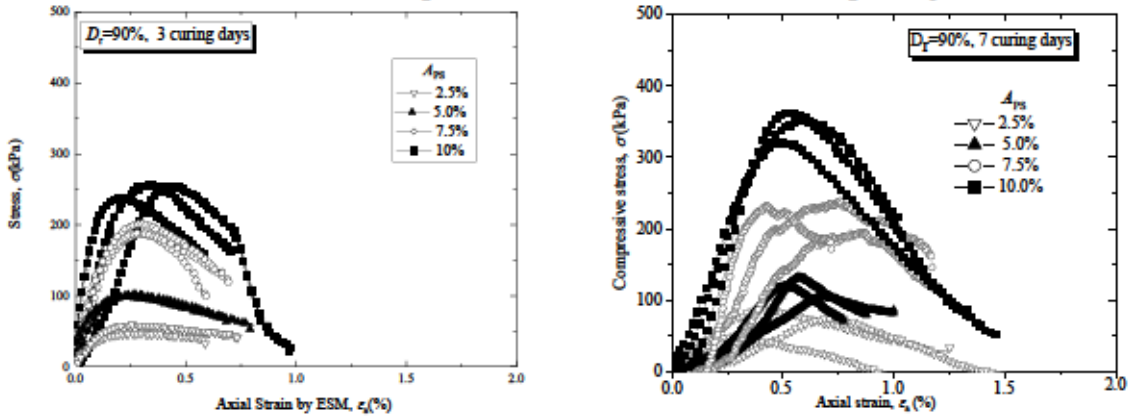


Figure C-7 Typical UCT stress-strain relationship of PSAS-treated sand for $w$=10%, $tp$=3days, $D_r$=90%: (a) $t$= 3days, (b) $t$= 7 days.

Table C-i UCT data record for PSAS-treated sand for w=10%, tp=3days, Dr=90% at t= 3days

| Specimen No. | $A_{PS}$(%) | Modifier Batch | Curing days, $t$ | $q_u$ | $\varepsilon_f$ | $E_{50}$ | $\rho_d$ | $e$ | $w$ | $D_r$ |
|---|---|---|---|---|---|---|---|---|---|---|
| | | | | (kN/m²) | (%) | (kN/m²) | (g/cm³) | | (%) | (%) |
| 1 | 2.5 | *Batch A* | 3 Days | 59.7318 | 0.403 | 22940 | 1.58 | 0.672 | 17.47% | 91.80% |
| 2 | 2.5 | *Batch A* | 3 Days | 51.867 | 0.602 | 13320 | 1.58 | 0.673 | 16.05% | 91.31% |
| 3 | 2.5 | *Batch A* | 3 Days | 39.92 | 0.328 | 36690 | 1.58 | 0.674 | 20.83% | 91.15% |
| 1 | 5 | *Batch A* | 3 Days | 120.06 | 0.171 | 14770 | 1.60 | 0.654 | 16.26% | 91.61% |
| 2 | 5 | *Batch A* | 3 Days | 95.31 | 0.577 | 11960 | 1.60 | 0.653 | 14.60% | 91.90% |
| 3 | 5 | *Batch A* | 3 Days | 108.810 | 0.668 | 16460 | 1.59 | 0.658 | 15.07% | 90.14% |
| 1 | 7.5 | *Batch A* | 3 Days | 209.9931 | 0.734 | 32190 | 1.60 | 0.645 | 19.30% | 91.99% |
| 2 | 7.5 | *Batch A* | 3 Days | 172.8114 | 0.533 | 21770 | 1.60 | 0.649 | 13.50% | 90.77% |
| 3 | 7.5 | *Batch A* | 3 Days | 207.1803 | 0.536 | 39660 | 1.60 | 0.648 | 12.93% | 91.03% |
| 1 | 10 | *Batch A* | 3 Days | 117.4935 | 0.734 | 59830 | 1.56 | 0.688 | 16.63% | 88.56% |
| 2 | 10 | *Batch A* | 3 Days | 129.4655 | 0.734 | 65920 | 1.57 | 0.677 | 16.91% | 91.60% |
| 3 | 10 | *Batch A* | 3 Days | 132.9695 | 0.629 | 56200 | 1.57 | 0.683 | 16.13% | 89.95% |

Table C-j UCT data record for PSAS-treated sand for w=10%, tp=3days, Dr=90% at t= 7days

| Specimen No. | $A_{PS}$(%) | Modifier Batch | Curing days, $t$ | $q_u$ | $\varepsilon_f$ | $E_{50}$ | $\rho_d$ | $e$ | $w$ | $D_r$ |
|---|---|---|---|---|---|---|---|---|---|---|
| | | | | (kN/m²) | (%) | (kN/m²) | (g/cm³) | | (%) | (%) |
| 1 | 2.5 | *Batch A* | 7 Days | 88.1 | 0.403 | 22942.70833 | 1.57 | 0.677 | 18.31% | 90.07% |
| 2 | 2.5 | *Batch A* | 7 Days | 76.5 | 0.602 | 13327.52613 | 1.57 | 0.677 | 16.05% | 90.03% |
| 3 | 2.5 | *Batch A* | 7 Days | 49.9 | 0.328 | 36691.17647 | 1.58 | 0.675 | 20.01% | 90.81% |
| 1 | 5 | *Batch A* | 7 Days | 133.4 | 0.171 | 14776.82222 | 1.59 | 0.657 | 16.26% | 90.57% |
| 2 | 5 | *Batch A* | 7 Days | 105.9 | 0.577 | 11963.93801 | 1.59 | 0.656 | 16.65% | 90.87% |
| 3 | 5 | *Batch A* | 7Days | 120.900 | 0.668 | 16464.78965 | 1.59 | 0.657 | 16.30% | 90.69% |
| 1 | 7.5 | *Batch A* | 7Days | 238.9 | 0.734 | 32196.7655 | 1.60 | 0.651 | 19.30% | 90.17% |
| 2 | 7.5 | *Batch A* | 7 Days | 196.6 | 0.533 | 21775.90887 | 1.60 | 0.650 | 16.32% | 90.62% |
| 3 | 7.5 | *Batch A* | 7 Days | 235.7 | 0.536 | 39660.33468 | 1.60 | 0.650 | 16.92% | 90.53% |
| 1 | 10 | *Batch A* | 7Days | 160.95 | 0.734 | 59832.71375 | 1.57 | 0.682 | 16.63% | 90.22% |
| 2 | 10 | *Batch A* | 7 Days | 177.35 | 0.734 | 65929.36803 | 1.57 | 0.681 | 16.91% | 90.60% |
| 3 | 10 | *Batch A* | 7 Days | 182.15 | 0.629 | 56208.6358 | 1.57 | 0.681 | 16.13% | 90.56% |

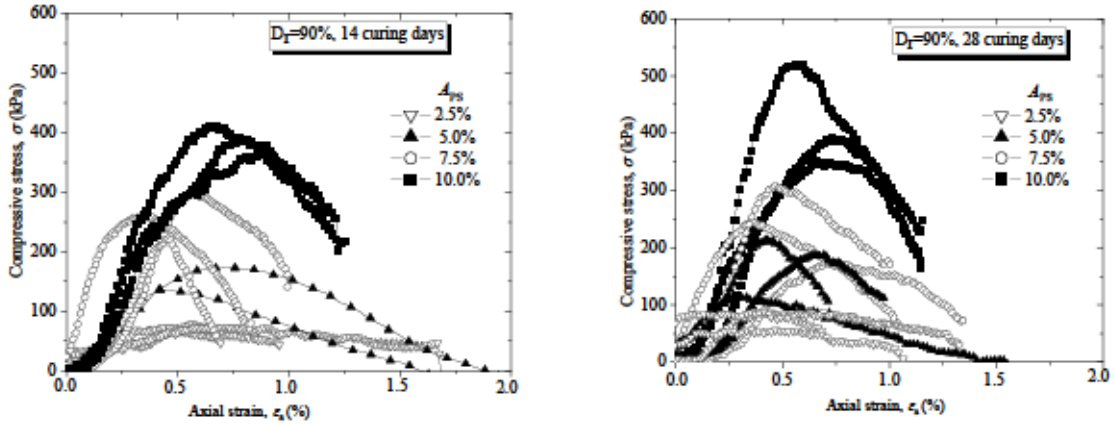


Figure C-8 Typical UCT stress-strain relationship of PSAS-treated sand for w=10%, tp=3days, Dr=90%: (c) t= 14days, (d) t= 28 days.

Table C-k UCT data record for PSAS-treated sand for w=10%, tp=3days, Dr=90% at t= 14days

| Specimen No. | $A_{PS}$(%) | Modifier Batch | Curing days, $t$ | $q_u$ (kN/m²) | $\varepsilon_f$ (%) | $E_{50}$ (kN/m²) | $\rho_d$ (g/cm³) | $e$ | $w$ (%) | $D_r$ (%) |
|---|---|---|---|---|---|---|---|---|---|---|
| 1 | 2.5 | *Batch A* | 14 Days | 80.05 | 0.6005 | 19710 | 1.58 | 0.676 | 19.12% | 90.53% |
| 2 | 2.5 | *Batch A* | 14 Days | 76.4 | 0.401 | 17760 | 1.58 | 0.675 | 19.74% | 90.88% |
| 3 | 2.5 | *Batch A* | 14 Days | 75.3 | 0.723 | 14590 | 1.58 | 0.675 | 18.16% | 90.88% |
| 1 | 5 | *Batch A* | 14 Days | 175.1 | 0.745 | 27530 | 1.59 | 0.657 | 22.20% | 90.63% |
| 2 | 5 | *Batch A* | 14 Days | 171.1 | 0.5 | 43200 | 1.59 | 0.658 | 21.14% | 90.37% |
| 3 | 5 | *Batch A* | 14 Days | 135.9 | 0.46 | 36720 | 1.59 | 0.658 | 20.69% | 90.35% |
| 1 | 7.5 | *Batch A* | 14 Days | 300.9 | 0.582 | 55510 | 1.60 | 0.650 | 16.59% | 90.41% |
| 2 | 7.5 | *Batch A* | 14 Days | 223.5 | 0.471 | 36750 | 1.60 | 0.651 | 18.58% | 90.30% |
| 3 | 7.5 | *Batch A* | 14 Days | 263.44 | 0.373 | 129130 | 1.60 | 0.651 | 16.29% | 90.14% |
| 1 | 10 | *Batch A* | 14 Days | 370.9 | 0.899 | 94130 | 1.57 | 0.680 | 20.43% | 90.91% |
| 2 | 10 | *Batch A* | 14 Days | 392.2 | 0.818 | 71560 | 1.57 | 0.683 | 21.49% | 90.08% |
| 3 | 10 | *Batch A* | 14 Days | 412.7 | 0.695 | 85260 | 1.57 | 0.681 | 17.85% | 90.65% |

Table C-l UCT data record for PSAS-treated sand for w=10%, tp=3days, Dr=90% at t= 28days

| Specimen No. | $A_{PS}$(%) | Modifier Batch | Curing days, $t$ | $q_u$ (kN/m²) | $\varepsilon_f$ (%) | $E_{50}$ (kN/m²) | $\rho_d$ (g/cm³) | $e$ | $w$ (%) | $D_r$ (%) |
|---|---|---|---|---|---|---|---|---|---|---|
| 1 | 2.5 | *Batch A* | 28 Days | 90.2 | 0.973 | 10250 | 1.58 | 0.676 | 19.67% | 90.40% |
| 2 | 2.5 | *Batch A* | 28 Days | 88.5 | 0.973 | 11490 | 1.58 | 0.675 | 17.04% | 90.74% |
| 3 | 2.5 | *Batch A* | 28 Days | 58.9 | 0.861 | 8890 | 1.58 | 0.675 | 19.87% | 90.82% |
| 1 | 5 | *Batch A* | 28 Days | 217.500 | 0.973 | 22840 | 1.59 | 0.659 | 18.65% | 90.02% |
| 2 | 5 | *Batch A* | 28 Days | 114.9 | 0.973 | 16990 | 1.59 | 0.656 | 19.34% | 90.80% |
| 3 | 5 | *Batch A* | 28 Days | 190.500 | 0.607 | 40870 | 1.59 | 0.658 | 17.27% | 90.26% |
| 1 | 7.5 | *Batch A* | 28 Days | 252.5 | 0.788 | 68980 | 1.60 | 0.649 | 17.00% | 90.94% |
| 2 | 7.5 | *Batch A* | 28 Days | 310.8 | 0.723 | 59310 | 1.60 | 0.651 | 17.74% | 90.23% |
| 3 | 7.5 | *Batch A* | 28 Days | 176.7 | 0.575 | 33720 | 1.60 | 0.650 | 17.52% | 90.53% |
| 1 | 10 | *Batch A* | 28 Days | 354.7 | 0.652 | 66920 | 1.57 | 0.682 | 16.14% | 90.36% |
| 2 | 10 | *Batch A* | 28 Days | 393.9 | 0.629 | 79090 | 1.57 | 0.681 | 18.46% | 90.44% |
| 3 | 10 | *Batch A* | 28 Days | 522.7 | 0.507 | 122120 | 1.57 | 0.682 | 19.57% | 90.21% |

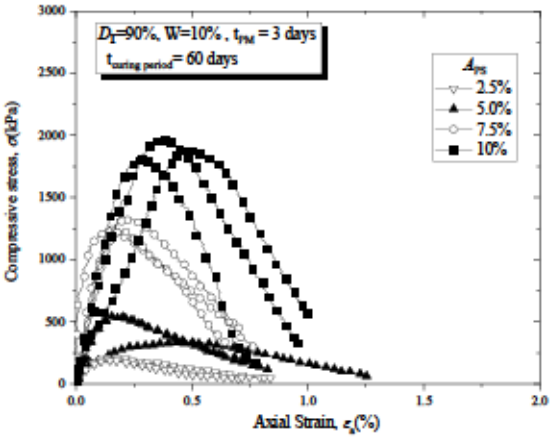


(e)

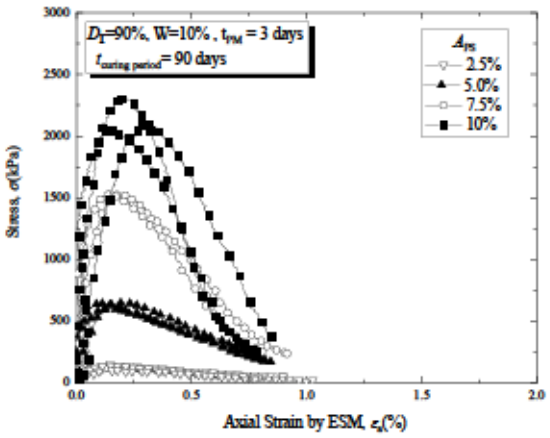


(f)

Figure C-9 Typical UCT stress-strain relationship of PSAS-treated sand for w=10%, tp=3days, Dr=90%: (e) t= 60days, (f) t= 90days.

Table C-m UCT data record for PSAS-treated sand for w=10%, tp=3days, Dr=90% at t= 60days

| Specimen No. | $A_{PS}$(%) | Modifier Batch | Curing days, $t$ | $q_u$ (kN/m²) | $\varepsilon_f$ (%) | $E_{50}$ (kN/m²) | $E_{0.02}$ (kN/m²) | $\rho_d$ (g/cm³) | $e$ | $w$ (%) | $D_r$ (%) |
|---|---|---|---|---|---|---|---|---|---|---|---|
| 1 | 2.5 | *BATCH B* | 60 Days | 190.1 | 0.211 | 288021 | 490650 | 1.58 | 0.676 | 23.02% | 90.29% |
| 2 | 2.5 | *BATCH B* | 60 Days | 187.8 | 0.205 | 268286 | 476000 | 1.57 | 0.676 | 23.24% | 90.27% |
| 3 | 2.5 | *BATCH B* | 60 Days | 163.53 | 0.189 | 215171 | 408300 | 1.58 | 0.675 | 22.89% | 90.86% |
| 1 | 5 | *BATCH B* | 60 Days | 339.55 | 0.236 | 273831 | 936167 | 1.59 | 0.658 | 26.86% | 90.13% |
| 2 | 5 | *BATCH B* | 60 Days | 484.7 | 0.225 | 526848 | 1256500 | 1.59 | 0.658 | 26.51% | 90.27% |
| 3 | 5 | *BATCH B* | 60 Days | 490.1 | 0.211 | 544556 | 1282000 | 1.59 | 0.657 | 26.41% | 90.53% |
| 1 | 7.5 | *BATCH B* | 60 Days | 1239.3 | 0.247 | 983571 | 3639000 | 1.60 | 0.650 | 27.51% | 90.56% |
| 2 | 7.5 | *BATCH B* | 60 Days | 1158.4 | 0.175 | 4633600 | 3268500 | 1.60 | 0.651 | 27.01% | 90.21% |
| 3 | 7.5 | *BATCH B* | 60 Days | 1132.3 | 0.215 | 1068208 | 3446500 | 1.60 | 0.650 | 27.49% | 90.52% |
| 1 | 10 | *BATCH B* | 60 Days | 1877.2 | 0.421 | 733281 | 5436500 | 1.57 | 0.680 | 20.07% | 90.85% |
| 2 | 10 | *BATCH B* | 60 Days | 1811.1 | 0.261 | 429171 | 6646000 | 1.57 | 0.681 | 25.69% | 90.40% |
| 3 | 10 | *BATCH B* | 60 Days | 1695.3 | 0.202 | 952416 | 4955500 | 1.57 | 0.681 | 25.71% | 90.59% |

Table C-n UCT data record for PSAS-treated sand for w=10%, tp=3days, Dr=90% at t= 90days

| Specimen No. | $A_{PS}$(%) | Modifier Batch | Curing days, $t$ | $q_u$ (kN/m²) | $\varepsilon_f$ (%) | $E_{50}$ (kN/m²) | $E_{0.02}$ (kN/m²) | $\rho_d$ (g/cm³) | $e$ | $w$ (%) | $D_r$ (%) |
|---|---|---|---|---|---|---|---|---|---|---|---|
| 1 | 2.5 | *BATCH B* | 90 Days | 129.3 | 0.217 | 195909 | 405500 | 1.58 | 0.675 | 26.26% | 90.71% |
| 2 | 2.5 | *BATCH B* | 90 Days | 125.8 | 0.186 | 209667 | 270050 | 1.58 | 0.675 | 25.95% | 90.77% |
| 3 | 2.5 | *BATCH B* | 60 Days | 92.1 | 0.225 | 124459 | 197100 | 1.58 | 0.674 | 24.40% | 90.92% |
| 1 | 5 | *BATCH B* | 90 Days | 563.1 | 0.182 | 686707 | 1358500 | 1.59 | 0.659 | 26.79% | 90.00% |
| 2 | 5 | *BATCH B* | 90 Days | 610.1 | 0.227 | 693295 | 1431500 | 1.59 | 0.658 | 27.62% | 90.14% |
| 3 | 5 | *BATCH B* | 90 Days | 599.2 | 0.146 | 651304 | 1646500 | 1.59 | 0.656 | 26.29% | 90.86% |
| 1 | 7.5 | *BATCH B* | 90 Days | 1438.6 | 0.213 | 2247813 | 4460500 | 1.60 | 0.649 | 24.42% | 90.90% |
| 2 | 7.5 | *BATCH B* | 90 Days | 1435.5 | 0.162 | 2175000 | 2473500 | 1.60 | 0.649 | 22.83% | 90.83% |
| 3 | 7.5 | *BATCH B* | 90 Days | 0 | 0.157 | 0 | 0 | 1.60 | 0.650 | 27.49% | 90.46% |
| 1 | 10 | *BATCH B* | 90 Days | 2156.4 | 0.2 | 3717931 | 4890500 | 1.57 | 0.683 | 22.43% | 90.12% |
| 2 | 10 | *BATCH B* | 90 Days | 1942.3 | 0.261 | 3034844 | 6267000 | 1.57 | 0.683 | 24.07% | 90.03% |
| 3 | 10 | *BATCH B* | 90 Days | 1981.2 | 0.202 | 1151860 | 4610500 | 1.57 | 0.682 | 25.88% | 90.23% |

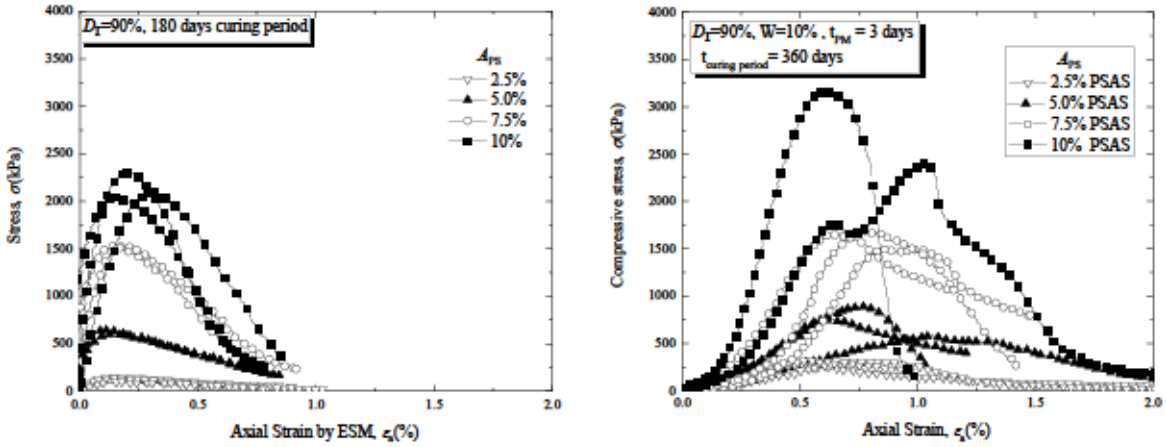


(g) (h)

Figure C-10 Typical UCT stress-strain relationship of PSAS-treated sand for w=10%, tp=3days, Dr=90%: (e) t= 180days, (f) t= 360days.

Table C-o UCT data record for PSAS-treated sand for w=10%, tp=3days, Dr=90% at t= 180days

| Specimen No. | $A_{PS}$(%) | Modifier Batch | Curing days, $t$ | $q_u$ (kN/m²) | $\varepsilon_f$ (%) | $E_{50}$ (kN/m²) | $E_{0.02}$ (kN/m²) | $\rho_d$ (g/cm³) | $e$ | $w$ (%) | $D_r$ (%) |
|---|---|---|---|---|---|---|---|---|---|---|---|
| 1 | 2.5 | *BATCH B* | 180 Days | 139.3 | 0.11 | 204853 | 827000 | 1.57 | 0.676 | 25.20% | 90.22% |
| 2 | 2.5 | *BATCH B* | 180 Days | 135.8 | 0.143 | 339500 | 1706000 | 1.58 | 0.675 | 25.19% | 90.73% |
| 3 | 2.5 | *BATCH B* | 180 Days | 92.1 | 0.208 | 121184 | 1246000 | 1.58 | 0.676 | 25.71% | 90.51% |
| 1 | 5 | *BATCH B* | 180 Days | 610.1 | 0.142 | 677889 | 3791500 | 1.59 | 0.658 | 24.30% | 90.33% |
| 2 | 5 | *BATCH B* | 180 Days | 599.1 | 0.159 | 665667 | 4954500 | 1.59 | 0.657 | 24.86% | 90.52% |
| 3 | 5 | *BATCH B* | 180 Days | 583.1 | 0.249 | 728875 | 20730000 | 1.59 | 0.659 | 25.49% | 90.01% |
| 1 | 7.5 | *BATCH B* | 180 Days | 1435.5 | 0.213 | 1595000 | 20730000 | 1.60 | 0.651 | 23.61% | 90.22% |
| 2 | 7.5 | *BATCH B* | 180 Days | 1438.6 | 0.193 | 1598444 | 23582500 | 1.60 | 0.651 | 25.69% | 90.23% |
| 3 | 7.5 | *BATCH B* | 180 Days | 0 | 0.154 | 0 | 16052500 | 1.60 | 0.651 | 25.24% | 90.17% |
| 1 | 10 | *BATCH B* | 180 Days | 2156.4 | 0.188 | 3478065 | 22538000 | 1.57 | 0.680 | 25.61% | 90.88% |
| 2 | 10 | *BATCH B* | 180 Days | 1942.3 | 0.18 | 2774714 | 33064000 | 1.57 | 0.682 | 24.16% | 90.36% |
| 3 | 10 | *BATCH B* | 180 Days | 1981.2 | 0.209 | 1151860 | 32286500 | 1.57 | 0.680 | 23.60% | 90.85% |

Table C-p UCT data record for PSAS-treated sand for w=10%, tp=3days, Dr=90% at t= 360days

| Specimen No. | $A_{PS}$(%) | Modifier Batch | Curing days, $t$ | $q_u$ (kN/m²) | $\varepsilon_f$ (%) | $E_{50}$ (kN/m²) | $E_{0.02}$ (kN/m²) | $r_d$ (g/cm³) | $e$ | $w$ (%) | $D_r$ (%) |
|---|---|---|---|---|---|---|---|---|---|---|---|
| 1 | 2.5 | *BATCH B* | 360 Days | 0 | 0.217 | 0 | 0 | 0.00 | 0.000 | 0.00% | 0.00% |
| 2 | 2.5 | *BATCH B* | 360 Days | 139.1 | 0.323 | 93986 | 380300 | 1.58 | 0.675 | 25.90% | 90.62% |
| 3 | 2.5 | *BATCH B* | 360 Days | 0 | 0.225 | 0 | 0 | 1.58 | 0.676 | 23.98% | 90.49% |
| 1 | 5 | *BATCH B* | 360 Days | 570.2 | 0.182 | 178188 | 2519500 | 1.59 | 0.657 | 20.92% | 90.48% |
| 2 | 5 | *BATCH B* | 360 Days | 0 | 0.227 | 0 | 0 | 1.59 | 0.658 | 22.53% | 90.33% |
| 3 | 5 | *BATCH B* | 360 Days | 498 | 0.335 | 184444 | 2020500 | 1.59 | 0.658 | 23.33% | 90.21% |
| 1 | 7.5 | *BATCH B* | 360 Days | 1191.5 | 0.213 | 242175 | 4391500 | 1.60 | 0.651 | 22.81% | 90.37% |
| 2 | 7.5 | *BATCH B* | 360 Days | 1245.4 | 0.162 | 300821 | 5003000 | 1.60 | 0.649 | 23.76% | 90.85% |
| 3 | 7.5 | *BATCH B* | 360 Days | 1606.6 | 0.157 | 247932 | 8010000 | 1.60 | 0.651 | 23.56% | 90.15% |
| 1 | 10 | *BATCH B* | 360 Days | 0 | 0.2 | 0 | 4890500 | 1.57 | 0.681 | 20.35% | 90.42% |
| 2 | 10 | *BATCH B* | 360 Days | 2735.8 | 0.261 | 506630 | 5297000 | 1.57 | 0.681 | 22.57% | 90.62% |
| 3 | 10 | *BATCH B* | 360 Days | 1963.7 | 0.202 | 288779 | 12186000 | 1.57 | 0.680 | 22.29% | 90.71% |

### C.2.3 Stress-strain relationship of PSAS treated sand for $w$=20%, $t_p$=0 days, $D_r$=50%

- *ELM: External Strain Measurement* *LSM: Local Strain measurement*

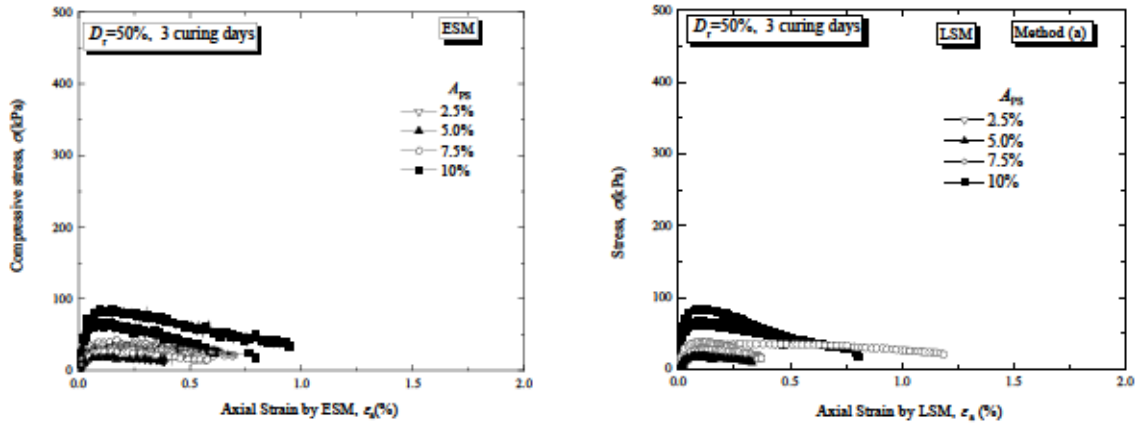


(a) (b)

Figure C-11 Typical UCT stress-strain relationship of PSAS-treated sand for w=20%, tp=0days, Dr=50%, t= 3days: (a) ESM, (b) LSM

Table C-q UCT data record for PSAS-treated sand for w=20%, tp=0days, Dr=50% at t= 3days

| Specimen No. | $A_{PS}$(%) | Modifier Batch | Curing days, $t$ | $q_u$ (kN/m$^2$) | $\varepsilon_f$ (%) | $E_{50}$ (kN/m$^2$) | $Ev$ (kN/m$^2$) | $\rho_d$ (g/cm$^3$) | $e$ | $w$ (%) | $D_r$ (%) |
|---|---|---|---|---|---|---|---|---|---|---|---|
| 1 | 2.5 | *BATCH 2* | 3 Days | 0 | 0.261 | 114200 | 83150 | 1.48 | 0.783 | 23.10% | 51.74% |
| 2 | 2.5 | *BATCH 2* | 3 Days | 0 | 0.257 | 200200 | 50510 | 1.48 | 0.785 | 23.24% | 51.03% |
| 3 | 2.5 | *BATCH 2* | 3 Days | 0 | 0.0962 | 254400 | 169000 | 1.48 | 0.780 | 22.94% | 52.58% |
| 1 | 5.0 | *BATCH 2* | 3 Days | 19.3 | 0.107 | 604400 | 437500 | 1.48 | 0.788 | 26.86% | 50.03% |
| 2 | 5.0 | *BATCH 2* | 3 Days | 0 | 0 | 227200 | 283500 | 1.48 | 0.783 | 26.51% | 51.56% |
| 3 | 5.0 | *BATCH 2* | 3 Days | 17.8 | 0.139 | 458600 | 312500 | 1.48 | 0.782 | 26.41% | 52.02% |
| 1 | 7.5 | *BATCH 2* | 3 Days | 38.58 | 0.127 | 1253000 | 914500 | 1.47 | 0.797 | 27.51% | 49.19% |
| 2 | 7.5 | *BATCH 2* | 3 Days | 35.25 | 0.193 | 1253000 | 826000 | 1.48 | 0.782 | 26.41% | 53.55% |
| 3 | 7.5 | *BATCH 2* | 3 Days | 27.3 | 0.136 | 828800 | 656500 | 1.47 | 0.790 | 26.98% | 51.29% |
| 1 | 10 | *BATCH 2* | 3 Days | 83.5 | 0.019 | 654600 | 597500 | 1.44 | 0.830 | 28.91% | 50.41% |
| 2 | 10 | *BATCH 2* | 3 Days | 61.6 | 0.094 | 995300 | 945500 | 1.44 | 0.827 | 28.69% | 51.26% |
| 3 | 10 | *BATCH 2* | 3 Days | 66.5 | 0.087 | 1825400 | 848800 | 1.44 | 0.832 | 29.06% | 49.84% |

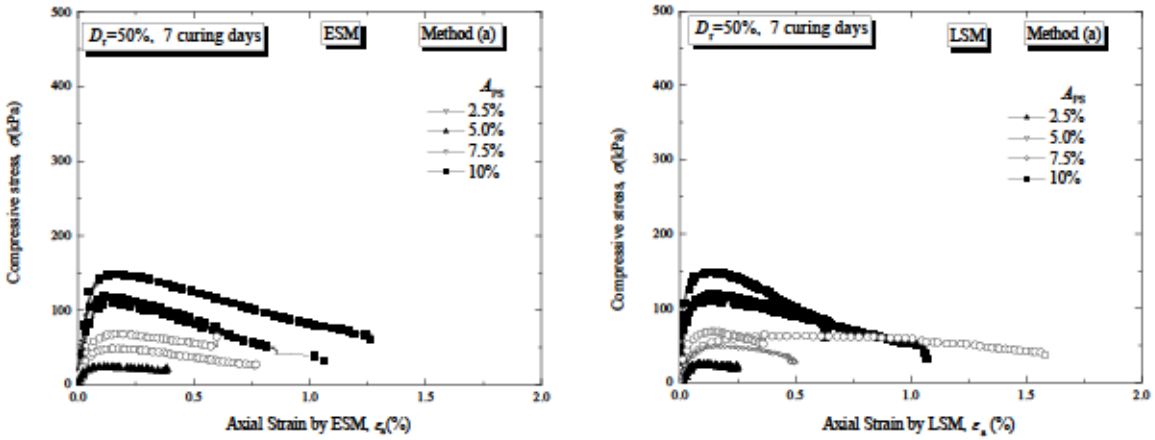


Figure C-12 Typical UCT stress-strain relationship of PSAS-treated sand for w=20%, tp=0days, Dr=50%, t= 7days: (a) ESM (b) LSM.

Table C-r UCT data record for PSAS-treated sand for w=20%, tp=0days, Dr=50% at t= 7days

| Specimen No. | $A_{PS}$(%) | Modifier Batch | Curing days, $t$ | $q_u$ (kN/m²) | $\varepsilon_f$ (%) | $E_{50}$ (kN/m²) | $E_{0.02}$ (kN/m²) | $\rho_d$ (g/cm³) | $e$ | $w$ (%) | $D_r$ (%) |
|---|---|---|---|---|---|---|---|---|---|---|---|
| 1 | 2.5 | *BATCH 2* | 7 Days | 0 | 0 | 0 | 0 | 1.48 | 0.787 | 22.64% | 50.33% |
| 2 | 2.5 | *BATCH 2* | 7 Days | 0 | 0 | 0 | 0 | 1.48 | 0.787 | 21.67% | 50.22% |
| 3 | 2.5 | *BATCH 2* | 7 Days | 0 | 0 | 0 | 0 | 1.48 | 0.787 | 25.58% | 50.24% |
| 1 | 5 | *BATCH 2* | 7 Days | 23.78 | 0.107 | 66056 | 116250 | 1.48 | 0.786 | 22.64% | 50.62% |
| 2 | 5 | *BATCH 2* | 7 Days | 0 | 0 | 0 | 0 | 1.48 | 0.787 | 24.59% | 50.56% |
| 3 | 5 | *BATCH 2* | 7 Days | 29.7 | 0.139 | 38077 | 69000 | 1.86 | 0.000 | 0.00% | |
| 1 | 7.5 | *BATCH 2* | 7 Days | 68.59 | 0.167 | 110629 | 176500 | 1.47 | 0.793 | 23.89% | 50.31% |
| 2 | 7.5 | *BATCH 2* | 7 Days | 62.64 | 0.273 | 101032 | 109200 | 1.47 | 0.789 | 21.69% | 51.54% |
| 3 | 7.5 | *BATCH 2* | 7 Days | 48.54 | 0.136 | 97080 | 114000 | 1.47 | 0.791 | 21.87% | 50.96% |
| 1 | 10 | *BATCH 2* | 7 Days | 148.4 | 0.157 | 265000 | 544500 | 1.44 | 0.831 | 20.59% | 50.17% |
| 2 | 10 | *BATCH 2* | 7 Days | 109.5 | 0.157 | 202778 | 329500 | 1.44 | 0.831 | 19.62% | 50.19% |
| 3 | 10 | *BATCH 2* | 7 Days | 118.3 | 0.133 | 369688 | 386000 | 1.44 | 0.829 | 21.16% | 50.87% |

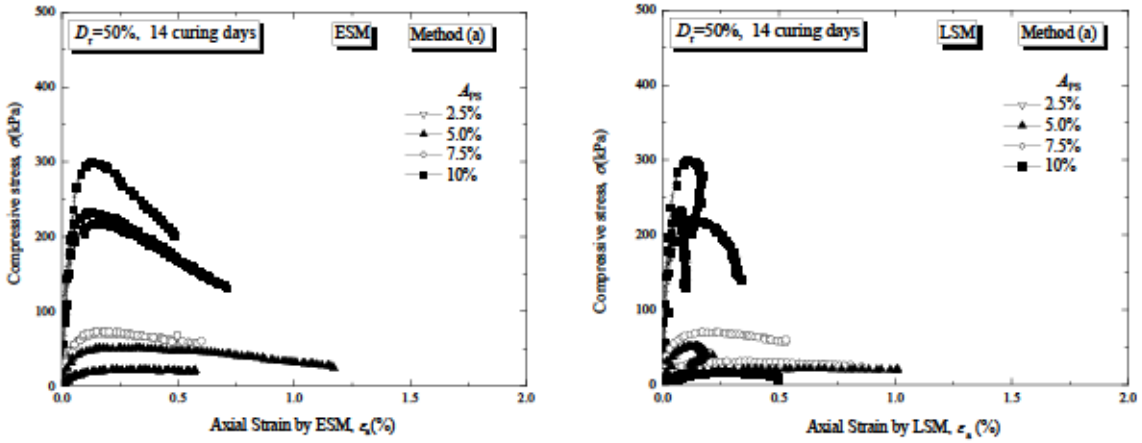


Figure C-13 Typical UCT stress-strain relationship of PSAS-treated sand for w=20%, tp=0days, Dr=50%, t= 14days: (a) ESM (b) LSM

Table C-s UCT data record for PSAS-treated sand for w=20%, tp=0days, Dr=50% at t= 14days

| Specimen No. | $A_{PS}$(%) | Modifier Batch | Curing days, $t$ | $q_u$ (kN/m²) | $e_f$ (%) | $E_{50}$ (kN/m²) | $E_{0.02}$ (kN/m²) | $r_d$ (g/cm³) | $e$ | $w$ (%) | $D_r$ (%) |
|---|---|---|---|---|---|---|---|---|---|---|---|
| 1 | 2.5 | *BATCH 2* | 14 Days | 0 | 0 | 0 | 0 | 1.48 | 0.785 | 23.02% | 50.84% |
| 2 | 2.5 | *BATCH 2* | 14 Days | 0 | 0 | 0 | 0 | 1.48 | 0.785 | 23.24% | 50.76% |
| 3 | 2.5 | *BATCH 2* | 14 Days | 0 | 0 | 0 | 0 | 1.48 | 0.786 | 22.89% | 50.55% |
| 1 | 5 | *BATCH 2* | 14 Days | 0 | 0 | 0 | 0 | 1.48 | 0.782 | 23.73% | 51.87% |
| 2 | 5 | *BATCH 2* | 14 Days | 15.73 | 0 | 14045 | 31000 | 1.48 | 0.787 | 22.33% | 50.48% |
| 3 | 5 | *BATCH 2* | 14 Days | 21.6 | 0 | 31765 | 29300 | 1.48 | 0.786 | 24.81% | 50.58% |
| 1 | 7.5 | *BATCH 2* | 14 Days | 70.1 | 0 | 250357 | 209400 | 1.47 | 0.791 | 25.56% | 50.95% |
| 2 | 7.5 | *BATCH 2* | 14 Days | 73.1 | 0 | 158913 | 212650 | 1.47 | 0.794 | 24.51% | 50.16% |
| 3 | 7.5 | *BATCH 2* | 14 Days | | | | | 1.47 | 0.794 | 25.57% | 50.11% |
| 1 | 10 | *BATCH 2* | 14 Days | 299.4 | 0 | 534643 | 824000 | 1.44 | 0.831 | 23.19% | 50.32% |
| 2 | 10 | *BATCH 2* | 14 Days | 216.5 | 0 | 386607 | 687500 | 1.44 | 0.828 | 21.29% | 50.91% |
| 3 | 10 | *BATCH 2* | 14 Days | 232 | 0 | 464000 | 836000 | 1.44 | 0.831 | 22.21% | 50.21% |

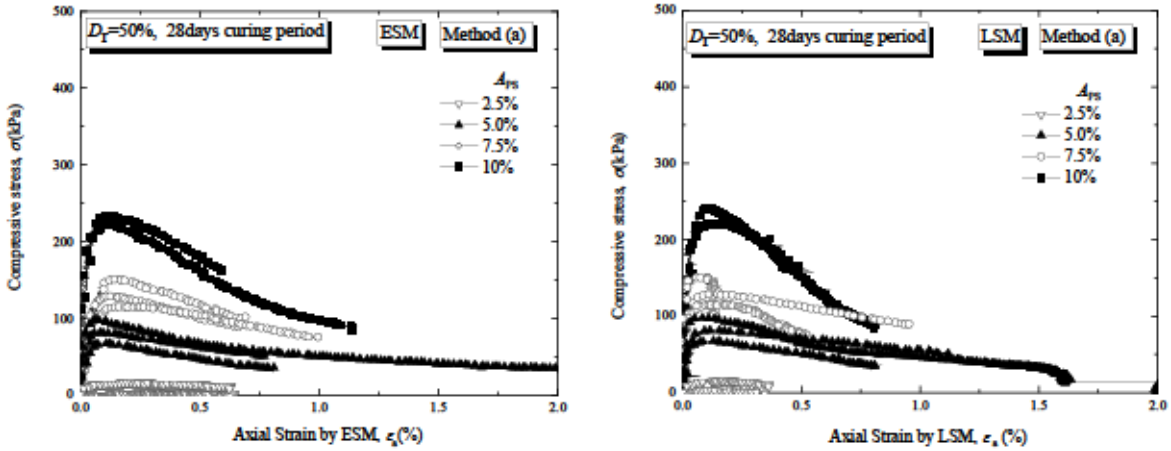


Figure C-14 Typical UCT stress-strain relationship of PSAS-treated sand for w=20%, tp=0days, Dr=50%, t= 28 days: (a) ESM (b) LSM

Table C-t UCT data record for PSAS-treated sand for w=20%, tp=0days, Dr=50% at t= 28days

| Specimen No. | $A_{PS}$(%) | Modifier Batch | Curing days, $t$ | $q_u$ (kN/m²) | $\varepsilon_f$ (%) | $E_{50}$ (kN/m²) | $E_{0.02}$ (kN/m²) | $\rho_d$ (g/cm³) | $e$ | $w$ (%) | $D_r$ (%) |
|---|---|---|---|---|---|---|---|---|---|---|---|
| 1 | 2.5 | *BATCH 2* | 28 Days | 7 | 0.063 | 43750 | 31000 | 1.48 | 0.787 | 26.52% | 50.19% |
| 2 | 2.5 | *BATCH 2* | 28 Days | 15.76 | 0.2036 | 39400 | 40145 | 1.48 | 0.787 | 24.78% | 50.28% |
| 3 | 2.5 | *BATCH 2* | 28 Days | 2.5 | 0.0962 | 5952 | 6600 | 1.48 | 0.787 | 24.43% | 50.11% |
| 1 | 5 | *BATCH 2* | 28 Days | 97.6 | 0.107 | 244000 | 436500 | 1.48 | 0.788 | 25.32% | 50.04% |
| 2 | 5 | *BATCH 2* | 28 Days | 67.6 | 0.119 | 160952 | 221500 | 1.48 | 0.787 | 25.20% | 50.33% |
| 3 | 5 | *BATCH 2* | 28 Days | 81.2 | 0.139 | 193333 | 247000 | 1.48 | 0.786 | 25.50% | 50.59% |
| 1 | 7.5 | *BATCH 2* | 28 Days | 128.9 | 0.117 | 157195 | 462500 | 1.47 | 0.792 | 23.75% | 50.53% |
| 2 | 7.5 | *BATCH 2* | 28 Days | 151.1 | 0.148 | 179881 | 683500 | 1.47 | 0.791 | 26.29% | 50.80% |
| 3 | 7.5 | *BATCH 2* | 28 Days | 115 | 0.249 | 261364 | 463500 | 1.47 | 0.794 | 26.71% | 50.19% |
| 1 | 10 | *BATCH 2* | 28 Days | 240.6 | 0.101 | 802000 | 635500 | 1.44 | 0.829 | 29.94% | 50.83% |
| 2 | 10 | *BATCH 2* | 28 Days | 233.7 | 0.104 | 730313 | 675500 | 1.44 | 0.832 | 31.15% | 50.02% |
| 3 | 10 | *BATCH 2* | 28 Days | 221.2 | 0.104 | 650588 | 752000 | 1.44 | 0.827 | 28.10% | 51.34% |

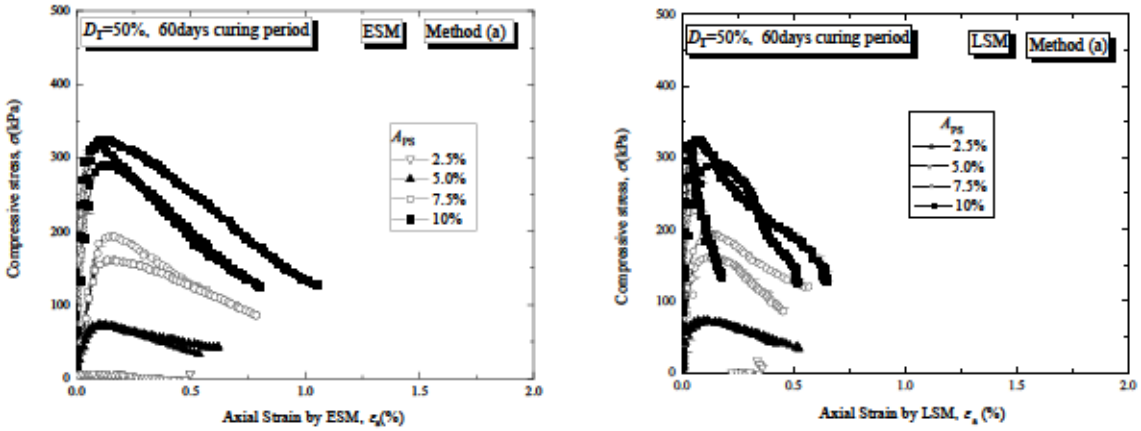


Figure C-15 Typical UCT stress-strain relationship of PSAS-treated sand for w=20%, tp=0days, Dr=50%, t= 60 days: (a) ESM (b) LSM.

Table C-u UCT data record for PSAS-treated sand for w=20%, tp=0days, Dr=50% at t= 60days

| Specimen No. | $A_{PS}$ (%) | Modifier Batch | Curing days, $t$ | $q_u$ (kN/m$^2$) | $\varepsilon_f$ (%) | $E_{50}$ (kN/m$^2$) | $E_{0.02}$ (kN/m$^2$) | $\rho_d$ (g/cm$^3$) | $e$ | $w$ (%) | $D_r$ (%) |
|---|---|---|---|---|---|---|---|---|---|---|---|
| 1 | 2.5 | *BATCH 2* | 60 Days | 25.9 | 0.006 | 161875 | 43167 | 1.48 | 0.785 | 23.02% | 50.74% |
| 2 | 2.5 | *BATCH 2* | 60 Days | 0 | 0.2036 | 0 | 0 | 1.48 | 0.786 | 23.24% | 50.61% |
| 3 | 2.5 | *BATCH 2* | 60 Days | 0 | 0.0962 | 0 | 0 | 1.48 | 0.786 | 22.89% | 50.57% |
| 1 | 5.0 | *BATCH 2* | 60 Days | 73.4 | 0.107 | 183500 | 220000 | 1.48 | 0.788 | 26.86% | 50.03% |
| 2 | 5.0 | *BATCH 2* | 60 Days | 71.4 | 0.11 | 170000 | 222500 | 1.48 | 0.788 | 26.51% | 50.09% |
| 3 | 5.0 | *BATCH 2* | 60 Days | 74.1 | 0.109 | 176429 | 247000 | 1.48 | 0.786 | 26.41% | 50.78% |
| 1 | 7.5 | *BATCH 2* | 60 Days | 193.3 | 0.117 | 254342 | 500000 | 1.47 | 0.792 | 27.51% | 50.68% |
| 2 | 7.5 | *BATCH 2* | 60 Days | 160.7 | 0.148 | 191310 | 375000 | 1.47 | 0.792 | 26.16% | 50.48% |
| 3 | 7.5 | *BATCH 2* | 60 Days | 164.7 | 0.249 | 205875 | 450000 | 1.47 | 0.793 | 28.95% | 50.30% |
| 1 | 10 | *BATCH 2* | 60 Days | 318.3 | 0.101 | 884167 | 1250000 | 1.44 | 0.830 | 28.91% | 50.41% |
| 2 | 10 | *BATCH 2* | 60 Days | 291 | 0.14 | 808333 | 850000 | 1.44 | 0.829 | 31.61% | 50.85% |
| 3 | 10 | *BATCH 2* | 60 Days | 324.3 | 0.104 | 1013438 | 1300000 | 1.44 | 0.829 | 30.89% | 50.73% |

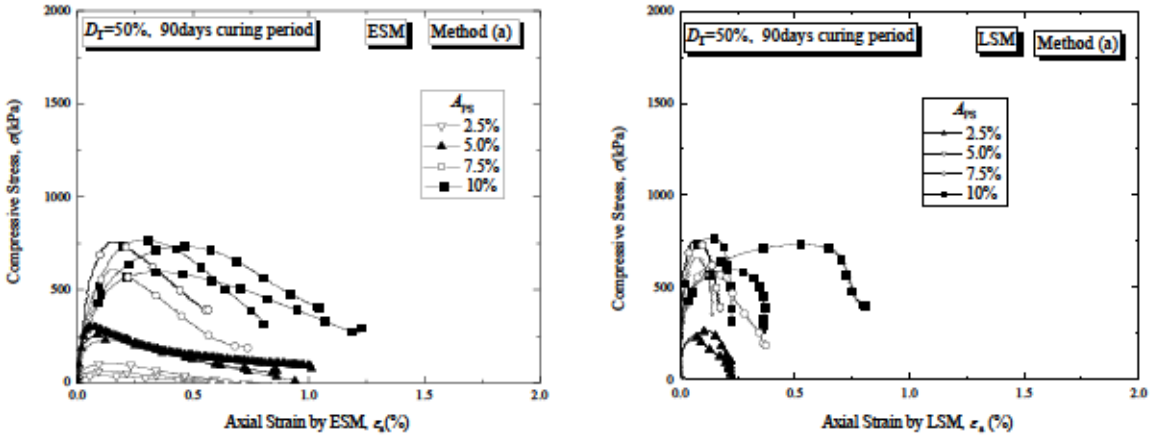


Figure C-16 Typical UCT stress-strain relationship of PSAS-treated sand for w=20%, tp=0days, Dr=50%, t= 90 days: (a) ESM (b) LSM.

Table C-v UCT data record for PSAS-treated sand for w=20%, tp=0days, Dr=50% at t= 90days

| Specimen No. | $A_{PS}$(%) | Modifier Batch | Curing days, $t$ | $q_u$ (kN/m²) | $\varepsilon_f$ (%) | $E_{50}$ (kN/m²) | $E_{0.02}$ (kN/m²) | $\rho_d$ (g/cm³) | $e$ | $w$ (%) | $D_r$ (%) |
|---|---|---|---|---|---|---|---|---|---|---|---|
| 1 | 2.5 | *BATCH 2* | 90 Days | 104.400 | 0.006 | 522000 | 130500 | | | | |
| 2 | 2.5 | *BATCH 2* | 90 Days | 62.7 | 0.2036 | 313500 | 78375 | 1.48 | 0.784 | 26.09% | 51.32% |
| 3 | 2.5 | *BATCH 2* | 90 Days | 36.300 | 0.096 | 121000 | 45375 | | | | |
| 1 | 5.0 | *BATCH 2* | 90 Days | 299.800 | 0.107 | 713810 | 1022000 | 1.48 | 0.785 | 23.71% | 50.93% |
| 2 | 5.0 | *BATCH 2* | 90 Days | 267.7 | 0.11 | 637381 | 972000 | 1.48 | 0.787 | 23.57% | 50.57% |
| 3 | 5.0 | *BATCH 2* | 90 Days | 231.800 | 0.109 | 551905 | 917000 | 1.48 | 0.785 | 25.90% | 50.98% |
| 1 | 7.5 | *BATCH 2* | 90 Days | 608.600 | 0.117 | 981613 | 2071500 | 1.47 | 0.792 | 30.82% | 50.47% |
| 2 | 7.5 | *BATCH 2* | 90 Days | 758.8 | 0.148 | 1084000 | 3061500 | 1.48 | 0.788 | 29.26% | 51.63% |
| 3 | 7.5 | *BATCH 2* | 90 Days | 662.500 | 0.249 | 946429 | 2430500 | 1.47 | 0.790 | 28.58% | 51.09% |
| 1 | 10.0 | *BATCH 2* | 90 Days | 596.200 | 0.101 | 876765 | 1869000 | 1.44 | 0.830 | 30.02% | 50.44% |
| 2 | 10.0 | *BATCH 2* | 90 Days | 732.9 | 0.14 | 1017917 | 1678000 | 1.44 | 0.831 | 31.45% | 50.28% |
| 3 | 10.0 | *BATCH 2* | 90 Days | 767.800 | 0.104 | 1279667 | 2729000 | 1.44 | 0.831 | 30.20% | 50.31% |

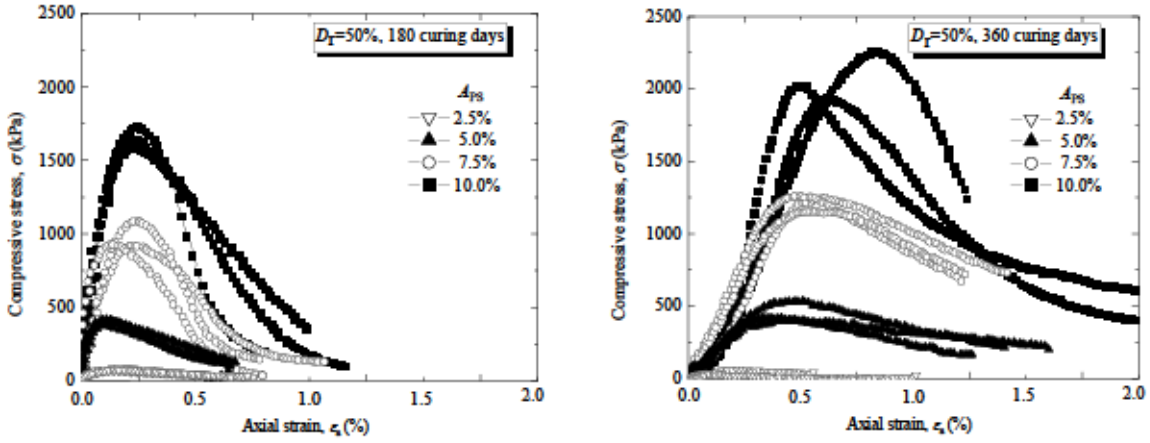


Figure C-17 Typical UCT stress-strain relationship of PSAS-treated sand for w=20%, tp=3days, Dr=50%: (a) t= 180 days, (b) t= 360 days.

Table C-w UCT data record for PSAS-treated sand for w=20%, tp=0days, Dr=50% at t= 180days

| Specimen No. | $A_{PS}$(%) | Modifier Batch | Curing days, $t$ | $q_u$ (kN/m²) | $\varepsilon_f$ (%) | $E_{50}$ (kN/m²) | $\rho_d$ (g/cm³) | $e$ | $w$ (%) | $D_r$ (%) |
|---|---|---|---|---|---|---|---|---|---|---|
| 1 | 2.5 | *Batch A* | 180 Days | 82.3 | 0.973 | 121029 | 1.48 | 0.786 | 19.67% | 50.47% |
| 2 | 2.5 | *Batch A* | 180 Days | 75.7 | 0.973 | 151400 | 1.48 | 0.786 | 17.04% | 50.58% |
| 3 | 2.5 | *Batch A* | 180 Days | 71.7 | 0.973 | 170714 | 1.48 | 0.786 | 19.87% | 50.55% |
| 1 | 5 | *Batch B* | 180 Days | 403 | 0.973 | 671667 | 1.48 | 0.787 | 18.65% | 50.32% |
| 2 | 5 | *Batch B* | 180 Days | 416.1 | 0.97 | 2080500 | 1.48 | 0.786 | 19.34% | 50.66% |
| 3 | 5 | *Batch B* | 180 Days | 381.4 | 0.973 | 1907000 | 1.48 | 0.786 | 17.27% | 50.87% |
| 1 | 7.5 | *Batch C* | 180 Days | 923.5 | 0.973 | 732937 | 1.47 | 0.791 | 17.00% | 50.85% |
| 2 | 7.5 | *Batch C* | 180 Days | 1087.6 | 0.973 | 776857 | 1.47 | 0.794 | 17.74% | 50.03% |
| 3 | 7.5 | *Batch C* | 180 Days | 928.2 | 0.973 | 663000 | 1.47 | 0.793 | 17.52% | 50.23% |
| 1 | 10 | *Batch D* | 180 Days | 1643.4 | 0.902 | 1676939 | 1.44 | 0.832 | 18.25% | 50.05% |
| 2 | 10 | *Batch D* | 180 Days | 1585.5 | 0.981 | 1524519 | 1.44 | 0.829 | 19.34% | 50.82% |
| 3 | 10 | *Batch D* | 180 Days | 1731.3 | 0.822 | 1292015 | 1.44 | 0.828 | 18.70% | 50.98% |

Table C-x UCT data record for PSAS-treated sand for w=20%, tp=0days, Dr=50% at t= 360days

| Specimen No. | $A_{PS}$(%) | Modifier Batch | Curing days, $t$ | $q_u$ (kN/m²) | $\varepsilon_f$ (%) | $E_{50}$ (kN/m²) | $\rho_d$ (g/cm³) | $e$ | $w$ (%) | $D_r$ (%) |
|---|---|---|---|---|---|---|---|---|---|---|
| 1 | 2.5 | *Batch A* | 360 Days | 32 | 0.973 | 45714 | 1.48 | 0.786 | 21.24% | 50.38% |
| 2 | 2.5 | *Batch A* | 360 Days | 65.9 | 0.973 | 32950 | 1.48 | 0.787 | 21.39% | 50.28% |
| 3 | 2.5 | *Batch A* | 360 Days | 28.9 | 0.973 | 68810 | 1.48 | 0.787 | 22.74% | 50.05% |
| 1 | 5 | *Batch B* | 360 Days | 535.1 | 0.505 | 161175 | 1.48 | 0.787 | 20.64% | 50.52% |
| 2 | 5 | *Batch B* | 360 Days | 406.2 | 0.452 | 152707 | 1.48 | 0.788 | 20.33% | 50.15% |
| 3 | 5 | *Batch B* | 360 Days | 420.7 | 0.345 | 166944 | 1.48 | 0.786 | 20.64% | 50.73% |
| 1 | 7.5 | *Batch C* | 360 Days | 1247.4 | 0.589 | 228462 | 1.47 | 0.793 | 18.95% | 50.28% |
| 2 | 7.5 | *Batch C* | 360 Days | 1260.9 | 0.486 | 331816 | 1.47 | 0.794 | 21.39% | 50.15% |
| 3 | 7.5 | *Batch C* | 360 Days | 1154.1 | 0.973 | 285668 | 1.47 | 0.791 | 21.95% | 50.86% |
| 1 | 10 | *Batch D* | 360 Days | 2255.8 | 0.816 | 286269 | 1.44 | 0.830 | 24.97% | 50.39% |
| 2 | 10 | *Batch D* | 360 Days | 2018.6 | 0.981 | 369707 | 1.44 | 0.829 | 25.84% | 50.74% |
| 3 | 10 | *Batch D* | 360 Days | 1934.1 | 0.822 | 293936 | 1.44 | 0.831 | 23.23% | 50.22% |

## C.2.4 Stress-strain relationship of PSAS treated sand for $w$=20%, tp=0 days, $D_r$=90%

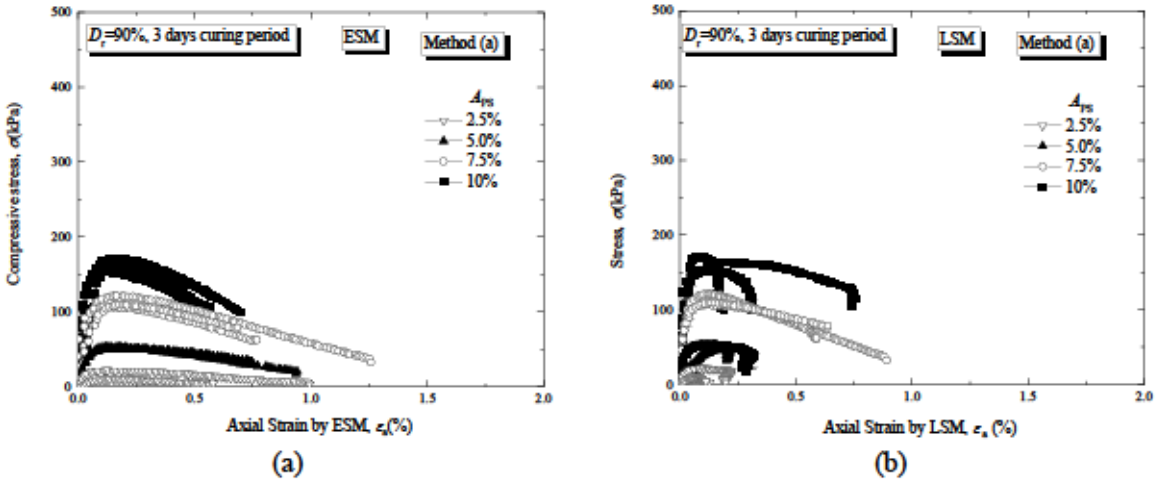


Figure C-18 Typical UCT stress-strain relationship of PSAS-treated sand for w=20%, tp=0days, Dr=90%, t= 3days: (a) ESM, (b) LSM

Table C-y UCT data record for PSAS-treated sand for w=20%, tp=0days, Dr=90% at t= 3days

| Specimen No. | $A_{PS}$(%) | Modifier Batch | Curing days, $t$ | $q_u$ (kN/m²) | $\varepsilon_f$ (%) | $E_{50}$ (kN/m²) | $E_V$ (kN/m²) | $\rho_d$ (g/cm³) | $e$ | $w$ (%) | $D_r$ (%) |
|---|---|---|---|---|---|---|---|---|---|---|---|
| 1 | 2.5 | *Batch A* | 3 Days | 0 | 0.112 | 0 | | | | 0.00% | |
| 2 | 2.5 | *Batch A* | 3 Days | 16.16 | 0.135 | 16490 | 15200 | 1.59 | 0.660 | 24.37% | 89.77% |
| 3 | 2.5 | *Batch A* | 3 Days | 0 | 0.089 | 0 | | | | 0.00% | |
| 1 | 5 | *Batch A* | 3 Days | 67.1 | 0.107 | 239643 | 256500 | 1.59 | 0.658 | 20.20% | 90.37% |
| 2 | 5 | *Batch A* | 3 Days | 71.5 | 0 | 0 | 239000 | 1.59 | 0.657 | 24.70% | 90.58% |
| 3 | 5 | *Batch A* | 3 Days | 70.6 | 0.139 | | 283000 | 1.60 | 0.654 | 19.10% | 91.52% |
| 1 | 7.5 | *Batch A* | 3 Days | 145.7 | 0.136 | 364250 | 449500 | 1.60 | 0.649 | 21.67% | 90.78% |
| 2 | 7.5 | *Batch A* | 3 Days | 161.4 | 0.154 | 201750 | 441500 | 1.60 | 0.646 | 19.66% | 91.69% |
| 3 | 7.5 | *Batch A* | 3 Days | 142.4 | 0.149 | 296667 | 472000 | 1.60 | 0.649 | 22.53% | 90.69% |
| 1 | 10 | *Batch A* | 3 Days | 320.1 | 0.195 | 2000625 | 1018000 | 1.57 | 0.685 | 20.50% | 89.45% |
| 2 | 10 | *Batch A* | 3 Days | 341.1 | 0.132 | 1137000 | 0 | 1.57 | 0.680 | 16.83% | 90.73% |
| 3 | 10 | *Batch A* | 3 Days | 285.2 | 0.134 | 1296364 | 946000 | 1.57 | 0.681 | 22.25% | 90.54% |

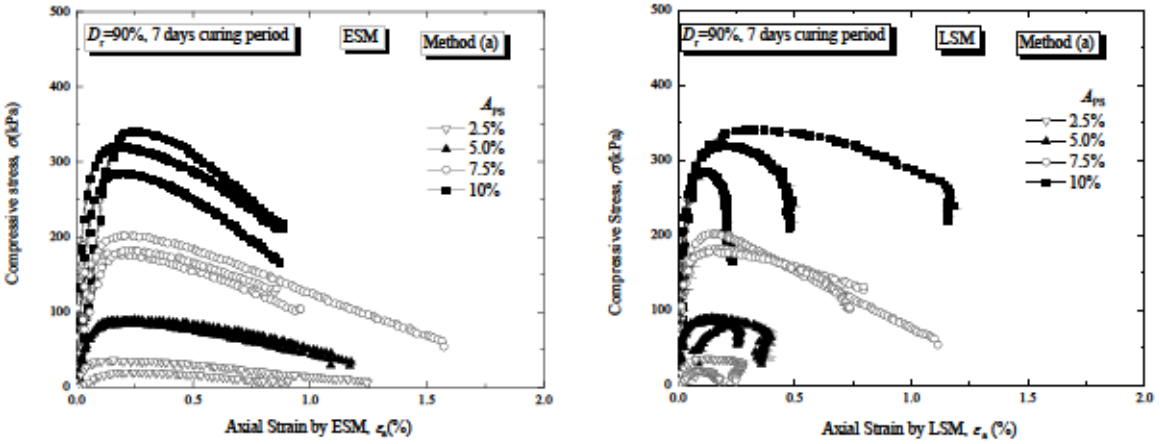


(a) (b)

Figure C-19 Typical UCT stress-strain relationship of PSAS-treated sand for w=20%, tp=0days, Dr=90%, t= 7days: (a) ESM, (b) LSM.

Table C-z UCT data record for PSAS-treated sand for w=20%, tp=0days, Dr=90% at t= 7days

| Specimen No. | $A_{PS}$(%) | Modifier Batch | Curing days, $t$ | $q_u$ (kN/m²) | $\varepsilon_f$ (%) | $E_{50}$ (kN/m²) | $E_{0.02}$ (kN/m²) | $\rho_d$ (g/cm³) | $e$ | $w$ (%) | $D_r$ (%) |
|---|---|---|---|---|---|---|---|---|---|---|---|
| 1 | 2.5 | *Batch A* | 7 Days | | | | | | | | |
| 2 | 2.5 | *Batch A* | 7 Days | 20.2 | 0.267 | 13649 | 28700 | 1.57 | 0.678 | 25.72% | 89.81% |
| 3 | 2.5 | *Batch A* | 7 Days | | | | | | | | |
| 1 | 5.0 | *Batch A* | 7 Days | 89.800 | 0.252 | 128286 | 281000 | 1.59 | 0.659 | 20.31% | 89.90% |
| 2 | 5.0 | *Batch A* | 7 Days | 88.9 | 0.178 | 148167 | 283500 | 1.59 | 0.657 | 24.70% | 90.56% |
| 3 | 5.0 | *Batch A* | 7 Days | 84.400 | 0.223 | 168800 | 338500 | 1.59 | 0.661 | 19.62% | 89.29% |
| 1 | 7.5 | *Batch A* | 7 Days | 182.2 | 0.227 | 178627 | 551000 | 1.60 | 0.652 | 21.87% | 90.04% |
| 2 | 7.5 | *Batch A* | 7 Days | 201.8 | 0.21 | 272703 | 546000 | 1.60 | 0.650 | 19.93% | 90.66% |
| 3 | 7.5 | *Batch A* | 7 Days | 178 | 0.159 | 296667 | 572500 | 1.60 | 0.653 | 22.79% | 89.70% |
| 1 | 10 | *Batch A* | 7 Days | 320.1 | 0.157 | 615577 | 1033500 | 1.57 | 0.682 | 20.31% | 90.14% |
| 2 | 10 | *Batch A* | 7 Days | 341.1 | 0.157 | 236875 | 586500 | 1.57 | 0.683 | 21.81% | 89.95% |
| 3 | 10 | *Batch A* | 7 Days | 285.2 | 0.133 | 570400 | 895000 | 1.57 | 0.680 | 22.17% | 90.81% |

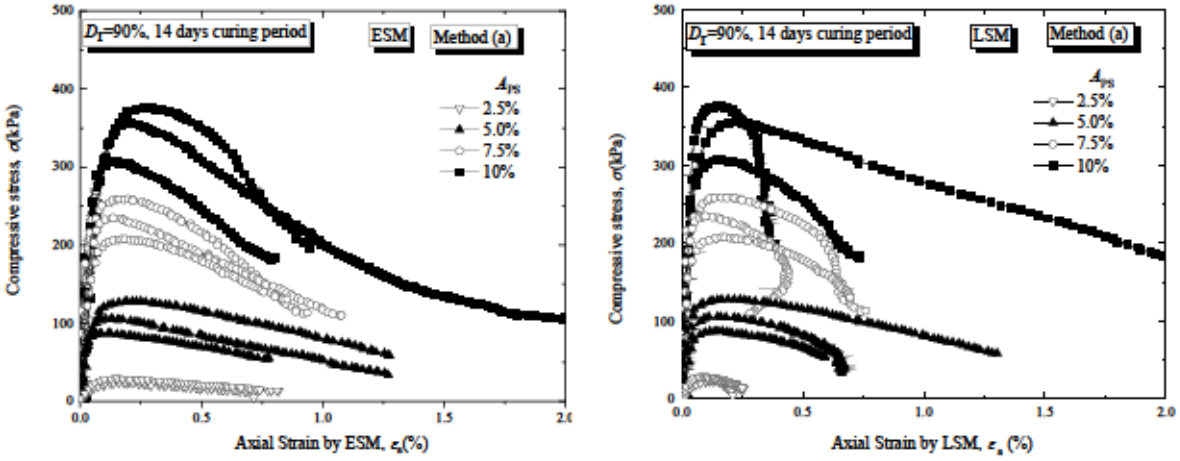


Figure C-20 Typical UCT stress-strain relationship of PSAS-treated sand for w=20%, tp=0days, Dr=90%, t= 17days: (a) ESM, (b) LSM.

Table C-aa UCT data record for PSAS-treated sand for w=20%, tp=0days, Dr=90% at t= 14days

| Specimen No. | $A_{PS}$(%) | Modifier Batch | Curing days, $t$ | $q_u$ (kN/m$^2$) | $\varepsilon_f$ (%) | $E_{50}$ (kN/m$^2$) | $E_{0.03}$ (kN/m$^2$) | $\rho_d$ (g/cm$^3$) | $e$ | $w$ (%) | $D_r$ (%) |
|---|---|---|---|---|---|---|---|---|---|---|---|
| 1 | 2.5 | *Batch A* | 14 Days | | 0.261 | 0 | | | | | |
| 2 | 2.5 | *Batch A* | 14 Days | 29.3 | 0.143 | 43088 | 68120 | 1.57 | 0.678 | 24.53% | 89.55% |
| 3 | 2.5 | *Batch A* | 14 Days | 24.1 | 0.208 | 41552 | 47900 | 1.57 | 0.678 | 25.35% | 89.69% |
| 1 | 5.0 | *Batch A* | 14 Days | 127.9 | 0.198 | 245962 | 409750 | 1.59 | 0.660 | 22.93% | 89.61% |
| 2 | 5.0 | *Batch A* | 14 Days | 105.8 | 0.117 | 377857 | 262850 | 1.59 | 0.657 | 22.06% | 90.53% |
| 3 | 5.0 | *Batch A* | 14 Days | 87.4 | 0.128 | 502299 | 179000 | 1.59 | 0.659 | 23.42% | 90.03% |
| 1 | 7.5 | *Batch A* | 14 Days | 234.7 | 0.137 | 434630 | 921500 | 1.60 | 0.654 | 19.94% | 89.47% |
| 2 | 7.5 | *Batch A* | 14 Days | 258.9 | 0.155 | 462321 | 776000 | 1.60 | 0.650 | 19.46% | 90.66% |
| 3 | 7.5 | *Batch A* | 14 Days | 207.6 | 0.136 | 494286 | 682000 | 1.60 | 0.651 | 20.82% | 90.40% |
| 1 | 10 | *Batch A* | 14 Days | 355.6 | 0.205 | 592667 | 815500 | 1.57 | 0.684 | 21.31% | 89.76% |
| 2 | 10 | *Batch A* | 14 Days | 376.5 | 0.269 | 495395 | 698000 | 1.57 | 0.681 | 18.96% | 90.54% |
| 3 | 10 | *Batch A* | 14 Days | 307.3 | 0.132 | 465606 | 940000 | 1.56 | 0.685 | 23.03% | 89.39% |

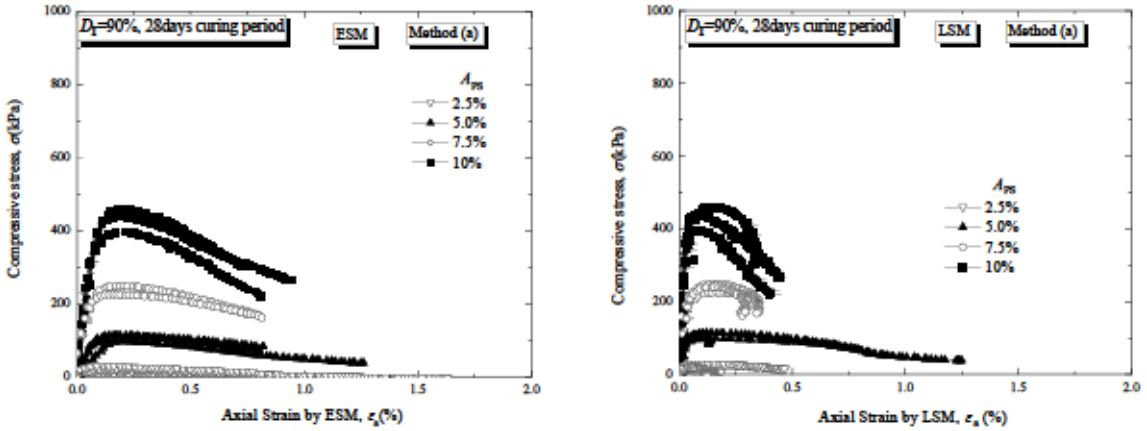


(a) (b)

Figure C-21 Typical UCT stress-strain relationship of PSAS-treated sand for $w$=20%, tp=0days, $D_r$=90%, $t$= 28 days: (a) ESM, (b) LSM.

Table C-bb UCT data record for PSAS-treated sand for w=20%, tp=0days, Dr=90% at t= 28days

| Specimen No. | $A_{PS}$(%) | Modifier Batch | Curing days, $t$ | $q_u$ (kN/m²) | $\varepsilon_f$ (%) | $E_{50}$ (kN/m²) | $E_{0.02}$ (kN/m²) | $\rho_d$ (g/cm³) | $e$ | $w$ (%) | $D_r$ (%) |
|---|---|---|---|---|---|---|---|---|---|---|---|
| 1 | 2.5 | *Batch A* | 28 Days | 29.2 | 0.11 | 265455 | 118500 | 1.58 | 0.675 | 26.11% | 90.76% |
| 2 | 2.5 | *Batch A* | 28 Days | 14.6 | 0.143 | 101389 | 84600 | 1.58 | 0.676 | 25.43% | 90.35% |
| 3 | 2.5 | *Batch A* | 28 Days | 17.9 | 0.208 | 124306 | 72500 | 1.58 | 0.675 | 24.49% | 90.87% |
| 1 | 5.0 | *Batch A* | 28 Days | 99.100 | 0.142 | 169692 | 391600 | 1.59 | 0.660 | 21.71% | 89.66% |
| 2 | 5.0 | *Batch A* | 28 Days | 114.3 | 0.159 | 150395 | 428000 | 1.59 | 0.663 | 22.79% | 88.58% |
| 3 | 5.0 | *Batch A* | 28 Days | 109.700 | 0.249 | 68563 | 368000 | 1.58 | 0.670 | 24.19% | 86.61% |
| 1 | 7.5 | *Batch A* | 28 Days | 249.3 | 0.213 | 461667 | 797500 | 1.60 | 0.650 | 21.16% | 90.44% |
| 2 | 7.5 | *Batch A* | 28 Days | 240.3 | 0.193 | 500625 | 699000 | 1.59 | 0.654 | 19.12% | 89.39% |
| 3 | 7.5 | *Batch A* | 28 Days | 225.5 | 0.154 | 626389 | 608500 | 1.59 | 0.660 | 21.48% | 87.75% |
| 1 | 10 | *Batch A* | 28 Days | 459.1 | 0.188 | 510111 | 1254500 | 1.57 | 0.684 | 23.51% | 89.81% |
| 2 | 10 | *Batch A* | 28 Days | 438.7 | 0.18 | 645147 | 1369000 | 1.56 | 0.685 | 24.17% | 89.38% |
| 3 | 10 | *Batch A* | 28 Days | 396.1 | 0.209 | 550139 | 1339500 | 1.55 | 0.696 | 24.91% | 86.37% |

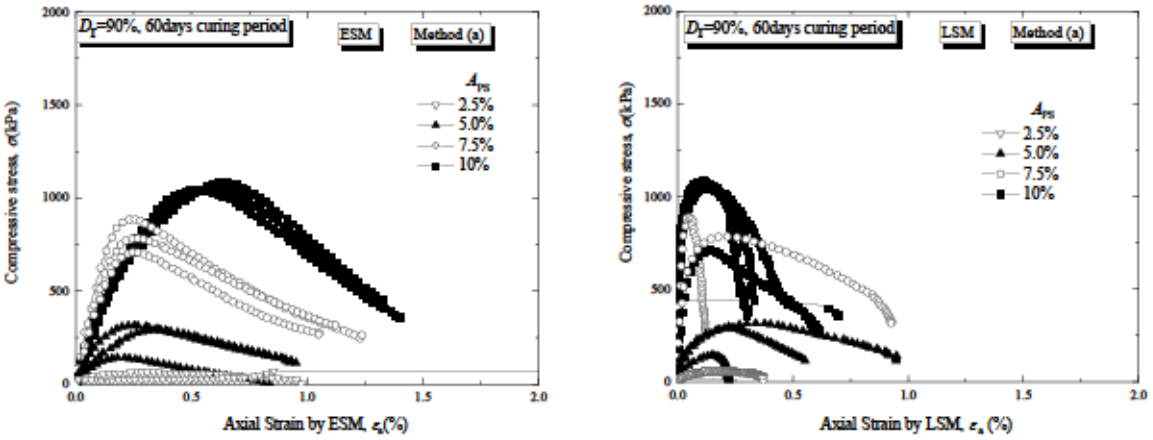


Figure C-22 Typical UCT stress-strain relationship of PSAS-treated sand for w=20%, tp=0days, Dr=90%, t= 60 days: (a) ESM, (b) LSM.

Table C-cc UCT data record for PSAS-treated sand for w=20%, tp=0days, Dr=90% at t= 60days

| Specimen No. | $A_{PS}$(%) | Modifier Batch | Curing days, $t$ | $q_u$ (kN/m²) | $\varepsilon_f$ (%) | $E_{50}$ (kN/m²) | $E_{0.02}$ (kN/m²) | $\rho_d$ (g/cm³) | $e$ | $w$ (%) | $D_r$ (%) |
|---|---|---|---|---|---|---|---|---|---|---|---|
| 1 | 2.5 | *Batch B* | 60 Days | | | | | | | | |
| 2 | 2.5 | *Batch B* | 60 Days | 0 | | | | | | | |
| 3 | 2.5 | *Batch B* | 60 Days | 62.300 | 0.163 | 84189 | 139000 | 1.57 | 0.677 | 20.24% | 90.16% |
| 1 | 5.0 | *Batch B* | 60 Days | 142.600 | 0.161 | 155000 | 2221500 | 1.59 | 0.656 | 21.08% | 90.97% |
| 2 | 5.0 | *Batch B* | 60 Days | 315.7 | 0.131 | 263083 | 1627000 | 1.60 | 0.653 | 18.40% | 91.85% |
| 3 | 5.0 | *Batch B* | 60 Days | 291.500 | 0.123 | 142892 | 3593500 | 1.59 | 0.659 | 21.04% | 89.93% |
| 1 | 7.5 | *Batch B* | 60 Days | 784.5 | 0.187 | 496519 | 4782000 | 1.60 | 0.650 | 23.93% | 90.57% |
| 2 | 7.5 | *Batch B* | 60 Days | 709.4 | 0.197 | 437901 | 6231000 | 1.60 | 0.648 | 23.81% | 91.08% |
| 3 | 7.5 | *Batch B* | 60 Days | 886.8 | 0.173 | 661791 | 3551000 | 1.60 | 0.646 | 20.60% | 91.76% |
| 1 | 10 | *Batch B* | 60 Days | 1081.4 | 2211 | 563229 | 4190500 | 1.57 | 0.680 | 20.72% | 90.87% |
| 2 | 10 | *Batch B* | 60 Days | 1047.6 | 0.13 | 557234 | 4153500 | 1.57 | 0.681 | 20.66% | 90.50% |
| 3 | 10 | *Batch B* | 60 Days | 1048.1 | 0.203 | 551632 | 4018000 | 1.57 | 0.682 | 21.94% | 90.26% |

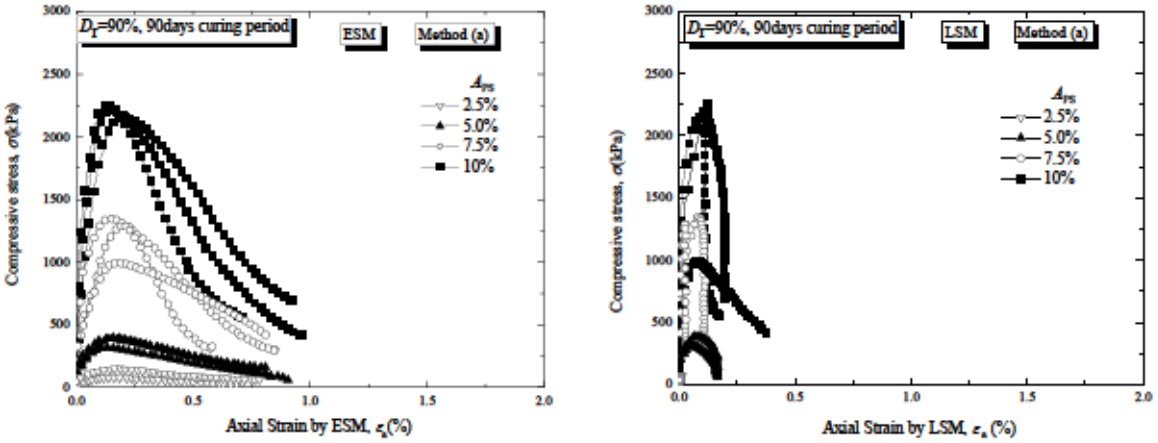


Figure C-23 Typical UCT stress-strain relationship of PSAS-treated sand for w=20%, tp=0days, Dr=90%, t= 90 days: (a) ESM, (b) LSM.

Table C-dd UCT data record for PSAS-treated sand for w=20%, tp=0days, Dr=90% at t= 90days

| Specimen No. | $A_{PS}$(%) | Modifier Batch | Curing days, $t$ | $q_u$ (kN/m²) | $\varepsilon_f$ (%) | $E_{50}$ (kN/m²) | $E_{a.o.i}$ (kN/m²) | $\rho_d$ (g/cm³) | $e$ | $w$ (%) | $D_r$ (%) |
|---|---|---|---|---|---|---|---|---|---|---|---|
| 1 | 2.5 | *Batch B* | 90 Days | 147.5 | 0.163 | 614583 | 184375 | 1.58 | 0.676 | 22.75% | 90.34% |
| 2 | 2.5 | *Batch B* | 90 Days | 76.8 | 0.142 | 116364 | 96000 | 1.57 | 0.679 | 23.70% | 89.20% |
| 3 | 2.5 | *Batch B* | 90 Days | | | | | | | 20.67% | 335.09% |
| 1 | 5.0 | *Batch B* | 90 Days | 394.800 | 0.161 | 548333 | 1381500 | 1.59 | 0.657 | 16.04% | 90.61% |
| 2 | 5.0 | *Batch B* | 90 Days | 389.1 | 0.131 | 1297000 | 1218000 | 1.59 | 0.657 | 21.50% | 90.51% |
| 3 | 5.0 | *Batch B* | 90 Days | 316.200 | 0.123 | 1581000 | 1299750 | 1.59 | 0.660 | 22.16% | 89.73% |
| 1 | 7.5 | *Batch B* | 90 Days | 1346.2 | 0.187 | 3205238 | 4782000 | 1.60 | 0.651 | 22.36% | 90.14% |
| 2 | 7.5 | *Batch B* | 90 Days | 1290.3 | 0.197 | 1433667 | 6231000 | 1.60 | 0.647 | 21.81% | 91.39% |
| 3 | 7.5 | *Batch B* | 90 Days | 992.5 | 0.173 | 1711207 | 3551000 | 1.60 | 0.648 | 22.64% | 91.03% |
| 1 | 10 | *Batch B* | 90 Days | 2215.7 | 2211 | 4616042 | 8654500 | 1.57 | 0.680 | 22.54% | 90.73% |
| 2 | 10 | *Batch B* | 90 Days | 2258.9 | 0.13 | 9412083 | 6290500 | 1.57 | 0.685 | 22.66% | 89.50% |
| 3 | 10 | *Batch B* | 90 Days | 2159.1 | 0.203 | 2998750 | 8217500 | 1.57 | 0.683 | 23.59% | 90.03% |

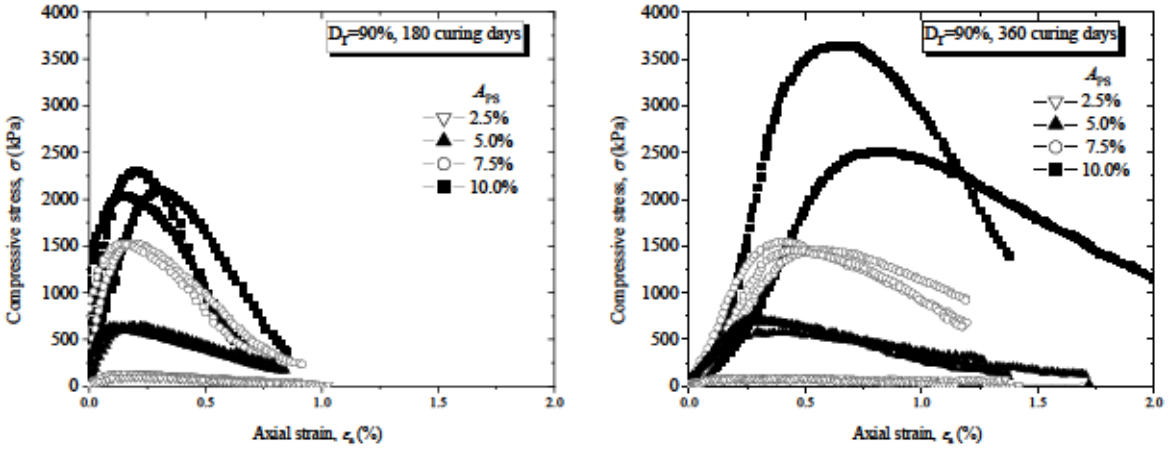


(a) (b)

Figure C-24 Typical UCT stress-strain relationship of PSAS-treated sand for w=20%, tp=0days, Dr=90%: (a) t= 180 days, (b) t= 360 days.

*Table C-ee* UCT data record for PSAS-treated sand for w=20%, tp=0days, Dr=90% at t= 180days

| Specimen No. | $A_{PS}$ (%) | Modifier Batch | Curing days, $t$ | $q_u$ (kN/m²) | $\varepsilon_f$ (%) | $E_{50}$ (kN/m²) | $\rho_d$ (g/cm³) | $e$ | $w$ (%) | $D_r$ (%) |
|---|---|---|---|---|---|---|---|---|---|---|
| 1 | 2.5 | *Batch B* | 180 Days | 142.5 | 0.973 | 169643 | 1.58 | 0.676 | 19.67% | 90.44% |
| 2 | 2.5 | *Batch B* | 180 Days | 137.6 | 0.973 | 237241 | 1.58 | 0.672 | 17.04% | 91.91% |
| 3 | 2.5 | *Batch B* | 180 Days | 100.4 | 0.973 | 135676 | 1.57 | 0.676 | 19.87% | 90.23% |
| 1 | 5 | *Batch B* | 180 Days | 647.2 | 0.973 | 719111 | 1.59 | 0.657 | 18.65% | 90.56% |
| 2 | 5 | *Batch B* | 180 Days | 639.5 | 0.973 | 710556 | 1.59 | 0.658 | 19.34% | 90.17% |
| 3 | 5 | *Batch B* | 180 Days | 599.6 | 0.973 | 1998667 | 1.59 | 0.658 | 17.27% | 90.25% |
| 1 | 7.5 | *Batch B* | 180 Days | 1526.1 | 0.973 | 1956538 | 1.60 | 0.646 | 17.00% | 91.76% |
| 2 | 7.5 | *Batch B* | 180 Days | 1523.2 | 0.973 | 1554286 | 1.60 | 0.651 | 13.69% | 90.19% |
| 3 | 7.5 | *Batch B* | 180 Days | | | | 1.60 | 0.650 | 17.52% | 90.48% |
| 1 | 10 | *Batch B* | 180 Days | 2305.5 | 0.902 | 2955769 | 1.57 | 0.681 | 16.14% | 90.63% |
| 2 | 10 | *Batch B* | 180 Days | 2040.3 | 0.981 | 2914714 | 1.57 | 0.683 | 18.46% | 89.92% |
| 3 | 10 | *Batch B* | 180 Days | 2082.3 | 0.822 | 1107606 | 1.57 | 0.683 | 14.54% | 90.01% |

Table C-ff UCT data record for PSAS-treated sand for w=20%, tp=0days, Dr=90% at t= 360 days

| Specimen No. | $A_{PS}$(%) | Modifier Batch | Curing days, $t$ | $q_u$ (kN/m²) | $\varepsilon_f$ (%) | $E_{50}$ (kN/m²) | $\rho_d$ (g/cm³) | $e$ | $w$ (%) | $D_r$ (%) |
|---|---|---|---|---|---|---|---|---|---|---|
| 1 | 2.5 | *Batch B* | 360 Days | 98.9 | 0.973 | 11239 | 1.57 | 0.677 | 19.67% | 90.00% |
| 2 | 2.5 | *Batch B* | 360 Days | 96.9 | 0.973 | 12584 | 1.58 | 0.675 | 17.04% | 90.87% |
| 3 | 2.5 | *Batch B* | 360 Days | 0 | 0 | | 1.58 | 0.675 | 19.87% | 90.57% |
| 1 | 5 | *Batch B* | 360 Days | 742.3 | 0.283 | 378724 | 1.59 | 0.658 | 18.65% | 90.13% |
| 2 | 5 | *Batch B* | 360 Days | 690.8 | 0.32 | 356082 | 1.59 | 0.658 | 19.34% | 90.34% |
| 3 | 5 | *Batch B* | 360 Days | 579.8 | 0.289 | 265963 | 1.59 | 0.659 | 17.27% | 90.08% |
| 1 | 7.5 | *Batch B* | 360 Days | 1544.4 | 0.401 | 543803 | 1.60 | 0.649 | 17.00% | 90.70% |
| 2 | 7.5 | *Batch B* | 360 Days | 1459.9 | 0.538 | 347595 | 1.60 | 0.651 | 13.69% | 90.37% |
| 3 | 7.5 | *Batch B* | 360 Days | 1453.6 | 0.435 | 376580 | 1.60 | 0.650 | 17.52% | 90.45% |
| 1 | 10 | *Batch B* | 360 Days | 3645.1 | 0.619 | 680056 | 1.57 | 0.682 | 16.14% | 90.32% |
| 2 | 10 | *Batch B* | 360 Days | 2509.9 | 0.784 | 326810 | 1.57 | 0.681 | 18.46% | 90.54% |
| 3 | 10 | *Batch B* | 360 Days | | | | | | | |

## C.2.5 Stress-strain relationship of OPC-treated sand for w=10%, tp=3 days, Dr=50%

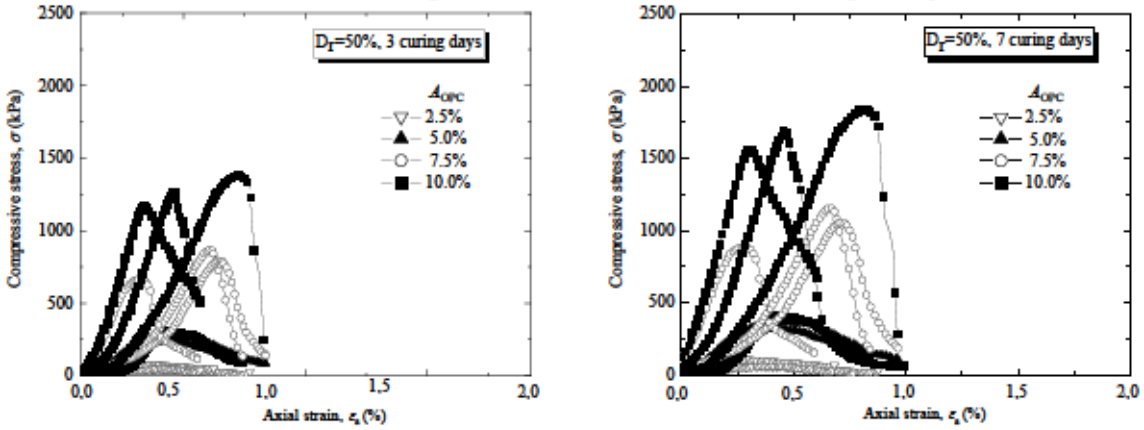


Figure C-25 Typical UCT stress-strain relationship of OPC-treated sand for w=10%, tp=3days, Dr=50%: (a) t= 3 days, (b) t= 7 days.

*Table C-gg UCT data record for OPC-treated sand for w=10%, tp=3days, Dr=50% at t= 3 days*

| Specimen No. | $A_{PS}$(%) | Modifier Batch | Curing days, $t$ | $q_u$ (kN/m²) | $\varepsilon_f$ (%) | $E_{50}$ (kN/m²) | $\rho_d$ (g/cm³) | $e$ | $w$ (%) | $D_r$ (%) |
|---|---|---|---|---|---|---|---|---|---|---|
| 1 | 2.5 | *Batch A* | 3 Days | 34.0 | 0.220 | 29050 | 1.50 | 0.764 | 22.35% | 49.37% |
| 2 | 2.5 | *Batch A* | 3 Days | 46.0 | 0.453 | 17650 | 1.51 | 0.762 | 22.22% | 50.46% |
| 3 | 2.5 | *Batch A* | 3 Days | 29.2 | 0.403 | 21780 | 1.51 | 0.742 | 20.84% | 50.82% |
| 1 | 5 | *Batch A* | 3 Days | 295.1 | 0.639 | 57100 | 1.53 | 0.748 | 22.40% | 52.55% |
| 2 | 5 | *Batch A* | 3 Days | 263.4 | 0.331 | 90430 | 1.52 | 0.755 | 22.91% | 51.63% |
| 3 | 5 | *Batch A* | 3 Days | 334.2 | 0.333 | 109940 | 1.52 | 0.750 | 22.53% | 51.79% |
| 1 | 7.5 | *Batch A* | 3 Days | 923.3 | 0.806 | 121990 | 1.54 | 0.735 | 22.43% | 52.48% |
| 2 | 7.5 | *Batch A* | 3 Days | 843.9 | 0.787 | 92530 | 1.54 | 0.717 | 21.12% | 50.86% |
| 3 | 7.5 | *Batch A* | 3 Days | 720.2 | 0.426 | 173000 | 1.55 | 0.708 | 20.46% | 53.11% |
| 1 | 10 | *Batch A* | 3 Days | 1245.5 | 0.453 | 259480 | 1.55 | 0.742 | 22.40% | 51.12% |
| 2 | 10 | *Batch A* | 3 Days | 1472.2 | 0.749 | 215480 | 1.54 | 0.763 | 23.86% | 50.81% |
| 3 | 10 | *Batch A* | 3 Days | 1350.2 | 0.605 | 250410 | 1.56 | 0.722 | 21.00% | 54.30% |

Table C-hh UCT data record for OPC-treated sand for w=10%, tp=3days, Dr=50% at t= 7 days

| Specimen No. | $A_{OPC}$(%) | Modifier Batch | Curing days, $t$ | $q_u$ (kN/m²) | $\varepsilon_f$ (%) | $E_{50}$ (kN/m²) | $\rho_d$ (g/cm³) | $e$ | $w$ (%) | $D_r$ (%) |
|---|---|---|---|---|---|---|---|---|---|---|
| 1 | 2.5 | *Batch A* | 7 Days | 79.6 | 0.22 | 29050 | 1.51 | 0.762 | 21.00% | 50.05% |
| 2 | 2.5 | *Batch A* | 7 Days | 107.7 | 0.453 | 17650 | 1.51 | 0.760 | 17.84% | 50.90% |
| 3 | 2.5 | *Batch A* | 7 Days | 68.4 | 0.403 | 21780 | 1.51 | 0.762 | 20.84% | 50.15% |
| 1 | 5 | *Batch A* | 7 Days | 368.9 | 0.639 | 57100 | 1.53 | 0.746 | 21.06% | 50.09% |
| 2 | 5 | *Batch A* | 7 Days | 329.2 | 0.331 | 90430 | 1.54 | 0.736 | 20.20% | 53.58% |
| 3 | 5 | *Batch A* | 7 Days | 417.8 | 0.333 | 109940 | 1.53 | 0.746 | 21.63% | 50.21% |
| 1 | 7.5 | *Batch A* | 7 Days | 1154.1 | 0.806 | 121990 | 1.55 | 0.726 | 21.08% | 50.48% |
| 2 | 7.5 | *Batch A* | 7 Days | 1054.9 | 0.787 | 92530 | 1.55 | 0.726 | 21.12% | 50.42% |
| 3 | 7.5 | *Batch A* | 7 Days | 900.3 | 0.426 | 173000 | 1.56 | 0.718 | 20.46% | 52.73% |
| 1 | 10 | *Batch A* | 7 Days | 1556.9 | 0.453 | 259480 | 1.56 | 0.721 | 20.68% | 50.23% |
| 2 | 10 | *Batch A* | 7 Days | 1840.2 | 0.749 | 215480 | 1.56 | 0.725 | 20.73% | 49.12% |
| 3 | 10 | *Batch A* | 7 Days | 1687.8 | 0.605 | 250410 | 1.56 | 0.723 | 21.00% | 49.71% |

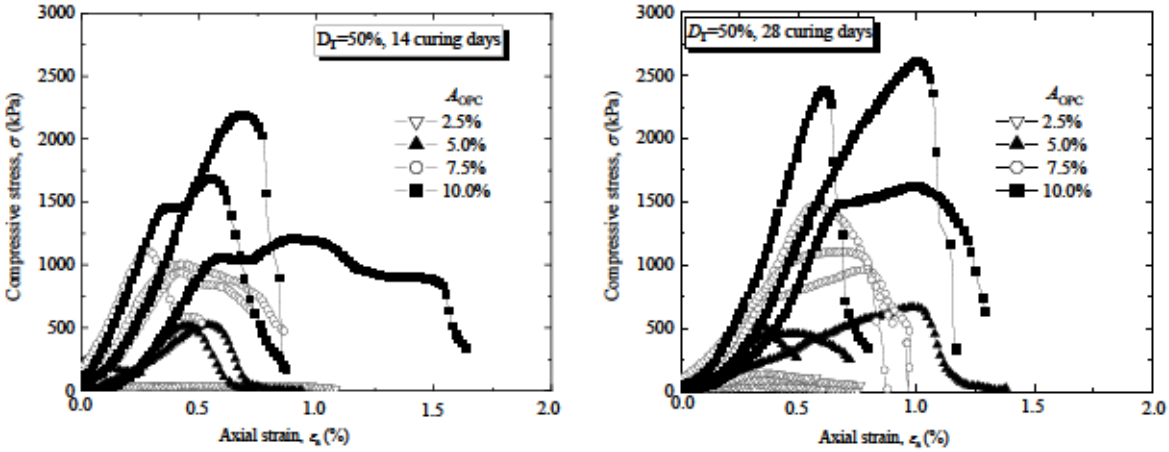


Figure C-26 Typical UCT stress-strain relationship of OPC-treated sand for w=10%, tp=3days, Dr=50%: (c) t= 14 days, (d) t= 28 days.

Table C-ii UCT data record for OPC-treated sand for w=10%, tp=3days, Dr=50% at t= 14days

| Specimen No. | $A_{OPC}$(%) | Modifier Batch | Curing days, $t$ | $q_u$ (kN/m²) | $\varepsilon_f$ (%) | $E_{50}$ (kN/m²) | $\rho_d$ (g/cm³) | $e$ | $w$ (%) | $D_r$ (%) |
|---|---|---|---|---|---|---|---|---|---|---|
| 1 | 2.5 | *Batch A* | 14 Days | 48 | 0.507 | 11820 | 1.50 | 0.7641 | 20.25% | 49.37% |
| 2 | 2.5 | *Batch A* | 14 Days | 50.6 | 0.567 | 10240 | 1.51 | 0.7613 | 21.22% | 50.39% |
| 3 | 2.5 | *Batch A* | 14 Days | 46.4 | 0.605 | 13100 | 1.51 | 0.7610 | 21.45% | 50.48% |
| 1 | 5 | *Batch A* | 14 Days | 279.8 | 0.261 | 106790 | 1.53 | 0.7451 | 21.86% | 50.50% |
| 2 | 5 | *Batch A* | 14 Days | 538.8 | 0.562 | 76970 | 1.53 | 0.7458 | 20.81% | 50.28% |
| 3 | 5 | *Batch A* | 14Days | 529.43 | 0.396 | 117130 | 1.53 | 0.7417 | 20.86% | 57.49% |
| 1 | 7.5 | *Batch A* | 14 Days | 1112.7 | 0.476 | 174400 | 1.55 | 0.7251 | 20.80% | 50.63% |
| 2 | 7.5 | *Batch A* | 14 Days | 941 | 0.439 | 180260 | 1.55 | 0.7246 | 20.05% | 50.78% |
| 3 | 7.5 | *Batch A* | 14 Days | 1005.6 | 0.629 | 128590 | 1.55 | 0.7240 | 20.22% | 50.97% |
| 1 | 10 | *Batch A* | 14 Days | 2193.8 | 0.752 | 391750 | 1.56 | 0.7208 | 19.62% | 50.25% |
| 2 | 10 | *Batch A* | 14 Days | 1693.3 | 0.748 | 132910 | 1.57 | 0.7195 | 19.88% | 50.59% |
| 3 | 10 | *Batch A* | 14 Days | 1216.9 | 0.769 | 226190 | 1.57 | 0.7181 | 22.10% | 50.98% |

Table C-jj UCT data record for OPC-treated sand for w=10%, tp=3days, Dr=50% at t= 28 days

| Specimen No. | $A_{OPC}$(%) | Modifier Batch | Curing days, $t$ | $q_u$ (kN/m²) | $\varepsilon_f$ (%) | $E_{50}$ (kN/m²) | $\rho_d$ (g/cm³) | $e$ | $w$ (%) | $D_r$ (%) |
|---|---|---|---|---|---|---|---|---|---|---|
| 1 | 2.5 | *Batch A* | 28 Days | 59.2 | 0.427 | 18380 | 1.51 | 0.762 | 20.76% | 50.16% |
| 2 | 2.5 | *Batch A* | 28 Days | 150.10 | 0.466 | 25440 | 1.51 | 0.761 | 22.58% | 50.35% |
| 3 | 2.5 | *Batch A* | 28 Days | 103.1 | 0.513 | 42950 | 1.51 | 0.761 | 23.43% | 50.43% |
| 1 | 5 | *Batch A* | 28 Days | 535.4 | 0.367 | 124510 | 1.53 | 0.746 | 24.68% | 50.21% |
| 2 | 5 | *Batch A* | 28 Days | 469.2 | 0.575 | 76410 | 1.53 | 0.748 | 24.22% | 49.49% |
| 3 | 5 | *Batch A* | 28 Days | 675.2 | 1.075 | 56360 | 1.53 | 0.745 | 23.51% | 50.54% |
| 1 | 7.5 | *Batch A* | 28 Days | 985.3 | 0.883 | 169870 | 1.55 | 0.726 | 23.57% | 50.41% |
| 2 | 7.5 | *Batch A* | 28 Days | 1500.8 | 0.668 | 274870 | 1.55 | 0.727 | 24.12% | 52.15% |
| 3 | 7.5 | *Batch A* | 28 Days | 1122.8 | 0.811 | 161320 | 1.55 | 0.727 | 22.54% | 52.18% |
| 1 | 10 | *Batch A* | 28 Days | 2639.2 | 0.982 | 288750 | 1.57 | 0.719 | 22.57% | 50.64% |
| 2 | 10 | *Batch A* | 28 Days | 1658.7 | 0.908 | 179902 | 1.56 | 0.721 | 21.90% | 50.09% |
| 3 | 10 | *Batch A* | 28 Days | 2417.6 | 0.563 | 355520 | 1.56 | 0.721 | 23.21% | 50.21% |

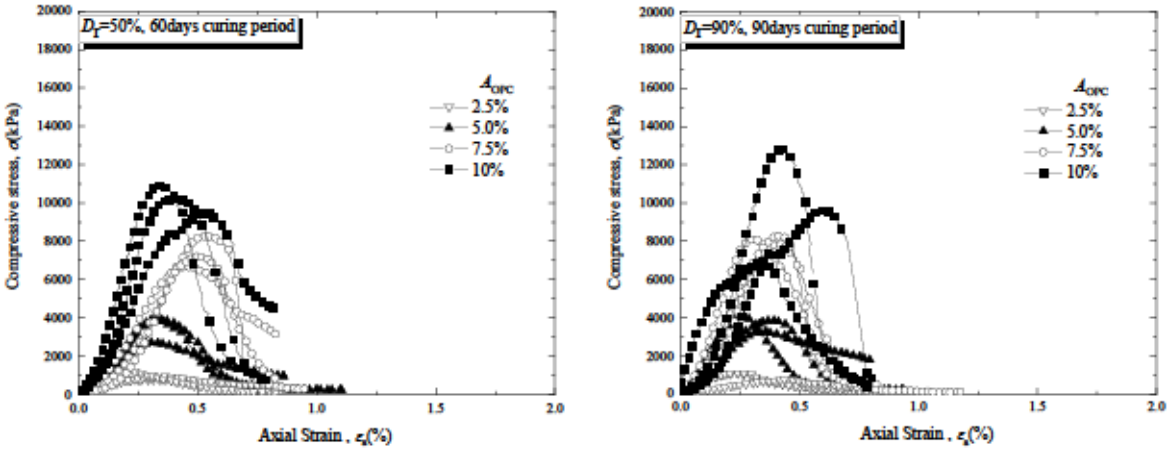


(e) (f)

Figure C-27 Typical UCT stress-strain relationship of OPC-treated sand for w=10%, tp=3days, Dr=50%: (e) t= 60 days, (f) t= 90 days.

Table C-kk UCT data record for OPC-treated sand for w=10%, tp=3days, Dr=50% at t= 60 days

| Specimen No. | $A_{OPC}$(%) | Modifier Batch | Curing days, $t$ | $q_u$ (kN/m²) | $\varepsilon_f$ (%) | $E_{50}$ (kN/m²) | $E_{0.02}$ (kN/m²) | $\rho_d$ (g/cm³) | $e$ | $w$ (%) | $D_r$ (%) |
|---|---|---|---|---|---|---|---|---|---|---|---|
| 1 | 2.5 | *BATCH B* | 60 Days | 768.9 | 0.11 | 413387 | 2162000 | 1.51 | 0.761 | 23.39% | 50.60% |
| 2 | 2.5 | *BATCH B* | 60 Days | 895.4 | 0.143 | 349766 | 3857000 | 1.51 | 0.761 | 23.53% | 50.41% |
| 3 | 2.5 | *BATCH B* | 60 Days | 1070.8 | 0.208 | 551959 | 3152000 | 1.51 | 0.762 | 23.25% | 50.16% |
| 1 | 5.0 | *BATCH B* | 60 Days | 3708.4 | 0.142 | 991551 | 10687500 | 1.53 | 0.746 | 25.00% | 50.04% |
| 2 | 5.0 | *BATCH B* | 60 Days | 3667.5 | 0.159 | 1125000 | 14210500 | 1.53 | 0.744 | 22.07% | 51.00% |
| 3 | 5.0 | *BATCH B* | 60 Days | 2594.2 | 0.249 | 781386 | 10348000 | 1.53 | 0.741 | 25.24% | 51.70% |
| 1 | 7.5 | *BATCH B* | 60 Days | 7968.1 | 0.213 | 1276939 | 26124500 | 1.55 | 0.725 | 25.90% | 50.72% |
| 2 | 7.5 | *BATCH B* | 60 Days | 6482.2 | 0.193 | 1276024 | 24363500 | 1.55 | 0.725 | 26.77% | 50.59% |
| 3 | 7.5 | *BATCH B* | 60 Days | 6949.6 | 0.154 | 1106624 | 12861000 | 1.55 | 0.727 | 26.47% | 50.16% |
| 1 | 10 | *BATCH B* | 60 Days | 10205.2 | 0.188 | 3189125 | 33489000 | 1.56 | 0.720 | 25.05% | 50.42% |
| 2 | 10 | *BATCH B* | 60 Days | 9145.4 | 0.18 | 1988130 | 38276500 | 1.57 | 0.720 | 27.15% | 50.47% |
| 3 | 10 | *BATCH B* | 60 Days | 9943.4 | 0.209 | 2437108 | 30153000 | 1.57 | 0.720 | 27.01% | 50.58% |

Table C-ll UCT data record for OPC-treated sand for w=10%, tp=3days, Dr=50% at t= 90 days

| Specimen No. | $A_{OPC}$(%) | Modifier Batch | Curing days, $t$ | $q_u$ (kN/m²) | $\varepsilon_f$ (%) | $E_{50}$ (kN/m²) | $E_{0.02}$ (kN/m²) | $\rho_d$ (g/cm³) | $e$ | $w$ (%) | $D_r$ (%) |
|---|---|---|---|---|---|---|---|---|---|---|---|
| 1 | 2.5 | *BATCH B* | 90 Days | 1015.1 | 0.11 | 939907 | 2402500 | 1.51 | 0.760 | 17.90% | 50.82% |
| 2 | 2.5 | *BATCH B* | 90 Days | 1038.7 | 0.143 | 590170 | 3129500 | 1.51 | 0.760 | 19.19% | 50.69% |
| 3 | 2.5 | *BATCH B* | 90 Days | 699.2 | 0.208 | 192088 | 1332500 | 1.51 | 0.762 | 22.89% | 50.01% |
| 1 | 5.0 | *BATCH B* | 90 Days | 3683.3 | 0.142 | 1058420 | 13472000 | 1.53 | 0.745 | 17.90% | 50.43% |
| 2 | 5.0 | *BATCH B* | 90 Days | 3698.3 | 0.159 | 1696468 | 13557000 | 1.53 | 0.745 | 21.66% | 50.53% |
| 3 | 5.0 | *BATCH B* | 90 Days | 3157.9 | 0.249 | 934290 | 11069500 | 1.53 | 0.746 | 18.81% | 50.18% |
| 1 | 7.5 | *BATCH B* | 90 Days | 7638.7 | 0.213 | 2598197 | 19164000 | 1.55 | 0.725 | 17.78% | 50.65% |
| 2 | 7.5 | *BATCH B* | 90 Days | 7450.9 | 0.193 | 1670605 | 21944000 | 1.55 | 0.727 | 18.05% | 50.16% |
| 3 | 7.5 | *BATCH B* | 90 Days | 7791.0 | 0.154 | 1947750 | 32661500 | 1.55 | 0.721 | 19.35% | 50.39% |
| 1 | 10 | *BATCH B* | 90 Days | 6505.6 | 0.188 | 4337067 | 19915000 | 1.56 | 0.722 | 18.57% | 50.14% |
| 2 | 10 | *BATCH B* | 90 Days | 11898.9 | 0.18 | 2620903 | 55874500 | 1.56 | 0.722 | 18.39% | 50.04% |
| 3 | 10 | *BATCH B* | 90 Days | 9169.3 | 0.209 | 1667145 | 26485500 | 1.57 | 0.719 | 16.16% | 50.86% |

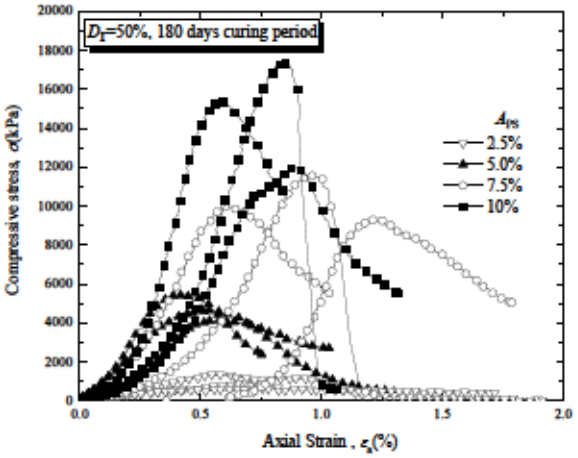


(g) (h)

Figure C-28 Typical UCT stress-strain relationship of OPC-treated sand for w=10%, tp=3days, Dr=50%: (g) t= 180 days, (h) t= 360 days.

Table C-mm UCT data record for OPC-treated sand for w=10%, tp=3days, Dr=50% at t= 180 days

| Specimen No. | $A_{OPC}$ (%) | Modifier Batch | Curing days, $t$ | $q_u$ (kN/m²) | $\varepsilon_f$ (%) | $E_{50}$ (kN/m²) | $\rho_d$ (g/cm³) | $e$ | $w$ (%) | $D_r$ (%) |
|---|---|---|---|---|---|---|---|---|---|---|
| 1 | 2.5 | *BATCH B* | 180 Days | 1089.8 | 0.11 | 143018 | 1.51 | 0.760 | 21.68% | 50.87% |
| 2 | 2.5 | *BATCH B* | 180 Days | 1246.3 | 0.143 | 222554 | 1.51 | 0.760 | 21.78% | 50.92% |
| 3 | 2.5 | *BATCH B* | 180 Days | 581.1 | 0.208 | 159643 | 1.51 | 0.762 | 22.89% | 50.07% |
| 1 | 5 | *BATCH B* | 180 Days | 4484.2 | 0.142 | 1072775 | 1.53 | 0.739 | 20.16% | 52.67% |
| 2 | 5 | *BATCH B* | 180 Days | 5144.1 | 0.159 | 1299015 | 1.53 | 0.745 | 21.66% | 50.43% |
| 3 | 5 | *BATCH B* | 180 Days | 4000.2 | 0.249 | 643119 | 1.53 | 0.744 | 22.49% | 50.86% |
| 1 | 7.5 | *BATCH B* | 180 Days | 9486.4 | 0.213 | 1382857 | 1.55 | 0.727 | 21.34% | 50.03% |
| 2 | 7.5 | *BATCH B* | 180 Days | 10520.5 | 0.193 | 818079 | 1.55 | 0.724 | 21.78% | 50.93% |
| 3 | 7.5 | *BATCH B* | 180 Days | 8916.9 | 0.154 | 1284856 | 1.55 | 0.725 | 21.57% | 50.72% |
| 1 | 10 | *BATCH B* | 180 Days | 14406.6 | 0.188 | 2040595 | 1.57 | 0.719 | 18.57% | 50.69% |
| 2 | 10 | *BATCH B* | 180 Days | 11211.1 | 0.18 | 1063672 | 1.57 | 0.715 | 18.39% | 51.77% |
| 3 | 10 | *BATCH B* | 180 Days | 15433.9 | 0.209 | 1447833 | 1.57 | 0.716 | 18.36% | 51.64% |

## C.2.6 Stress-strain relationship of OPC-treated sand for w=10%, tp=3 days, Dr=90%

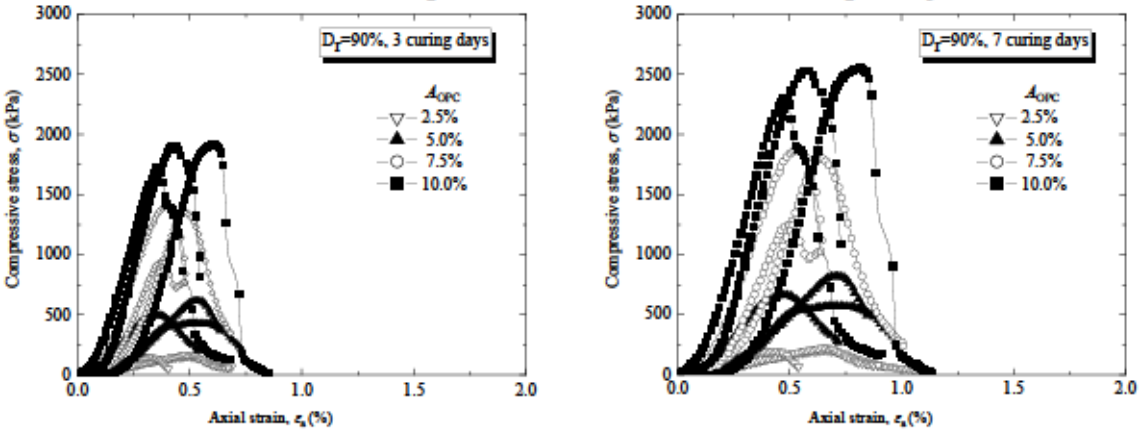


Figure C-29 Typical UCT stress-strain relationship of OPC-treated sand for *w*=10%, *tp*=3days, *Dr*=90%: (g) t= 3 days, (h) t= 7 days.

Table C-nn UCT data record for OPC-treated sand for w=10%, tp=3days, Dr=90% at t= 3 days

| Specimen No. | $A_{OPC}$ (%) | Modifier Batch | Curing days, *t* | $q_u$ (kN/m²) | $\varepsilon_f$ (%) | $E_{50}$ (kN/m²) | $\rho_d$ (g/cm³) | *e* | *w* (%) | $D_r$ (%) |
|---|---|---|---|---|---|---|---|---|---|---|
| 1 | 2.5 | *Batch A* | 3 Days | 166.0 | 0.347 | 34780 | 1.61 | 0.651 | 10.40% | 90.51% |
| 2 | 2.5 | *Batch A* | 3 Days | 154.1 | 0.206 | 47350 | 1.61 | 0.653 | 13.52% | 89.60% |
| 3 | 2.5 | *Batch A* | 3 Days | 178.7 | 0.355 | 38330 | 1.60 | 0.654 | 12.11% | 89.26% |
| 1 | 5 | *Batch B* | 3 Days | 542.6 | 0.262 | 129440 | 1.63 | 0.624 | 10.16% | 90.75% |
| 2 | 5 | *Batch B* | 3 Days | 663.5 | 0.462 | 89760 | 1.63 | 0.629 | 11.79% | 89.00% |
| 3 | 5 | *Batch B* | 3 Days | 466.1 | 0.381 | 76450 | 1.63 | 0.627 | 11.93% | 89.69% |
| 1 | 7.5 | *Batch C* | 3 Days | 1464.2 | 0.443 | 243370 | 1.66 | 0.596 | 9.25% | 90.09% |
| 2 | 7.5 | *Batch C* | 3 Days | 1513.8 | 0.313 | 302260 | 1.66 | 0.594 | 7.78% | 90.74% |
| 3 | 7.5 | *Batch C* | 3 Days | 1019.4 | 0.351 | 181500 | 1.66 | 0.596 | 7.58% | 90.18% |
| 1 | 10 | *Batch D* | 3 Days | 2067.2 | 0.538 | 406280 | 1.68 | 0.575 | 7.24% | 89.31% |
| 2 | 10 | *Batch D* | 3 Days | 2048.9 | 0.356 | 407810 | 1.69 | 0.575 | 10.86% | 89.53% |
| 3 | 10 | *Batch D* | 3 Days | 1859.4 | 0.281 | 413570 | 1.69 | 0.567 | 8.34% | 91.55% |

Table C-oo UCT data record for OPC-treated sand for w=10%, tp=3days, Dr=90% at t= 7 days

| Specimen No. | $A_{OPC}$ (%) | Modifier Batch | Curing days, *t* | $q_u$ (kN/m²) | $\varepsilon_f$ (%) | $E_{50}$ (kN/m²) | $\rho_d$ (g/cm³) | *e* | *w* (%) | $D_r$ (%) |
|---|---|---|---|---|---|---|---|---|---|---|
| 1 | 2.5 | *Batch A* | 7 Days | 210.1 | 210.1 | 34780 | 1.60 | 0.655 | 14.14% | 89.07% |
| 2 | 2.5 | *Batch A* | 7 Days | 195.1 | 195.1 | 47350 | 1.61 | 0.651 | 12.79% | 90.28% |
| 3 | 2.5 | *Batch A* | 7 Days | 226.2 | 226.2 | 38330 | 1.61 | 0.650 | 11.04% | 90.67% |
| 1 | 5 | *Batch A* | 7 Days | 678.3 | 678.3 | 129440 | 1.64 | 0.624 | 11.98% | 90.68% |
| 2 | 5 | *Batch A* | 7 Days | 829.4 | 829.4 | 89760 | 1.64 | 0.625 | 11.79% | 90.50% |
| 3 | 5 | *Batch A* | 7 Days | 582.6 | 582.6 | 76450 | 1.64 | 0.625 | 11.93% | 90.51% |
| 1 | 7.5 | *Batch A* | 7 Days | 1830.2 | 1830.2 | 243370 | 1.68 | 0.594 | 7.25% | 90.90% |
| 2 | 7.5 | *Batch A* | 7 Days | 1892.2 | 1892.2 | 302260 | 1.68 | 0.593 | 7.78% | 91.09% |
| 3 | 7.5 | *Batch A* | 7 Days | 1274.2 | 1274.2 | 181500 | 1.68 | 0.595 | 7.58% | 90.54% |
| 1 | 10 | *Batch A* | 7 Days | 2584.0 | 2584 | 406280 | 1.71 | 0.570 | 7.24% | 90.86% |
| 2 | 10 | *Batch A* | 7 Days | 2561.1 | 2561.1 | 407810 | 1.72 | 0.570 | 7.61% | 90.88% |
| 3 | 10 | *Batch A* | 7 Days | 2324.3 | 2324.3 | 413570 | 1.71 | 0.573 | 8.34% | 90.01% |

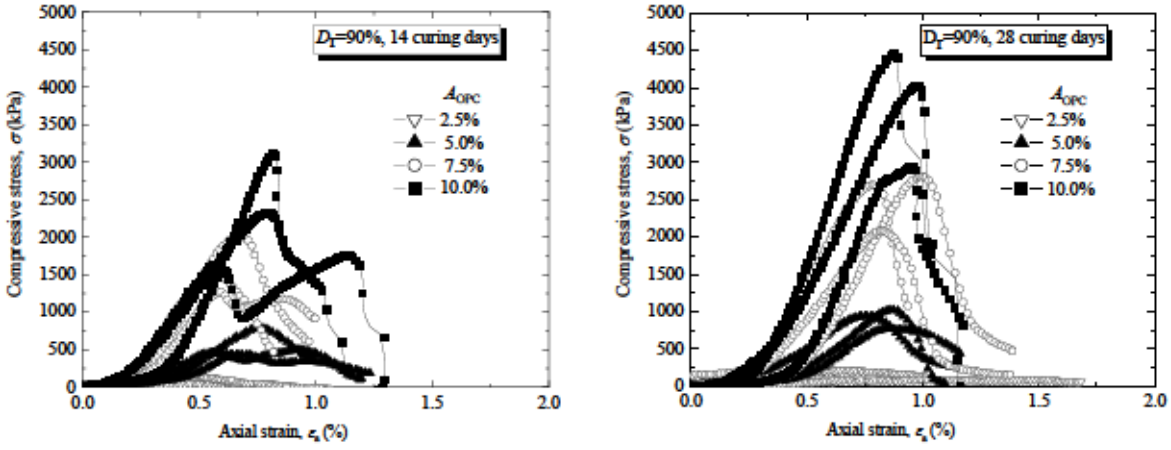


Figure C-30 Typical UCT stress-strain relationship of OPC-treated sand for w=10%, tp=3days, Dr=90%: (c) t= 14 days, (d) t= 28 days.

Table C-pp UCT data record for OPC-treated sand for w=10%, tp=3days, Dr=90% at t= 14 days

| Specimen No. | $A_{OPC}$ (%) | Modifier Batch | Curing days, $t$ | $q_u$ (kN/m²) | $\varepsilon_f$ (%) | $E_{50}$ (kN/m²) | $\rho_d$ (g/cm³) | $e$ | $w$ (%) | $D_r$ (%) |
|---|---|---|---|---|---|---|---|---|---|---|
| 1 | 2.5 | *Batch A* | 14 Days | 0 | 0 | 0 | 1.61 | 0.652 | 14.14% | 90.14% |
| 2 | 2.5 | *Batch A* | 14 Days | 161.5 | 0.403 | 35730 | 1.61 | 0.651 | 12.79% | 90.49% |
| 3 | 2.5 | *Batch A* | 14 Days | 223.2 | 0.378 | 56640 | 1.61 | 0.650 | 11.04% | 90.90% |
| 1 | 5 | *Batch A* | 14 Days | 469.2 | 0.457 | 79520 | 1.64 | 0.625 | 11.98% | 90.44% |
| 2 | 5 | *Batch A* | 14 Days | 508.5 | 0.752 | 71820 | 1.64 | 0.625 | 11.79% | 90.50% |
| 3 | 5 | *Batch A* | 14 Days | 790.3 | 0.764 | 82490 | 1.64 | 0.624 | 11.93% | 90.89% |
| 1 | 7.5 | *Batch A* | 14 Days | 1556.3 | 0.457 | 316320 | 1.68 | 0.595 | 7.25% | 90.60% |
| 2 | 7.5 | *Batch A* | 14 Days | 2028.9 | 0.526 | 354700 | 1.68 | 0.596 | 7.78% | 90.11% |
| 3 | 7.5 | *Batch A* | 14 Days | 1294.6 | 0.423 | 247060 | 1.68 | 0.596 | 7.58% | 90.21% |
| 1 | 10 | *Batch A* | 14 Days | 3137.5 | 0.633 | 379840 | 1.72 | 0.569 | 7.24% | 90.96% |
| 2 | 10 | *Batch A* | 14 Days | 1803.5 | 0.467 | 296620 | 1.72 | 0.570 | 7.61% | 90.89% |
| 3 | 10 | *Batch A* | 14 Days | 2363 | 0.699 | 311741 | 1.71 | 0.572 | 8.34% | 90.13% |

Table C-qq UCT data record for OPC-treated sand for w=10%, tp=3days, Dr=90% at t= 28 days

| Specimen No. | $A_{OPC}$ (%) | Modifier Batch | Curing days, $t$ | $q_u$ (kN/m²) | $\varepsilon_f$ (%) | $E_{50}$ (kN/m²) | $\rho_d$ (g/cm³) | $e$ | $w$ (%) | $D_r$ (%) |
|---|---|---|---|---|---|---|---|---|---|---|
| 1 | 2.5 | *Batch A* | 28 Days | 221.2 | 0.343 | 85070 | 1.61 | 0.649 | 14.38% | 91.23% |
| 2 | 2.5 | *Batch A* | 28 Days | 244.5 | 0.396 | 65720 | 1.61 | 0.652 | 14.00% | 90.11% |
| 3 | 2.5 | *Batch A* | 28 Days | 96.6 | 0.642 | 29630 | 1.61 | 0.647 | 13.93% | 91.94% |
| 1 | 5 | *Batch A* | 28 Days | 963.5 | 0.621 | 197430 | 1.64 | 0.626 | 11.85% | 90.13% |
| 2 | 5 | *Batch A* | 28 Days | 784.8 | 0.393 | 216790 | 1.64 | 0.626 | 11.38% | 90.23% |
| 3 | 5 | *Batch A* | 28 Days | 1033.9 | 0.337 | 243840 | 1.64 | 0.625 | 12.88% | 90.51% |
| 1 | 7.5 | *Batch A* | 28 Days | 2720.6 | 0.526 | 260590 | 1.68 | 0.596 | 11.79% | 90.51% |
| 2 | 7.5 | *Batch A* | 28 Days | 2856.2 | 0.497 | 629110 | 1.68 | 0.595 | 11.66% | 90.42% |
| 3 | 7.5 | *Batch A* | 28 Days | 2116.4 | 0.534 | 421590 | 1.67 | 0.600 | 12.41% | 88.88% |
| 1 | 10 | *Batch A* | 28 Days | 4077.5 | 0.654 | 629240 | 1.70 | 0.582 | 11.56% | 87.64% |
| 2 | 10 | *Batch A* | 28 Days | 4526.0 | 0.57 | 850750 | 1.70 | 0.582 | 11.99% | 87.67% |
| 3 | 10 | *Batch A* | 28 Days | 2993.8 | 0.482 | 787840 | 1.71 | 0.572 | 11.34% | 90.16% |

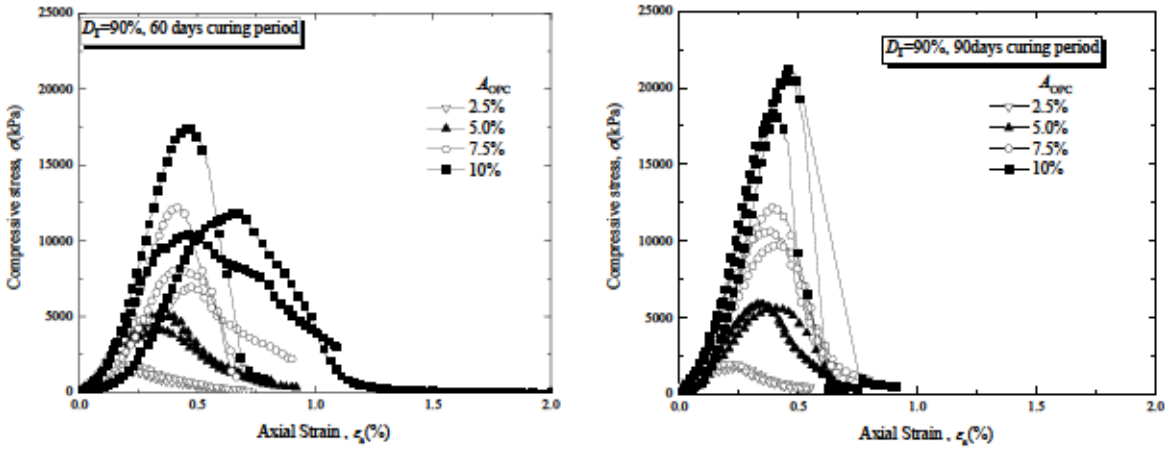


Figure C-31 Typical UCT stress-strain relationship of OPC-treated sand for *w*=10%, *tp*=3days, $D_r$=90%: (e) *t*= 60 days, (f) *t*= 90 days.

Table C-rr UCT data record for OPC-treated sand for w=10%, tp=3days, Dr=90% at t= 60 days

| Specimen No. | $A_{OPC}$(%) | Modifier Batch | Curing days, *t* | $q_u$ (kN/m²) | $\varepsilon_f$ (%) | $E_{50}$ (kN/m²) | $Ev$ (kN/m²) | $\rho_d$ (g/cm³) | *e* | *w* (%) | $D_r$ (%) |
|---|---|---|---|---|---|---|---|---|---|---|---|
| 1 | 2.5 | *BATCH B* | 60 Days | 1319.4 | 0.11 | 114200 | 83150 | 1.61 | 0.651 | 12.10% | 90.32% |
| 2 | 2.5 | *BATCH B* | 60 Days | 1512.9 | 0.143 | 200200 | 50510 | 1.61 | 0.651 | 12.56% | 90.41% |
| 3 | 2.5 | *BATCH B* | 60 Days | 1319.4 | 0.208 | 254400 | 169000 | 1.61 | 0.649 | 13.51% | 90.99% |
| 1 | 5 | *BATCH B* | 60 Days | 4771.7 | 0.142 | 604400 | 437500 | 1.64 | 0.625 | 15.19% | 90.37% |
| 2 | 5 | *BATCH B* | 60 Days | 4807.4 | 0.159 | 227200 | 283500 | 1.64 | 0.625 | 13.56% | 90.49% |
| 3 | 5 | *BATCH B* | 60 Days | 3882.1 | 0.249 | 458600 | 312500 | 1.64 | 0.626 | 12.07% | 90.03% |
| 1 | 7.5 | *BATCH B* | 60 Days | 6472.9 | 0.213 | 1253000 | 914500 | 1.68 | 0.594 | 10.32% | 90.82% |
| 2 | 7.5 | *BATCH B* | 60 Days | 7763.5 | 0.193 | 1253000 | 826000 | 1.68 | 0.594 | 11.37% | 90.86% |
| 3 | 7.5 | *BATCH B* | 60 Days | 11084.6 | 0.154 | 828800 | 656500 | 1.68 | 0.597 | 12.35% | 90.08% |
| 1 | 10 | *BATCH B* | 60 Days | 11379.1 | 0.188 | 654600 | 597500 | 1.71 | 0.572 | 10.58% | 90.18% |
| 2 | 10 | *BATCH B* | 60 Days | 16503.9 | 0.18 | 995300 | 945500 | 1.72 | 0.568 | 11.38% | 91.36% |
| 3 | 10 | *BATCH B* | 60 Days | 10043.4 | 0.209 | 1825400 | 848800 | 1.71 | 0.572 | 11.16% | 90.21% |

Table C-ss UCT data record for OPC-treated sand for w=10%, tp=3days, Dr=90% at t= 90 days

| Specimen No. | $A_{OPC}$ (%) | Modifier Batch | Curing days, *t* | $q_u$ (kN/m²) | $\varepsilon_f$ (%) | $E_{50}$ (kN/m²) | $E_{0.02}$ (kN/m²) | $\rho_d$ (g/cm³) | *e* | *w* (%) | $D_r$ (%) |
|---|---|---|---|---|---|---|---|---|---|---|---|
| 1 | 2.5 | *BATCH B* | 90 Days | 1606.5 | 0.11 | 1575000 | 4223250 | 1.61 | 0.653 | 12.10% | 89.60% |
| 2 | 2.5 | *BATCH B* | 90 Days | 1844.2 | 0.143 | 2426579 | 5995500 | 1.61 | 0.652 | 12.56% | 90.20% |
| 3 | 2.5 | *BATCH B* | 90 Days | 1761.1 | 0.208 | 1222986 | 7159000 | 1.61 | 0.650 | 13.51% | 90.83% |
| 1 | 5 | *BATCH B* | 90 Days | 5369.1 | 0.142 | 1383789 | 17282000 | 1.64 | 0.629 | 15.19% | 89.14% |
| 2 | 5 | *BATCH B* | 90 Days | 5419.1 | 0.159 | 1593853 | 17267500 | 1.64 | 0.624 | 13.56% | 90.68% |
| 3 | 5 | *BATCH B* | 90 Days | 5396.6 | 0.249 | 1707785 | 23164500 | 1.64 | 0.623 | 12.07% | 91.05% |
| 1 | 7.5 | *BATCH B* | 90 Days | 11271.2 | 0.213 | 2762549 | 41702000 | 1.68 | 0.598 | 10.32% | 89.53% |
| 2 | 7.5 | *BATCH B* | 90 Days | 10092.8 | 0.193 | 2900230 | 50955000 | 1.68 | 0.599 | 11.37% | 89.32% |
| 3 | 7.5 | *BATCH B* | 90 Days | 9272.8 | 0.154 | 2365510 | 29393000 | 1.68 | 0.599 | 12.35% | 89.40% |
| 1 | 10 | *BATCH B* | 90 Days | 19041.4 | 0.188 | 3950498 | 83073000 | 1.67 | 0.576 | 10.58% | 89.15% |
| 53 | 10 | *BATCH B* | 90 Days | 18756.3 | 0.18 | 3460572 | 75199500 | 1.67 | 0.576 | 11.38% | 89.27% |
| 3 | 10 | *BATCH B* | 90 Days | 16596.3 | 0.209 | 3841736 | 56243500 | 1.68 | 0.574 | 11.16% | 89.83% |

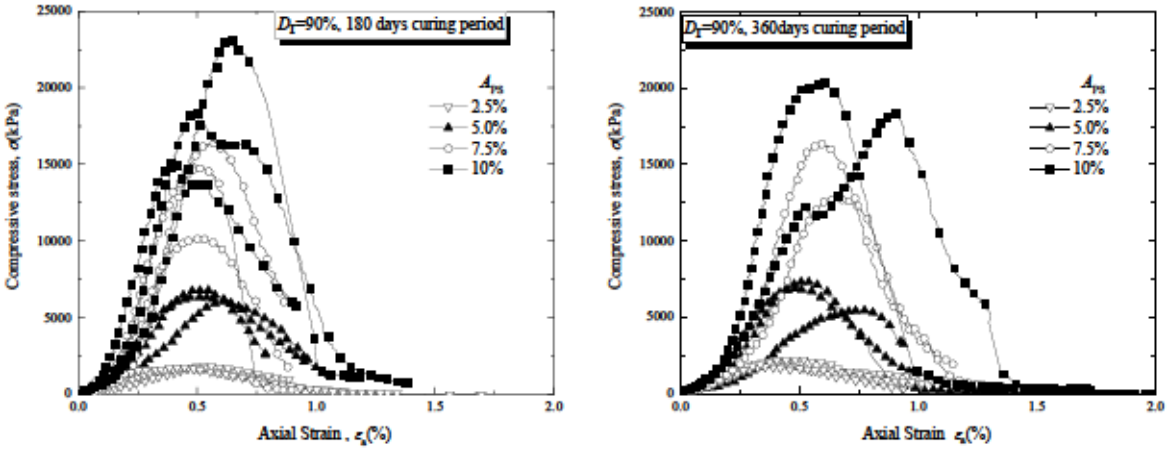


(g) (h)

Figure C-32 Typical UCT stress-strain relationship of OPC-treated sand for w=10%, tp=3days, Dr=90%: (e) t= 180 days, (f) t= 360 days.

Table C-tt UCT data record for OPC-treated sand for w=10%, tp=3days, Dr=90% at t= 180 days

| Specimen No. | $A_{OPC}$ (%) | Modifier Batch | Curing days, $t$ | $q_u$ (kN/m²) | $\varepsilon_f$ (%) | $E_{50}$ (kN/m²) | $\rho_d$ (g/cm³) | $e$ | $w$ (%) | $D_r$ (%) |
|---|---|---|---|---|---|---|---|---|---|---|
| 1 | 2.5 | *BATCH B* | 180 Days | 1688.4 | 0.11 | 302581 | 1.60 | 0.654 | 12.10% | 89.16% |
| 2 | 2.5 | *BATCH B* | 180 Days | 1601.7 | 0.143 | 428262 | 1.61 | 0.648 | 12.56% | 91.46% |
| 3 | 2.5 | *BATCH B* | 180 Days | 1636.9 | 0.208 | 601801 | 1.61 | 0.650 | 13.51% | 90.79% |
| 1 | 5 | *BATCH B* | 180 Days | 5959.2 | 0.142 | 832291 | 1.64 | 0.626 | 15.19% | 90.25% |
| 2 | 5 | *BATCH B* | 180 Days | 6378.9 | 0.159 | 1190093 | 1.64 | 0.626 | 13.56% | 90.05% |
| 3 | 5 | *BATCH B* | 180 Days | 6184.5 | 0.249 | 1332866 | 1.64 | 0.626 | 12.07% | 90.25% |
| 1 | 7.5 | *BATCH B* | 180 Days | 15242 | 0.213 | 2248083 | 1.68 | 0.597 | 10.32% | 90.07% |
| 2 | 7.5 | *BATCH B* | 180 Days | 9720.4 | 0.193 | 1847985 | 1.68 | 0.596 | 11.37% | 90.09% |
| 3 | 7.5 | *BATCH B* | 180 Days | 13797.9 | 0.154 | 2555167 | 1.68 | 0.595 | 12.35% | 90.67% |
| 1 | 10 | *BATCH B* | 180 Days | 17028.4 | 0.188 | 2895986 | 1.72 | 0.569 | 10.58% | 90.92% |
| 2 | 10 | *BATCH B* | 180 Days | 14118.9 | 0.18 | 3151540 | 1.71 | 0.572 | 11.38% | 90.15% |
| 3 | 10 | *BATCH B* | 180 Days | 21435.9 | 0.209 | 2646407 | 1.71 | 0.572 | 11.16% | 90.28% |

Table C-uu UCT data record for OPC-treated sand for w=10%, tp=3days, Dr=90% at t= 360 days

| Specimen No. | $A_{OPC}$ (%) | Modifier Batch | Curing days, $t$ | $q_u$ (kN/m²) | $\varepsilon_f$ (%) | $E_{50}$ (kN/m²) | $\rho_d$ (g/cm³) | $e$ | $w$ (%) | $D_r$ (%) |
|---|---|---|---|---|---|---|---|---|---|---|
| 1 | 2.5 | *BATCH B* | 360 Days | 1915.6 | 0.11 | 573533 | 1.60 | 0.654 | 12.10% | 89.16% |
| 2 | 2.5 | *BATCH B* | 360 Days | 1635.9 | 0.143 | 511219 | 1.61 | 0.648 | 12.56% | 91.46% |
| 3 | 2.5 | *BATCH B* | 360 Days | 2126.8 | 0.208 | 542551 | 1.61 | 0.650 | 13.51% | 90.79% |
| 1 | 5 | *BATCH B* | 360 Days | 6860.7 | 0.142 | 1203632 | 1.64 | 0.626 | 15.19% | 90.25% |
| 2 | 5 | *BATCH B* | 360 Days | 5224.4 | 0.159 | 666378 | 1.64 | 0.626 | 13.56% | 90.05% |
| 3 | 5 | *BATCH B* | 360 Days | 6523.1 | 0.249 | 1336701 | 1.64 | 0.626 | 12.07% | 90.25% |
| 1 | 7.5 | *BATCH B* | 360 Days | 12171.2 | 0.213 | 1477087 | 1.68 | 0.597 | 10.32% | 90.07% |
| 2 | 7.5 | *BATCH B* | 360 Days | 15466.6 | 0.193 | 2101440 | 1.68 | 0.596 | 11.37% | 90.09% |
| 3 | 7.5 | *BATCH B* | 360 Days | 0 | 0.154 | 0 | 1.68 | 0.595 | 12.35% | 90.67% |
| 1 | 10 | *BATCH B* | 360 Days | 19486.7 | 0.188 | 3205049 | 1.72 | 0.569 | 10.58% | 90.92% |
| 2 | 10 | *BATCH B* | 360 Days | 16842.5 | 0.18 | 3107472 | 1.71 | 0.572 | 11.38% | 90.15% |
| 3 | 10 | *BATCH B* | 360 Days | 16596.3 | 0.209 | 3841736 | 1.71 | 0.572 | 11.16% | 90.28% |

## C.3 Monotonic triaxial tests

### C.3.1 Normative references

The following standards shall constitute a part of this standard by virtue of being referenced in this standard. The latest versions of these standards shall apply (including supplements)

JGS 0520 Preparation of soils specimens for triaxial tests

Matters not prescribed in this standard shall be in accordance with the following related codes and standards.

JGS 0522 Method for consolidated -undrained triaxial compression tests on soils

JGS 0523 Method for consolidated -undrained triaxial compression test on soils with pore water pressure measurements

JGS 0524 Method for consolidated-drained triaxial compression test on soils

If a coarse-grained soil with maximum particles size exceeding about 20 mm is tested, the test specimen used in the test shall be prepared and installed in accordance with the following standards.

JGS 0530 preparation of the specimens of coarse granular materials for triaxial tests.

### C.3.2 Triaxial test apparatus and setting.

The triaxial test is most often performed on a cylindrical specimen, as shown in Fig. D.gg. Principal stresses are applied to the specimen, as indicated in Fig. D.gg First, a confining pressure, $\sigma_3$, is applied to the specimen. This pressure acts all around and therefore on all planes in the specimen. Then an additional stress difference, $\sigma_d$, is applied in the axial direction. The stress applied externally to the specimen in the axial direction is.

$$\sigma_1 = \sigma_d + \sigma_3$$

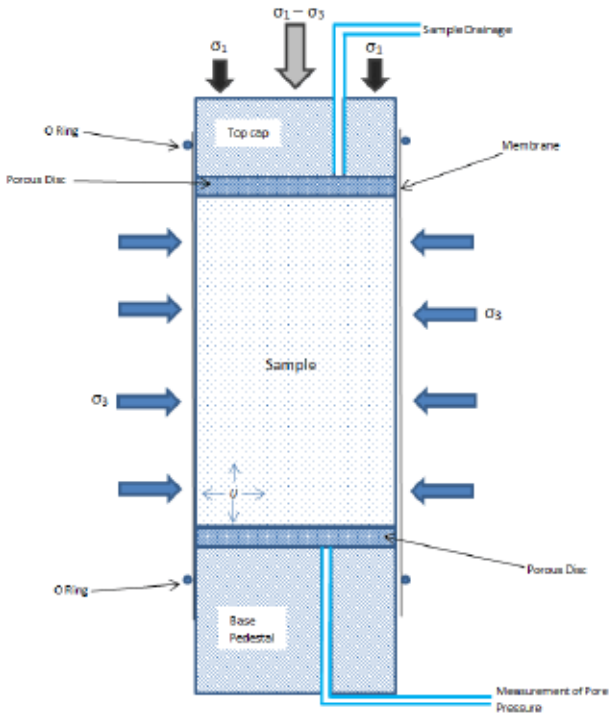


Figure C-33 Stress condition in a typical triaxial test

σ1: Vertical (axial) Stress or vertical load applied to the sample it is also known as the Major Principal Stress and can also be expressed as σv

σ3: Confining Pressure or as cell pressure it is also known as the Minor Principal Stress and can also be called σh

U: Pore Pressure it can be expressed as Uw (Pore Water Pressure (P.W.P))

σ1– σ3– Deviator Stress (the stress due to the axial load applied to the specimen in excess of the confining pressure)

In the general case, three principal stresses, $\sigma_1$, $\sigma_2$, and $\sigma_3$ may act on a soil element in the field. However, only two different principal stresses can be applied to the specimen in the conventional triaxial test. The intermediate principal stress, $\sigma_2$, can only have values as follows:

$\sigma_2 = \sigma_3$: Triaxial compression

$\sigma_2 = \sigma_3$: Triaxial extension

The condition of the triaxial extension can be achieved by applying negative stress differences to the specimen. This merely produces a reduction in compression in the extension direction, but no tension occurs in the specimen. The state of stress applied to the specimen is in both cases axisymmetric.

The test is performed using the triaxial apparatus, as seen in the schematic illustration in Fig.D.hh. The specimen is surrounded by a cap and a base and a membrane. This unit is placed in a triaxial cell in which the cell pressure can be applied. The cell pressure acts as hydrostatic confinement for the specimen, and the pressure is, therefore, the same in all directions.

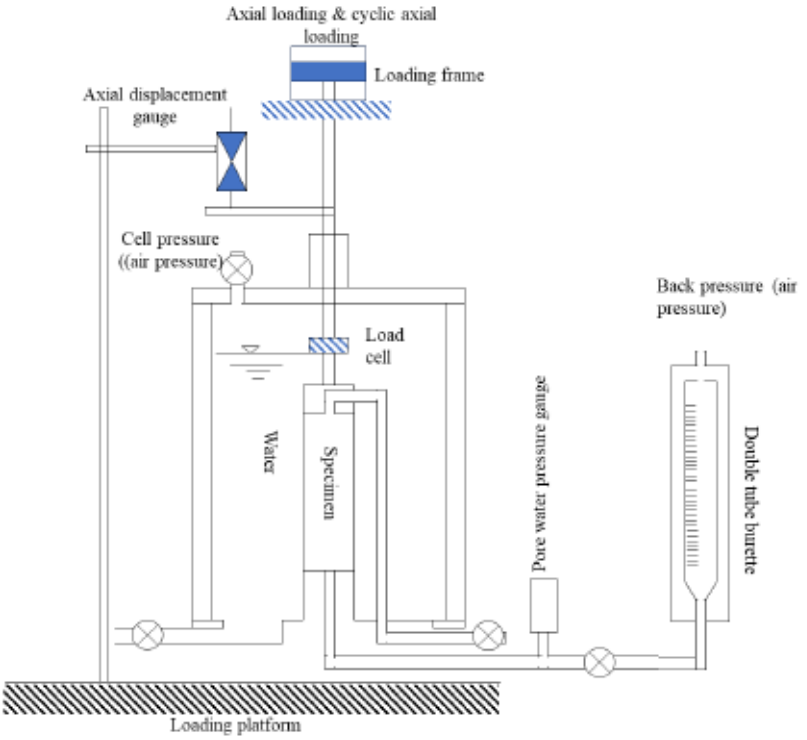


Figure C-34 Schematic illustration of triaxial apparatus

Besides, a deviator load can be applied through a piston that goes through the top of the cell and loads the specimen in the axial direction. The vertical deformation of the specimen may be measured by a dial gage attached to the piston which travels the same vertical distance as the cap sitting on top of the specimen. Drainage lines are connected to the water-saturated specimen through the base (or both the cap and the base) and connected to a burette outside the triaxial cell. This allows for measurements of the volume changes of the specimen during the test. Alternatively, the connection to the burette can be shut off thereby preventing the specimen from changing volume. Instead, the pore water pressure can be measured on a transducer connected to the drainage line.

The following quantities are measured in a typical triaxial test:

a) Confining pressure
b) Deviator load
c) Vertical (or axial) deformation
d) Volume changes or pore water pressure.

These measurements constitute the database from which other quantities can be derived [e.g., stress difference ($\sigma_1 - \sigma_3$), axial strain $\varepsilon_1$, and volumetric strain $\varepsilon_v$].

### C.3.3 Terms and definitions

- **Axial stress**: Refers to the stress acting in the longitudinal direction of the specimen.
- **Lateral stress:** refers to the stress acting in the radial direction of the test specimen.
- **Principal stress difference:** Refers to the differences in the axial stress and the lateral stress. The value of stress is defined at the mid-height of the test specimen.
- **Isotropic stress state refers** to the state of stress when the axial stress is equal to the lateral stress.
- **Cell pressure:** refers to the pressure applied within the triaxial pressure cell; the lateral stress is equal to the cell pressure.
- **Back pressure**: refers to the pressure applied to the test specimen to achieve a higher degree of saturation of the test specimen while keeping effective stress constant.
- **Consolidation stress:** refers to the difference between the extremally period stress on the test specimen and the back pressure during consolidation process.

**Undrained Compressive strength of soil** refers to the maximum principal stress difference that can be applied to the soil specimen when no pore water can flow in or out of the specimen.

### C.3.4 Types of triaxial test

Many variations of test procedure are possible with the triaxial apparatus, but the three principal types of tests are as follows:

1. Unconsolidated-Undrained (UU). The specimen is subjected to a specified confining pressure and then the principal stress difference is applied immediately, with no drainage/consolidation being permitted at any stage of the test. The test procedure is standardized in JGS 0522
2. Consolidated-Undrained (CU). Drainage of the specimen is permitted under a specified confining

pressure until consolidation is complete; the principal stress difference is then applied with no further drainage being permitted. Pour water pressure measurements may be during the undrained part of the test to determine strength parameters in terms of effective stresses. The consolidation phase is isotropic in most standard testing, denoted by CIU. Modern computer-controlled triaxial machines (also known as stress path cells) use hydraulic pressure control units to control the cell (confining) pressure, back pressure and ram load (axial stress) independently (fig ). Such an apparatus can therefore apply a "no-lateral strain" condition where stresses are anisotropic, mimicking the one-dimensional compression that occurs in an oedometer test.

3. Consolidated-Drained (CD). Drainage of the specimen is permitted under a specific confining pressure until consolidated is complete, with drainage still being permitted, the principal stress difference is then applied at a rate slow enough to ensure that the excess pore water pressure is main.

### C.3.5 Equipment conditions in the laboratory

Equipment used for preparation and mounting of specimens conforms to the following requirement.

- Negative pressure generator

  The negative pressure generator develops a negative pressure enough to bring the rubber sleeve into close contact with the inner surface of the mold. When in the preparation of the specimen using the negative pressure method, it can be applied to make the specimen free stand.

- Rubber sleeve

  This rubber sleeve must be longer than the rubber sleeve expander, its inner diameter in a natural state should be about 95% of the diameter of the specimen. The rubber thickness is about 0.15mm.

- Rubber sleeve expander

  This Rubber sleeve expander has a cylindrical shape with height and inner diameter about 5-10% greater than the height and diameter of the specimen. The design of the expander ensures that the rubber sleeve fits tightly to the inner surface of the expander under an applied negative pressure.

- Filter

For the filter, its permeability is greater to suit margin of the specimen. It fitting to the cap and pedestal allows to drain both upward and downward lo-compressibility material with the smallest possible coefficient of friction.

- O-ring and rubber cord

  O-rings is set tightly to prevent leakage; the inner diameter of the O-rings is about 80% of the diameter of the specimen.

- Instrument for measuring specimen size

  The specimen diameter is measured using a caliper or a steel rule with a Vernier.

- Weighing scale

  Methods of preparing and mounting specimens

  The method used for the specimen preparation is the negative pressure method.

### C.3.6 Negative pressure method used for sample preparation.

The negative pressure method is used for samples obtained in a loosened state and that cannot be formed into large pieces by compaction and consolidation.it is used also to make loosened samples freestanding.

Preparation and measurement of the specimen using negative pressure method.

Using this method, the specimen is prepared as follows:

- After Assemble the pedestal, rubber sleeve, and mould apply negative pressure to bring the rubber sleeve into close contact with the inner surface of the mold.
- Fill the moil d with the sample material. When the material reaches the prescribed height of the mold, smooth the upper surface of the specimen.

### C.3.7 Method used to fill the mould with sample material. JGS 0520

- Natural Toyoura sand

Wet tamping method is used for the preparation of the specimen of natural Toyoura sand.

With a spoon or an applicator nozzle, place the sample material in the mould in several batches, using a push rod or compact it each time. During the application of the methods in the laboratory, compaction was done by tapping the lower part of the mould with a wood hammer or by using a wood battle to facilitate compaction.

- Shortly we Place a cap on the top of the specimen, draw the rubber sleeve around the cap, and use an O-ring, etc., to seal the rubber sleeve against the cap.
- After that an appropriate negative pressure is applied to the specimen and the mould is removed.
- We Measure the diameter of the specimen to a precision of 0.1 mm or better at the outside of the rubber sleeve, taking measurement at the top and bottom of the specimen and at one point near the middle. the mean of the measured values is taken, and we correct the thickness of the rubber sleeve as measured in advance and $D_i$(cm) of the specimen is determined.

  The measurement of the specimen diameter and height is taken after increasing the negative pressure to 30kN/m2. In fact, the negative pressure must remain lower than the prescribed effective stress in the sideways direction at the termination of consolidation.
- Measure the height of the specimen to a precision of 0.1mm or better at three or more points and obtain the mean value to determine the initial height Hi(cm) of the specimen.
- To determine the mass of the specimen, we take the mass of the whole original sample before forming the specimen and then measure the residual amount after preparing the specimen to a precision of 0.1g or better. At the end the difference obtained is considered as the specimen mass. Alternatively, the whole sample is collected and weighted after testing.
- Split a representative quantity from the original sample and measure the water content to determine the initial water content $w_i$ (%) of the specimen as needed.

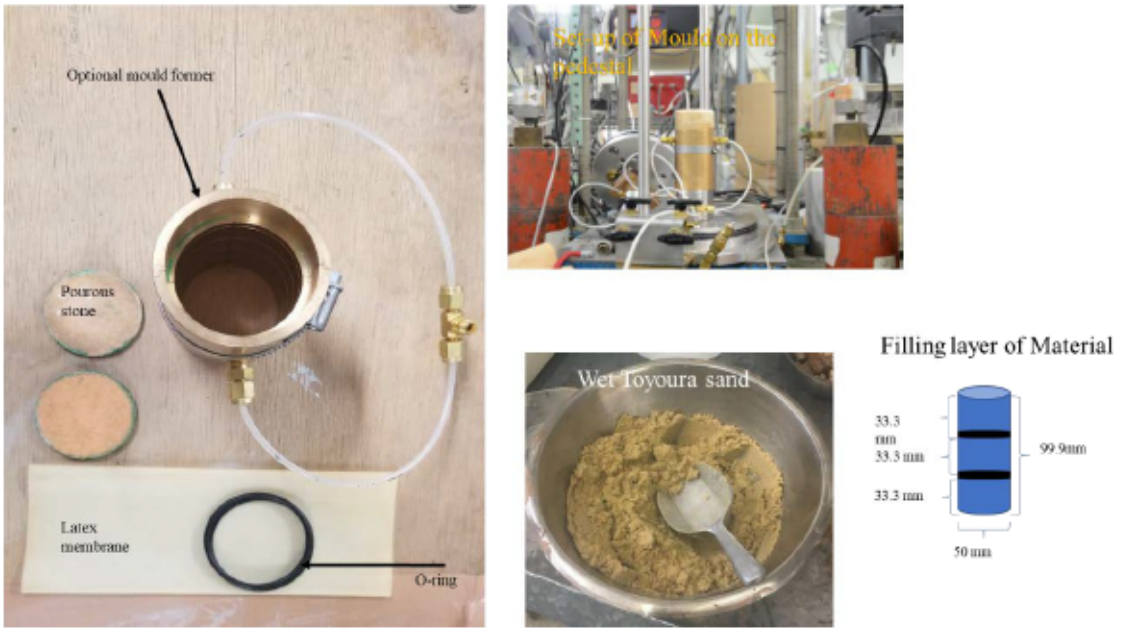


Figure C-35 Sample preparation equipment-Sample setup

### C.3.8 Saturation of specimen

Refer to the following for the method available to saturate the specimen. Volume changes that occur as a result of the saturation process are measured as required.

- Combine appropriate methods as needed to increase the degree of saturation of the specimen.
  In the need of increasing the degree of saturation of a specimen, a combination of the following four methods must be used according to the soil type and the state of the specimen.
  a) Passed deaerated water through the specimen under cell pressure.
  b) Apply enough back pressure.
  c) Apply method a) and b) after replacing void air inside the specimen under cell pressure.
  d) Extraction of air from within the specimen by applying a negative pressure of about 90kN/m2 to the specimen and to the pressure cell without changing the effective isotropic stress. Apply deaerated water while applying the negative pressure as needed.
- When using back pressure, apply the back pressure up kN/m2 to the specimen and the isotropic pressure concurrently without changing the effective isotropic stress inside the specimen.A back pressure of 95 kN/m2 is used. the back pressure increases gradually in order to avoid large fluctuation in effective stress inside the specimen.

### C.3.9 Consolidation process

The consolidation process is carried out in accordance with the following requirements for consolidation:

- We make first zero adjustment to the displacement transducer and pore water pressure transducer and confirm that pore water pressure measurement system is indicating the desired value of back pressure $u_b$ (kN/m2) by opening the valve on the pore water pressure measurement system. At the same time take the initial value of the burette.
- After we close the drainage valve connected to the burette. Increase only the isotropic stress to make

the difference between the isotropic stress and the back pressure equal to the desired value of consolidation stress.

If the loading piston is not rigidly connected to the cap, set the load measuring device, the piston, and the cap in contact with each other before this process.

- Open the drainage valve to start consolidation.
- Record readings of the volume change $\Delta V_t$ (cm3) and the axial deformation $\Delta H_t$ (cm) of the test specimen at appropriate time intervals during consolidation and plot them. Consolidation shall be continued at least until the end of primary consolidation. Measure the volume change $\Delta V_c$ (cm3) (which is supposed to be the amount of water expelled from the specimen) and axial deformation ΔHc (cm) due to consolidation.
- Close the drainage valve connected to the burette and increase the isotropic stress by the amount Δσ(kN/m2), wait for the change in pore water pressure caused by stabilize, and measure the pore pressure increment $\Delta u$ (kN/m2) after stabilization and the time required for stabilization.
- Return the isotropic stress to its original value, wait for the value of the pore water pressure to stabilize and open drainage valve.

### C.3.10 Axial compression process

The axial compression process is carried out in accordance with the following requirements.

- Check and adjust the origins of the axial load and deformation gauge readings.
- Close the drainage valve.
- Compress the test specimen continuously with a constant strain rate keeping the cell pressure constant.
- Record the axial compression force P(N), the axial deformation ΔH(cm), and the pore water pressure $u$(kN/m2) during compression.
- Terminate the compression when more than 3%axial strain has been reached after the maximum value of the axial load reading, or when the load reading has been reduced to about 2/3 of its maximum value, or when an axial strain of 15%has been reached.
- Remove the test specimen form the triaxial pressure chamber, and observe and record the deformed shape and failure mode of the test specimen,
- Measure the oven-dried mass of the specimen $m_s$ (g)

### C.3.11 Data record for Triaxial test

- Initial state of the specimen before consolidation

The volume $V_0$(cm3) and the height $H_0$(cm) of the test specimen prior to consolidation is calculated from the following equations.

$V_0 = V_i - \Delta V_i$

$H_0 = H_i - \Delta H_i$ where $V_i$ : initial volume of the specimen (cm3) $H_i$ : Initial height of the specimen cm

(

$\Delta V_i$ : volume change of the test specimen from the initialed to the state prior to the consolidation (cm3)

$\Delta H_i$ : change of the test specimen from the initialed to the state prior to the consolidation (cm3).

- Consolidation process

The method of calculation for the consolidation process is describe as follows:

- The volume of the test specimen after consolidation, Vc(cm3) is calculated as follows:

$V_c = V_0 - \Delta V_c$

Where?

$\Delta V_c$ : volume change of the test specimen due to consolidation.

The void ratio after consolidation (prior to axial compression) is calculated from the following equation.

$e_c = \frac{V_c \rho_s}{m_s} - 1$

Calculate the height of the specimen after consolidation Hc (cm)

$$H_c = H_0 - \Delta H_c$$

Where $\Delta H_c$ : change in test specimen height due to consolidation (cm)

- The area of the test specimen's cross section after consolidation

$$A_c = \frac{V_c}{H_c}$$

- Dry density of the specimen after consolidation $\rho_{dc}$ (g/cm3) is calculated as follows:

$$\rho_{dc} = \frac{m_s}{V_c}$$

Where $m_s$: dry weight of the specimen

Pore pressure coefficient, B-value

The B-value of the specimen after consolidation is calculated from the following equation.

$B = \frac{\Delta u}{\Delta \sigma}$ where?

$\Delta\sigma$ amount of isotropic stress increment (kN/m2)

$\Delta u$ : amount of pore water pressure increment (kN/m2) caused by $\Delta\sigma$

Axial compression process

The method of calculation for the axial compression process is as follows.

The axial strain of the specimen

$\varepsilon_a = \frac{\Delta H}{H_c} \times 100$

Where?

$\Delta H$ : axial deformation of the specimen in the axial compression process(cm)

The principal stress difference $(\sigma_a - \sigma_r)$ (kN/m2) and pore water pressure increment ue (kN/m2) due to the axial compression at axial strain of $\varepsilon_a$(%) shall be calculated from this equation.

$\sigma_a - \sigma_r = \frac{P}{A_c}\left[1 - \frac{\varepsilon_a}{100}\right] \times 100 \quad u_e = u - u_b$

Where?

P: axial compression force (N) applied to the test specimen at the axial strain $\varepsilon_a$(%) setting P=0 during isotropic consolidation.

$\sigma_a$: axial stress (kN/m2) acting on the test specimen.

$\sigma_r$: lateral stress (kN/m2) acting on the test specimen.

u : pore water pressure in the specimen (kN/m2)

$u_b$ : back pressure (kN/m2)

- Draw the graphs with principal stress difference and the pore water pressure on the vertical axis versus axial strain on the horizontal axis, to obtain the principal stress difference-axial strain curve and the pore water pressure increment due to axial compression-axial strain curve.
- Obtain minimum principal stress difference $(\sigma_a - \sigma_r)_{max}$in the axial strain range of 0 <$\varepsilon_a$<15% from the graph and take it to be the compressive strength.
- Calculate effective principal stresses, $\sigma'_a$(kN/m2) and $\sigma'_b$(kN/m2) in the axial compression process from the following equations and draw an effective stress path diagram with $\frac{\sigma_a-\sigma_r}{2}$ on the vertical versus $(\sigma'_a + \sigma'_r)/2$ on the horizontal axis.

$\sigma'_r = \sigma_r - u \quad \sigma'_a = (\sigma_a - \sigma_r) + \sigma'_r$

- Calculate the effective axial stress $\sigma'_{af}$ (kN/m2) and the effective lateral stress $\sigma'_{rf}$ (kN/m2) at the maximum principal stress difference from the following equations.

$\sigma'_{rf} = \sigma_{rf} - u_f \quad \sigma'_{af} = (\sigma_a - \sigma_r)_{max} + \sigma'_{rf}$

Where $u_f$: pore water pressure at the maximum principal stress difference (kN/m2).

## C.4 Method for cyclic undrained triaxial test on soils-Japanese geotechnical society standard (JGS 0541 -2009)

### C.4.1 Scope

This standard specifies methods of testing to obtain the relationship between the number of load cycles to reach a specific double amplitude strain and a specific excess pore water pressure and the single amplitude of the cyclic deviator stress under undrained conditions of the cyclic stress amplitude ratio, for saturated specimen that were consolidated under isotropic stress conditions. The standard applies mainly to saturated sandy soils.

Note 1: Sandy soils referred to here is soil that consists mainly of sand fraction.

Note 2: Soils that have been saturated after the test specimen is prepared are included. Also, this standard is also applicable to saturated cohesive soils and gravelly soils.

### C.4.2 Cyclic deviator stress

The difference between the two stresses in the cyclic undrained loading process. The stress value shall be defined at the mid-height of the specimen.

### C.4.3 Cyclic stress amplitude ratio

Half the single amplitude of the cyclic deviator stress divided by the effective confining pressure.

### C.4.4 Equipment for cyclic triaxial test

- The cyclic triaxial apparatus shall include a triaxial pressure cell, a cell pressure and back pressure supply device, an axial loading device, and load, displacement, volume change, pore water pressure measuring and recording devices, and shall satisfy the following conditions.

Note: an example of a cyclic triaxial apparatus is shown in Fig.D.hh

The test equipment shall have sufficient capacity and load resistance with respect to the maximum cell pressure, back pressure, the maximum axial compressive load and the maximum axial tensile load on the specimen.

Note1: The triaxial cell shall be fixed to a loading platform or similar, so that the triaxial cell is not raised up when the maximum axial tensile load is acting.

Note 2: In order to produce a triaxial extensile stress state during cyclic loading, normally a triaxial cell in which the load piston and the cap are rigidly connected is used (see Fig. D.hh of JGS 0522 Method for consolidated undrained triaxial compression test on soils), and the load piston and cap shall be rigidly connected before setting the specimen in the triaxial cell. If the specimen is set in the triaxial cell without rigidly connecting load piston and cap, the load piston and the cap shall be connected after a sufficiently large effective stress is applied to the specimen.

- The specimen shall be covered with the cap, pedestal, and a rubber sleeve, it shall be possible to apply the required cell pressure, back pressure, and axial load, and it shall be possible to supply and drain water at the top and the bottom ends of the specimen. Also, the volume change of the pore water pressure measurement line due to water pore pressure changes shall be sufficiently small.

Note 1: the diameter of the cap and pedestal shall be the same as the diameter of the specimen as standard. The two surfaces of the cap and pedestal shall be flat and parallel to each other and shall be normal to the piston.

Note 2: the volume change of the pore water pressure measurement line (see fig 2) that induces the pore water meter pressure receiving unit, and the water drainage line between the specimen and the water drainage valve shall be measured. If the volume of the specimen is V, and the volume of the pore water pressure measurement line for a change in pore water pressure, $\Delta u$ is $\Delta V$, then $\{(\Delta V/V)/\Delta u\}$ should be $<5\times10\text{-}6$ m2/kN.

- During isotropic consolidation, it shall be possible to continuously apply the required cell pressure, back pressure, and axial stress within a range of fluctuation of ± 2 kN/m2, and ± 1.0% for pressures more than 200 kN/m2. Also, during consolidation it shall be possible to measure the axial displacement and volume change of the specimen with an allowable tolerance in the height of the specimen and the volume of ±0.02% and 0.05%, respectively.

Note: the volume change of the specimen during isotropic consolidation is assumed to the quantity of water drained from the specimen and may be measured using burette or other device with equal or better performance. The burette shall have a structure to enable the back pressure to be applied and should have a structure so that the water level in the burette does not change due to changes in the back pressure.

- In the undrained state which is the condition of cyclic triaxial test conducted in this research after isotropic consolidation, the cyclic load was applied until the double amplitude axial strain DA as defined in section 6.3 is more than 5%, and the wave form shown a sine wave with a frequency of 0.1 to 1Hz as standard. The following conditions was always satisfied until the cyclic axial load reaches DA=2%.
- The fluctuation in the sum of the single amplitude Pc of the compressive load and the single amplitude PE of the extensile load defined from the isotropic stress state, (Pc+PE) shall be less than 10%

  $0.9 \leq Pc/PE \leq 1.1$

Note 1: the single amplitude Pc of the compressive load and the single amplitude PE of the extensile load shall be defined from the isotropic stress state as shown in fig.3 In the figure, P is the cyclic axial load which is taken to be zero under isotropic stress state. The axial load acting on the load piston is the sum of the cyclic axial load P and the force acting on the load piston due to cell pressure.

Note 2: the load frequency needs to be limited to the range 0.1 to 1.0 Hz if it has been confirmed that the effect on the test results is negligible.

Note3: A cyclic axial load other than a sine wave may be used if it has been confirmed that the cyclic axial load amplitude can be accurately controlled and measured. However, a rectangular or trapezoidal wave shall not be used.

Note: 4 During cyclic axial loading, the cell pressure shall not fluctuate due to the load piston entering and exiting the triaxial pressure cell.

- During the cyclic loading, it shall be possible to continuously apply the required cell pressure to within a range of fluctuation of pressure of ±2 kN/m2 for pressure less than 200 kN/m2, and ±1 kN/m2 for pressure more than 200 kN/m2.
- During cyclic loading, it shall be possible to continuously measure the pore water pressure and if necessary, the cell pressure to within allowable tolerance of ±2kN/m2 less than 200 kN/m2, and ±1 kN/m2 for pressure more than 200 kN/m2.

Note: An electric pressure transducer shall be used to measure the pore water pressure during cyclic loading.

- During cyclic loading it shall be possible to continuously measure the cyclic axial load acting on the specimen to within an allowable tolerance of 0.5% of the required load and amplitude. However, when the load cell is outside the triaxial cell pressure cell, the single amplitude friction for F at the bearing of the triaxial pressure chamber based on the cell pressure shall satisfy the following condition.

$F < 0.02 \times$ (effective confining pressure $\sigma 0'$) $\times$ (specimen cross-sectional area)

The axial displacement during cyclic loading shall be capable of being measured to within an allowance tolerance of ±0.05% of the height of the specimen.

During the cyclic loading it shall be possible to continuously record the pore water pressure, cyclic

axial load, axial displacement, if necessary, the cell pressure

Test method

Preparation of the specimen shall be accordance with JGS 0520 preparation of soil specimen for triaxial tests. (See section D.3.7)

5.2 Checking the degree of saturation of the specimen.

Before consolidation and if necessary, after consolidation, the pore water pressure coefficient B (B value) shall be measured. The B value shall be obtained under an isotropic stress state.

The B value before consolidation shall be obtained by the following method.

Close the water drainage valve.

Increment the isotropic stress Δσ for 1 to 2 minutes. Δσ shall be about 50 kN/m2 as standard. However, after Δσ is applied the cell pressure shall not exceed the cell pressure at completion of isotropic consolidation.

When the pore water pressure has settled to a constant value, the increment in the pore water pressure Δu shall be measured.

Calculate the pore pressure coefficient B (=Δu/ Δσ). When the B value is higher than 0.95, either open the water drainage value and start isotropic consolidation or open the drainage valve after incrementing the isotropic stress to a prescribed value when consolidation is completed. If the B value is smaller than 0.95, reduce the isotropic stress by Δσ and return to the beginning, and increase the degree of saturation by method described in JGS 0520preparation of soil specimens for triaxial tests, section 4.6a), so that the B value is 0.95% higher.

Instead of obtaining the B value before starting consolidation, it may be obtained by the method described in section 5.2a) above, at a stress stage lower than the prescribed consolidation stress, however, the primary consolidation at that stress stage shall be completed.

For specimens with B value 0.95 or higher and consolidation 8hours or less, the B value after consolidation need not to be obtained. However, if air remains within the triaxial pressure cell and if there is a possibility that air has entered the specimen through the cell water due to the cell pressure being applied for 8hours or longer, the B value after consolidation shall be obtained by the following method.

After primary consolidation of the specimens is completed, close the water drainage valve.

Reduce the isotropic stress by Δσ for 1 to 2 min. Δσ shall be about 50kN/m2 as standards.

Measure the reduction in pore water pressure Δuu.

At the time as 2) increment the isotropic stress by Δσ

Measure the increment in pore pressure Δu1.

Calculate the pore water pressure coefficient B {= (Δuu+ Δu1)/(2 Δσ)}

Open the water drainage valve.

When the B value is 0.96 or higher, go to section5.4 when the B value is smaller than 0.95, increase the degree of saturation by method described in JGS 0520preparation of soil specimens for triaxial tests, section 4.6a), so that the B value is 0.95% higher.

C.4.5 5.3 Consolidation process

The test shall be carried out in accordance with the following requirements for the consolidation process.

Carry out consolidation with a constant back pressure by applying isotropic stress to the specimen up to prescribed consolidation stress σ'c.

Consolidation shall be continued until at least the primary consolidation is complete.

Measure the volume change of the specimen (assumed to be equal to the quantity of water drained from the specimen) ΔVc (cm3) and the axial displacement of the specimen ΔHc (cm) due to consolidation.

5.4 cyclic undrained loading process

The test shall be carried out in accordance with the following requirements for the cyclic undrained loading process.

Confirm the isotropic stress state with the prescribed effective confining pressure $\sigma_0$'

$0.98<\sigma'_{ac}/\sigma'_{rc}<1.02$

(b) Close the water drainage valve

(c) Apply the cyclic axial load, and continuously record the axial load, axial displacement, pore water pressure, and if necessary, the cell pressure. The first wave shall be the compressive load.

Terminate the cyclic loading if the number of cycles exceeds about 200, or if (ΔL/Hc) ×100 is 5% or higher where, ΔL is the double amplitude of axial displacement (ΔH) of the specimen during cyclic loading and Hc is the height of the specimen after consolidation.

Deformation and failure state of the specimen shall be observed and recorded.

Measure the dry mass $m_s$ of the specimen (g).

C.4.6 5.5 tests with cyclic loading amplitude varied.

This shall refer to a series carried out under the same effective confining pressure, using the necessary number of similar specimens, but with the cyclic loading amplitude varied as appropriate.

Note: the number of specimens necessary to obtain the relationship between the cyclic load amplitude and the number of cycles under the same effective confining pressure shall be minimum of 4. The magnitude of the cyclic axial load amplitude shall be adjusted so that at least 2 specimens have the number of load cycle in the range of about 5 to 50 and a double axial strain DA of 5%, for Toyoura sand and DA of 0.1% for PSAS-treated sand.

C.4.7 Typical Undrained cyclic result obtained.

# D APPENDIX- IV. Effects of dry-wet cycles on the mechanical properties of sand treated with paper sludge ash-based stabilizer.

## D.1 Specimen Test Procedure and measurement condition

- 1st step: After prepare the specimen
  - Measure mass $m_0$
- 2nd step: wetting process
  - Measure Mass $m_1$ before immersion $=m_0$
  - Measure Mass $m_2$ after wetting condition
  - Calculated water content during wetting ($W_w$)
- 3rd step: drying process
  - Measure Mass $m_3$ before air drying process$=m_2$
  - Measure Mass $m_4$ After air drying process
  - Calculated water content during drying process ($W_d$)
- 4th step: Conduct UCT on the dry specimen of each

Figure D-1 test program for each specimen

## D.2 Unconfined compression test results for specimen cured under dry-wet cycle process.

### D.2.1 T=40°C Dry-wet cycle Stress-strain relationship of PSAS treated sand for w=20%, tp=1 days, Dr=50%

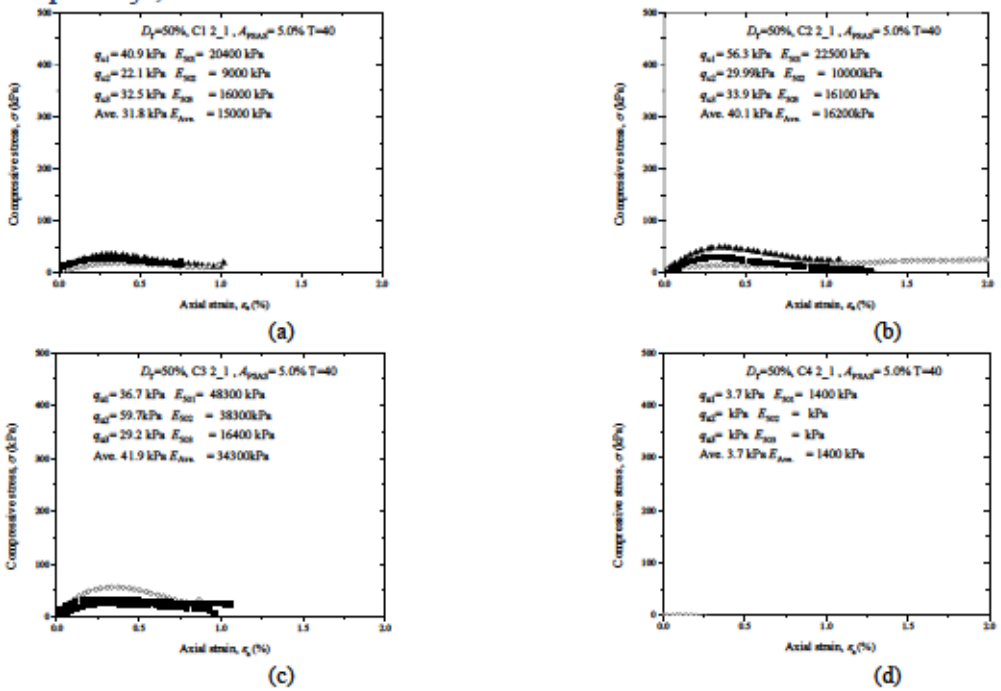


Figure D-2 T=40°C Typical UCT stress-strain relationship of PSAS-treated sand for w=20%, tp=1days, Dr=50%, APS=5%: (a) C1, (b) C2, (c)= C3, and (d)=C4 .

### D.2.2 T=40°C Dry-wet cycle Stress-strain relationship of PSAS treated sand for w=20%, tp=1 days, Dr=90%

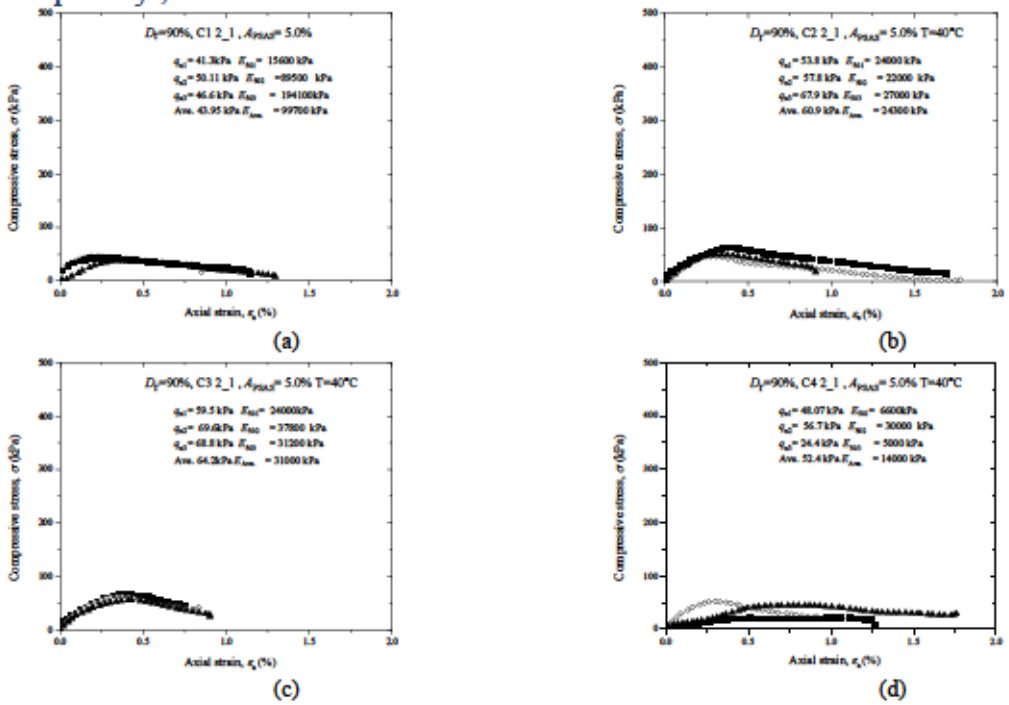


Figure D-3 T=40°C Typical UCT stress-strain relationship of PSAS-treated sand for w=20%, tp=1days, Dr=90%, $A_{PS}$=5%: (a) C1, (b) C2, (c)= C3, and (d)=C4 .

Table D-aUCT data record for PSAS-treated sand for w=20%, tp=1days, Dr=90% at C1

| Mixtures | Particle density (cm3) | Diameter (cm) | Height (cm) | Volume (cm3) | Wet density (g/cm3) | e (After) | Dr (%) |
|---|---|---|---|---|---|---|---|
| 5.00% | 2.64 | 4.98 | 9.32 | 181.54 | 1.92 | 0.66 | 90.45% |
| | 2.64 | 4.98 | 9.39 | 182.80 | 1.91 | 0.66 | 90.05% |
| | 2.64 | 4.98 | 9.05 | 176.28 | 1.98 | 0.66 | 89.21% |

Table D-bUCT data record for PSAS-treated sand for w=20%, tp=1days, Dr=90% at C2

| Mixtures | Particle density (cm3) | Diameter (cm) | Height (cm) | Volume (cm3) | Wet density (g/cm3) | e (After) | Dr (%) |
|---|---|---|---|---|---|---|---|
| 5.00% | 2.64 | 4.98 | 9.62 | 187.28 | 1.82 | 0.66 | 90.29% |
| | 2.64 | 4.98 | 9.59 | 186.78 | 1.83 | 0.66 | 90.12% |
| | 2.64 | 4.98 | 9.40 | 183.00 | 1.84 | 0.66 | 90.46% |

Table D-cUCT data record for PSAS-treated sand for w=20%, tp=1days, Dr=90% at C3

| Mixtures | Particle density (cm3) | Diameter (cm) | Height (cm) | Volume (cm3) | Wet density (g/cm3) | e (After) | Dr (%) |
|---|---|---|---|---|---|---|---|
| 5.00% | 2.64 | 4.98 | 9.29 | 180.85 | 1.87 | 0.66 | 90.54% |
| | 2.64 | 4.98 | 9.39 | 182.80 | 1.84 | 0.66 | 90.75% |
| | 2.64 | 4.98 | 9.70 | 188.94 | 1.80 | 0.66 | 90.45% |

Table D-dUCT data record for PSAS-treated sand for w=20%, tp=1days, Dr=90% at C4

| Mixtures | Particle density (cm3) | Diameter (cm) | Height (cm) | Volume (cm3) | Wet density (g/cm3) | e (After) | Dr (%) |
|---|---|---|---|---|---|---|---|
| 5.00% | 2.64 | 4.98 | 9.25 | 180.17 | 1.99 | 0.66 | 90.43% |
| | 2.64 | 4.98 | 9.49 | 184.75 | 1.98 | 0.66 | 90.32% |
| | 2.64 | 4.98 | 9.62 | 187.28 | 1.95 | 0.66 | 88.83% |